

UPC-2024 Course Notes

**Methods of Continuum Mechanics
in Rock Physics and Seismic Exploration**

Igor B. Morozov

January 2025

Contents

1	INTRODUCTION	9
1.1	Scope and objectives	9
1.2	Physical terminology	10
1.2.1	Energy, attenuation, phase lags, and Q	12
1.3	Porous rock	13
1.4	Heterogeneities and scales	14
1.4.1	Microscopic and mesoscopic deformations	16
	Wave-induced fluid flows	17
1.4.2	Macroscopic picture	20
	Characteristic times and frequencies	21
1.5	Observations of elasticity and anelasticity	23
1.5.1	Transient deformations	24
1.5.2	Forced harmonic oscillations	27
1.5.3	Seismic waves	30
1.6	First-principle, effective and empirical moduli	32
1.7	Theories of Relaxation Phenomena	35
1.7.1	Traditional approach: the viscoelastic model	35
1.7.2	Approach of this course: continuum mechanics	36
1.8	Structure of next chapters	38
2	THE VISCOELASTIC MODEL	40
2.1	Mathematical principles	41
2.2	Phenomenology	45
2.2.1	Time-domain and frequency-domain pictures	45
2.2.2	Time domain: Creep function	46
2.2.3	Frequency domain: Dispersion band and Absorption peak	48

2.3	Kramers-Krönig (causality) relations	49
2.4	Kinetic equation	51
2.5	Zener's (standard linear solid) equation	52
2.6	Spring-dashpot diagrams	54
2.7	Linear viscoelastic solids	56
2.7.1	Maxwell's body	56
2.7.2	Kelvin-Voigt's body	58
2.7.3	Standard linear (Zener's) solid	59
2.7.4	Burgers' body	64
2.7.5	Generalized linear solids	65
2.8	Quasi-static (kinetic) character of viscoelastic equations	65
2.9	Problems with the viscoelastic approach	67
2.9.1	Treatment of heterogeneity	68
2.9.2	Treatment of non-viscoelastic forces	69
2.9.3	Boundary conditions	69
2.9.4	Nonphysical wave solutions	70
2.10	Laboratory assignments	70
	Lab 2.1: Dispersion and attenuation spectra of linear solids	70
	Lab 2.2: Explore Burgers' model	70
3	VARIATIONAL APPROACH IN PHYSICS	72
3.1	d'Alembert's principle	73
3.2	Hamiltonian action	74
3.3	Dissipation pseudo-potential	75
3.4	Constraints	76
3.5	Non-mechanical equations and Fréchet derivatives	77

4	LAGRANGIAN MECHANICS	80
4.1	Generalized coordinates	80
4.2	Euler-Lagrange equations	82
4.3	Mechanical energy	83
4.4	Dissipation of mechanical energy	84
4.5	Mass-Stiffness-Damping (MSD) model	86
4.5.1	Quasi-static variables	89
	Separation of dynamic and quasi-static variables	90
	Time-stepping equations	91
	Frequency-domain form	92
4.6	Oscillations and waves	92
	Plane-wave dispersion and attenuation	93
4.7	Examples	95
4.7.1	Linear oscillator with damping	95
4.7.2	Linked oscillators	100
4.8	Equipartitioning of energy	102
4.9	Attenuation coefficient	103
4.10	Quality factors	105
4.10.1	Q of a free-oscillation mode	105
4.10.2	Q -factors in forced oscillation experiments	105
	Kinetic-, potential-, and total-energy based Q s	106
	Strain-stress phase-lag Q	108
4.10.3	Conclusion about Q	109
4.11	Laboratory assignments	110
	Lab 4.1: Model the mechanical system in Figure 4.3	110
	Lab 4.2: Calculate the Q spectrum for the system in Figure 4.3	110
	Lab 4.3: Model forced oscillations of the system in Figure 4.3	111

5	LAGRANGIAN MECHANICS OF MACROSCOPIC SOLIDS OR FLUIDS	112
5.1	Media with internal structure (“General Linear Solid”)	116
5.1.1	GLS with displacement-type internal variables	116
5.1.2	GLS with arbitrary scalar internal variables	117
5.2	Equations of motion	119
5.2.1	Wave modes	121
5.3	Constitutive relations	122
5.3.1	Elasticity: Hooke’s law	123
5.3.2	Viscous surface friction: Navier-Stokes law	124
5.3.3	Body-force drag friction: Darcy’s law	125
5.4	Effects of micropores on material properties	126
5.5	Wave-Induced Fluid Flows (WIFF)	130
5.6	Biot’s Poroelastic Model	132
5.6.1	Relations between displacements, strains, and elastic parameters	134
5.6.2	Gassmann’s equation	138
5.6.3	Wave modes	139
5.7	Biot’s model with variable secondary porosity	141
5.8	Rigorous continuum-mechanics (GLS) form of the viscoelastic model	143
5.8.1	Linear solids	144
	Maxwell’s solid	144
	Kelvin-Voigt solid	147
	Standard linear (Zener’s) solid	147
	Burgers’ solid	149
	Generalized standard linear solid	150
5.8.2	Kinetic (massless) internal variables	153
5.9	Extended Generalized Standard Linear Solid	155
5.9.1	Selection of internal-friction material properties	156
5.10	Effective media (homogenization)	157

5.11	Model discretization for numerical modeling	158
5.11.1	Finite-element discretization using basis functions (Galerkin's method)	158
	Implementation of boundary conditions	162
	Construction of basis functions	164
5.11.2	Finite-difference discretization by spatial gridding	168
5.12	Problems and laboratory assignments	170
	Lab 5.1: Model a Maxwell's body	170
	Lab 5.2: Model a Zener's body	170
	Lab 5.3: Zener's body with finite internal mass	170
	Lab 5.4: Modification of bulk and shear elastic moduli by secondary porosity	171
	Problem 5.1: Creep in the standard linear solid	171
	Problem 5.2: Equivalence of two forms of the SLS	171
	Problem 5.3: Memory equation for strain	172
	Problem 5.4: Memory equation for stress	172
	Problem 5.5: Strain-stress relations for SLS	172
6	EFFECTS OF TEMPERATURE	173
6.1	Adiabatic and isothermal elastic moduli	177
6.2	Heat flows	179
6.2.1	Macroscopic heat flow	181
6.2.2	Local (internal) heat flow	182
6.3	General Linear Solid with multiple temperatures (GLST)	183
6.4	Biot's Model with Internal Temperatures	184
6.5	Mass-Stiffness-Damping model with temperature (MSDT)	187
6.6	Temperature Waves	189
6.7	Problems and Laboratory Assignments	191
7	APPLICATIONS	192
7.1	Static equilibrium	195

7.2	Plane Waves	196
7.2.1	P waves	196
7.2.2	S waves	197
7.2.3	Extensional waves in an infinite rod	197
7.3	Low-frequency forced oscillations of cylindrical rock samples	201
7.3.1	Approximation of uniform deformation	202
7.3.2	Detailed modeling of Biot's rock with thermoelastic effects	208
	Construction of finite elements and basis functions	208
	Construction of model vector	212
	Observables	213
	Governing equations	215
	Boundary conditions	216
	Solution	217
7.3.3	Detailed modeling of Biot's rock with local extended SLS	217
7.3.4	Detailed modeling of Biot's rock with local WIFF	218
7.4	Laboratory assignments	219
	Lab 7.1: Velocity dispersion and attenuation of plane P and S waves	219
	Lab 7.2: Extensional waves in a rod	220
	Lab 7.3: Modeling Young's modulus experiment with rock cylinder	222
	Lab 7.4: Poisson's ratios for poroelasticity	223
8	BIBLIOGRAPHY	225
9	APPENDICES	227
9.1	Variational principles for heat transfer	227
	Stationary heat conduction	227
	Stationary heat convection	229
	Nonstationary heat conduction	230
9.2	Symmetry of the kinetic-coefficient matrix	231
9.3	Orthogonalization and normalization of finite-element basis functions	233
9.4	Frequency-dependent effective moduli with thermal effects	234

1 Introduction

At the beginning of this and each of subsequent chapters, I list their **key points**:

- Main problems and objectives
 - Scales of measurement and microstructure, importance of the macroscopic scale, homogenization
 - Types of anelastic phenomena: transient deformations, oscillations, waves
 - Two approaches to anelasticity:
 - Conventional: the viscoelastic model
 - Approach of this course: macroscopic continuum mechanics
-

1.1 *Scope and objectives*

In this course, I attempt giving a unified and rigorous, and yet simple and practical, approach to analyzing many problems in rock physics and seismology. The scope of problems will include:

- 1) Static and quasi-static deformations of bodies of arbitrary shapes;
- 2) Pore-fluid flow through rock: Darcy law and poroelasticity;
- 3) Linear creep and stress relaxation within rock;
- 4) Deformation of media with complex internal structures, such as compounds and multiple porosities;
- 5) Elasticity and anelasticity;
- 6) Attenuation of seismic waves;
- 7) Thermal effects during rock deformation.

As all other physical phenomena, these effects can be described by methods of mechanics and thermodynamics. I will focus on methods using strictly macroscopic-scale material

properties and laws. These macroscopic laws correspond to the scales of all observations in the laboratory and field.

1.2 Physical terminology

There exists a broadly used but somewhat intricate terminology related to classification of deformations of solids (e.g., Cooper, 2002). This classification is usually illustrated on the example of a body undergoing an instantaneous (step-function) loading from zero stress followed by a similar unloading after certain amount of time. Such experiments are described in section 0. However, I try describing materials not just by their behavior in certain specific experiments but in terms of universal physical properties which should be active in *any* experiments.

Assume that the body and its surrounding environment does not change its composition, microstructure, etc., and returns to the original state after one loading/unloading cycle. Based on the dissipation of mechanical energy into heat, such deformations can be elastic (with zero dissipation) or inelastic (with positive dissipation) (Table 1.1). Thermodynamically, such processes are classified as reversible and irreversible, respectively, because processes with net zero loss of heat (and presumably no other changes) can typically be performed in reverse time order.

TABLE 1.1 Classification of viscoelastic behavior of materials
(modified after Cooper, 2002)

<i>Deformation type</i>	Viscoelastic		
	Elastic	Inelastic	
<i>Thermodynamic type</i>	Reversible ¹ (no dissipation of heat)	Irreversible ¹ (heat dissipates)	
<i>Time dependence of strain</i> ²	Synchronous with stress	Delayed relative to stress ³	
<i>Deformation sub-type</i>		Anelastic	Plastic
<i>Recoverability by unloading</i> ²	Recoverable	Recoverable	Not recoverable

¹) In a loop of loading/unloading.

²) In a step-function stress experiment.

³) Also postulated time dependence of strain-stress relations in viscoelastic model.

From the viewpoint of the viscoelastic model (Chapter 2), the distinctive property of a viscoelastic body is the delayed stress-strain response for inelastic processes (Table 1.1). However, from the mechanical argument further in this course, the delay in the observed strain response is only a consequence of internal friction within the material. Moreover, as also shown below, there exists no definite strain-stress response within rock at all.

Among the inelastic deformations, anelastic and plastic processes are differentiated (Table 1.1). For anelastic deformations, the body returns to its original shape after each loading/unloading cycle (maybe after some time after the stress is removed). Plastic deformations are characterized by material flows, *i.e.* permanent changes in the shape of the body after the end of the loading/unloading cycle. Note that the term “not recoverable” in Table 1.1 may not be rigorously accurate, because practically any creep can in principle be “recovered” by additional reshaping of the body. What is meant here is “deformation recovered by itself.” This is a phenomenological description of the expected result of some experiment but not a specification of its mechanism.

Peeking ahead in our discussion of continuum mechanics, the difference between anelastic and plastic effects can be illustrated in Figure 1.1. Plastic behavior always requires some internal variable, which is additive to the strain and has zero elastic energy

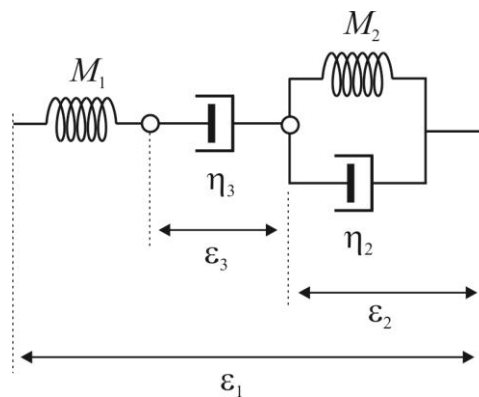


FIGURE 1.1.

Burgers' model of deformation. Stress σ is applied to the ends of this sequence of mechanical elements and causes observed deformation ϵ_1 . This deformation includes an anelastic part (involving both elasticity and viscosity, ϵ_2), plastic part (viscosity only, ϵ_3), and pure elastic part (the unlabeled deformation of the spring M_1).

Note that anelastic deformations almost always include movements of some internal degrees of freedom (white dots in this plot) which are not observed in the mechanical strain-stress testing experiment.

(*i.e.*, no elastic spring connected in parallel). The middle segment (ε_3) in Figure 1.1 is an example of such “plastic” variable. For very slow deformations, this variable will be the only one varying continuously and creating the plastic flow. In other words, plastic behavior requires some “flowing” structure present the system; this is not just a matter of selecting effective strain-stress laws. By contrast, the anelastic element (ε_2 in Figure 1.1) shows zero deformation at zero stress, and its deformation is reversible.

Because plasticity implies a certain construction of the medium rather than just a constitutive law, we do not significantly differentiate between the anelastic and plastic subtypes in Table 1.1. The major distinction lies between:

- Conservative deformations (elastic deformations of solids, frictionless flows in fluids) and
- Inelastic processes dissipating the mechanical energy.

1.2.1 Energy, attenuation, phase lags, and Q

When talking about wave “attenuation” and “energy dissipation,” it is important to clearly understand the meanings of these terms. These concepts are often interpreted empirically and intuitively, but in reality, they may not be easy to specify for a given experiment, and they may mean not what you think. Let us consider these concepts separately and in most general terms.

First, “attenuation” is often equated with the Q -factor not just the inverse Q -factor for a wave or a stress-strain phase lag measured in a subresonant lab experiment. Q -factors differ for different shapes of oscillating bodies (like a drum or string) and different wave modes. As it will be further explained in the course, the notion of a Q -factor is extremely tricky when applied to traveling waves or materials like rock. The Q -factor is also often explained through the strain-stress phase lag observed in a rock-physics experiment. However, in porous rock, there exist multiple types of strains, such as the strain of the average rock frame, different types of mineral grains, and of different parts of the pore volume and fluids. Each of these strains has a counterpart stress and consequently the corresponding phase lags and Q s. Because of heat flows between grains and pore fluids,

there is also a strain-stress phase lag related to thermoelasticity (coupling between deformations and temperature variations) In addition, within aseismic wave in a reservoir or in a deforming rock sample, there exist multiple types of waves: primary (“fast”) waves and secondary (“slow”) waves, P and S waves, and also waves related to boundary conditions like tube and surface waves. All these waves also have (generally) different strain-stress phase lags and Q -factors. Consequently, phase lags and Q -factors only describe certain types of experiments, and it is difficult to view them as material properties.

Similarly, by the law of energy conservation, the total energy is constant and does not dissipate. The energy also comes in multiple forms (kinetic, elastic, heat, chemical, surface adhesion, electric, etc.) which are extremely difficult to measure in rock. This is why I specifically emphasize the mechanical energy in the definition of inelastic processes above. Mechanical energy is a sum of the potential and kinetic energies associated with movements of grains and patches of gas or fluid within rock (but not, for example, their heat and electric or chemical energy). However, this energy is also impossible to measure in a real experiment, and we always observe only a part of the total mechanical energy. This observable mechanical energy is, for example, the work of the loading force applied to the end platen of a rock sample in a laboratory experiment. The measured work of the loading force is not the complete mechanical energy – it does not include the individual energies of deforming pores and pore fluids.

Thus, when explaining rock-physics observations, we should not rely on intuitive analogies but need to always use rigorous physical terminology and look for correct physical properties of the materials.

1.3 *Porous rock*

Still need some comments about the notion of porous rock

Emphasize strictly macroscopic properties... No such things as microcracks of certain shapes, connecting pores, ...

1.4 *Heterogeneities and scales*

Rock bodies contain internal structures with different characteristic spatial dimensions called scales. As above, when considering scales, it is important to clearly define this term. In particular, we need to differentiate between the observational scale of bodies used in the experiments and scales of the rock structure itself. In this regard, there exist only two scales:

- Observational scale, at which is any distance understood deterministically (e.g., dimensions of bodies or rock samples). Thus, this scale is only dependent on the
- Sub-observational scale, which is not covered by current deterministic equations. For example, such scale includes random layering between reflectors identified within a reservoir, distances between fractures, grain sizes, sizes of pores and patches of saturation. Any detail of the experiment at this scale must be described in terms of some averaged properties, which will vary on the observational scale. For example, when studying seismic responses of variable saturation within a rock cylinder, the shapes and sizes of saturation patches must be reduced to variations of average saturation or saturation tensor (below). This procedure of reducing the detail of sub-observational scale to observable properties is called creation of an effective-medium model, or homogenization.

Three characteristic scales are recognized for seismic properties (Figure 1.2):

- The longer, macroscopic scale of investigation or engineering application. This scale covers distances from several centimeters to meters and given by seismic wavelengths, thicknesses of key layers, dimensions of identifiable scatterers in the subsurface, and dimensions of samples in the laboratory testing.
- The shorter, microscopic scale of about a micrometer or smaller. At this scale, the rock represents an extremely complex arrangement of grains, volumes of pore fluids, bitumen, crystals of minerals, etc.
- The mesoscopic scale intermediate between the scales above (typically

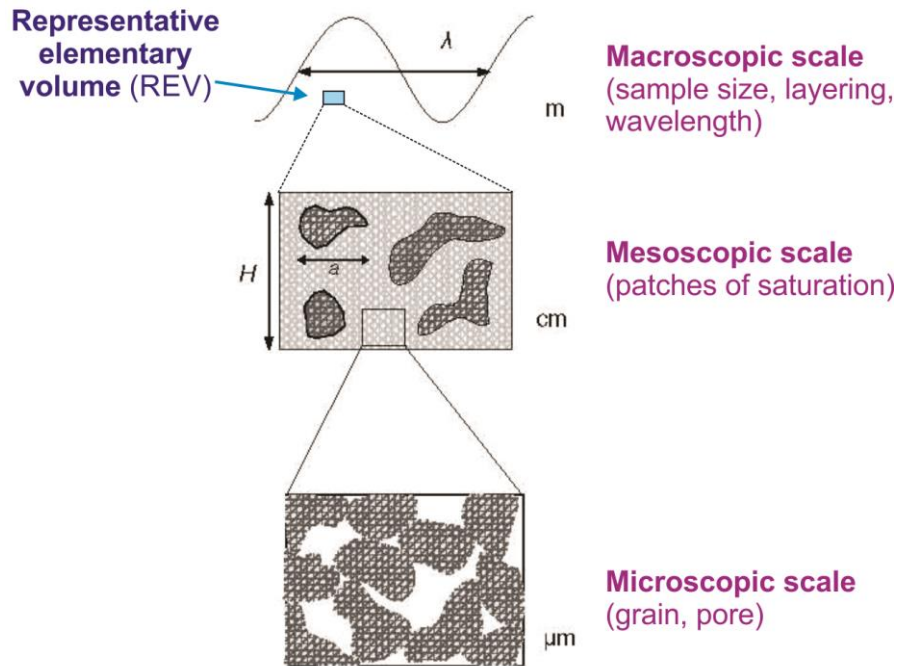


FIGURE 1.2.

Scales of structures within rock (modified after Müller et al., 2010)

about 1 cm). At this scale, grains are not recognized but groups of grains, fractures and larger cavities are viewed as the structure.

For laboratory measurements on rock cores or ultrasonic measurements with centimeter-long waves, the mesoscopic scale may overlap with the macroscopic one. In such cases, we will only talk about the macroscopic scale.

For laboratory and field observations with oscillations and waves or deformations of reservoirs, the differentiation of scales is somewhat different. We are only able to see the macroscopic scale, which is much larger than the size of the representative elementary volume (REV) (Figure 1.2, top). Usually, the REV is larger than the mesoscopic scale unless a small rock sample is being studied. Therefore, it is better to always look for REV-scale material properties summarizing the mesoscopic and microscopic-scale rock structure.

The REV is described by relatively few averaged medium properties and 'effective medium' equations of continuum mechanics discussed further in this course. These

parameters and equations are obtained by averaging the complex structures and deformation patterns at the microscopic and mesoscopic scales. This procedure of approximating the heterogeneous by effective-medium properties and equations is often called homogenization of micro- and meso-structures.

In the following subsections, I summarize the microscopic/mesoscopic scale phenomena and how they generally appear in REV-scale effective media.

1.4.1 Microscopic and mesoscopic deformations

At the microscopic and mesoscopic spatial scales, the rock structure is extremely complex, and deformation occur by numerous physical mechanisms. Lakes (2009) gave a classification of microscopic mechanisms that can be responsible for inelastic behavior of solids (Table 1.1). I added dislocation-based (q) and scattering (r) mechanisms to Lakes' classification. In this table, the asterisks indicate the most fundamental mechanisms which arise due to the most inherent properties and observed even in ideal perfect crystals.

Columns in Table 1.1 show check marks for the different mechanism contributing to macroscopic (observable on the scale of our experiments) physical phenomena:

- Column *Viscosity* indicates the microscopic or mesoscopic phenomena that create average viscous forces, similar to the viscosity of a fluid. This mechanism is not considered in conventional approaches, but in will be principal mechanism of anelasticity in chapter 5.
- Column *Thermal* indicates effects causing variation of temperature and heat flows between parts of the medium (chapter 6).
- Column *Kinetic* marks phenomena due to random vibration of particles, similar to the Brownian motion and reversible chemical reactions. This is the principal mechanism used in the viscoelastic model (chapter 2).
- Column *Scattering* indicates a special group of 'elastic' relaxation processes which occur without loss of the total mechanical energy. This mechanism is controlled by the shapes of heterogeneities and sometimes by the shape of the whole body studied. We will not consider this mechanism in this course.

Wave-induced fluid flows

The pore-fluid related mechanism (p) in Table 1.1 is the most important in

TABLE 1.1 Mechanisms of internal mechanical friction in materials

Mechanism	Viscosity (due to strain rates)	Thermal (due to thermal flows)	Kinetic (due to internal variables)	Scattering (due to elastic effects)
1) Atomic and molecular processes:	✓			
a) Relaxation by motion of solute atoms, in metals or on strain gradient;			✓	
b) Relaxation by dislocation motion (amplitude or frequency dependent); a special case is the “high-temperature background” (increase of Q with frequency);			✓	
c) Relaxation by molecular rearrangement in polymers;	✓		✓	
d) Relaxation by atom pair reorientation;			✓	
e) Relaxation by diffusion of atoms (at high temperature in metals);	✓		✓	
f) Relaxation by phase transitions;			✓	
g) Relaxation by electron viscosity;	✓		✓	
h) Relaxation by point-defect motion			✓	
2) Coupled-field effects:				
i) Thermoelastic dissipation*;		✓		
j) Fluid flow effects in porous materials containing fluids;	✓			
k) Piezoelectric and magnetoelastic effects;	✓			
l) Phonon-phonon scattering*;	✓			✓
m) Electron-phonon scattering.				✓
3) Effects due to heterogeneity:				
n) Relaxation in multiphase structured materials;				✓
o) Grain boundary slip in polycrystalline materials, such as metals, ceramics, or rocks;	✓			
p) Filtration fluid flows in porous materials.	✓			
q) Movement of dislocations in crystalline lattices;	✓			
r) Elastic scattering (reflections and wave mode conversions) on heterogeneities and boundaries of the body.				✓

*) Fundamental, inherent to all materials.

exploration seismics and called the wave-induced fluid flow (WIFF) there. This term is not particularly accurate because such flows occur not only in waves but in practically any types of deformations. For example, a steady-state pore-fluid flow during a permeability

measurement in a rock sample is also such as flow. However, WIFF is usually used to explain the variations of attenuation and velocities of harmonic waves, and consequently this name has become customary and broadly used.

Figure 1.3 shows several types of WIFF phenomena. Note that these phenomena can occur on all three of the structural scales (microscopic, mesoscopic, or macroscopic scales) and depend on the shape of the pore space within rock and sometimes on the size and shape of the whole rock body (e.g., case (d) in Figure 1.3).

The “wave-induced fluid flows” are often modeled in detail, by simulating some micro- and/or meso-scale structures (Figure 1.3) and using computer modeling to simulate

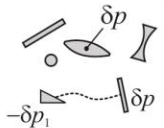
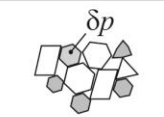
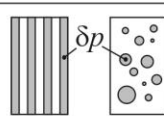
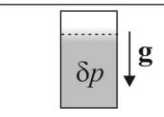
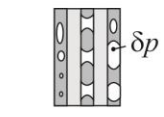
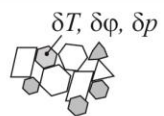
a		Type I WIFF: trapped pore fluids, micropores of various shapes, communicating micropores, squirt flows, multiple porosities	Microscopic
b		Grains, inclusions, ice, bitumen	
c		Type II WIFF: patchy saturation, thin layers	Macroscopic
d		Laboratory-scale WIFF Gravity-driven saturation layering	
e		Capillary effects, gas bubbles	
f		Thermoelastic, piezoelectric effects	

FIGURE 1.3.

Several types of microscopic, mesoscopic, and macroscopic-scale effects of pore fluids within rock. These effects called the wave-induced pore-fluid flow (WIFF) modify the velocities and attenuation of seismic waves. Effects (b) and (f) can occur for fluids or solid grains.

Note the complexity and variability of possible effects. The detail of these effects in a given rock are likely impossible to constrain, but the averaged macroscopic properties (pressures δp , electric potentials $\delta \phi$, temperature variations δT , etc.) can be used to characterize the rock.

the detailed fluid flow through it. By also measuring the average stresses and strains or energies within the modeled body, macroscopic ‘effective-medium’ relations are derived. However, although providing a complete detail, this approach contains a major difficulty: the modeled structure is always *only an example of a possible rock structure*. The modeled structure does not accurately represent any rock sample, and a myriad of other microstructures produce practically identical effects on a wave traveling through this medium. The results of modeling do not allow differentiating between the individual cases in Figure 1.3, and only averaged properties of the models can be constrained from experimental data. In particular, the ‘type-I, ‘type-II’ and ‘laboratory-scale’ WIFF are differentiated simply based on the sizes of the structures involved (much less than grain size ($\sim 1 \mu\text{m}$), grain size, and over 1 cm, respectively) and their aspect ratios (like planar cracks vs. spheres).

In this course, we try obtaining an effective-medium description of WIFF (as well as of any other process in Table 1.1) directly, by starting from observable macroscopic properties of the material and performing modeling strictly in terms of these properties.

1.4.2 Macroscopic picture

The micro- and mesoscale structures shown Figure 1.3 can be described by macroscopically- (REV-scale) averaged material properties. Some of these properties are well known, and some of them may be difficult to obtain but are in principle measurable:

- **Density and porosity**, mass fraction of various minerals and fluids (saturation).
- **Structural parameters**: distributions of sizes and shapes of grains and pores, fractures, microcracks and micropores.
- **Permeability parameters**: tortuosity, shapes and connectivity of pores.
- **Elastic moduli** measured under various conditions (bulk, shear, Young’s, drained, undrained, unjacketed for porous rock, isothermal, adiabatic). The General Linear Solid (GLS) model discussed further in this course shows that there exist many more types of such averaged elastic properties.
- **Average effects of viscosity** (bulk or shear) of fluids in primary and

secondary pores. Similar to elastic properties, there exist many material properties of this type.

- **Surface tension** parameters: surface tension, average contact angles, wettability, average radii of capillary menisci.
- **Electrical and magnetic properties.**
- **Average properties of thermal microstructure:** specific heat and heat conductivity between grains, pores, fluids, etc..

Our ultimate goal is to learn constraining the above macroscopic parameters from laboratory observations and wave velocities measured in the field and to apply these parameters to modeling seismic waves and interpreting reservoir conditions.

Characteristic times and frequencies

How do we recognize each of the “relaxation mechanisms” in Table 1.1 and Figures 1.2 and 1.3 within real rock? Unfortunately, these mechanisms only represent hypotheses explaining frequency dependencies of attenuation ($\chi(f)$, $Q^{-1}(f)$) and modulus dispersion observed in forced harmonic-oscillation mechanical testing (Figure 1.4). These spectra do not allow identification of the precise micro- or microscopic mechanisms (rows in Table 1.1, but they provide relatively clear distinction between groups of mechanisms given by the columns of that table (Figure 1.4).

In the attenuation spectra, the most valuable information constraining the mechanisms is the frequency (or multiple frequencies, or sometimes broader bands) of absorption peaks (Figure 1.4). From an observed characteristic frequency f_r , the characteristic “relaxation times” of the system is obtained as $\tau_r = 1/2\pi f_r$. Values of these relaxation times and frequencies are used, for example, for differentiating between the type I, type II, and the ‘global-flow’ (‘laboratory-scale’) WIFF in Figure 1.3. The characteristic time can be related two types of phenomena:

- Elastic scattering (for example, free oscillations or wave reflections). In such cases, a characteristic time τ_r indicates the presence of structure (e.g., layering, or pores) with characteristic dimension l :

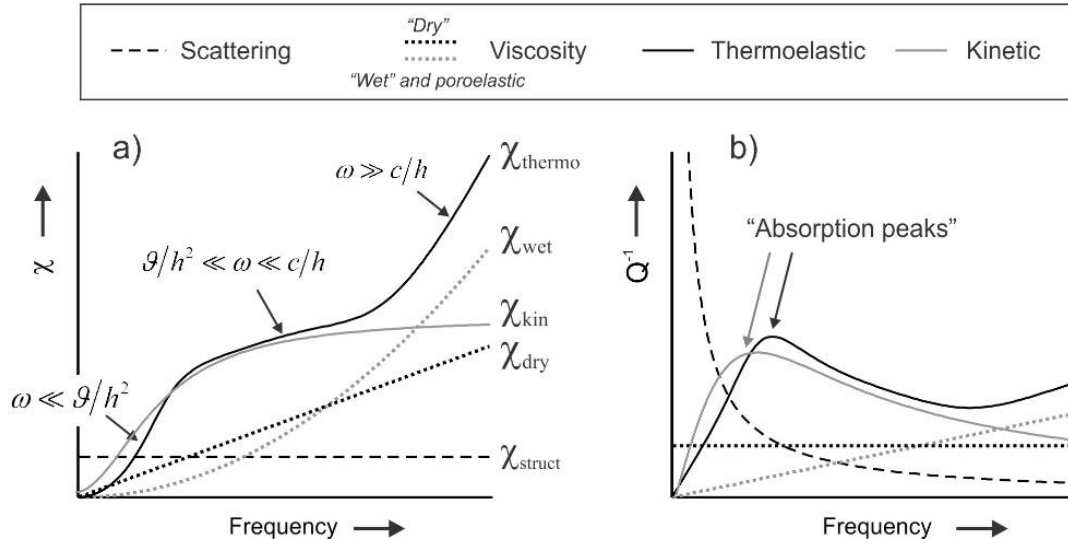


FIGURE 1.4

Schematic frequency dependencies of wave energy dissipation for different mechanisms of anelasticity in a material without internal variables: a) temporal attenuation coefficient χ (chapter 5), b) inverse quality factor $Q^{-1} = 2\chi/\omega$. Scaling of the axes is arbitrary.

For viscosity, two functions are shown, corresponding to linear ‘wet’, gray dotted line), and nonlinear (‘dry’, black dotted line). The ‘wet’ viscosity case also represents the saturated porous rock. Expressions in the labels in (a) indicate three different regimes of thermoelastic dissipation (chapter 6).

$$l \approx c\tau_r, \quad (1.1)$$

where c is the characteristic wave velocity. For rock, these elastic resonances occur at extremely high frequencies (Gigahertz). However, in laboratory testing, seismic-range frequencies f_r may occur due to resonances within the measurement apparatus.

- Anelastic relaxation due to internal friction within rock. In this case, the measured characteristic time τ_r suggests the presence of characteristic viscosity η of the mechanical system:

$$\eta \approx M\tau_r, \quad (1.1)$$

where M is the characteristic value of the elastic modulus. Unfortunately, a part of this viscosity may also occur within the measurement apparatus.

These parameters l and η are largely empirical and are sensitive to numerous parameters of the micro- or meso-scale structure. The magnitudes of χ can be reasonably estimated from first principles only for thermoelastic mechanisms. Note that in the viscoelastic model (next section and chapter 2), the dissipation strength and the relaxation times for kinetic processes are also totally empirical characteristics.

Note that for a material without internal deformation variables (Figure 1.4), the scattering, thermoelastic dissipation, and kinetic processes are the only mechanisms predicting the characteristic absorption peak in $Q^{-1}(f)$ (Figure 1.4b). Peak in $Q^{-1}(f)$ are indeed often observed, and from them, frequencies f_r are identified and material parameters l or η estimated. By contrast, the common viscosity without internal deformation variables leads to $Q^{-1}(f)$ monotonically increasing with frequency. This comparison shows that for real rock, there are (disregarding scattering) three general groups of mechanisms that can explain observations:

- 1) Kinetic effects (generalized to the viscoelastic model; this will be discussed in chapter 2);
- 2) Viscosity with internal deformations (like pore-fluid flows; chapter 5);
- 3) Thermoelastic effects (chapter 6).

1.5 *Observations of elasticity and anelasticity*

One of the key tasks in rock physics consists in explaining the anelastic relaxation phenomena, as defined in Table 1.1. Generally, relaxation means some observable property of a rock body *apparently* changing with time, such as a deformed body gradually returning to its original shape after the load is removed. Relaxation phenomena are observed in three forms:

- Time-delayed responses of strains and stresses in mechanical loading experiments;
- Frequency-dependent and phase-shifted ($M(f)$) and attenuation ($Q^{-1}(f)$) under time-harmonic loading at varying frequencies;
- Variations of wave velocities and attenuation with frequency. These

variations also cause changing shapes of wave packets with propagation time (dispersion).

Let us briefly consider these three types of phenomena.

1.5.1 Transient deformations

Consider, a rock sample subjected to mechanical testing in the laboratory or a volume of rock on which a seismic wave pulse is incident. If a sudden increase of stress σ is applied to the body, its deformation will first jump to a certain initial level ε_U (Figure 1.5). This initial strain is called ‘unrelaxed’, and the modulus (stiffness) associated with this initial deformation equals $M_U^{\text{def}} = \sigma/\varepsilon_U$. If the applied stress σ is kept constant at $t > 0$, internal flows occur within the body, and the strain increases further until ‘relaxed’ strain ε_R is achieved, and the rock is equilibrated. In this limit, a weaker, ‘relaxed’ stress-strain response will be obtained: $M_R^{\text{def}} = \sigma/\varepsilon_R$. The process of relaxation depends on time as $\exp(-t/\tau_\varepsilon)$, where τ_ε is the relaxation time for strain. If the load is suddenly removed at

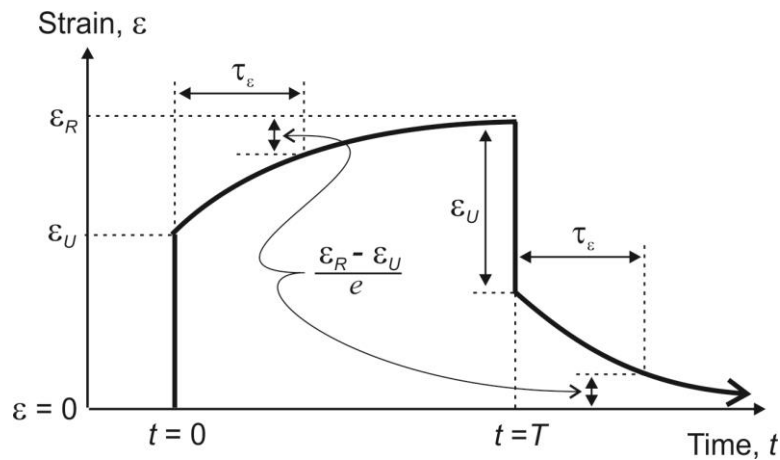


FIGURE 1.5.

Linear relaxation of strain in a rock sample. After a step in stress σ is applied at time $t = 0$, the initial strain becomes ε_U (‘unrelaxed’), and it gradually approaches the ‘relaxed’ strain $\varepsilon_U > \varepsilon_R$ at $t \rightarrow \infty$. After the loading stress is removed at time $t = T$, the relaxation process is repeated in the opposite direction.

Note that with periodic loading and unloading, the pattern of strain lags behind the stress. This is an indication of the stress-strain phase delay for periodic processes.

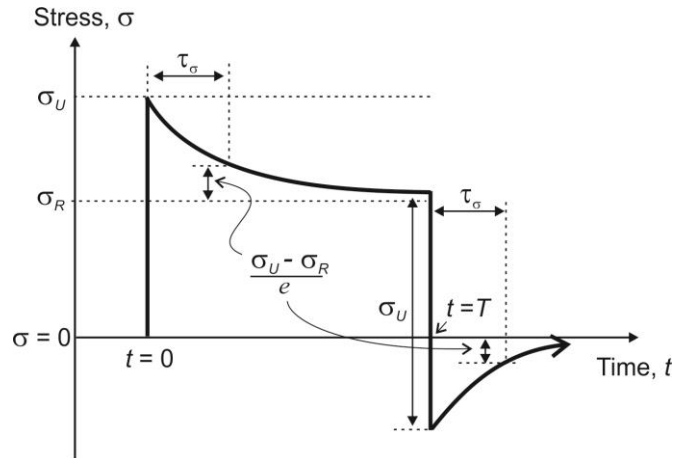


FIGURE 1.6.

Linear relaxation of stress in a rock sample. After a step in strain ε is applied at time $t = 0$, the initial stress ‘overshoots’ the equilibrium value and becomes σ_U (‘unrelaxed’). With time increasing, the stress gradually reduces to the ‘relaxed’ (equilibrium) stress $\sigma_R < \sigma_U$ at $t \rightarrow \infty$. After the strain is removed at time $t = T$, the stress relaxation process is repeated in the opposite direction.

time T , the process is repeated with opposite polarity of strain variations (Figure 1.5). As a result, the pattern of strain variations $\varepsilon(t)$ is delayed in time relative to the stress $\sigma(t)$ (Figure 1.5).

Another way to assess relaxation phenomena in rocks is to conduct a stress relaxation experiment (Figure 1.6). Such experiments are somewhat more difficult to implement because they require maintaining a fixed strain and accurately measuring significant pressure. However, such experiments are important because they observe the constant-deformation regime, in contrast to the constant-pressure regime in Figure 1.5. In this experiment, a sudden increase of strain ε is created at time $t = 0$ and maintained constant after that. At $t = 0$, the stress in the body will jump to the unrelaxed level $\sigma_U = M_U \varepsilon$, and then it will gradually decrease to the relaxed level $\sigma_R = M_R \varepsilon$ (Figure 1.6). If the strain is returned to $\varepsilon = 0$ after time $t = T$, the stress “overshoots” in the opposite direction and eventually relaxes to the zero level (Figure 1.6). The relaxation processes also exponentially depend on time, but with a different (stress) relaxation time τ_σ , which turns out to be smaller than τ_ε . If the deformation pattern is repeated, the “sawtooth” pattern of stress $\sigma(t)$ is advanced relative to $\varepsilon(t)$ in this case (Figure 1.6).

In the constant-loading experiment (Figure 1.5; $\sigma = \text{const}$), the output measured quantity is the compliance of the rock sample

$$J(t) = \frac{\varepsilon(t)}{\sigma}. \quad (1.1)$$

From the constant-strain experiment (Figure 1.6; $\varepsilon = \text{const}$), the empirical (effective) modulus is measured:

$$M(t) = \frac{\sigma(t)}{\varepsilon}. \quad (1.2)$$

From these figures, note the two general properties of the empirical modulus and compliance (Figures 1.5 and 1.6):

- $J(t)$ increases from the level of $J_U = 1/M_U$ at $t = 0$ to $J_R = 1/M_R$ at $t \rightarrow \infty$ (1.3a)

- $M(t)$ decreases from $M = M_U$ at $t = 0$ to M_R at $t \rightarrow \infty$ (1.3b)

1.5.2 Forced harmonic oscillations

In the second type of manifestation of anelastic relaxation, Figure 1.7 schematically shows a laboratory experiment measuring shear-wave attenuation in a rock sample. An harmonically oscillating loading torque (shear stress) $\sigma(t) = \sigma_0 \cos(2\pi ft)$ is applied to the upper face of the cylindrical rock specimen, and phase-delayed shear strain $\varepsilon(t) = \varepsilon_0 \cos(2\pi ft + \delta)$ is measured by measuring the shearing angles of the specimen and the aluminum standard (Figure 1.7). Such experiments are the primary rock-physics tool in laboratory studies of reservoir rock. The typical results are schematically

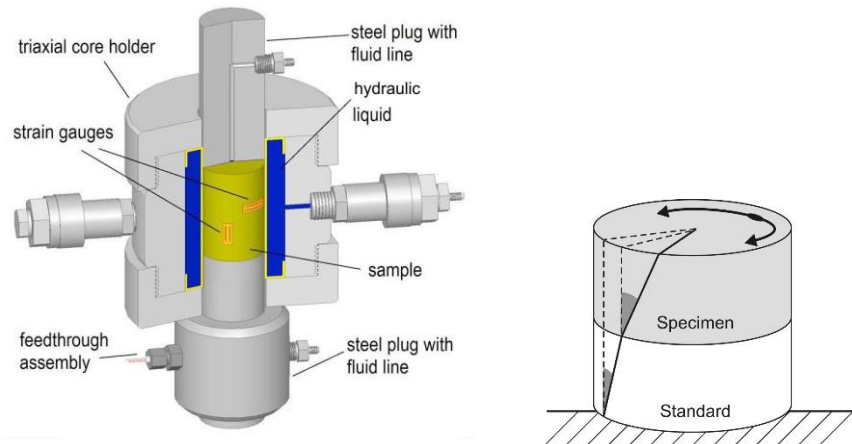


FIGURE 1.7

Left: An apparatus for Young's modulus measurements (from Mikhaltsevitch et al., 2015). A jacketed cylindrical rock core (greenish yellow) is placed in a column with an aluminum cylinder (standard), so that they receive a common vertical pressure oscillating in time. The resulting axial and transverse strains are measured by a strain gauges attached to the sample (yellow) and also to the standard. Confining pressure (may also be oscillating) is applied using hydraulic fluid surrounding the sample (blue). Pore-fluid pressure is regulated via the fluid line(s) connected at the end(s) of the sample.

Right: Principle of torsional phase-lag Q measurements for shear deformation (Jackson and Paterson, 1993). From the two shaded angles, the ratio of strains in the sample and the aluminum standard element is determined. Because the torque within the specimen and standard is the same, the shear strain of the standard and its shear modulus can be used to determine the stress/strain ratio within the specimen.

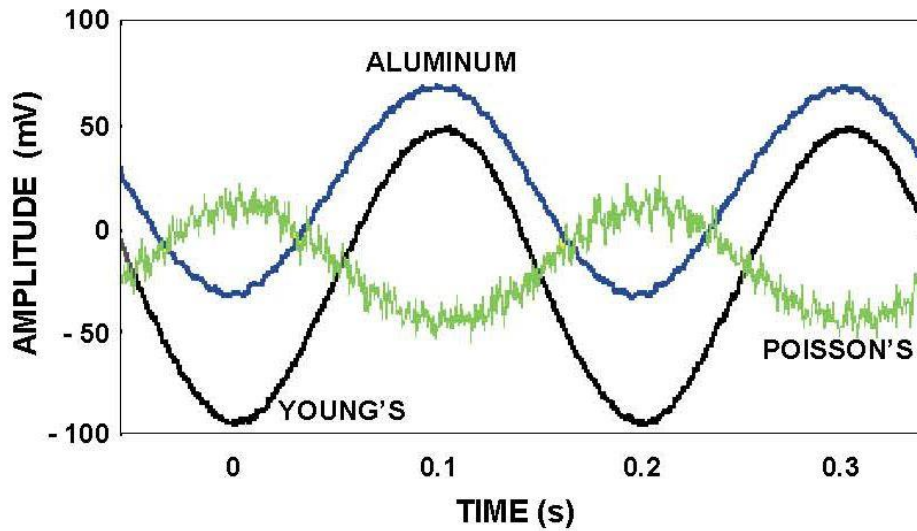


FIGURE 1.8.

Subresonant measurements of Young's modulus (from Batzle et al., 2001, The Leading Edge) A sinusoidal axial pressure at frequency 5 Hz is applied to a column consisting of an aluminum standard and the rock sample. Vertical strain gauges (Figure 1.7, left) measure Young's modulus deformation (black and blue curves), and horizontal gauges give the Poisson's ratio (green). Note the slight phase lag of the black curve relative to the blue one – this is the measured Q^{-1} (eq. 1.4).

shown in Figures 1.8 and 1.9. The resulting empirical modulus (Fourier transform of $M(t)$ above) $M(f)$ is complex-valued and frequency-dependent, and its complex argument is the phase delay $\delta(f)$ of the cosine function $\varepsilon(t)$ with respect to $\sigma(t)$. The stress-strain phase delay δ (Figure 1.8) is the key measured quantity, and it is usually presented in the form of another quantity denoted Q (“quality factor”):

$$Q^{-1} \stackrel{\text{def}}{=} -\frac{\text{Im } M}{\text{Re } M} = \arctan \delta. \quad (1.4)$$

Therefore, the complex-valued $M(\omega)$ can be expressed through its real part $M' \stackrel{\text{def}}{=} \text{Re } M$ and the Q^{-1} :

$$M = M'(1 - iQ^{-1}). \quad (1.5)$$

The real part M' of the viscoelastic modulus and its Q^{-1} are usually reported from seismic-frequency laboratory experiments (Figure 1.9).

The Q is usually associated with a material property summarizing the tendency of the material to dissipate the mechanical energy into heat, and thereby to cause seismic wave attenuation. However, the existence of such a material property is actually difficult to establish¹.

The relaxation times τ_ε and τ_σ (Figures 1.5 and 1.6) represented in the frequency domain by another pair of characteristic features (Figure 1.9):

- The characteristic frequency f_0 . With increasing attenuation (that is, viscosity of the material), f_0 reduces.
- Ratio M_U/M_R of the high- and low-frequency limits of modulus $M(f)$.

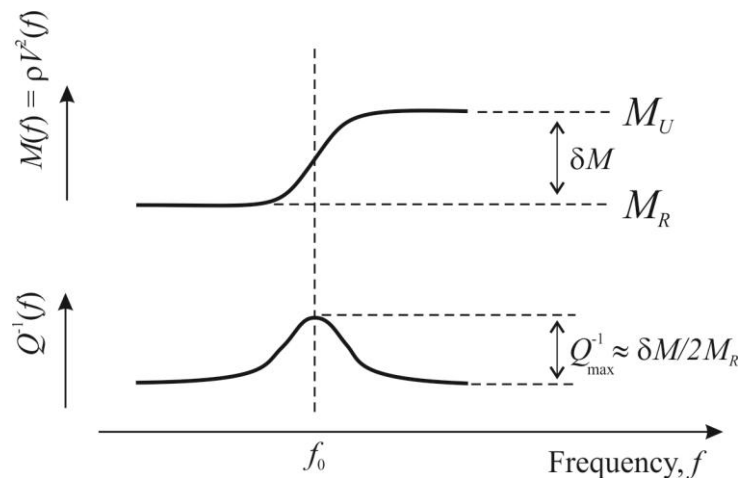


FIGURE 1.9.

Schematic modulus dispersion and attenuation spectra observed in experiments with seismic waves and rock samples. The dynamic modulus M undergoes a step (“dispersion”) by some amount of “modulus defect” δM near frequency f_0 , and the attenuation factor Q^{-1} shows a peak of height proportional to $\delta M/M$ at the same frequency. These particular shapes of the dispersion transition and attenuation peak can be modeled by the standard linear solid (Zener) model (chapter 5).

The existence of the relaxation frequency f_0 , the different M_R , M_U , the frequency dependent $M(f)$ with phase delays $\delta(f)$ and $Q^{-1}(f)$ are indicators of modulus-dispersion and attenuation phenomena. These parameters give a phenomenological description of the process of relaxation. Generally, these parameters are also sensitive to the details of the specific experiments, such as sizes of rock samples or boundary conditions². Our goal in this course is to explain this phenomenology by the laws of physics and identify the true physical properties of the material and the physical laws governing the process.

To select the physical properties and laws explaining rock anelasticity, there exist two general approaches outlined in the following subsections. These approaches differ fundamentally: the first approach postulates purely mathematical principles and modifies mechanical laws specifically for modeling anelastic deformations in solids, but the second approach relies entirely on standard physics.

1.5.3 Seismic waves

Anelastic relaxation phenomena are also important for seismic waves, as illustrated in Figure 1.10 for coda waves. Codas in earthquake seismology consist of waves randomly scattered from the crust around the seismic station, similarly to a reflection seismogram in from a surface source in exploration seismology. Increased anelasticity of the medium is observed from shorter duration of the wavetrain $T_{1/2}$ and reduction of wave frequencies. These effects are also associated with a larger effective Q^{-1} of the medium (bottom of Figure 1.10).

Obtaining properties of seismic waves from mechanical properties of the medium may be a complex task. This procedure is described in chapters 5 through 7. In practice, the viscoelastic model is commonly used (next section and chapter 2). In this model, the variation of velocity and Q -factor of a wave with oscillation frequency f are explained through the variation of the effective complex-valued modulus of the medium $M(f)$. Assuming that the density ρ is not affected by anelasticity³, the phase velocity of a wave

² This is indeed the case for f_0 and Q^{-1} for porous fluid-saturated rock, particularly in laboratory experiments with small rock samples or thin layering in the field.

³ However, in reality, for waves in porous fluid-saturated rock or grainy media, the density also contains a frequency-dependent imaginary part. See chapters 5 and 7.

equals

$$c(\omega) = \sqrt{\frac{M(\omega)}{\rho}}, \quad (1.6)$$

where $\omega = 2\pi f$ is the angular frequency. For different wave types, modulus $M(\omega)$ in this formula can be different: shear modulus μ for S waves, P-wave modulus $M = \lambda + 2\mu$ for P waves, Young's modulus $E = \frac{9K\mu}{3K + \mu}$ for extensional waves in a rod (where λ is the Lamé modulus and K is the bulk modulus), or flexural modulus for transverse waves in a bar. Any pair of these moduli (for example, (K, μ) , or (λ, μ)) can have an arbitrary frequency dependence and a Q^{-1} such as shown in Figure 1.9). Each of these moduli may possess different frequency dependencies.

As a result of frequency dependencies of the moduli, phase velocities of the waves change from the “relaxed” limit $c_R = \sqrt{M_R/\rho}$ at $\omega \rightarrow 0$ to “unrelaxed” $c_U = \sqrt{M_U/\rho}$ at $\omega \rightarrow \infty$. This change of velocity (usually increase, $c_U > c_R$) is called velocity dispersion.

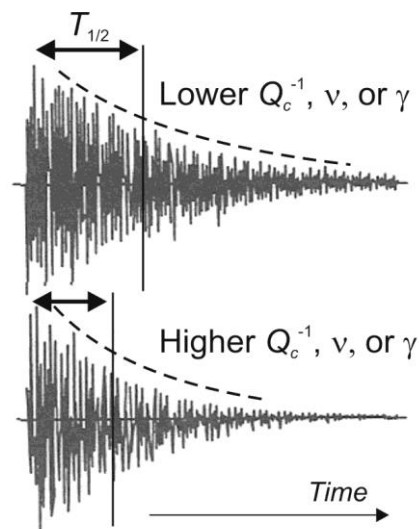


FIGURE 1.10

Schematic seismograms showing seismic coda waves with lower and higher attenuation. Higher apparent attenuation is recognized from shorter duration of the coda $T_{1/2}$, which can be described by larger values of Q^{-1} , ν , or γ (parameters ν and γ describe the geometrical spreading; I do not discuss them in this course).

To describe wave attenuation, we need to first consider the expression for particle displacement (or velocity, acceleration) for a harmonic wave:

$$u(x, t) = u_0 \exp \left[-i\omega \left(t - \frac{x}{c} \right) \right]. \quad (1.7)$$

A complex-valued modulus $M(\omega)$ leads to a complex-valued wave slowness in this equation, which for small Q^{-1} equals (eq. 1.5):

$$\frac{1}{c} = \sqrt{\frac{\rho}{M}} \approx \sqrt{\frac{\rho}{M'}} \left(1 + \frac{i}{2} Q^{-1} \right) = \frac{1}{c'} \left(1 + \frac{i}{2} Q^{-1} \right), \quad \text{where } c' = \sqrt{M'/\rho}. \quad \text{Therefore, the}$$

amplitude of displacement (eq. 1.7) exponentially decreases with travel distance x as:

$$u(x, t) = u_0 \exp \left[-i\omega \left(t - \frac{x}{c'} \right) \right] \exp \left(-\frac{\omega T}{2} Q^{-1} \right). \quad (1.8)$$

where $T = x/c'$ is the wave travel time to point x . The last exponential factor here can also be expressed through the regular frequency: $\exp \left(-\frac{\omega T}{2} Q^{-1} \right) = \exp \left(-\frac{\pi f T}{Q} \right)$, which is the definition of the Q -factor for a wave (Aki and Richards, 2002). The meaning of this Q is that upon propagation by one wavelength ($\Delta T = 1/f$), the amplitude of the wave decreases by factor $\exp(-\pi Q^{-1})$.

Thus, the Q -factor for a frequency-dependent modulus $M(f)$ of a uniform medium is also the Q of a wave in this medium. This is the third way of observing the anelastic (relaxation, viscoelastic) property of rock.

1.6 First-principle, effective and empirical moduli

The goal of theoretical rock-physics models and laboratory experiments consists in measuring certain material properties which should further be useful to predict reservoir properties. However, one has to clearly understand what material properties are measured in a given experiment and how they relate to theoretical models. This question is not so simple because mechanical properties are never measured directly, and the key observed

properties like attenuation and dispersion may be relatively weak and complex.

As shown in the preceding section, material properties are commonly assessed by transforming the experimental data into some types of frequency-dependent moduli. However, it is important to differentiate between three different meanings of the term “modulus”:

- 1) The (or first-principle, ab initio) modulus. This modulus is the key concept used in physics-based theories like the one described in this course. This is a true material property which enters rigorous equations of mechanics. This modulus can only be elastic, and it is time- and frequency-independent. This modulus is *never seen in any experiments* and has to be inverted by carefully interpreting the observations.
- 2) The empirical modulus. This modulus is typically some stress to strain ratio *measured in a laboratory or field experiment* (section 1.5). From different experiments, various kinds of such time- and frequency-dependent moduli are derived. These stress/strain ratios are usually designed so that they reduce to the elastic modulus in some idealized cases, such as for static or abruptly changing loading of a rock sample, or for an ideal elastic body. However, most practical experiments are far from these limiting cases, and extensive efforts may be needed for extracting true material properties from the measured empirical moduli.
- 3) The effective modulus. This property is *derived theoretically*, as a model for the stress/strain ratios in bodies of certain simple shapes (such as boundless uniform media, cylinders, or spheres) but with complex internal microstructure (such as pores and inclusions). The meaning of the term “effective” relates to averaging the effects of small-scale heterogeneities. Examples of effective-medium theories are the viscoelastic theory (chapter 2) and Biot’s model of porous rock (chapter 5). The effective modulus usually turns out to be frequency-dependent, but this dependency may be due to the size and shape of the body. Similarly to the first-principle modulus, the effective modulus is *not measured directly* but it can be compared to the empirical modulus if derived for the appropriate experimental environment (shape of the body, thermal regime, boundary conditions, etc.).

Unfortunately, in today's applied studies, it is usually assumed that the measured empirical moduli are equivalent to the effective modulus of a "viscoelastic" material of the sample, and that this modulus would be the same for waves traveling in large bodies of the same material. This assumption serves as a basis for most data interpretations and publications. Nevertheless, this assumption still represents a major fallacy of the conventional method of rock-physics interpretation. As was pointed out by J. E. White long ago (in 1986), this fallacy is particularly strong for fluid-saturated porous rock. The fallacy consists in ignoring differences between the first-principle, empirical, and effective moduli above:

- Porous rock contains a relatively independent pore-fluid flow, and therefore it cannot be described by only two bulk and shear effective moduli. In particular, the drag (Darcy) friction by pore fluid is a body force, and it not included in the surface (Cauchy) stress σ measured in the lab.
- For porous rock, the empirical moduli measured in the lab contain inertial effects, and therefore they are different from the effective-media moduli (which are modeled without inertial effects).
- The measured empirical moduli are not properties of the material of the rock specimen. These ratios depend on numerous other factors: the size and shape of the body, its heterogeneity and permeability, placements of strain gauges and pore-fluid supply tubes, properties of the "dead volume" (buffer containing pore fluids), friction of the fluid within the various pipelines in the apparatus, heterogeneous patterns of pore-fluid saturation and flows within the rock sample, and also on the thermal regime of the experiment (e.g., Figure 1.7).

Theoretically, the above assumption is justified by the viscoelastic model and presenting materials as arrangements of springs and dashpots (see chapter 2). The obvious advantage of this approach is simplicity: one does not have to study the actual mechanism of internal friction and to differentiate between the effects of solid viscosity, Darcy, thermoelastic and other types of friction. Instead of all this detail, only an *ad hoc*, complex-valued and frequency-dependent viscoelastic modulus is obtained. Note that in

experimental studies, this frequency-dependent modulus is often called “elastic”, which is also an imprecise term. Elastic moduli are always frequency-independent.

1.7 Theories of Relaxation Phenomena

In this course, we consider only linear mechanical interactions, and therefore only the linear viscoelastic model.

1.7.1 Traditional approach: the viscoelastic model

The conventional approach to explaining anelastic deformations in materials science, engineering, and seismology is based on the so-called viscoelastic theory. The key hypothesis of this theory is that the time-dependent moduli $M(t)$ and compliances $J(t)$ or the frequency-dependent moduli $M(f)$ and Q -factors measured in certain experiments (preceding section) truly belong to the material and operate in all other cases, and particularly in seismic waves.

The viscoelastic model is inspired by generalizing observations of creep within rock. In creep experiments, the compliance function $J(t)$ is measured nearly directly, by recording transient deformation. When loading is abruptly applied to a rock body and then kept constant, the body deforms almost instantaneously (“elastic” deformation) and then continues to slowly deform in the same direction for an extended period of time (from several seconds to several days, creep).

Figure 1.11 shows three creep regimes occurring with a sufficiently large stress applied for a long time. In a field seismic or laboratory attenuation experiment, stresses are weak, and only the transient creep regime is sampled. During periodic weak loading and unloading the rock passes through the elastic stage (labeled OA in Figure 1.11), transient creep (AP), elastic unloading (PQ), transient relaxation creep (PR), and finally returns to the undeformed state. The segments AP and QR in this diagram are the same as the relaxation curves in Figure 1.5.

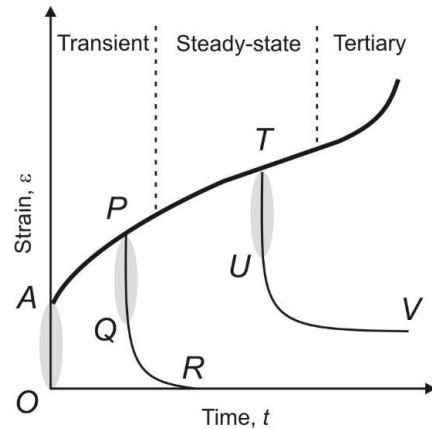


FIGURE 1.11

Schematic creep curve showing the transient (primary), steady-state (secondary), and tertiary creep regimes (Griggs, 1940). Upward-sloping curve shows step-function loading and downward curves show unloading. Letters indicate different regimes: of deformation: OA – elastic deformation, AP – transient creep, PQ – elastic unloading, PR – transient relaxation creep. Gray ellipses indicate the intervals of high velocities, and interpreted energy dissipation.

Note that the transient creep (path $O-A-P-Q-R$) is reversible, which means that the system returns to zero-deformation state when the load is removed. After steady-state creep ($T-U-V$), the system is left with a residual deformation.

The distinction between the “elastic” and “creep” deformation stages in creep (Figure 1.11) experiments pose an interesting question: during which of these two stages does the mechanical energy dissipation predominantly occur? To answer this question, note that the “elastic” deformations (highlighted by gray) occur much faster than the transient creep, and because of high velocities, they are likely to cause the largest energy dissipation.

1.7.2 Approach of this course: continuum mechanics

Despite what is often thought, theoretical models cannot be judged solely on their ability to fit data. The data may be easily fittable by multiple theories, some of which may still be unacceptable or incompatible. Rock-physics experiments produce relatively limited amounts of data, such as only one time-domain curve in Figures 1.5 or 1.6, or a pair of mutually related curves in Figure 1.9. These data usually sample only one spatial location such as the average volume of the rock specimen. As explained in the preceding subsection, such data *can always be explained* by some ‘phenomenological’ time- or frequency-dependent modulus $M(t)$ or $M^*(f)$, but *the value of this explanation may be uncertain*.

Prior to fitting data, models of relaxation should be designed consistently with basic principles of other physical theories. For the mechanics of solids and fluids, the principles most important for us are:

- Instantaneous interactions (acceleration of any point at time t is caused by forces acting at the same time);
- Local interactions (forces at a given point \mathbf{x} depending on only few spatial derivatives of stresses and material properties);
- Within a continuous medium, there may (and consequently generally should) exist body forces (applied to elementary volumes) as well as surface stresses (applied to surfaces of elementary volumes).

In addition, a very general observation can be made from the observed character of band-limited modulus-dispersion spectra in Figure 1.9:

- The existence of low- and high-frequency plateaus in the dispersion spectra suggests (at least) two deformation modes within the solid, and consequently the existence of some internal variable(s) within the medium. Relative movement of these internal variables cause the observed relaxation effects create the appearance of ‘material memory’ for a body.

These principles form the basis of the “General Linear Solid” (GLS) model in this course (chapter 5). The canonical text showing application of these principles to numerous areas in physics is the eleven-volume Course of Theoretical Physics by Landau and Lifshitz, written from 1940s to 1970s. For applications to the continuum mechanics of solids, see its volume 7 (Landau and Lifshitz (1986) in *Bibliography*). However, these texts are of intended for theoretical physicists, and here, I only present selected and simplified content useful for applied geophysicists.

In comparison to the conventional viscoelastic approach outlined in the preceding section, not that the continuum-mechanics approach:

- Does not allow arbitrary time-dependent “material memory”.
 - Instead, it considers separate elastic and two types of viscous forces.
- Instead of the material memory, it seeks internal variables within the material.

- With appropriate selection of internal variables, the continuum-mechanics approach reproduces arbitrary viscoelastic models.
- As special cases, predicts equations (2.2) and the empirical time-dependent quantities M , J , and the frequency-dependent Q^{-1} in them.
 - However, the continuum-mechanics approach recognizes these quantities as properties of the whole body rather than material properties.

1.8 *Structure of next chapters*

In the next chapters, I start with a summary of the standard viscoelastic theory (chapter 2). Chapter 2 describes the phenomenology of this theory, its mathematical principles, causality (Kramers-Krönig) relations, and the use and meaning of spring-dashpot diagrams and several commonly used models. At the end of chapter 2, I explain the quasi-static character of the viscoelastic approximation and discuss its limitations.

Chapters 3 and 4 give simple introductions to variational methods in mechanics and to Lagrangian form of analytical mechanics. Chapter 4 describes procedures for model discretization and the general forms of equations of motion arising in most problems. In addition chapter 4 contains a brief summary of rigorous approach to standard viscoelasticity.

Using the Lagrangian formulation, chapter 5 describes the framework of the General Linear Solid (GLS) and its key special cases: Biot's poroelastic model, arbitrary mechanically-implementable viscoelastic models, and a generalization of the viscoelastic models called the Extended generalized standard linear solid. Chapter 5 also gives several types of differential equations arising from the Lagrangian models without and with temperature variations.

Based on these general approaches, chapter 6 discusses modifications of the Lagrangian models by variations of temperature during deformation (thermoelasticity). Here again, I briefly describe the standard thermoelasticity with wavelength-scale heat flows and also extend it to local heat flows within the internal GLS material structure. This completes the theoretical part of the course.

Chapter 7 describes applications of the GLS models to several key cases: static equilibrium, low-frequency laboratory experiments with rock sample in the, and plane waves.

Quick exercises related to current discussions are given in text boxes and laboratory assignments for practical Matlab calculations are given at the ends of key chapters.

2 The Viscoelastic Model

Key points:

- Mathematical principles:
 - Boltzmann's after-effect
 - Correspondence principle
 - Phenomenology: creep, modulus and velocity dispersion, Q
 - Convolutional-integral and time-differential strain-stress relations
 - Causality and Kramers-Krönig relations
 - Kinetic equation
 - Zener's and related equations
 - Linear solids
 - Time-domain responses and empirical-modulus and attenuation spectra
 - Quasi-static character of the viscoelastic model
-

The viscoelastic model of anelasticity is extremely popular in materials science and engineering, and it also extends to scales as large as Earth's and planetary tides, rotation of the Earth (Chandler wobble), and geodynamic processes. In time scale, this model is thought to work from milliseconds (seismic periods) to tens of thousands of years (postglacial rebound of the continents). The viscoelastic model is also commonly used in exploration seismology and studies of reservoir rock, which are the focus of this course.

The linear viscoelastic theory is based upon an intuitive interpretation of rock inelasticity as "imperfect elasticity." This model is empirical and can be viewed as a phenomenological extrapolation of the empirical strain-stress relations measured in creep

and other experiments. This extrapolation does not consider any physical laws but is performed using purely mathematical methods described in this chapter. By contrast, later in this course (starting in chapter 5), we will study the actual mechanics of internal friction within an attenuating medium.

2.1 *Mathematical principles*

The goal of the viscoelastic model is to predict the time-dependent stress $\sigma(t)$ for a measured strain $\varepsilon(t)$ or vice versa, to predict strain $\varepsilon(t)$ if the stress $\sigma(t)$ is known. The model is based not on any physical considerations, such as, for example, it does not attempt to decide whether the stress is caused by the strain or vice versa. Instead of considering the physics, specific physics two principles for direct mathematical generalization laboratory observations are advanced:

- 1) Linearity of the strain-stress relation: If we consider two measurements with strain functions $\varepsilon_1(t)$ and $\varepsilon_2(t)$, and the corresponding stress functions $\sigma_1(t)$ and $\sigma_2(t)$, and implement a new experiment with combined deformation $\varepsilon(t_1) = c_1\varepsilon_1(t_1) + c_2\varepsilon_2(t_1)$ at any time t_1 , then the time-dependent stress measured at arbitrary time t_2 in this experiment will be $\sigma(t_2) = c_1\sigma_1(t_2) + c_2\sigma_2(t_2)$. This requirement of mathematical linearity of functional mapping $\varepsilon(t) \rightarrow \sigma(t)$ and vice versa, $\sigma(t) \rightarrow \varepsilon(t)$, is called the Boltzmann's principle ("memory," or "after-effect," *Nachwirkung* in German). Linearity is naturally expected from weak elastic interactions occurring in seismic deformations, and it also holds for the so-called Newtonian (i.e. usual) viscosity. Note that linear relations between stress and strain perturbations $\delta\sigma(t_1) \propto \delta\varepsilon(t_2)$ hold even for different times t_1 and t_2 , if the $\varepsilon(t)$ if $\sigma(t)$ are causally unrelated to each other but occur due to some external reason.
- 2) The correspondence principle connecting the elastic and anelastic cases. This principle is much more subtle and more hypothetical. This principle relates the behavior of a given material to its "elastic counterpart," i.e. the same material but

without anelasticity. For an elastic system, the observed strain and stress measured at the same point⁴ are related by

$$\sigma(t) = M\varepsilon(t), \quad \text{and} \quad \varepsilon(t) = J\sigma(t), \quad (2.1)$$

where M is a material property (constant) called elastic modulus, and $J = 1/M$ is the compliance. The correspondence principle states that for an anelastic system, quantities M and J become functions of time, and relations (2.1) become integrals over all preceding times $\tau \leq t$:

$$\sigma(t) = \int_{-\infty}^t M(t-\tau)\varepsilon(\tau)d\tau, \quad (2.2a)$$

and

$$\varepsilon(t) = \int_{-\infty}^t J(t-\tau)\sigma(\tau)d\tau, \quad (2.2b)$$

where M is the time-dependent viscoelastic modulus. The integrations over preceding times are selected in order to enforce causality of these relations. The elastic case corresponds to singular functions $M(t) = M\delta(t)$ and $J(t) = J\delta(t)$, where $\delta(t)$ is the Dirac delta function equal zero at all $t \neq 0$ and satisfying $\int_{-\infty}^{\infty} \delta(\tau)d\tau = 1$. By taking the Laplace or Fourier transforms (next section), relations (2.2a) and (2.2b) become multiplications by complex-valued, frequency-dependent moduli and compliances:

$$\sigma(f) = M(f)\varepsilon(f), \quad \text{and} \quad \varepsilon(f) = J(f)\sigma(f), \quad (2.2c)$$

where $J(f) = 1/M(f)$. In the elastic limit, $M(f) = M$ and $J(f) = J$ (frequency-independent).

⁴ Note that I call this principle ‘hypothetical’ because the above conditions are unrealizable in practice. No elastic counterpart exists for a real material, and the stress and strain are never measured at the same point. Stresses within a given material are also not related to strains by any definite relation (see next chapters in this text).

Function $M(t)$ and its Fourier transform $M(f)$ in eqs. (2.2) are assumed to represent a phenomenological (effective) property of the anelastic material called the viscoelastic modulus. The character of this modulus as being extended in time is also referred to as phenomenological “memory” of the material, which is implemented by “memory variables” in numerical modeling.

In the frequency domain, another real-valued quantity

$$Q(f) = -\frac{\operatorname{Re} M(f)}{\operatorname{Im} M(f)}, \quad (2.2d)$$

is derived from $M(f)$ and called the quality factor of the medium⁵.

The viscoelastic modulus function $M(t)$ in eq. (2.2a) contains a singularity at $t = 0$, which is useful to isolate using Dirac’s delta function $\delta(t)$ (Figure 2.1a):

$$M(t) = M_U \delta(t) + \tilde{M}(t), \quad (2.3)$$

where M_U is the unrelaxed modulus (chapter 1) and $\tilde{M}(t)$ is a continuous function varying

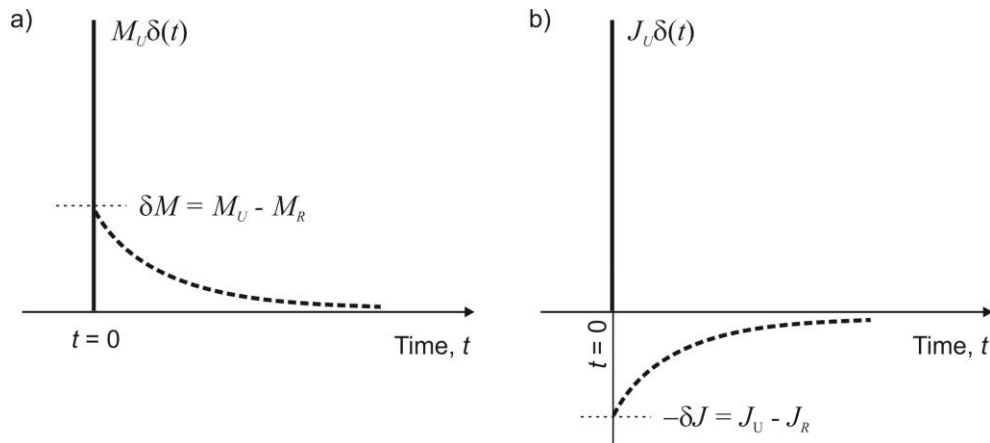


FIGURE 2.1

Schematic shapes of: a) viscoelastic modulus function $M(t)$, b) compliance function $J(t)$. Solid lines show the singular parts proportional to Dirac’s delta function $\delta(t)$, and dashed lines show the relaxation parts $-\tilde{M}(t)$ and $\tilde{J}(t)$ in eqs. (2.3) and (2.7).

⁵ Note that in the notation used in this course, $\operatorname{Im} M^* \leq 0$, and therefore $Q > 0$.

from $\delta M = M_U - M_R$ at $t = 0$ to zero at $t \rightarrow \infty$. With this separation of the unrelaxed part, eq. (2.2a) gives a combination of a response synchronous with $\varepsilon(t)$ and a delayed stress relaxation:

$$\sigma(t) = M_U \varepsilon(t) + \int_{-\infty}^t \tilde{M}(t-\tau) \varepsilon(\tau) d\tau . \quad (2.4)$$

Thus, the viscoelastic stress equals the elastic stress $M_U \varepsilon(t)$ caused by a constant modulus M_U plus additional time-dependent stress

$$r(t) = \int_{-\infty}^t \tilde{M}(t-\tau) \varepsilon(\tau) d\tau . \quad (2.5)$$

This additional stress is called memory variable and often used to implement viscoelastic models in time-domain (finite-difference or finite-element) wave modeling codes.

Similarly to the empirical modulus, the compliance function $J(t)$ contains a delta-function singularity of magnitude $J_U = 1/M_U$ (unrelaxed compliance) at $t = 0$ (solid line in Figure 2.1b). Isolating this singularity, the compliance function becomes

$$J(t) = J_U \delta(t) + \tilde{J}(t), \quad (2.6)$$

where $\tilde{J}(t)$ is a continuous function varying from $-\delta J = J_U - J_R$ at $t = 0$ to zero at $t \rightarrow \infty$ (Figure 2.1b). Equation (2.2b) then becomes

$$\varepsilon(t) = J_U \sigma(t) + \int_{-\infty}^t \tilde{J}(t-\tau) \sigma(\tau) d\tau . \quad (2.7)$$

Similarly to the stress “material memory” (eq. 2.5), the term $\int_{-\infty}^t \tilde{J}(t-\tau) \sigma(\tau) d\tau$ here can be viewed as an additional after-effect “strain memory,” but this concept does not seem to be used in modeling software.

Justifications for assuming the correspondence principle in geophysics are given by many authors, but always by explaining a relation between *a single* strain history $\varepsilon(t)$ and the corresponding stress history $\sigma(t)$ (for example, see Nowick and Berry (1972) or

Lakes (2009), and references therein). This single pair of stress and strain functions is sufficient for describing deformation of a finite body or for a wave in a homogeneous medium. In these cases, it is indeed true that any pair of dependencies ($\sigma(t)$, $\varepsilon(t)$) can be related by convolutional integrals like eqs. (2.2a and b). This relation can be constructed even if functions $\sigma(t)$ and $\varepsilon(t)$ are physically unrelated to each other (such as parameters measured in different parts of the body) but caused by some common source $f(t)$. For nearly any pair of functions ($\sigma(t)$, $\varepsilon(t)$), functions $M(t)$ and $J(t)$ can be obtained by the filtering operation called deconvolution.

2.2 Phenomenology

In this section, we discuss two general groups of observations leading to the viscoelastic model. Our goal here to show that from both time-domain and frequency-domain experiments three quantities are typically extracted from the observations:

- The relaxed and unrelaxed moduli (M_R and M_U). These moduli represent two basic elastic properties of the body or medium.
- Some type of relaxation time τ or characteristic frequency $f_0 = 1/\tau$. This is the principal measure of attenuation (inelasticity) within the material.

These three parameters give the end-member case on which the interpretation is usually based. In more complex cases, there may be multiple relaxation times τ (“relaxation mechanisms”) with accordingly variable M_R and M_U .

2.2.1 Time-domain and frequency-domain pictures

Time-dependent functions $M(t)$ and $J(t)$ can also be represented in other domains emphasizing different aspects of deformation. In materials science (usually dealing with causal functions $u(t)$ decaying in time), the Laplace transformation is often used, in which the time variable t is replaced with Laplace variable Laplace s representing the decay rate of the function. In seismic applications, oscillatory functions $u(t)$ are of primary interest, and the most useful transformation is the Fourier transform. The Fourier transform replaces a $u(t)$ with function $U(\omega)$ of angular oscillation frequency $\omega = 2\pi f$:

$$U(\omega) = \int d\omega e^{i\omega t} u(t), \quad (2.8a)$$

where f is the regular frequency⁶. The inverse transformation shows that the signal $u(t)$ is represented as a sum of oscillatory harmonics $e^{-i\omega t}$ multiplied by weights $U(\omega)$:

$$u(t) = \frac{1}{2\pi} \int d\omega e^{-i\omega t} U(\omega). \quad (2.8b)$$

The frequency-dependent weights $U(\omega)$ are called spectra. Note that as all measured physical quantities, the time-domain functions $M(t)$ and $J(t)$ are real-valued, but the corresponding frequency-domain spectra $M(\omega)$ and $J(\omega)$ are complex-valued. Magnitudes of these values like $|M(\omega)|$ are the amplitude spectra (or spectral amplitudes), and their arguments $\text{Arg}M(\omega)$ are the phase spectra.

In the frequency (or Laplace, Z-transform) domain, the integral relations of section 2.1 become simple and reduce to complex multiplications or divisions shown in eqs. (2.2c).

2.2.2 Time domain: Creep function

The modulus $M(t)$, compliance $J(t)$ and other functions of viscoelasticity are inspired by time-dependent strain-stress responses measured in laboratory experiments. In most time-domain experiments, the time-dependent $\varepsilon(t)$ resulting from application of a step-function stress $\sigma = \sigma_0 \theta(t)$ is measured. The resulting strain response is often represented as a combination of the initial unrelaxed compliance J_U and a nondimensional creep function $\phi(t)$:

$$\frac{\varepsilon(t)}{\sigma} = J_U [1 + \phi(t)]. \quad (2.9)$$

The creep function is related to function $\tilde{J}(t)$ in eq. (2.7) by $\phi(t) = M_U \int_{-\infty}^t \tilde{J}(t-\tau) d\tau$ and

⁶ Note that in other texts, opposite signs of ‘ $i\omega t$ ’ in the forward and Fourier transforms (eqs. (2.8)) are often used.

is therefore expected to satisfy causality ($\phi(t) \equiv 0$ for $t \leq 0$) and continuously increase with t . If there exists a finite limit $\phi(t)|_{t \rightarrow \infty} = \text{const}$, then the ‘relaxed’ (static, final-state; chapter 1) modulus equals $M_R = \frac{M_U}{1 + \phi(\infty)}$.

The creep is studied phenomenologically, and numerous empirical forms of creep functions have been proposed. For example, in the Andrade law, the creep is a combination of a steady-state creep proportional to t and an additional power-law creep:

$$\phi(t) = M_U \left(\frac{t}{\eta} + \beta t^n \right), \quad (2.10)$$

where parameters η and β describe the linear and nonlinear viscosities, respectively. Exponent n is usually below one ($n \approx 0.2-0.4$). Ratio $\tau = \frac{\eta}{M_U}$ plays the role of the characteristic relaxation time mentioned above.

From experiments with magmatic rocks under low stresses measured over time ranges from about 30 s to 10 weeks, Lomnitz (1956) proposed the following logarithmic law for the creep function:

$$\phi(t) = \begin{cases} 0 & \text{for } t < 0, \\ q \ln(1 + at) & \text{for } t \geq 0, \end{cases} \quad (2.11)$$

where parameter a is some characteristic frequency (f_0 above). The inverse of this frequency, $\tau = 1/a$, can be viewed as the relaxation time during which the transition from the elastic- to creep-type deformation occurs. This parameter is difficult to constrain from the data, but it is expected that a is high, so that that $t \gg \tau$ within the observation time range. Lomnitz (1956) used $a = 1000$ Hz and argued that but this characteristic frequency could also be as high as the vibration frequency of a vacancy in the crystal lattice, which could be 10^4-10^{10} Hz. However, the characteristic frequency could also be a resonant frequency of the *measurement apparatus*, which is likely to be about $\sim 100-10,000$ Hz.

2.2.3 Frequency domain: Dispersion band and Absorption peak

In the frequency domain, a limited frequency band of positive modulus dispersion ($\text{Re}M(f)$ increasing with frequency) and band-limited attenuation (a peak in $Q^{-1}(f)$) are often observed or expected. Zener's viscoelastic strain-stress relation discussed in section 2.5 is very popular because it explains such band-limited seismic attenuation and dispersion spectra (Figures 2.2 and 2.3).

Note that despite its notation as a ' Q ', the peak value of the quality factor Q_m is in fact unrelated to attenuation and represents a combination of elastic properties of the system. As shown in section 2.3, the peak Q^{-1} for Zener's body equals $Q_m^{-1} = Q^{-1}(\omega_m) = \frac{\delta M}{2\bar{M}}$, where $\delta M = M_U - M_R$ is called the modulus defect (difference between the unrelaxed and relaxed moduli), and $\bar{M} = \sqrt{M_R M_U}$ is the geometric mean of the two moduli. Thus, the peak inverse Q -factor equals half of the ratio of the modulus defect to the average modulus, which is a pure elastic property.

As noted above, the frequency of the peak $f_0 = \omega_m/2\pi$ is the characteristic parameter representing 'attenuation' (i.e., internal friction) in Zener's model. As illustrated by the Zener's model and also shown in most experiments studying porous rock saturated with fluids variable viscosities, f_0 is inversely proportional to the viscosity of the agent (e.g., fluid) causing attenuation.

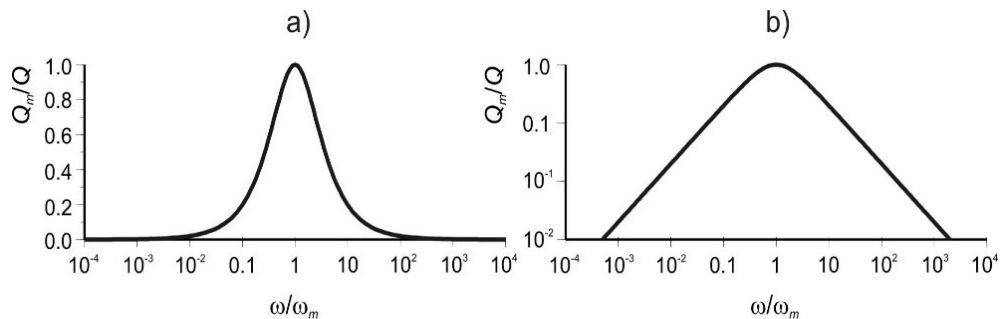


FIGURE 2.2

Absorption peak for the standard linear solid in eq. (2.30): a) linear scale in Q^{-1} , and b) logarithmic scale.

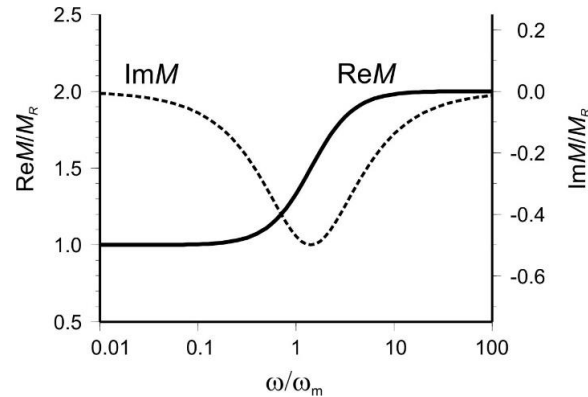


FIGURE 2.3

Real and imaginary parts of $M(\omega)$ for a standard linear solid with $M_U/M_R = 2$. Frequency ω_m is the frequency of the peak in $Q^{-1}(\omega)$. Note that for this ratio of the elastic moduli, $Q_m^{-1} \approx 0.35$ in Figures 2.2. The $\text{Re}M$ curve illustrates the modulus dispersion.

Exercise

Derive relations (2.29a) and (2.29b) from equations above them.

2.3 Kramers-Krönig (causality) relations

Regardless of the physical mechanism, because $J(t)$ and $M(t)$ are real-valued and causal functions, their frequency-domain counterparts $J(\omega)$ and $M(\omega)$ are constrained by two very general mathematical relations. First, the real-valued character of (for example) $M(t)$ means that the frequency-domain spectra at negative frequencies $\omega < 0$ are uniquely determined by the spectra at $\omega > 0$:

$$\begin{cases} \text{Re } M(-\omega) = \text{Re } M(\omega), \\ \text{Im } M(-\omega) = -\text{Im } M(\omega). \end{cases} \quad (2.12)$$

That is, $\text{Re}M(\omega)$ is an even function of frequency, and $\text{Im}M(\omega)$ is an odd function of frequency. These relations follow directly from the definition of the Fourier transform (2.8a) for a real-valued function $u(t)$.

The second relation is similarly general and describes causality. Causality means that function $M(t)$ (for example) equals zero for all $t < t_0$, where t_0 is some time at which, for example, the mechanical-loading experiment is started. This requirement means that $M(t)$ satisfies relation $M(t) \equiv M(t)\theta(t-t_0)$, where $\theta(t)$ is the Heavyside function (equal zero for all $t < 0$, $1/2$ for $t = 0$, and one for $t > 0$). After the Fourier transform (eqs. 2.8) and using eqs. (2.12), this equation shows that the imaginary part of $M(\omega)$ must be related to the real part and vice versa:

$$\begin{cases} \operatorname{Re} M(\omega) = \frac{2}{\pi} \text{P.v.} \int_0^{\infty} d\omega' \frac{\operatorname{Im} M(\omega')}{\omega'^2 - \omega^2}, \\ \operatorname{Im} M(\omega) = -\frac{2\omega}{\pi} \text{P.v.} \int_0^{\infty} d\omega' \frac{\operatorname{Re} M(\omega')}{\omega'^2 - \omega^2}, \end{cases} \quad (2.13)$$

where P.v. denotes the Cauchy's principal value of the integrals (integrals evaluated by skipping the infinitesimal vicinity of radius $a \rightarrow 0$ around the singularity at $\omega' = \omega$). These equations are called the Kramers-Krönig relations.

For $M(\omega)$ with band-limited dispersion and attenuation as described in the preceding section (I will not discuss the precise mathematical conditions for this approximation), the P.v. integrals can be approximated by derivatives of the integrands, and several differential forms of the Kramers-Krönig relations are obtained. In particular, such a relation shows if a band-limited $Q^{-1}(f)$ is measured, then regardless of the physical mechanism, it should be proportional to the derivative of the measured modulus dispersion:

$$\frac{2}{\pi} Q^{-1} \approx \frac{d[\ln(\operatorname{Re} M)]}{d[\ln \omega]} = \frac{d(\operatorname{Re} M)}{d\omega} \frac{\omega}{\operatorname{Re} M}. \quad (2.14)$$

Thus, frequency-domain laboratory measurements of moduli and Q like shown in Figure 1.9 are not mutually independent. Both the $M(f)$ and $Q^{-1}(f)$ essentially represent measurements of a single stress-strain response in the time domain, and consequently they are related.

The general importance of the Kramers-Krönig relations for waves is in emphasizing the fact that a system with attenuation (Q^{-1}) must also exhibit modulus dispersion and vice

versa. The peak attenuation and the fastest-growing dispersion occur at the same frequencies. Recall that the peak value Q_m^{-1} also measures the total amount of dispersion (eq. 2.29b).

2.4 Kinetic equation

The time or frequency dependencies of the linear viscoelastic moduli can be expressed by linear relations for time derivatives, called kinetic (or kinematic) equations. Such equations describe, for example, diffusion processes, such as dissipation of heat or chemical reactions. Because of this affinity to heat, kinetic equations are useful for describing thermal effects.

For a given (thermodynamic) variable ξ (such as strain), the kinetic equation expresses its rate of change $\dot{\xi} = \frac{d\xi}{dt}$ through its current value ξ and some equilibrium ('relaxed') value $\bar{\xi}$:

$$\dot{\xi} = -\frac{1}{\tau_r} [\xi - \bar{\xi}(\sigma, T)]. \quad (2.15)$$

Thus, the key parameter of the kinetic equation is the characteristic (relaxation) time τ_r . This time has the meaning of the ratio of the deviation from the equilibrium ($\xi - \bar{\xi}$) to the rate of approaching it.

The equilibrium value $\bar{\xi}(\sigma, T)$ may depend on some external factors, for which we take the applied stress σ and temperature T as an example (eq. 2.15). Whenever σ and T change, the equilibrium level $\bar{\xi}(\sigma, T)$ also changes, and by eq. (2.15), $\xi(t)$ starts approaching the new equilibrium variations cause in a time-delayed fashion. If the equilibrium is constant $\bar{\xi}(\sigma, T) = \bar{\xi} = \text{const}$, then eq. (2.15) gives an exponential approach of $\xi(t)$ to $\bar{\xi}$ with characteristic time τ_r :

$$\xi(t) = \bar{\xi} + C \exp\left(-\frac{t}{\tau_r}\right), \quad (2.16)$$

where C is an arbitrary constant. Such exponential approaches to the equilibrium level are shown in Figures 1.5 and 1.6.

2.5 Zener's (standard linear solid) equation

A commonly used form of viscoelastic strain-stress relations are described by the Zener's, or standard linear solid equation. This equation postulates that at any time, a combination of the stress and its rate of change equals a similar combination of the strain and strain rate:

$$\sigma + \tau_\sigma \dot{\sigma} = M_R (\varepsilon + \tau_\varepsilon \dot{\varepsilon}). \quad (2.17a)$$

This equation can be viewed as a generalization of the kinetic equation (eq. 2.15) applied to both strain and stress simultaneously. With constant stress ($\dot{\sigma} = 0$), eq. (2.17a) is a kinetic equation for strain (taking $\xi(t) = \varepsilon(t)$ and $\bar{\xi} = \sigma/M_R$), with relaxation time $\tau_r = \tau_\varepsilon$. Vice versa, with constant strain ($\dot{\varepsilon} = 0$), this equation is a kinetic equation for stress $\sigma(t)$, with relaxation time t_σ . Consequently, $M_R = \frac{\bar{\sigma}}{\bar{\varepsilon}}$ is the relaxed modulus (modulus observed at equilibrium, when both $\dot{\sigma} = 0$ and $\dot{\varepsilon} = 0$).

Equation (2.17a) can also be written as an equivalence of two differential operators acting on functions of time $\sigma(t)$ and $\varepsilon(t)$:

$$\left(1 + \tau_\sigma \frac{d}{dt}\right) \sigma = M_R \left(1 + \tau_\varepsilon \frac{d}{dt}\right) \varepsilon. \quad (2.17b)$$

In another useful form, for time-harmonic deformations⁷ with $\sigma(t) = \sigma_0 e^{-i\omega t}$ and

⁷ Note that time derivatives of harmonic functions are proportional to the functions themselves; for example: $\dot{u} = \frac{\partial u}{\partial t} = -i\omega u$.

$\varepsilon(t) = \varepsilon_0 e^{-i\omega t}$, this equation simply means a specific form of the frequency-dependent complex modulus:

$$M(\omega) \stackrel{\text{def}}{=} \frac{\sigma_0}{\varepsilon_0} = M_R \frac{1 - i\omega\tau_\varepsilon}{1 - i\omega\tau_\sigma}. \quad (2.17c)$$

The unrelaxed modulus M_U is defined as the modulus obtained for very fast stress and strain variations. In this case, the rate-related terms $\tau_\sigma \dot{\sigma}$ and $\tau_\varepsilon \dot{\varepsilon}$ will dominate the other two terms in eq. (2.17a), and therefore the ratio of the stress and strain rates would equal $\frac{\dot{\sigma}}{\dot{\varepsilon}} = M_R \frac{\tau_\varepsilon}{\tau_\sigma}$. This ratio must equal the unrelaxed modulus, and therefore

$M_U = M_R \frac{\tau_\varepsilon}{\tau_\sigma}$. Thus, it turns out that:

- The ratio of relaxation times is an elastic property equal the ratio of the unrelaxed and relaxed moduli:

$$\frac{\tau_\varepsilon}{\tau_\sigma} = \frac{M_U}{M_R}. \quad (2.18)$$

Since $M_U \geq M_R$, the relaxation times in eqs. (2.17) must always satisfy relation $\tau_\varepsilon \geq \tau_\sigma$.

- There is only one relaxation-time parameter in Zener's eqs. (2.17a), which can be taken as

$$\tau_r = \sqrt{\tau_\sigma \tau_\varepsilon}. \quad (2.19)$$

Parameters M_R , M_U , τ_s , and τ_ε are the four “material properties” required for describing a viscoelastic linear solid. Note that M_U is not included in Zener's eq. (2.17), and therefore this equation does not describe the viscoelastic model completely. Only certain solutions of this equation must be selected, which refer to mechanically-implementable models and have the correct value of M_U . In section 2.7, I review several such mechanical models known as linear solids and derive their time-domain and spectral

properties.

The selection of solutions by a given value of M_U can be done as follows. As noted

above (eq. 2.16), solutions to eqs. (2.17a or b) are $\varepsilon(t) = \sigma \left[\frac{1}{M_R} - C_1 \exp\left(-\frac{t}{\tau_\varepsilon}\right) \right]$ when

$\dot{\sigma} = 0$ (relaxation of strain) and $\sigma(t) = \varepsilon \left[M_R + C_2 \exp\left(-\frac{t}{\tau_\sigma}\right) \right]$ when $\dot{\varepsilon} = 0$ (relaxation of

stress). These solutions contain two arbitrary constants C_1 and C_2 . As explained in section 2.9, these two degrees of freedom actually indicate a problem with the viscoelastic model. This problem is resolved by requiring, in addition to equation (2.17), that the stress/strain ratio measured immediately after the loading or deformation is applied

(at $t = +0$) equal the unrelaxed modulus: $\frac{\sigma(0)}{\varepsilon(0)} = M_U$. This requirement is satisfied by

mechanically implementable systems, such as those discussed in the next section. From the

two solutions, the initial stress/strain ratio equals $\frac{\sigma(0)}{\varepsilon(0)} = \left(\frac{1}{M_R} - C_1 \right)^{-1}$ and

$\frac{\sigma(0)}{\varepsilon(0)} = M_R + C_2$. Therefore, the arbitrary coefficients in $\varepsilon(t)$ and $\sigma(t)$ are set by the

expected unrelaxed modulus: $C_1 = \frac{1}{M_R} - \frac{1}{M_U}$ and $C_2 = M_U - M_R$.

2.6 Spring-dashpot diagrams

The viscoelastic model is often illustrated using combinations of springs and mechanical dampers (“dashpots”) arranged so that they provide the desired time- and/or frequency dependent strain-stress responses. These desired responses are specified by:

- 1) Achieving the desired response at extreme low frequencies. At low frequencies, all dashpots produce zero forces and can accommodate arbitrary deformations. In this way, either finite “relaxed” response with modulus M_R is obtained from the springs only, or “plastic” response with unlimited deformation with zero stress is achieved.

- 2) Achieving the desired response at extreme high frequencies. In this limit, each dashpot has zero displacement, and the unrelaxed modulus M_U is again obtained by the resulting combination of springs.
- 3) Achieving the desired frequency band across which the transition between regimes 1) and 2) occurs. This frequency band is controlled by the viscosities of the dashpots.

The high-frequency regime takes place when a sudden change of the external force occurs (like experiment 2) in the preceding section), and the low-frequency regime takes place if the external force is kept steady (like experiment 1)).

In the theory of linear viscoelasticity, spring-dashpot diagrams are supposed to be understood *not* as models of the internal construction of rock but only as ways of providing certain shapes of the time-dependent strain-stress response $M(t)$ of the medium. Nevertheless, the time dependencies of $M(t)$ are nonunique and depend on the external forces applied to the linear solid (for example, on whether the solid is kept at constant pressure or fixed deformation). Also, identical $M(t)$ responses may correspond to different combinations of springs and dashpots, and so the whole concept of time- and frequency dependent material properties is rather complicated and unreliable.

What the spring-dashpot arrangements show uniquely is the dependence of the stress on the strain and/or strain rate of the deformation. As seen from the following subsections, by following the different chains of spring and dashpots, the stress σ experienced by any element is always given by linear combinations of the strains and strain rates of all elements

$$\sigma = \sum_{\text{springs } i} M_i \varepsilon_i + \sum_{\text{dashpots } j} \eta_j \dot{\varepsilon}_j, \quad (2.20)$$

where the strains ε_i with $i \geq 2$ correspond to some internal variables. The two terms in these equations represent the elasticity and viscosity of the system, respectively, M_i denote the various elastic moduli, and η_j denotes the viscosities of the dashpots contributing to stress σ .

In analytical mechanics (chapter 5), all eqs. (2.20) are described very compactly by the Lagrangian and dissipation functions. Therefore, the best and easiest way for

understanding the spring-dashpot arrangements such as shown in Figure 2.4 is to view them as diagrams of internal variables and construction of the Lagrangian and dissipation functions for the medium.

2.7 *Linear viscoelastic solids*

The internal variables in the linear solids (e.g., the white dot in Figure 2.4) are considered as unobservable, and therefore they can be selected in various ways. However, it is convenient to select them so that these variables become responsible for internal friction within the medium. This can be achieved by selecting ε_i (with $i \geq 2$) to be the deformations of the dashpot elements in the linear solids.

There are several commonly used configurations of such spring-dashpot systems called linear solids, or linear bodies. Five types of these configurations are summarized in the following subsections.

2.7.1 Maxwell's body

The Maxwell's body consists of a spring and a dashpot connected in series (Figure 2.4). The connection point between these elements represents an internal strain variable of this system, which is denoted ε_2 (white dot in Figure 2.4). Variable $\varepsilon_1 = \varepsilon$ is the observed strain of the body, and let us denote s the stress applied to the ends of this diagram. I keep this notation of internal variables for consistency with mechanical descriptions of the same linear bodies in chapter 5.

The strain-stress equations of equilibrium for such diagrams can be obtained from the following simple rules:

- For elements connected in series, the stress is common to all of them. Therefore, the stress can be used as an independent variable, and the strains derived from it.
- For elements connected in parallel, the strains are equal, and they can be used for parameterizing the deformation.
- For a spring element, the strain and stress on it are related by $\sigma = M\varepsilon$;

- For a dashpot element, the strain rate and stress are related by $\sigma = \eta \dot{\epsilon}$.

From these rules, we see that $\dot{\epsilon}_2 = \sigma/\eta$ in Figure 2.4, and the observable strain $\epsilon_1 = \epsilon$ and stress are related by equation

$$\sigma + \frac{\eta}{M} \dot{\sigma} = \eta \dot{\epsilon}. \quad (2.21)$$

This is a limiting case of Zener's equation (2.17) with finite stress relaxation time $\tau_\sigma = \frac{\eta}{M}$, the relaxed modulus tending to zero as $M_R \rightarrow 0$, and strain relaxation time simultaneously tending to infinity as $\tau_\epsilon = \frac{\eta}{M_R}$. The unrelaxed modulus (ratio of the coefficients in terms containing $\dot{\epsilon}$ and $\dot{\sigma}$) is $M_U = M$.

The complex-valued, frequency-dependent modulus $M(\omega)$ can be easily obtained from eq. (2.21c):

$$M(\omega) = \frac{\sigma(\omega)}{\epsilon(\omega)} = \frac{-i\omega\eta}{1-i\omega\tau_\sigma}. \quad (2.22)$$

At low frequencies, this modulus is pure imaginary and proportional to the frequency: $M(\omega) \approx -i\omega\eta$, which is the effect of the dashpot. At high frequencies, this modulus approaches $M(\omega \rightarrow \infty) \approx M$ (the unrelaxed modulus).

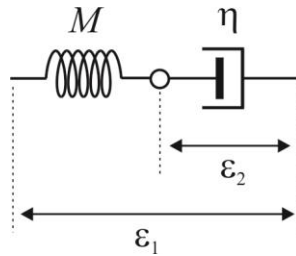


FIGURE 2.4.

Maxwell's linear solid. This model contains one internal variable ϵ_2 (white dot) connected by one spring (M) and dashpot (η) arranged in a series. Labels and notation are as in Figure 2.4.

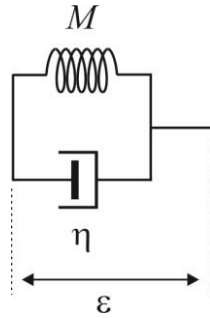


FIGURE 2.5.
Kelvin-Voigt's linear solid. Labels and notation are as in Figure 2.4.

2.7.2 Kelvin-Voigt's body

In a Kelvin-Voigt's body, there are no internal variables, and the spring and dashpots are connected in parallel (Figure 2.5). The strain-stress relation represented by this diagram is

$$\sigma = M\epsilon + \eta\dot{\epsilon}. \quad (2.23)$$

This equation means that the relaxed (static, steady-state) modulus is $M_R = M$, strain relaxation time $\tau_\epsilon = \frac{\eta}{M}$, stress relaxation time $\tau_\sigma = 0$, and therefore the unrelaxed modulus is infinite: $M_U = \infty$.

The frequency-dependent modulus $M(\omega)$ can be obtained as in the preceding subsection and equals

$$M(\omega) = M(1 - i\omega\tau_\epsilon) = M - i\omega\eta. \quad (2.24)$$

At low frequencies, this modulus is near-elastic (real-valued and constant): $M(\omega \rightarrow 0) \approx M$. At high frequencies, the viscosity of the dashpot dominates the forces, and $M(\omega \rightarrow \infty) \approx -i\omega\eta$.

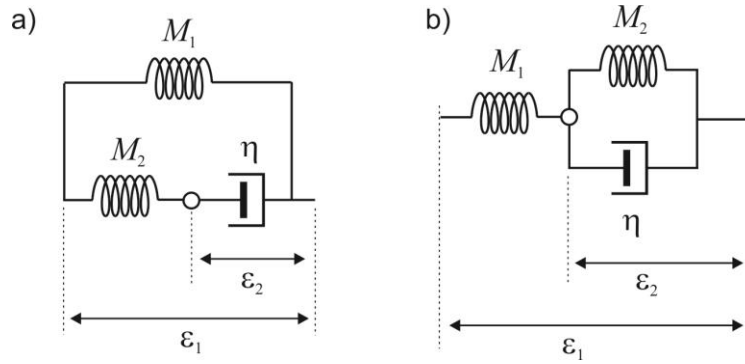


FIGURE 2.6.

Two forms of Zener's linear solid (also called the Standard linear solid, SLS): a) using a Maxwell's body with a spring attached in parallel, b) using a Kelvin-Voigt body with a spring in series. Labels and notation are as in Figure 2.4.

2.7.3 Standard linear (Zener's) solid

The Zener's linear solid (also called the "standard linear solid," or SLS) is a mechanical system implementing Zener's strain-stress equations (2.17) with nonzero coefficients. This mechanical system can be obtained in two ways: by using a Maxwell's solid with an additional elastic element attached in parallel with it (Figure 2.6a), or using a Kelvin-Voigt body with an additional spring connected in series (Figure 2.6b). In either case, the model requires one internal variable (white dots in the figure).

The Zener's equation (2.17) is easily obtained by using the diagram in Figure 2.6a. For the elastic spring, $\sigma_1 = M_1 \varepsilon$, and for the Maxwell's-body chain, eq. (2.21) gives

$\sigma_2 + \frac{\eta}{M_2} \dot{\sigma}_2 = \eta \dot{\varepsilon}$. Evaluating $\left(1 + \frac{\eta}{M_2} \frac{d}{dt}\right)(\sigma_1 + \sigma_2)$, the desired strain-stress relation is:

$$\sigma + \frac{\eta}{M_2} \dot{\sigma} = M_1 \varepsilon + \eta \left(1 + \frac{M_1}{M_2}\right) \dot{\varepsilon}. \quad (2.25)$$

Therefore, the relaxed modulus equals $M_R = M_1$, unrelaxed modulus $M_U = M_1 + M_2$,

strain relaxation time $\tau_\varepsilon = \eta \left(\frac{1}{M_1} + \frac{1}{M_2}\right)$, and stress relaxation time $\tau_\sigma = \frac{\eta}{M_2}$. Note that

conditions $M_U \geq M_R$ and $\tau_\varepsilon \geq \tau_\sigma$ are satisfied for any (non-negative) values of mechanical

properties.

The Zener's equations (2.17) are very important because they often capture the key features of observations with rock samples in the laboratory. The corresponding functions $M(t)$, $J(t)$, $\phi(t)$, $M(f)$, and $Q^{-1}(f)$ are often used for fitting attenuation data and to recognize absorption peaks. The creep function obtained by solving eq. (2.17) for $\epsilon(t)$ with constant stress is:

$$\phi(t) = \left(\frac{\tau_\epsilon}{\tau_\sigma} - 1 \right) \left(1 - e^{-t/\tau_\epsilon} \right). \quad (2.26)$$

From eqs. (2.17), the complex modulus $M(\omega)$ equals (Figure 2.3 was shown earlier):

$$M(\omega) = M_R \frac{1 - i\omega\tau_\epsilon}{1 - i\omega\tau_\sigma}. \quad (2.27)$$

and inverse quality factor (Figure 2.2):

$$Q^{-1}(\omega) = \frac{\omega(\tau_\epsilon - \tau_\sigma)}{1 + \left(\frac{\omega}{\omega_m} \right)^2}. \quad (2.28)$$

where $\omega_m = 1/\sqrt{\tau_\epsilon\tau_\sigma}$.

The $Q^{-1}(\omega)$ spectrum (eq. 2.28) exhibits a peak at $\omega = \omega_m$ with maximum value of

$$Q_m^{-1} = \frac{\omega_m(\tau_\epsilon - \tau_\sigma)}{2} = \frac{\beta^{-1} - \beta}{2}, \quad (2.29a)$$

where the dimensionless parameter β is defined by $\beta = \sqrt{\frac{\tau_\sigma}{\tau_\epsilon}} = \sqrt{\frac{M_R}{M_U}}$. Relation (2.29a) can

also be written as

$$Q_m^{-1} = \frac{\delta M}{2M}, \quad (2.29b)$$

where $\delta M = M_U - M_R$ is the modulus defect, and $\bar{M} = \sqrt{M_R M_U}$ is the geometric mean of the two moduli. Thus, the peak Q^{-1} is determined entirely by the elastic properties of this system.

Using the peak attenuation value Q_m^{-1} and frequency ω_m , the expression for the $Q^{-1}(\omega)$ spectrum (eq. 2.28) can be written in a convenient form:

$$Q^{-1}(\omega) = 2Q_m^{-1} \frac{\omega/\omega_m}{1 + \left(\frac{\omega}{\omega_m}\right)^2}. \quad (2.30)$$

This equation shows that the shape of the absorption peak is completely fixed and only scaled along both frequency and magnitude axes. In order to produce the desired absorption spectra, this standard shape is only replicated and scaled by ω_m in frequency and by Q_m^{-1} in magnitude. Peaks of $Q^{-1}(\omega)$ of this form resulting from a single relaxation frequency ω_m are called Debye peaks.

In terms of mechanical elements of Zener's model (Figure 2.6a), the frequency of the attenuation peak equals

$$\omega_m = \frac{1}{\sqrt{\tau_\varepsilon \tau_\sigma}} = \frac{1}{\eta} \frac{M_2}{\sqrt{1 + \frac{M_2}{M_1}}}. \quad (2.31)$$

Thus, the frequency of the peak is inversely proportional to the viscosity of the dashpot.

If the low-frequency limit of the modulus M_R (equal M_1) and two parameters of the attenuation peak ω_m and Q_m^{-1} are measured from some data, the Zener's model becomes completely constrained. The relaxation times can be obtained as

$$\tau_\varepsilon = \frac{1}{\omega_m} \left[Q_m^{-1} + \sqrt{Q_m^{-2} + 1} \right], \quad \text{and} \quad \tau_\sigma = \frac{1}{\omega_m^2 \tau_\varepsilon}. \quad (2.32)$$

Therefore, if we measure M_R , M_U , and $\omega_0 = 2\pi f_0$ from frequency-domain data (Figure 1.9),

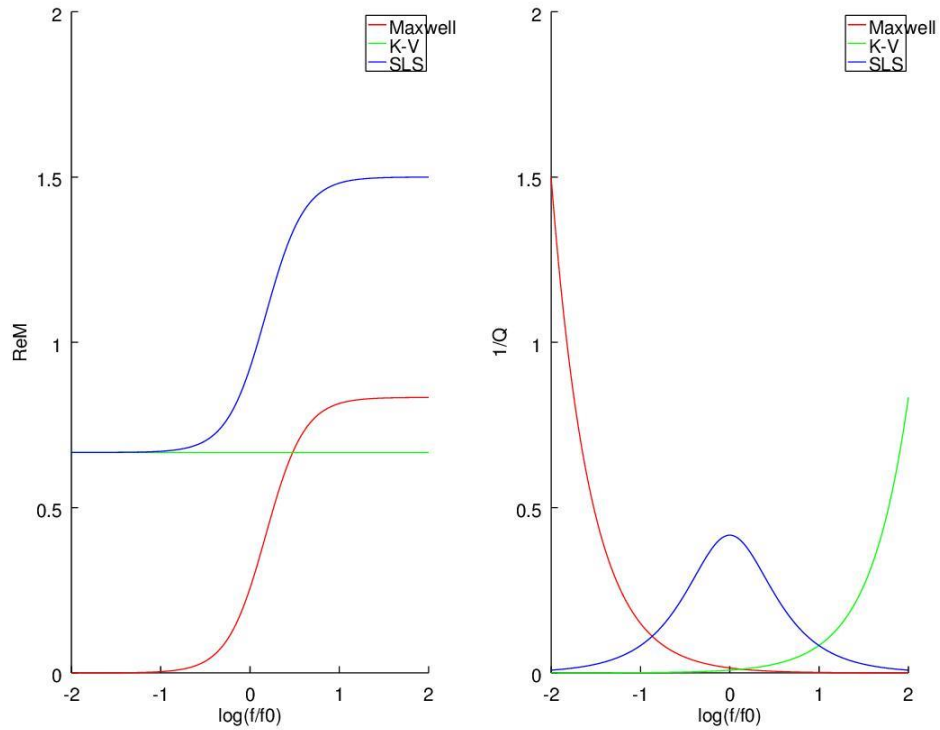


FIGURE 2.7.

Comparison of spectra $\text{Re}M(f)$ and $Q^{-1}(f)$ for Maxwell, Kelvin-Voigt, and Zener's bodies. Frequencies are normalized so that the frequency of the Zener's body peak equals 1.0. Moduli are normalized so that the geometric mean modulus $\bar{M} = \sqrt{M_R M_U} = 1$. Value of $\beta = 1.5$ (relative deviation of M_R or M_U from \bar{M}) is selected. In Kelvin-Voigt's and Maxwell's bodies, the value of η (dashpot viscosity) is taken equal that in Zener's body. For the Maxwell's and Kelvin-Voigt's bodies, Q^{-1} values were multiplied by 0.01 before plotting.

we obtain

$$\tau_\varepsilon = \frac{1}{\beta\omega_0}, \quad \text{and} \quad \tau_\sigma = \frac{\beta}{\omega_0}. \quad (2.33)$$

Figure 2.7 shows a comparison of the spectra predicted for observations in a laboratory forced-oscillation experiment for the three type of linear bodies considered above. Note that $\text{Re}M$ behave similarly for Maxwell's and Zener's (SLS) bodies, with nonzero MR for Zener's body. The spectra of Q^{-1} are most contrasting, with SLS showing a dissipation (relaxation) peak. Figure 2.8 shows how the spectra for Maxwell's and

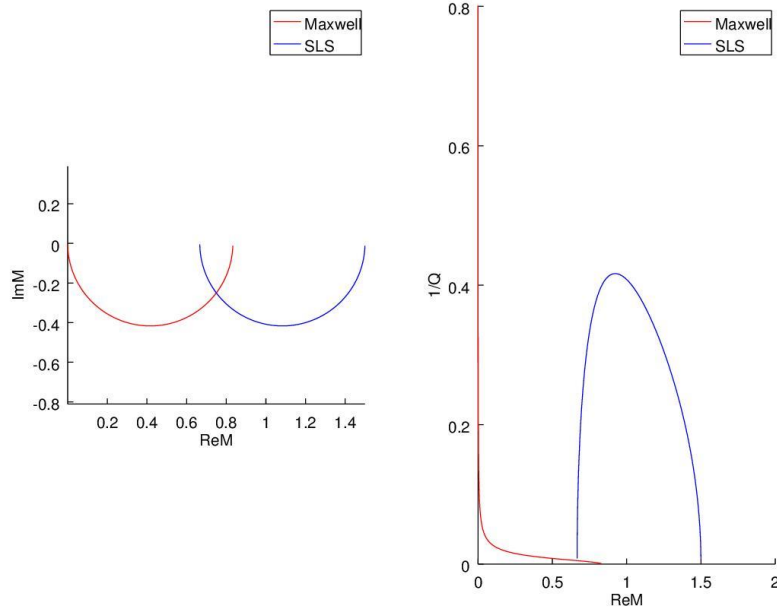


FIGURE 2.8.

Left: spectra of Maxwell's and Zener's (SLS) bodies in the complex plane of modulus M ; Right: cross-plots of Q^{-1} with $\text{Re}M$.

Zener's bodies look in the complex plane of M and in cross-plots of the inverse Q -factor with M .

Exercise

Derive parameters M_R , τ_ε , and τ_σ of Zener's equation from the mechanical parameters M_1 , M_2 , and η for the second form of Zener's body in Figure 2.6b.

Suggestions: This is easier to do in the frequency domain. Assume a harmonic stress function $\sigma(t) = \sigma_0 e^{-i\omega t}$, then express the strains of the elastic element M_1 on the left and of the Kelvin-Voigt body on the right. The resulting strain $\varepsilon(t)$ is a sum of these strains. Verify that the ratio $\sigma(t)/\varepsilon(t)$ has the form of Zener's equation (2.17c) and identify the three parameters in this equation.

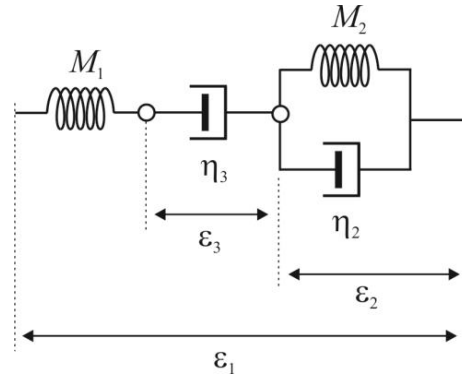


FIGURE 2.9.

Burgers' body. Labels and notation as in Figure 2.4.

2.7.4 Burgers' body

The Burger's solid adds to Zener's one an additional degree of freedom (variable number three in Figure 2.9) for which free static deformation is allowed. Therefore, the relaxed (static) modulus of this system equals zero, and the complex-valued effective modulus at near-zero frequencies is pure imaginary as in a Maxwell's body with two dashpots connected in series: $M(\omega) \approx -i\omega(\eta_1^{-1} + \eta_2^{-1})^{-1}$. At high frequencies, the dashpots do not move, and the unrelaxed modulus is due to a series of two springs (as in Zener's body): $M_U = (M_1^{-1} + M_2^{-1})^{-1}$. Between these limits, an expression for the complex modulus can be obtained by viewing the system in Figure 2.9 as a Maxwell body and a Kelvin-Voigt body connected in series:

$$M(\omega) = \left(M_{\text{Maxwell}}^{-1} + M_{\text{Kelvin-Voigt}}^{-1} \right)^{-1} = \left[\frac{1 - i\omega \frac{\eta_1}{M_1}}{-i\omega \eta_1} + (M_2 - i\omega \eta_2)^{-1} \right]^{-1}. \quad (2.34)$$

Because of the two internal degrees of freedom, this spectrum does not reduce to the Zener's linear solid equation (2.17).

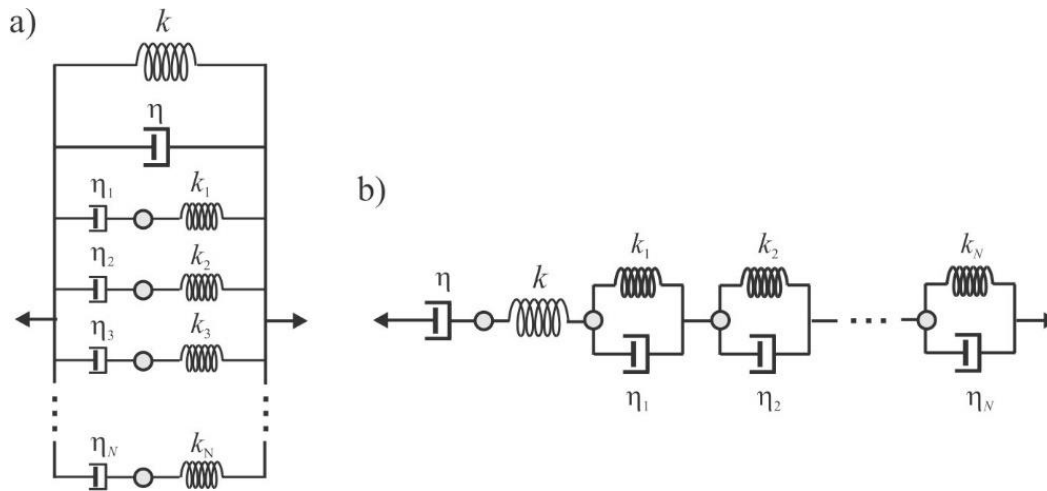


FIGURE 2.10

Combinations of elementary linear solids: a) Generalized Maxwell solid (with $\eta = 0$, this is also the Generalized Standard Linear, or Wiechert solid); b) Generalized Voigt model. Because of larger numbers of internal variables (gray circles), these systems can have broader spectral bands of dissipation.

2.7.5 Generalized linear solids

By combining multiple linear solids of the types above, mechanical systems with broad dispersion and attenuation frequency bands can be obtained (Figure 2.10). The arrangement of a Kelvin-Voigt solid with multiple Maxwell solids is called the Generalized Maxwell solid (Figure 2.10a). Similarly, a Generalized Voigt solid is obtained by combining the Burgers' model with multiple Voigt elements in a series (Figure 2.10b). The Generalized Maxwell solid without the main damper ($\eta = 0$) is called the Generalized Standard Linear solid (GSLs; also Generalized Zener's, or Wiechert's) model of material rheology (Figure 2.10a). The GSLs model is commonly used to implement band-limited attenuation in finite-difference codes for modeling seismic wavefields.

2.8 *Quasi-static (kinetic) character of viscoelastic equations*

In each of the forms of the viscoelastic relations discussed in this chapter (e.g., eq. (2.2) or Zener's equation (2.17)), the equations have the general form:

$$\mathbf{F}_\varepsilon \{ \boldsymbol{\varepsilon}(t) \} = \mathbf{F}_\sigma \{ \boldsymbol{\sigma}(t) \}, \quad (2.35)$$

where $\mathbf{F}_\varepsilon\{\dots\}$ and $\mathbf{F}_\sigma\{\dots\}$ are some integral or differential operators applied to the strain or stress as functions of time only. Such type of equations uniquely relating the force applied to some body to its deformation *and vice versa* represents a condition of some type of equilibrium. For example, the equilibrium may consist in a static deformation of a solid body or a steady-state flow of viscous fluid between two plates. Because the equilibrium may occur with loading forces slowly variable in time, this is a quasi-static equilibrium.

Three key features differentiate equations of equilibrium like shown in eq. (2.35) from dynamic equations of mechanics:

- 1) Equations of equilibrium are insensitive to the masses (densities) in the mechanical system. Indeed, if a body is near static equilibrium, all accelerations are near zero and the inertial forces are negligible compared to the elastic or viscous forces, and therefore the mass can be considered as equal zero. Zero masses attributed to all internal variables are key features of all viscoelastic bodies (section 2.7). Because of the zero masses, the internal variables are always equilibrated with current deformation $\boldsymbol{\varepsilon}(t)$.
- 2) Dynamic equations of motion are formulated not for strains and stresses as in eq. (2.35) but for displacements. Schematically, the general form of dynamic equations (second Newton's law) is:

$$\mathbf{m} \frac{\partial^2 \mathbf{u}(t)}{\partial t^2} = \mathbf{F} \left\{ \mathbf{u}(t), \frac{\partial \mathbf{u}(t)}{\partial t} \right\}, \quad (2.36)$$

where \mathbf{u} is a vector of all displacements in the system, \mathbf{m} is the mass (generally, a matrix for a complex system), and \mathbf{F} is the force dependent on $\mathbf{u}(t)$ and its gradients.

- 3) Equation (2.35) is *symmetric* in the sense that it can be used for predicting $\boldsymbol{\varepsilon}(t)$ from a measured $\boldsymbol{\sigma}(t)$, and vice versa. This is another indicator of an equation of equilibrium. This equation does not describe the deformation uniquely and allows, for example, two arbitrary constants C_2 and C_3 described in section 2.4.

By contrast to the equilibrium equation (2.35), the dynamic equation (2.36) is causal

in the sense that its right-hand side represents the cause (mechanical forces) and the left-hand side represents the effect of these forces. This equation predicts the acceleration of each point of the body from the displacements, velocities, and their gradients given in the right-hand side.

2.9 *Problems with the viscoelastic approach*

Time- and frequency-dependent material properties in equations (2.35) often allow explaining laboratory observations quite easily. For example, spectra like shown in Figure 1.9 measured for a rock sample are commonly interpreted as representing the effective modulus $M(f)$ of its material, and this modulus is used to predict propagation of seismic waves. However, do functions $M(t)$ or $M(f)$ truly represent a material property?

To answer this question, it is important to realize several strong limitations of the viscoelastic model:

- 1) Inherent quasi-static approximation;
- 2) Treatment of the heterogeneity of the medium;
- 3) Disregard of non-viscoelastic forces such as Darcy-type pore-flow friction;
- 4) Use of boundary conditions;
- 5) Nonphysical wave solutions arising in the presence of contrasts in material properties.

The first of these limitations was described in the preceding section, and the other three are explained in the following subsections.

Thus, only in limited cases, viscoelastic functions such as $M(t)$ or $Q(f)$ can be viewed as material properties. These limited cases are quite restrictive:

- Modeling of laboratory samples in which the deformation can be considered as homogenous. In addition, for fluid-saturated porous rock, only fixed (usually undrained) pore-flow conditions should be used. The resulting viscoelastic functions strongly depend on these conditions. Under drained conditions (when pore flow is allowed), limitation 3) above becomes

significant.

- Waves in media with no pore-flow effects and far from any boundaries.

In many applications of the viscoelastic model (see standard texts such as by Carcione and also many software algorithms), dynamic equations like (2.36) or body forces like gravity are added to the viscoelastic equations. However, these additions are performed in an artificial manner and still based on assumed time-dependent mechanical properties. We do not discuss these methods here because in the following chapters, a rigorous approach free from the above problems is given.

2.9.1 Treatment of heterogeneity

The viscoelastic model was originally designed for explaining quasi-static deformations with negligible spatial variations, such as creep of the whole rock sample in a lab experiment. In this case, the time is the only significant independent variable, and there exists only one complex-valued function $M(t)$ or $J(t)$ describing the whole system. In heterogeneous media with spatially-variable $\sigma(\mathbf{x}, t)$ and $\varepsilon(\mathbf{x}, t)$, deformations occur *not* by time-only dependent stress-strain relations (2.35) at point \mathbf{x} . From physics, it is known that heterogeneous deformations are driven by spatial gradients of pressure, which lead to multiple types of waves and material and heat flows. For example, stress σ at point \mathbf{x} and time t is affected by the deformations of *adjacent points* at earlier times, and *not* by the earlier strain values at the same point \mathbf{x} . At time t after an application of stress, the strain at point \mathbf{x} is affected by boundaries and material-property contrasts at distance ct from this point, where c is the wave or some flow velocity within the medium.

Since for a heterogeneous medium or a finite body (which are the usual cases) both $\sigma(\mathbf{x}, t)$ and $\varepsilon(\mathbf{x}, t)$ depend on the deformation of the whole body, relations (2.35) are (generally) only mathematical identities satisfied by this deformation. For a given experiment, it is often a difficult task to determine whether the resulting phenomenological $M(t)$ and $J(t)$ are dependent on the shape of the body or not. To evaluate this dependence, one has to utilize rigorous physics-based models such as described further in this course.

2.9.2 Treatment of non-viscoelastic forces

In addition to the problem of spatial heterogeneity, the viscoelastic model contains another serious problem in application to rocks: it considers only forces produced by surface stresses σ (more rigorously called the Cauchy stress tensor σ_{ij} ; see below in this course). An important example of body force acting within fluid-saturated porous rock is the Darcy friction of the fluid flowing through the pores of porous rock. The rate of this flow and the resulting force are controlled by the property called permeability of the rock.

Permeability is responsible for a significant portion of anelasticity (in fact, *all* of it in Biot's model of porous rock; see section 5.6 on page 132) is caused not by the surface stress σ (eqs. 2.35) but by body-force friction. Thus, for porous rock, eqs. (2.35) are not applicable. Similarly, thermal relaxation (chapter 6 below) also may occur by means of heat flowing out of point \mathbf{x} or toward it, but not by a time-memory process at the same point. Several heuristic approximations to combining Biot's and thermoelastic effects with viscoelasticity have been proposed (known as 'poro-viscoelasticity' and 'thermo-viscoelasticity'), but I will not go into them here. Instead, I will follow an approach starting from physical observations rather than from hypothesized mathematical principles.

2.9.3 Boundary conditions

A complicated problem of the viscoelastic model is in an incomplete treatment of boundary conditions. When two solid bodies are joined together, the displacements and

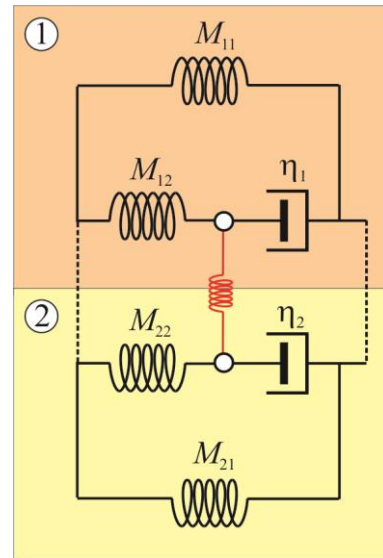


FIGURE 2.11

Boundary conditions at a welded contact of two Zener's bodies (labels 1 and 2) with different mechanical properties.

The displacements and stresses for the observable displacement must be equal (dashed solid lines). However, the internal variables can also be connected, for example, by an elastic force shown by red spring.

stresses at the boundary must be equal. This condition is shown by dashed lines in Figure 2.11. However, if the bodies are viscoelastic as, for example, the two Zener bodies in Figure 2.11, they contain internal variables (white dots) for which some boundary conditions also need to be specified.

In viscoelasticity, these internal variables are considered as non-interacting (and so no connection between them in the diagram) and quasi-static (section 2.8). However, in real rock, the internal degrees of freedom such as the network of microcracks may interact with the boundary. The interaction may be elastic or viscoelastic, as schematically shown by the red spring element in Figure 2.11.

2.9.4 Nonphysical wave solutions

Another serious problem with application of the viscoelastic model to seismic waves is in producing nonphysical wave solutions in layered media, or upon reflection from interfaces. Such nonphysical solutions have to be avoided by special mathematical conventions. For more on this subject, see, for example, Ruud (2006), Krebes and Daley (2007), and Vavryčuk (2010).

2.10 *Laboratory assignments*

Lab 2.1: Dispersion and attenuation spectra of linear solids

Write a Matlab or Octave program to calculate and plot the modulus dispersion ($\text{Re}M(f)$) and attenuation ($Q^{-1}(f)$) spectra for Maxwell's, Kelvin-Voigt's and Zener's solids.

Lab 2.2: Explore Burgers' model

Write a Matlab or Octave program to plot $\text{Re}M(f)$ and $Q^{-1}(f)$ for Burgers' model (Figure 5.9; eq. 2.34) with some $M_1 = 1$, $\eta_3 = 1$ (in some appropriate units), and try a couple values for M_2 and η_2 . Compare the results to the spectra of Maxwell's body (on the left in Figure 5.9) and Kelvin-Voigt's body (on the right in this Figure).

3 Variational Approach in Physics

Key points:

- Variational approach to mechanics and differential equations
 - D'Alembert's principle of virtual work and Hamiltonian action principle
 - Potential and pseudo-potential
 - Constraints
-

Large systems of differential equations arising in the mechanics of solids and fluids can often be presented very compactly in the form of a variational principle minimizing (more precisely, extremizing) a single functional. The variational principle gives a powerful and elegant way for summarizing all equations, perform transformations of variables, investigating the possible types of interactions, and determining the conservation laws. In this chapter, I describe the general ideas of variational approaches for differential equations, and in chapter 4, these ideas will be further detailed for Lagrangian mechanics.

Consider, for example, the differential equations governing the motion of N_p particles. The number of particles can range from $N_p = 1$ to a very large number such as the number of atoms in a solid body. The particles interact and are also subjected to forces (external and due to mutual interactions), so that so that the k^{th} particle is subjected to a total force vector \mathbf{F}_k . The second Newton's law then states that under the action of the force, the particle will attain acceleration

$$\mathbf{a}_k = \ddot{\mathbf{x}}_k = \frac{\mathbf{F}_k}{m_k}, \quad (3.1)$$

where m_k is the mass of the k^{th} particle, \mathbf{x}_k is the vector of its coordinates, and overdots denote derivatives with respect to time: $\ddot{\mathbf{x}}_k \stackrel{\text{def}}{=} \partial^2 \mathbf{x}_k / \partial t^2$. Equation (3.1) is convenient for

evaluating the change of velocity of any particular particle, but for considering the whole system of particles, it is more convenient to write it as a balance of the applied and inertial forces in the frame of reference of each particle:

$$m_k \ddot{\mathbf{x}}_k - \mathbf{F}_k = \mathbf{0}. \quad (3.2)$$

When describing finite-difference modeling algorithms, this equation is often called the “conservation of momentum”. However, better avoid this terminology because it does not add much to the understanding of eq. (3.2). The concept of momentum is yet to be defined (chapter 4) and not needed here. Equation (3.1) has an additional value of pointing the significance of the force \mathbf{F}_k (in the right-hand side) is *the cause* of acceleration \mathbf{a}_k (left-hand side).

Equation (3.2) gives zero at any t , for each particle and at any point on its true trajectory $\mathbf{x}_k(t)$. Therefore, it would be useful to present the trajectories of all N_p particles as a stationary point (usually minimum) of some functional (a correspondence assigning a real number to the set of all trajectories $\mathbf{x}_k(t)$) $S\{\mathbf{x}_k(t)\}$. This functional is called the Hamiltonian action. To obtain this functional, let us look at the d’Alembert’s principle of virtual work first.

3.1 d’Alembert’s principle

Let $\mathbf{x}_k(t)$ be the true trajectory of k th particle, and consider arbitrary infinitesimal deviations of all particles from their trajectories: $\mathbf{x}'_k(t) = \mathbf{x}_k(t) + \delta\mathbf{x}_k(t)$. Since all of the net forces in equation (3.2) equal zero, each of them can be multiplied by $\delta\mathbf{x}_k(t)$ and summed, producing the virtual work (work due to the arbitrary perturbations), which will equal zero:

$$\delta W = \sum_{k=1}^{N_p} (m_k \ddot{\mathbf{x}}_k - \mathbf{F}_k) \delta\mathbf{x}_k = 0. \quad (3.3)$$

Thus, the d’Alembert’s principle states that the true trajectories $\mathbf{x}_k(t)$ are such that an arbitrary deviation from them results in zero virtual work δW .

The virtual work δW is a differential form (a linear functional of infinitesimal deviations $\delta \mathbf{x}_k(t)$) and not a functional of $\mathbf{x}_k(t)$. This means that if δW is virtual work, there exists no functional $W\{\mathbf{x}_k(t)\}$ whose variation gives the δW . For this reason, the d'Alembert's principle (3.3) is called quasi-variational.

3.2 Hamiltonian action

To obtain the functional of Hamiltonian action and a variational principle for it, the virtual work δW is integrated over time:

$$\delta S = \int_{t_1}^{t_2} \delta W dt = \int_{t_1}^{t_2} \sum_{k=1}^{N_p} (m_k \ddot{\mathbf{x}}_k - \mathbf{F}_k) \delta \mathbf{x}_k dt = 0. \quad (3.4)$$

The two types of forces in the parentheses give the change of the kinetic energy for each particle $\int_{t_1}^{t_2} m_k \ddot{\mathbf{x}}_k \delta \mathbf{x}_k dt = \int_{t_1}^{t_2} \delta T_k dt$ (where $T_k = \frac{1}{2} m_k \dot{\mathbf{x}}_k^2$, and you need to use integration by parts and condition $\delta \mathbf{x}_k(t_1) = \delta \mathbf{x}_k(t_2) = 0$), and elastic energy $\mathbf{F}_k \delta \mathbf{x}_k = -\delta U_k$ (which is simply the definition of elastic energy). Therefore, δS is an increment of a functional S , which is called the Hamiltonian action and defined as

$$S = \int_{t_1}^{t_2} L dt, \quad (3.5)$$

where

$$L = \sum_{k=1}^{N_p} (T_k - U_k). \quad (3.6)$$

is the Lagrangian function of the system of particles. All equations of motion are then contained in the principle of stationary (extremal) Hamiltonian action:

$$\delta S = \delta \left[\int_{t_1}^{t_2} L dt \right] = 0 \quad (3.7)$$

for arbitrary infinitesimal variations of trajectories $\delta\mathbf{x}_k(t)$. In most cases, it is much easier to determine the two scalar energies than to write all the vector equations of motion (3.1). In chapter 4, we will obtain the differential equations on $\mathbf{x}_k(t)$ which allow finding this extremum $\delta S = 0$.

Thus, the Lagrangian of a mechanical system is the difference between the total kinetic and potential (elastic) energies of all particles (eq. 3.6). However, note that the Lagrangian can also have other forms. For example, for a charged particles in a magnetic field, the effect of the magnetic field is represented by terms in L proportional to particle velocities:

$$L_{mag} = \sum_{k=1}^{N_p} \left(-\frac{q_k}{c} \dot{\mathbf{x}}_k \cdot \mathbf{A} \right), \quad (3.8)$$

where q_k is the electric charge of k th particle, and \mathbf{A} is the vector potential of the magnetic field at point \mathbf{x}_k (this vector potential is another vector field defined so that the magnetic induction field \mathbf{B} is the curl of \mathbf{A} : $\mathbf{B} = \nabla \times \mathbf{A}$). Denominator c in eq. (3.8) is a constant related to the selected electromagnetic units, and it equals the speed of light in the Gaussian CGS (centimeter-gram-second) system.

The variational principle gives a much more powerful way for formulating and solving equations of motion than eqs. (3.1) or (3.2). Instead of following the trajectory of each particle in time, we consider all possible values of \mathbf{x}_k *at all times* as independent variables in a (highly) multidimensional space, and determine the stationary point of S . This stationary point is the true trajectory of all particles.

3.3 Dissipation pseudo-potential

In the expressions for potential energies U_k , forces \mathbf{F}_k depend on coordinates \mathbf{x}_k only, and consequently they can be presented as gradients of the total potential energy of the

system: $U = \sum_{k=1}^{N_p} U_k$: $\mathbf{F}_k = -\partial U / \partial \mathbf{x}_k$. Thus, using the variational principle, these forces can

be found by: 1) perturbing the particle trajectories by arbitrary deviations $\delta\mathbf{x}_k(t)$,

and 2) presenting the resulting perturbation of the time integral of the elastic energy U as linear combinations of these $\delta\mathbf{x}_k$ at different times:

$$\delta \left[\int_{t_1}^{t_2} U dt \right] = - \sum_{k=1}^{N_p} \int_{t_1}^{t_2} \mathbf{F}_k \delta\mathbf{x}_k dt . \quad (3.9)$$

The coefficients of $\delta\mathbf{x}_k$ in these linear combinations are the forces \mathbf{F}_k .

Forces \mathbf{F}_k may also depend not on the coordinates \mathbf{x}_k of the particles but on their velocities $\dot{\mathbf{x}}_k$. In particular, such velocity-dependent forces are those caused by magnetic fields and forces of friction. For example, if each of these particles is a sphere of radius r moving through fluid with viscosity η , then it will experiences a viscous friction force $\mathbf{F}_k = -6\pi r \eta \dot{\mathbf{x}}_k$ (the Stokes' law). Such forces can also be described as gradients of a time (and volume) integral as eq. (3.9), but using arbitrary *velocity perturbations* $\delta\dot{\mathbf{x}}_k$ and pseudo-potential, or dissipation function D instead of U :

$$\delta \left[\int_{t_1}^{t_2} D dt \right] = - \sum_{k=1}^{N_p} \int_{t_1}^{t_2} \mathbf{F}_k \delta\dot{\mathbf{x}}_k dt . \quad (3.10)$$

For the example of Stokes' friction in this paragraph, $D = 3\pi\eta \sum_{k=1}^{N_p} r_k \dot{\mathbf{x}}_k^2$ for N_p particles in the same fluid.

According to eq. (3.10), the dissipation function is used in the same way as the potential energy U but viewing particle velocities rather than coordinates as independent variables.

3.4 Constraints

Often, in addition to a system of differential equations such as (3.2), it is required that the system satisfies additional constraints. For example, in mechanics of porous solids, such constraints can be boundary conditions at the free surface or open or closed conditions

for pore-fluid flow across various boundaries. Such constraints can also be naturally included in the system of final equations by using the variational approach.

Using the example of a system particles (eq. 3.2), let us assume that it is also required that the particles move along certain surfaces satisfying constraints

$$B_j(\mathbf{x}_1, \mathbf{x}_2, \mathbf{x}_3, \dots) = 0, \quad (3.11)$$

where B_j is the j th constraint function dependent on all \mathbf{x}_k . To include these constraints into the equations, we only need to modify the Lagrangian as $L \rightarrow L + L_c$, where

$$L_c = \sum_{j=1}^{N_c} \lambda_j B_j, \quad (3.12)$$

and parameters λ_j are Lagrange multipliers. These multipliers are functions of time and treated as additional variables of the mechanical system. To visualize the physical meaning of this variable, note that if function B_j in eq. (3.11) represents some distance from the j th constraint surface, then λ_j is the external force required to hold the system on this surface.

The Hamiltonian action of the system with constraints equals $S_c = \int_{t_1}^{t_2} (L + L_c) dt$, and

it can be viewed as a functional of both original variables $\mathbf{x}_k(t)$ and the additional variables $\lambda_j(t)$. Because $\lambda_j(t)$ are determined so that the boundary conditions (eq. 3.11) are satisfied, the additional term in the Lagrangian L_c equals identically zero for the solution.

Therefore, the resulting $\mathbf{x}_k(t)$ achieve extremum of the original action: $\delta \left[\int_{t_1}^{t_2} L dt \right] = 0$ within

the constrained subspace of coordinates \mathbf{x}_k .

3.5 *Non-mechanical equations and Fréchet derivatives*

Variational methods can also be useful to derive compact forms for non-mechanical equations. How to decide for which equations this can be done? Consider a differential

equation:

$$F(u) = 0. \quad (3.13)$$

where u is some variable or field, and F contains a combination of differential operators, which can possibly be nonlinear. This equation can be linearized at the vicinity of function u by using the concept of Fréchet derivatives. The Fréchet derivative is the linear operator \hat{F}'_u defined so that if we perturb function u by adding to it an arbitrary function ϕ multiplied by an infinitesimal factor ε (say, $u(\mathbf{x}) \rightarrow u(\mathbf{x}) + \varepsilon\phi(\mathbf{x})$), then the relative perturbation of $F(u)$ (called the Fréchet differential) is the partial derivative of $F(u)$ with respect to ε :

$$\hat{F}'_u\phi = \lim_{\varepsilon \rightarrow 0} \frac{F(u + \varepsilon\phi) - F(u)}{\varepsilon} = \left. \frac{\partial}{\partial \varepsilon} [F(u + \varepsilon\phi)] \right|_{\varepsilon=0}. \quad (3.14)$$

Thus, for small perturbation δu in the vicinity of function u , eq. (3.13) is approximated as $F(u + \delta u) \approx F(u) + \hat{F}'_u\delta u$, or the increment of $F(u)$ equals

$$\delta F(u) = \hat{F}'_u\delta u. \quad (3.15)$$

The answer to the question of this section is: a variational principle for eq. (3.13) exists if the Fréchet derivative operator is symmetric in the following sense:

$$\int \psi \hat{F}'_u\phi dV = \int \phi \hat{F}'_u\psi dV, \quad (3.16)$$

where the integration is carried out over the volume of the body, and functions ϕ and ψ and their derivatives equal zero at all edges of volume V . If functions u (and therefore ϕ and ψ) also depend on time, time integration should also be included, and similarly, the arbitrary trial functions ϕ and ψ and their derivatives would be zero at the endpoint times t_1 and t_2 .

Exercises

- 1) Considering coordinates $\mathbf{x}_k(t)$ as function $u(t)$ above, derive expressions for the Fréchet derivative $\hat{F}'_{\mathbf{x}_k}$ for the Newton's second law (eq. 3.1):

$$F(\mathbf{x}_k) = m_k \ddot{\mathbf{x}}_k - \mathbf{F}_k .$$

Hint: Note that this $\hat{F}'_{\mathbf{x}_k}$ will be a differential operator which must be applied to the trial functions $\phi(t)$.

- 2) Show that these derivatives satisfy the symmetry relation (3.16).

4 Lagrangian Mechanics

Key points:

- Generalized variables
 - Conservative and dissipative mechanical systems
 - Euler-Lagrange equations
 - Attenuation coefficient and Q
 - Examples of simple and multidimensional damped mechanical oscillators
-

In Lagrangian analytical mechanics, the deformation of a rock body or wave-propagating medium in any experimental environment is completely described by giving the functional forms of the Lagrangian (denoted L) and dissipation functions (D) for this environment. The Lagrangian L is usually the difference of the total kinetic and elastic energies of the body (eq. (3.6)). However, in general, the Lagrangian does not have to be separable into the potential and kinetic energies.

4.1 *Generalized coordinates*

In chapter 1, I described the Lagrangian variational approach using coordinates of particles comprising the mechanical system. However, the description does not have to use only such coordinates, and any type of “generalized coordinates”, $\mathbf{q}(t)$ can be used. For example, if the mechanical system is the subsurface with a distribution of elastic moduli and density, vector \mathbf{q} would include positions of the macroscopic “representative elementary volume” (REV) within the medium, or we could use spatially variable strains or magnitudes of certain spatial harmonics as the generalized coordinates. Thus, the number of generalized variables can be small or very large in wave modeling, but for any number of variables, the principle of Hamiltonian action yields the equations of motion.

As shown in eq. (3.5), all time- or frequency-domain equations of motion are obtained by employing the Hamiltonian principle of extremal action $S\{\mathbf{q}(t)\} = \int_{t_1}^{t_2} L dt$. The trajectory is in the space of generalized coordinates $q_i(t)$ which are arbitrary variables describing the state of the mechanical system. The braces $\{\dots\}$ in this notation mean that S is a functional, i.e. a function whose argument is a function of time, that is, values of all variables \mathbf{q} taken at all times.

The principle of extremal action states that the trajectory $\mathbf{q}_{\text{true}}(t)$, corresponding to the true motion of the system is such that $\delta S = 0$. This equation means that for a small arbitrary deviation of all variables $\delta\mathbf{q}(t)$ such that $\delta\mathbf{q} = 0$ and $\delta\dot{\mathbf{q}} = 0$ at the endpoints $t = t_1$ and $t = t_2$, the action is unchanged: $S\{\mathbf{q}_{\text{true}} + \delta\mathbf{q}\} = S\{\mathbf{q}_{\text{true}}\} + o\{\delta\mathbf{q}\}$. In this relation, the “little $o\{\dots\}$ ” denotes some functional which for a small $\delta\mathbf{q}$ tends to zero faster than $\delta\mathbf{q}$. For example, if $\delta\mathbf{q}$ is characterized by some small measure ε (such as the peak or average seismic strain), then $o(\varepsilon)$ would consist of arbitrary terms of functional orders higher than ε , such as ε^2 , ε^3 , etc.

The variation of action (eq. 3.5) also represents an integral over time:

$$\delta S = \int_{t_1}^{t_2} \frac{\delta S}{\delta q_i} \delta q_i(t) dt, \quad (4.1)$$

where summation over all indices i is implied. The derivative $\frac{\delta S}{\delta q_i}$ is a functional derivative, which is the derivative of S with respect to the time-variant function $q_i(t)$ at any time t . Note that the definition of this derivative is similar to that of the Fréchet differential (eq. 3.15), except that because of time integration, $\frac{\delta S}{\delta q_i}$ is an ordinary function and not operator.

4.2 Euler-Lagrange equations

The functional derivative $\frac{\delta S}{\delta q_i}$ can be evaluated from partial derivatives of the Lagrangian function with respect to its arguments. Function L is usually a function of the generalized coordinates q_i and the corresponding “generalized velocities” denoted \dot{q}_i :

$L = L(\mathbf{q}, \dot{\mathbf{q}})$. Then, because $S = \int_{t_1}^{t_2} L dt$ for an evolution of the system from time t_1 to t_2 ,

the perturbation of the action equals $\delta S = \int_{t_1}^{t_2} \left(\frac{\partial L}{\partial q_i} \delta q_i + \frac{\partial L}{\partial \dot{q}_i} \delta \dot{q}_i \right) dt$. The part of the integral

containing $\delta \dot{q}_i$ in the integrand can be transformed by integration by parts:

$$\delta S = \int_{t_1}^{t_2} f \delta \dot{q}_i dt = \int_{t_1}^{t_2} f \frac{d(\delta q_i)}{dt} dt = - \int_{t_1}^{t_2} \frac{df}{dt} \delta q_i dt \quad (\text{recall that we consider } \delta q_i \text{ equal zero at both}$$

end points, and therefore the terms corresponding to the limits of this integration interval

equal zero). Therefore, δS equals $\delta S = \int_{t_1}^{t_2} \left(\frac{\partial L}{\partial q_i} - \frac{d}{dt} \frac{\partial L}{\partial \dot{q}_i} \right) \delta q_i dt$. Thus, $\frac{\delta S}{\delta q_i} = \frac{d}{dt} \frac{\partial L}{\partial \dot{q}_i} - \frac{\partial L}{\partial q_i}$.

The above δS must equal zero for *arbitrary* $\delta \mathbf{q}$, which gives us the equation that must be satisfied by the motion of the dynamic system $\mathbf{q}(t)$:

$$\frac{d}{dt} \frac{\partial L}{\partial \dot{q}_i} - \frac{\partial L}{\partial q_i} = 0. \quad (4.2)$$

This differential equation is called the Euler-Lagrange equation.

In the Euler-Lagrange equation (4.2), the derivative $Q_i \stackrel{\text{def}}{=} \frac{\partial L}{\partial \dot{q}_i}$ is the “generalized force”, which corresponds to the usual force \mathbf{F} in Newton’s laws (eq. (3.1) and also see

example below). The derivative with respect to velocity $p_i \stackrel{\text{def}}{=} \frac{\partial L}{\partial \dot{q}_i}$ is called the “generalized

momentum”, which generalizes the concept of the usual momentum $\mathbf{p}_k = m\mathbf{x}_k$ of a single

particle. In this notation, equation (4.2) is simply

$$\frac{dp_i}{dt} = Q_i, \quad (4.3)$$

which represents the second Newton's law with respect to arbitrary coordinates of the system generalizing eq. (3.1)). This equation is also valid when the "mass" of the system varies with time or spatial coordinates.

The Lagrangian describes the internal interactions within the system (elasticity and inertia). If an external force is present, such as the seismic source, the force is added to the right-hand side of eq. (4.3):

$$\frac{dp_i}{dt} = Q_i + F_i. \quad (4.4)$$

The external force F_i is also "generalized" and corresponds to the character of the generalized variable q_i . For example, if q_i is the coordinate of a point of an elastic medium, then F_i would be the corresponding component (X , Y , or Z) of the ordinary body force applied to the point. If q_i is a rotation angle of a body, F_i should be the torque applied to the body, and so on.

All components i of the external force F_i can also be obtained as derivative of a Lagrangian function $F_i = \frac{\partial L_F}{\partial q_i}$ by taking $L_F = q_i F_i$. Therefore, all external forces can be included in the Lagrangian by taking:

$$L(\mathbf{q}, \dot{\mathbf{q}}) \stackrel{\text{def}}{=} T - U + q_i F_i. \quad (4.5)$$

Note that the meaning of the added term $q_i F_i$ is the work by the external force applied when the generalized variable is shifted by q_i . This term can also be included in the potential energy U .

4.3 Mechanical energy

Next, function $H \stackrel{\text{def}}{=} p_i \dot{q}_i - L$ is called the "generalized energy." If expressed through

p_i instead of \dot{q}_i , this function is called the Hamiltonian. The generalized energy has an important property: if L does not explicitly depend in time t (as above) and contains no external forces, then the energy H is constant with time:

$$\frac{dH}{dt} = \frac{d}{dt}(p_i \dot{q}_i) - \frac{\partial L}{\partial q_i} \dot{q}_i - \frac{\partial L}{\partial \dot{q}_i} \ddot{q}_i = \frac{d}{dt}(p_i \dot{q}_i) - \dot{p}_i \dot{q}_i - p_i \ddot{q}_i \equiv 0. \quad (4.6)$$

This is the law of conservation of mechanical energy. Thus, time-independent Lagrangian functions describe conservative systems.

Other conservation laws are also obtained from the symmetries of the Lagrangian. For example, if the Lagrangian *does not explicitly depend* on some coordinate q_i , then the corresponding generalized force is zero: $Q_i = \frac{\partial L}{\partial q_i} = 0$, and consequently the corresponding momentum is conserved (eq. 4.4): $\frac{dp_i}{dt} = 0$. For example, this q_i can be the coordinate of the center of mass of a closed mechanical system, and then this relation means the conservation of momentum for the system. If this q_i is the orientation angle of a system, then p_i is the angular momentum, with the corresponding conservation law.

4.4 Dissipation of mechanical energy

To describe a non-conservative system with mechanical-energy dissipation, we need to add a frictional force in the right-hand sides of eqs. (4.2) or (4.3). Let us denote this force R_i :

$$\frac{dp_i}{dt} = Q_i + R_i. \quad (4.7)$$

Force R_i represents effects like viscous friction (see example in the following section). As outlined in section 3.3, this force can be obtained as a derivative of the dissipation function D with respect to velocities \dot{q}_i :

$$R_i \stackrel{\text{def}}{=} -\frac{\partial D}{\partial \dot{q}_i}. \quad (4.8)$$

Sign ‘-’ in this expression means that the force of friction acts in the direction opposite to velocity \dot{q}_i , and function D is non-negative and increases with \dot{q}_i . To understand its meaning, evaluate the derivative of the total energy (4.6) using eqs. (4.7) and (4.8):

$$\frac{dH}{dt} = \frac{d}{dt}(p_i \dot{q}_i) - \dot{p}_i \dot{q}_i - p_i \ddot{q}_i = R_i \dot{q}_i = -\dot{q}_i \frac{\partial D}{\partial \dot{q}_i}. \quad (4.9)$$

This shows that D is indeed responsible for the energy dissipation rate (power). In many cases of ‘linear’ dissipation (in all cases for rock considered in this course), the dissipation function is a quadratic function of the generalized velocities: $D = \frac{1}{2} \Upsilon \dot{q}_i \dot{q}_i$ (similar to the kinetic energy). In such cases, the dissipated power (4.9) equals $\frac{dH}{dt} = -\Upsilon \dot{q}_i \dot{q}_i = -2D$. This relation shows that for linear dissipation, the dissipation function can be understood as half the mechanical energy dissipated per unit time.

Finally, from the above, the Euler-Lagrange equations for i th generalized coordinate with energy dissipation are

$$\frac{d}{dt} \frac{\partial L}{\partial \dot{q}_i} - \frac{\partial L}{\partial q_i} + \frac{\partial D}{\partial \dot{q}_i} = 0. \quad (4.10)$$

When modeling continuous media, variables q_i often represent functions of spatial coordinates \mathbf{x} , and therefore in addition to \mathbf{q} and time derivatives $\dot{\mathbf{q}}$, the Lagrangian and dissipation functions depend on spatial derivatives of \mathbf{q} . Let us denote the spatial derivative with respect to coordinate x_j by comma in the subscript: $q_{i,j} \stackrel{\text{def}}{=} \frac{\partial q_i}{\partial x_j}$. Then, with the use of

dependencies on $q_{i,j}$ in functions L and D , the Euler-Lagrange equations (4.10) become modified with additional spatial derivatives:

$$\frac{\partial}{\partial t} \frac{\partial L}{\partial \dot{q}_i} + \frac{\partial}{\partial x_j} \frac{\partial L}{\partial q_{i,j}} - \frac{\partial L}{\partial q_i} + \frac{\partial D}{\partial \dot{q}_i} - \frac{\partial}{\partial x_j} \frac{\partial D}{\partial \dot{q}_{i,j}} = 0. \quad (4.11)$$

Note again that summations over spatial coordinates j are implied in this equation.

Thus, for a system of arbitrary complexity and geometry, the complete equations of motion become readily available once we decide on the forms of functions $L(\mathbf{q}, \dot{\mathbf{q}})$ and $D(\mathbf{q}, \dot{\mathbf{q}})$ for the system. In the following section, I illustrate these functions for a well-known mechanical system with only one degree of freedom (linear oscillator), and in the next chapter 5 – for a continuous medium usually used for modeling seismic waves.

4.5 *Mass-Stiffness-Damping (MSD) model*

Numerical modeling and inversion always use parameterizations of the continuous displacement fields by some finite vector of variables \mathbf{q} , which is only dependent on time. For a 3-D gridded model, this vector may contain about a million elements, but this is still a discrete problem. For such finite systems, the (quadratic) Lagrangian and dissipation functions reduce to only three quadratic forms of vectors \mathbf{q} and its time derivative $\dot{\mathbf{q}}$:

$$\begin{cases} L = \frac{1}{2} \dot{\mathbf{q}}^T \mathbf{M} \dot{\mathbf{q}} - \frac{1}{2} \mathbf{q}^T \mathbf{S} \mathbf{q}, \\ D = \frac{1}{2} \dot{\mathbf{q}}^T \mathbf{D} \dot{\mathbf{q}}, \end{cases} \quad (4.12)$$

where the three mechanical-property matrices are:

- 1) the mass matrix \mathbf{M} giving the kinetic energy of the system for all possible variations of variables $\mathbf{q}(t)$;
- 2) the stiffness matrix \mathbf{S} describing the elastic energy. This matrix is often denoted \mathbf{K} , but I reserve this symbol for bulk modulus and for the poroelastic model.
- 3) the damping matrix \mathbf{D} containing a similar description of all dissipation effects. This matrix is often denoted \mathbf{C} , but I will use ‘ \mathbf{D} ’ for association with “damping” and difference from specific heat.

We will call this model mass-stiffness-damping (MSD).

Note that after discretization (i.e., evaluation of the spatial derivatives $\partial_i \mathbf{u}$ through differences of \mathbf{u} , evaluation of spatial integrals, accounting for boundary conditions, etc.), there is no longer any formal distinction between the body-force (Darcy type) and viscous (Navier-Stokes type) friction in eqs. (4.12). As shown in chapter 6 below, thermoelastic temperature variations within the material can also be described by the general quadratic forms (4.12). The differences between these are embedded in the structure of matrices \mathbf{M} , \mathbf{D} , and \mathbf{S} . These differences may also be unnoticeable in the resulting solutions $\mathbf{q}(t)$ or $\mathbf{q}(f)$, and therefore they may be impossible to resolve by considering only a limited set of experiments⁸.

Equations (4.12) are the same as functions L and D for a multidimensional linear oscillator (examples shown in section 4.7) except that the displacement is a vector and the mass, rigidity, and damping of this multidimensional “oscillator” are matrices. The Euler-Lagrange equations from eq. (4.12) are also those for an oscillator:

$$\frac{d}{dt} \frac{\partial L}{\partial \dot{\mathbf{q}}} - \frac{\partial L}{\partial \mathbf{q}} + \frac{\partial D}{\partial \dot{\mathbf{q}}} = \mathbf{M}\ddot{\mathbf{q}} + \mathbf{D}\dot{\mathbf{q}} + \mathbf{S}\mathbf{q} = \mathbf{f}, \quad (4.13)$$

where \mathbf{f} is the vector of external force applied by the seismic source. Basically, these equations only state that some combination of displacements and their first and second time derivatives is proportional to the external force. If the external force is absent ($\mathbf{f} = \mathbf{0}$), this equation describes free oscillations (for example, of a rock sample in the laboratory or the whole Earth) or all types of seismic waves. With a different construction of matrices \mathbf{M} , \mathbf{S} , and \mathbf{D} , these equations describe finite-element models of solid bodies or wave-propagating media. Because relations (4.12) and (4.13) are so general, they apply to fluid-saturated media or thermoelastic effects.

⁸ This is why viscoelastic models (disregarding the GLS matrix \mathbf{d} and replacing it with $\boldsymbol{\eta}$) are always successful in matching $M(f)$ spectra from experiments with rock samples in the laboratory. The average effect of Darcy friction (\mathbf{d}) is presented as that of $\boldsymbol{\eta}$ in, for example, Maxwell’s or Zener’s viscoelastic model. Similarly, effects of thermoelastic heat dissipation can always be interpreted as caused by “wave-induced fluid flows”, i.e. pure mechanical friction (matrix $\boldsymbol{\eta}$). All of these effects are principally contained in matrix \mathbf{D} .

Oscillations of this multidimensional mechanical system take the form of numerous traveling or standing waves. The shape of the specific wave depends on boundary conditions (size and shape of the body) and the location(s) and time dependence of sources $\mathbf{f}(t)$ operating within the medium.

In full-waveform inversion or for modeling forced oscillations of a rock sample in the lab, the time-spatial domain eq. (4.13) is often transformed into the frequency-spatial (“ f - x ”) domain. This transformation is done by replacing the time derivatives of any function y by $\frac{dy}{dt} = -i\omega y$ (this means that all time dependencies are of the form $y(t) = y_0 e^{-i\omega t}$). Equation (4.13) then becomes the inhomogeneous Helmholtz equation:

$$\left(-\omega^2 \mathbf{M} - i\omega \mathbf{D} + \mathbf{S}\right) \mathbf{q} = \mathbf{f}_\omega, \quad (4.14)$$

where \mathbf{f}_ω is the Fourier component of the external force at frequency ω . Combined with the appropriate boundary conditions, these equations can be solved by matrix inverse:

$$\mathbf{q} = \mathbf{G} \mathbf{f}_\omega, \quad (4.15)$$

where

$$\mathbf{G} = \left(-\omega^2 \mathbf{M} - i\omega \mathbf{D} + \mathbf{S}\right)^{-1}, \quad (4.16)$$

is the frequency-domain response function for the mechanical system.

In practice, evaluation of this inverse of a large matrix requires some effort, such as evaluation of the singular-value decomposition and including the boundary and “radiation” conditions. The product $\mathbf{q} = \mathbf{G} \mathbf{f}$ can also be found in the time domain, by time-stepping the differential equations (4.13). These numerical modeling methods will be described in the next sections.

In the viscoelastic approach, the specific dependence of the terms $(\mathbf{S} - i\omega \mathbf{D})$ on frequency in eq. (4.14) is abandoned, and this combination is replaced with the “viscoelastic modulus”:

$$\mathbf{S} - i\omega\mathbf{D} \rightarrow \mathbf{S}(\omega) \stackrel{\text{def}}{=} \mathbf{S}_{\text{elastic}} \left[\mathbf{I} - i\mathbf{Q}^{-1}(\omega) \right], \quad (4.17)$$

where $\mathbf{S}_{\text{elastic}}$ is the rigidity matrix for an “elastic” model which would exist in the absence of attenuation, and \mathbf{Q}^{-1} is a diagonal matrix of “inverse Q -factors” defined at every point within the subsurface. The frequency dependence of $\mathbf{Q}^{-1}(\omega)$ is generally arbitrary, and it may be estimated from well-log or laboratory experiments. However, most commonly, \mathbf{Q}^{-1} is taken as constant within the frequency band. Note that this frequency dependence is drastically different from the linear dependence $\omega\mathbf{C}$ in eq. (4.14) and therefore, the “constant- Q ” model disagrees with the basic physics described above. Nevertheless, this model is used in most seismic wave modeling and inversion software.

4.5.1 Quasi-static variables

When performing time stepping the dynamic system using eq. (4.13), the accelerations have to be evaluated as

$$\ddot{\mathbf{q}} = \mathbf{M}^{-1}(\mathbf{f} - \mathbf{S}\mathbf{q} - \mathbf{D}\dot{\mathbf{q}}). \quad (4.18)$$

In some cases, the inverse \mathbf{M}^{-1} does not exist, and some combinations of variables cannot be inverted from this expression. This uncertainty occurs for combinations of variables \mathbf{q}_{QS} representing zero or negligibly small eigenvalues of matrix \mathbf{M} , i.e. \mathbf{q}_{QS} satisfying relation $\mathbf{M}\mathbf{q}_{\text{QS}} = \mathbf{0}$. These massless variables can be called quasi-static (and hence the notation), which means that that they near-instantaneously equilibrate with the applied elastic and friction forces, and their inertial forces are negligible. Important examples of such variables \mathbf{q}_{QS} are the divergent fluid flows within microcracks in squirt-flow models or thermoelastic temperature perturbations within a grainy solid. These examples will be considered in chapter 7.

Although the problem of nonexistent matrix \mathbf{M}^{-1} can be alleviated by using some pseudo-inverse of \mathbf{M} , a more reliable way of treating this problem is to utilize the quasi-static variables explicitly. In the following subsections, I show how dynamic (with mass) and quasi-static (massless) variables can be separated and obtain separate time-stepping

equations for each of these groups.

Separation of dynamic and quasi-static variables

We will differentiate between massless and with-mass modes of deformation by zero and nonzero (significant) eigenvalues of matrix \mathbf{M} . Each of these subsets is represented by all possible linear combinations the respective eigenvectors of matrix \mathbf{M} . For example, let us denote the number of elements of vector \mathbf{q} by N and assume that the quasi-static subspace contains N_{QS} eigenvectors. An arbitrary quasi-static deformation can be described by an N_{QS} -element vector \mathbf{q}_{QS} containing magnitudes of displacement for each of the quasi-static modes. Let us define an N by N_{QS} matrix \mathbf{E}_{QS} with columns containing unit vectors in the direction of each of the quasi-static eigenvectors. Then, in the model space, the above quasi-static deformation will be given by matrix product

$$\mathbf{q} = \mathbf{E}_{QS} \mathbf{q}_{QS}. \quad (4.19)$$

Inversely, for an arbitrary model vector \mathbf{q} , matrix product

$$\mathbf{q}_{QS} = \mathbf{E}_{QS}^T \mathbf{q}, \quad (4.20)$$

(where T denotes the matrix transpose) gives the contribution from each of the quasi-static modes in the total deformation \mathbf{q} . Combining these operations extracts from an arbitrary deformation \mathbf{q} its quasi-static part \mathbf{q}' (which is still a N -element vectopr in the complete model space):

$$\mathbf{q}' = \mathbf{E}_{QS} \mathbf{E}_{QS}^T \mathbf{q}. \quad (4.21)$$

Subtraction

$$\mathbf{q} - \mathbf{q}' = (\mathbf{I} - \mathbf{E}_{QS} \mathbf{E}_{QS}^T) \mathbf{q}, \quad (4.22)$$

removes the quasi-static modes from vector \mathbf{q} and leaves only the dynamic ones. This relation can also be written as $\mathbf{q}' = \mathbf{E}_{DYN} \mathbf{E}_{DYN}^T \mathbf{q}$, where \mathbf{E}_{DYN} is a matrix of all normalized

eigenvectors for dynamic modes.

The transformation matrix \mathbf{E}_{QS} also transforms expressions for various types of energies and dissipation functions. For example, if the elastic energy is given by the stiffness-matrix quadratic form (eqs. (4.12)) $U = \frac{1}{2} \mathbf{q}^T \mathbf{S} \mathbf{q}$, then the part of elastic energy belonging to the quasi-static modes equals $U_{\text{QS}} = \frac{1}{2} \mathbf{q}_{\text{QS}}^T \mathbf{S}_{\text{QS}} \mathbf{q}_{\text{QS}}$, where the quasi-static stiffness matrix is (from eq. 4.19))

$$\mathbf{S}_{\text{QS}} = \mathbf{E}_{\text{QS}}^T \mathbf{S} \mathbf{E}_{\text{QS}}. \quad (4.23)$$

Time-stepping equations

To obtain differential equations suitable for time-stepping the system with dynamic and quasi-static modes, we can isolate the terms with highest time derivatives in eq. (4.13) and project them onto the respective subspaces of deformation modes. Let us represent the model as a sum of dynamic (with mass) and quasi-static (massless) deformations:

$$\mathbf{q} = \mathbf{E}_{\text{DYN}} \mathbf{q}_{\text{DYN}} + \mathbf{E}_{\text{QS}} \mathbf{q}_{\text{QS}}. \quad (4.24)$$

Note that the two subspaces are orthogonal, so that $\mathbf{E}_{\text{DYN}}^T \mathbf{E}_{\text{QS}} = \mathbf{0}$ and $\mathbf{E}_{\text{QS}}^T \mathbf{E}_{\text{DYN}} = \mathbf{0}$.

For dynamic modes, time-stepping equations can be obtained by left-multiplying eq. (4.13) with matrix $\mathbf{E}_{\text{DYN}}^T$ and using eq. (4.24) in the left-hand side, which gives

$$\mathbf{M}_{\text{DYN}} \ddot{\mathbf{q}}_{\text{DYN}} = \mathbf{E}_{\text{DYN}}^T (\mathbf{f} - \mathbf{D}\dot{\mathbf{q}} - \mathbf{S}\mathbf{q}). \quad (4.25)$$

where $\mathbf{M}_{\text{DYN}} = \mathbf{E}_{\text{DYN}}^T \mathbf{M} \mathbf{E}_{\text{DYN}}$. The $N_{\text{DYN}} \times N_{\text{DYN}}$ matrix \mathbf{M}_{DYN} is invertible, and therefore vector \mathbf{q}_{DYN} can be incremented using acceleration

$$\ddot{\mathbf{q}}_{\text{DYN}} = \mathbf{M}_{\text{DYN}}^{-1} \mathbf{E}_{\text{DYN}}^T (\mathbf{f} - \mathbf{D}\dot{\mathbf{q}} - \mathbf{S}\mathbf{q}). \quad (4.26)$$

For quasi-static modes, the mass term vanishes after the projection, and the leading

time derivative comes from the mechanical-friction or heat dissipation term:

$$\mathbf{D}_{\text{QS}} \dot{\mathbf{q}}_{\text{QS}} = \mathbf{E}_{\text{QS}}^T (\mathbf{f} - \mathbf{S}\mathbf{q}), \quad (4.27)$$

where $\mathbf{D}_{\text{QS}} = \mathbf{E}_{\text{QS}}^T \mathbf{D} \mathbf{E}_{\text{QS}}$. This matrix should also be invertible, and vector \mathbf{q}_{QS} can be incremented using its generalized velocity

$$\dot{\mathbf{q}}_{\text{QS}} = \mathbf{D}_{\text{QS}}^{-1} \mathbf{E}_{\text{QS}}^T (\mathbf{f} - \mathbf{S}\mathbf{q}). \quad (4.28)$$

Frequency-domain form

In frequency domain, the quasi-static approximation of eq. (4.15) is obtained directly by dropping the mass term:

$$\mathbf{q} = (-i\omega \mathbf{D} + \mathbf{S})^{-1} \mathbf{f}_\omega. \quad (4.29)$$

This matrix equation describes the stationary motion of a damped multidimensional linear oscillator under low-frequency, harmonically oscillating loading. In particular, this equation can be used to model subresonant experiments with rock samples (see chapter 7). At low frequencies, inertial forces are negligible, and elastic forces are balanced by viscous ones.

4.6 Oscillations and waves

Let us return to the general equation of frequency-domain deformation in the mass-stiffness-damping form (eq. 4.14):

$$(-\omega^2 \mathbf{M} - i\omega \mathbf{D} + \mathbf{S}) \mathbf{q} = \mathbf{f}_\omega. \quad (4.14 \text{ repeated})$$

In the absence of the source in the right-hand side ($\mathbf{f} = \mathbf{0}$; ‘homogeneous’ equation), solutions of this equation represent free oscillations. For an infinite medium, these oscillation patterns travel in space and form waves. For a finite body, these waves reflect from boundaries and form a complex spatial pattern synchronously oscillating in time.

These waves interfere constructively at a set of resonance frequencies ω_n , where $n = 0, 1, 2, \dots$ is the free oscillation mode number. The lowest-frequency oscillation with $n = 0$ is called the fundamental mode. The n^{th} mode is described by the generalized eigenvalue problem:

$$\omega_n^2 \mathbf{M} \mathbf{q}^{(n)} = (\mathbf{S} - i\omega_n \mathbf{D}) \mathbf{q}^{(n)}, \quad (4.30)$$

where vector $\mathbf{q}^{(n)}$ gives the spatial distribution of the oscillation/wave mode, and ω_n is its frequency. Because of the matrix character of this eigenvalue equation, it is only satisfied by certain vectors $\mathbf{q}^{(n)}$ (eigenvectors, or eigenmodes), and ω_n^2 above is the eigenvalue corresponding to the n^{th} mode. In the next section and chapter 7, I give several specific forms of this general equation and its solutions.

Plane-wave dispersion and attenuation

To characterize the mechanical behaviour of materials, two types of experiments with certain types of oscillations are often used: plane waves in homogeneous media and low-frequency forced harmonic oscillations. For plane waves, measurement of wave velocities at variable frequencies leads to observations of velocity dispersion (frequency dependence $V(f)$) and attenuation (attenuation coefficient $\alpha(f)$). For forced oscillations, another pair of parameters is used: the effective modulus (stress/strain ratio) $M(f)$ and strain-stress phase lag, or Q-factor $Q(f)$ ⁹. In this subsection, I consider the plane-wave case on the general example of a MSDT medium (eq. 6.29).

For a plane harmonic wave at angular frequency ω traveling in a homogeneous medium, the spatial shape of the wave is determined by equation (4.14), which becomes in this case

⁹ In fact, when interpreting low-frequency laboratory experiments, effective moduli and Q are also often defined for waves using elastic relations like $V = \sqrt{M/\rho}$. However, this elastic relation is invalid for rock with $N > 1$, simply because there exist multiple types of M , multiple ρ , and multiple wave modes in such rock. In addition, for waves, the primary attenuation factors are the geometric spreading and scattering, which need to be accounted for before evaluate These factors are extremely variable and strongly different for traveling waves and rock samples in laboratory. Therefore, the moduli and Q inferred for waves need to be understood very carefully (and often skeptically) in each specific case.

$$\left(-\omega^2\bar{\mathbf{M}} - i\omega\bar{\mathbf{D}} + \bar{\mathbf{S}}\right)\mathbf{q} = \mathbf{0}. \quad (4.31)$$

This is an eigenvalue equation for \mathbf{q} , with the eigenvalue required to equal zero. There are generally as many solutions to this equation as the number of independent variables in vectors \mathbf{q} and \mathbf{q}_T combined minus one. The one missing mode is due to the invariance of all equations with respect to a constant shift in all temperatures (because temperatures enter all equations only through spatial and time derivatives).

At an arbitrary angular frequency $\omega = 2\pi f$, the spatial dependence of all variables in the plane wave can be written as $\mathbf{q}(t) = \mathbf{q}_0 e^{ikx}$, where k is the generally complex-valued wavenumber. For example, for a wave traveling forward along axis X , $\text{Re } k > 0$ and the amplitudes decay also forward, which means that $\text{Im } k \geq 0$. The real and imaginary parts of k give the wavelength and attenuation coefficient:

$$\lambda = \frac{2\pi}{\text{Re } k}, \quad \text{and} \quad \alpha = \frac{1}{\text{Im } k}, \quad (4.32)$$

and the phase and group velocity

$$V = \lambda f = \frac{\omega}{\text{Re } k}, \quad \text{and} \quad U = \frac{d\omega}{d(\text{Re } k)}. \quad (4.33)$$

For a MSDT medium, parameter k is embedded in matrices $\bar{\mathbf{S}}$ and $\bar{\mathbf{D}}$, which contain spatial derivatives (through matrices \mathbf{S} , \mathbf{D} , Ψ , and \mathbf{A}), and therefore solving eq. (4.31) for zero eigenvalues yields the wave modes and the corresponding wavenumbers k at frequency ω . In the resulting $k(\omega)$ dependence, characteristic dispersion and attenuation patterns are associated with different variables. This dependence can be described by several general features:

- 1) In the zero-frequency limit, the deformation is elastic and satisfies equation $\bar{\mathbf{S}}\mathbf{q}_0 = \mathbf{0}$. Due to the specific form of matrix $\bar{\mathbf{S}}$ with respect to the temperature variables, this equation is satisfied only with $\mathbf{q}_{T0} = \text{const}$, which means that the quasi-static limit is isothermal (thermal equilibrium).

- 2) If mechanical friction is present in the medium through a nonzero matrix \mathbf{D} , then its action on the low-frequency eigenmodes \mathbf{q}_0 will be can be characterized by an effective viscoelastic modulus $\mathbf{S}^* = \mathbf{S} - i\omega\mathbf{D}$, as $\mathbf{S}^*\mathbf{q}_0 = (\mathbf{S} - i\omega\mathbf{D})\mathbf{q}_0$. This means that the effective modulus, $V(\omega)$, and $\alpha(\omega)$ will increase with frequency as ω^2 (as common with viscous friction).
- 3) In many cases, the mass and damping (viscosity and thermal) matrices are such that there exist deformation modes (eigenvectors) \mathbf{q}_{hi} with zero eigenvalues of matrix $\bar{\mathbf{M}}^{-1}\bar{\mathbf{S}}\mathbf{q}_{hi} = \mathbf{0}$. Such modes represent the high-frequency limit of wave deformation. Note that these modes are also elastic. For example, such modes correspond to fluid flows between two sets of pores (s squirt or saturation-patch flows) or heat flows between pores and/or grains within the material. For variables \mathbf{q}_T , the above condition can be expressed as $\mathbf{C}\dot{\mathbf{q}}_T = -\Psi\mathbf{q}_T - \mathbf{A}\mathbf{q} = \mathbf{0}$, which means zero heat flows between parts of the medium. The deformation regime with zero heat flows is called adiabatic.

4.7 Examples

To illustrate the Lagrangian models above, let us consider an elementary example of a linear oscillator and then extend it to a more realistic structure.

4.7.1 Linear oscillator with damping

The damped linear oscillator is the simplest system exhibiting mechanical energy dissipation. Most characteristics of attenuative processes, including the definition of Q , arise from either explicit inferences or implicit analogies to this system. The concept of the linear oscillator is a mathematical abstraction belonging to the field of theoretical mechanics (Landau and Lifshitz, 1976), however, its realizations are pervasive in nearly every area of physics and engineering, such as mechanics, electrodynamics, optics, and quantum mechanics.

A linear oscillator is a mechanical system described by only two parameters, which are its mass m and the natural frequency ω_0 . These parameters are factors of the functional

forms for the kinetic and potential energies, respectively. The energy forms are quadratic with respect to both the displacement, \mathbf{r} , and velocity, $\dot{\mathbf{r}}$, and the Lagrangian is:

$$L(\mathbf{r}, \dot{\mathbf{r}}) = \frac{m}{2} \dot{\mathbf{r}}^2 - \frac{m\omega_0^2}{2} \mathbf{r}^2. \quad (4.34)$$

The energy of the oscillator is then:

$$H = \dot{\mathbf{r}} \frac{\partial L}{\partial \dot{\mathbf{r}}} - L = \frac{m}{2} \dot{\mathbf{r}}^2 + \frac{m\omega_0^2}{2} \mathbf{r}^2. \quad (4.35)$$

The energy is preserved in time, and the oscillator's movement consists of infinite oscillations at frequency ω_0 near the point $\mathbf{r} = 0$.

In order to introduce energy dissipation in this system, a “damping,” or viscous-friction force is required. For slow flows in fluids, the (Newtonian) friction force is proportional and directed opposite to the velocity. By using the two oscillator parameters, such force can be expressed through a dimensionless constant ξ :

$$\mathbf{f}_D = -\xi m \omega_0 \dot{\mathbf{r}}. \quad (4.36)$$

In a variational formulation, this force is described by the Rayleigh dissipation function:

$$D = \xi \omega_0 \frac{m}{2} \dot{\mathbf{r}}^2 = \xi \omega_0 E_k. \quad (4.37)$$

Note that the oscillator's dissipation function is proportional to its *kinetic energy* E_k . Half of the proportionality factor between E_k and D is the attenuation coefficient, $\chi = \omega_0 \xi / 2$ (Figure 4.1; section 4.9 below), and its inverse is the “relaxation time,” $\tau_0 = 1/\chi$.

With the above Lagrangian and dissipation functions, the differential equation of motion becomes:

$$m\ddot{\mathbf{r}} = -m\omega_0^2 \mathbf{r} - \xi m \omega_0 \dot{\mathbf{r}}. \quad (4.38)$$

For weak dissipation ($\xi \ll 1$), its general solution is

$$\mathbf{r}(t) = \text{Re} \left[\mathbf{A} \exp(-i\omega_0^* t) \right], \quad (4.39)$$

where the complex-valued frequency is (see section 4.9)

$$\omega_0^* \approx \omega_0 \left(\pm 1 - \frac{i\xi}{2} \right), \quad (4.40)$$

and \mathbf{A} is an arbitrary complex-valued amplitude. Because \mathbf{r} is real-valued, it is sufficient to consider only the solution with non-negative $\omega_0 = \text{Re } \omega_0^*$ (for negative frequency, we have $A(-\omega_0) \equiv A^*(\omega_0)$; the asterisk denotes complex conjugation here; section 2.3). The imaginary part of ω_0^* describes the logarithmic amplitude decrement of the free oscillation with time. Similar complex frequencies arise for the Earth's normal modes, surface waves, and in lab attenuation measurements using standing waves.

With the use of the complex frequency and $\mathbf{r}(t)$, eq. (4.38) takes the form of the free-oscillator eq. (4.37):

$$m\ddot{\mathbf{r}} = -m\omega_0^{*2}\mathbf{r}. \quad (4.41)$$

If an external force $f(t)$ is added to the right-hand side of eq. (4.38), then:

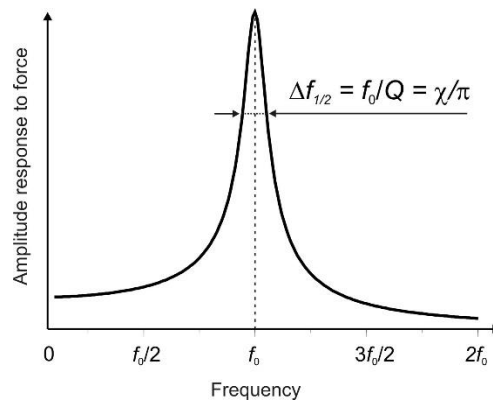


FIGURE 4.1

Definition of the quality factor for a linear oscillator. In a steady-state oscillation, Q measures the relative width of the resonance peak: $\Delta f = f_0/Q$, defined at the level of $1/\sqrt{2}$ of the maximum amplitude. Example with $Q = 10$ shown.

$$A(\omega) = \frac{f(\omega)}{m} \Lambda(\omega), \quad (4.42)$$

where the shape of its frequency-domain response to $f(\omega)$ is determined by the complex frequency alone,

$$\Lambda(\omega) = \frac{1}{\omega_0^{*2} - \omega^2}. \quad (4.43)$$

Thus, the displacement-amplitude response to a harmonic force exhibits a spectral peak centered at ω_0 , with parameters χ and $\xi (= Q^{-1})$ controlling its absolute and relative widths, respectively (Figure 4.1). Note that in practical observations, it is the *absolute* width of the spectrum that is measured, and Q only inferred from it. In terms of χ , eq. (4.43) reads:

$$\Lambda(\omega) = \frac{1}{\omega_0^2 - 2i\chi\omega - \omega^2}. \quad (4.44)$$

This expression allows measuring χ in the observed power spectra by fitting, for example, the following normalized density function to the observed power spectrum:

$$|\tilde{\Lambda}(\omega)|^2 = \frac{1}{\left(\frac{\omega_0^2 - \omega^2}{2\omega_0\chi}\right)^2 + 1}. \quad (4.45)$$

Exercises

From eq. (4.44) for forced oscillations at frequency ω , express, as functions of time:

- 1) Kinetic energy E_k ;
- 2) Potential energy E_p ;
- 3) Total mechanical energy $E_{mech} = E_p + E_k$;
- 4) Averages of the above quantities over an oscillation period,

denoted \bar{E}_p , \bar{E}_k , and \bar{E}_{mech} .

5) Mechanical-energy decay rate $\dot{\bar{E}}_{mech} = \frac{d\bar{E}_{mech}}{dt}$;

6) Attenuation coefficient $\chi = -\frac{\dot{\bar{E}}_{mech}}{\bar{E}_{mech}}$.

Show that the time-averaged kinetic energy is related to the average potential energy as $\bar{E}_k = (\omega/\omega_0)^2 \bar{E}_p$.

Note that the kinetic and potential energies equal each other only at the natural frequency ($\omega = \omega_0$). This criterion can be used for determining the natural frequency ω_0 . This is also one of the reasons for the difficulties with defining a Q factor for forced oscillations.

The inverse quantity $1/\Lambda(\omega)$ to eq. (4.44) gives the stress/strain ratio (Figure 4.2), which can be compared to the empirical moduli and Q -factors for viscoelastic solids

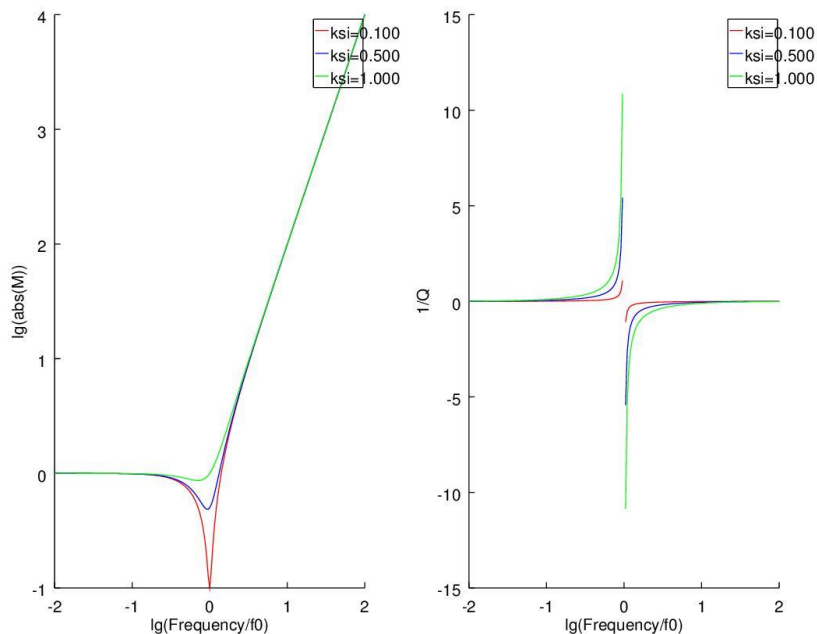


FIGURE 4.2

Logarithm of the complex magnitude (left) and Q -factor (right) of the stress to strain ratio for a mechanical oscillator with three values of ξ (legend).

(chapters 1 and 2). Near the resonance frequency, the stress/strain response drops for lower ξ , and at large frequencies, the response increases proportionally to f^2 (Figure 4.2a). The Q factor increases near linearly at low frequencies, and above ω_0 , it becomes negative (because of the negative real part of $\Lambda(\omega)$ and phase lag close to 180°).

4.7.2 Linked oscillators

A system of interlinked linear oscillators (multidimensional oscillator) represents a close analogy to the elastic medium, and it helps understanding the behavior of a rock sample in the laboratory or causes of multiple types of waves in the field. In this section, I explain how the spectra of oscillations and the various observable quantities in such systems can be modeled. This modeling can also be viewed as a simplified approach to “digital rock”.

Consider a network of linear damped oscillators connected with springs and dampers. Such systems can be drawn as graphs with vertices corresponding to the masses and displacements, and edges representing deformations (strains) (Figure 4.3). Springs of this graph correspond to the elastic-energy terms in the Lagrangian and dashpots denote the terms in the dissipation function. Let us denote the (X, Y) coordinates of the masses as the generalized coordinates, with zero values corresponding to the state of equilibrium. Both the kinetic and potential energies are quadratic functions of these coordinates, which can be expressed in the MSD form (section 4.5) as

$$E_k = \frac{1}{2} \dot{\mathbf{q}}^T \mathbf{M} \dot{\mathbf{q}} \quad \text{and} \quad E_p = \frac{1}{2} \mathbf{q}^T \mathbf{S} \mathbf{q}, \quad (4.46)$$

respectively. Both of the above forms must be symmetric and positive definite, and therefore all eigenvalues of both \mathbf{M} and \mathbf{S} are non-negative. Furthermore, the kinetic energy is always positive, and consequently matrix \mathbf{M} has no zero eigenvalues and has an inverse, \mathbf{M}^{-1} .

For a harmonic oscillation at frequency ω , each of the coordinates varies as $q_i(t) = \hat{q}_i \sin(\omega t + \varphi_i)$, and the distribution of amplitudes $\hat{\mathbf{q}}$ and frequency ω given by the eigenvalue equation from section 4.5:

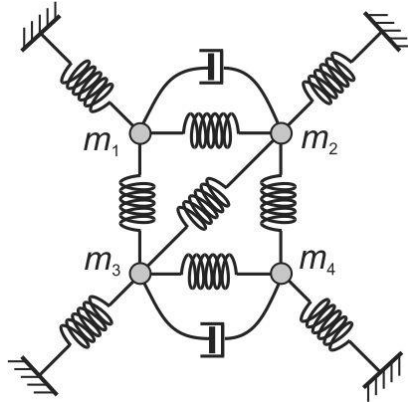


FIGURE 4.3
Four interlinked linear damped oscillators illustrating a complex mechanical system.

$$(\omega^2 \mathbf{M} - \mathbf{S}) \hat{\mathbf{q}} = 0. \quad (4.47)$$

This relation means that $\hat{\mathbf{q}}$ represent an eigenvector of matrix $\mathbf{M}^{-1}\mathbf{S}$, with ω^2 being the corresponding (always non-negative) eigenvalues. The number of such modes equals the number of degrees of freedom in the system (for example, twice the number of masses for 2-D oscillations in Figure 4.3). However, some of the modes may be degenerate, *i.e.* having equal values of ω . For each mode, the total, time-averaged mechanical energy equals:

$$\bar{E}_{mech} = \frac{1}{2} \hat{\mathbf{q}}^T (\omega^2 \mathbf{M} + \mathbf{S}) \hat{\mathbf{q}}. \quad (4.48)$$

Newtonian dissipation in such a system (dashpots in Figure 4.3) is also given by a symmetric, positive definite quadratic form:

$$D = \frac{1}{2} \dot{\mathbf{q}}^\dagger \mathbf{D} \dot{\mathbf{q}}, \quad (4.49)$$

(with complex-valued \mathbf{q} , we have to use Hermitian conjugation instead of the transpose) so that the time-average energy increase (dissipation) rate for the selected mode equals:

$$\dot{\bar{E}}_{mech} = -\frac{1}{t} \int_0^t \dot{q}_i \frac{\partial D}{\partial \dot{q}_i} d\tau = -\frac{\omega^2}{2} \hat{\mathbf{q}}^\dagger \mathbf{D} \hat{\mathbf{q}}. \quad (4.50)$$

Therefore, the attenuation coefficient and the Q for the selected mode are:

$$\chi = \frac{-\dot{\hat{E}}_{mech}}{2\hat{E}_{mech}} = \frac{\omega^2}{2} \frac{\hat{\mathbf{q}}^\dagger \mathbf{D} \hat{\mathbf{q}}}{\hat{\mathbf{q}}^\dagger (\omega^2 \mathbf{M} + \mathbf{S}) \hat{\mathbf{q}}}, \text{ and } Q = \frac{\omega}{2\chi}. \quad (4.51)$$

Equations (4.51) should not be understood as $\chi \propto \omega^2$ and $Q \propto \omega^{-1}$, because ω here is a constant determined by the selected mode $\hat{\mathbf{q}}$. However, if pairs (ω, Q) are compiled across the different modes, an approximate “scaling relation” $Q(\omega)$ may appear (see Lab 4.2). Similar empirical relations are commonly observed, for example, for the Earth’s free oscillations, surface waves, and also the well-known general “frequency dependence of Q .” This frequency dependence is believed to be $Q \propto \omega^{0.15-0.4}$ for all waves and across the entire seismic frequency band.

Above, we considered the case of weak dissipation and did not include the effect of D on shifting the resonant frequencies. If operator \mathbf{D} is not diagonal on the eigenvectors of matrix $\mathbf{M}^{-1}\mathbf{S}$, dissipation would also intermix the modes, and the motion may no longer be harmonic.

4.8 Equipartitioning of energy

Equation (4.47) shows that for a normal mode in any system (standing wave), the energy is equipartitioned, so that the average kinetic energy equals the average potential energy. This equality of the kinetic and potential energies in a wave is sometimes called the Rayleigh principle.

Because the kinetic energy is proportional to ω^2 , the oscillation eigenfrequency ω_0 , can be determined from the energy equipartitioning using the ratio of the time-averaged potential and kinetic energies \hat{E}_p and \hat{E}_k evaluated for the appropriate distribution of amplitudes $\hat{\mathbf{q}}$ but taken at frequency $\omega = 1$:

$$\omega_0 = \sqrt{\frac{\hat{E}_p}{\hat{E}_k}}, \quad (4.52)$$

With the average potential and kinetic energies being equal, their spatial distributions and time dependencies differ for oscillations of a finite body or in a traveling wave (Figure 4.4). In a body, the oscillation is a standing wave, in which the energies oscillate at frequency 2ω , the kinetic energy is opposite in phase relative to the potential one, and their sum is constant (Figure 4.4a). By contrast, in a wave traveling in a homogeneous medium, the kinetic and potential energies equal each other at any time and point (Figure 4.4b). The whole pattern of energy highs and lows travels with the wave.

4.9 Attenuation coefficient

In the viscoelastic model, the above calculation of the eigenfrequency is also extended to attenuation, although at the expense of making the moduli, energies, and action complex-valued. Because \hat{E}_p is proportional to the elastic moduli (spring constants k in our examples in Figure 4.3), a shift of each modulus into the complex plane, $k \rightarrow k - ik/Q_k$ would accordingly shift the potential energy of the mode: $\hat{E}_p \rightarrow \hat{E}_p + i \text{Im} \hat{E}_p$ (where $\text{Im} \hat{E}_p < 0$, and I retain the notation \hat{E}_p for $\text{Re} \hat{E}_p$ for brevity). The eigenfrequency (4.52) would then attain a negative imaginary part (for weak energy dissipation, $\text{Im} \hat{E}_p \ll \hat{E}_p$), which we denote $(-\chi)$. The complex-valued angular frequency of the oscillation is therefore

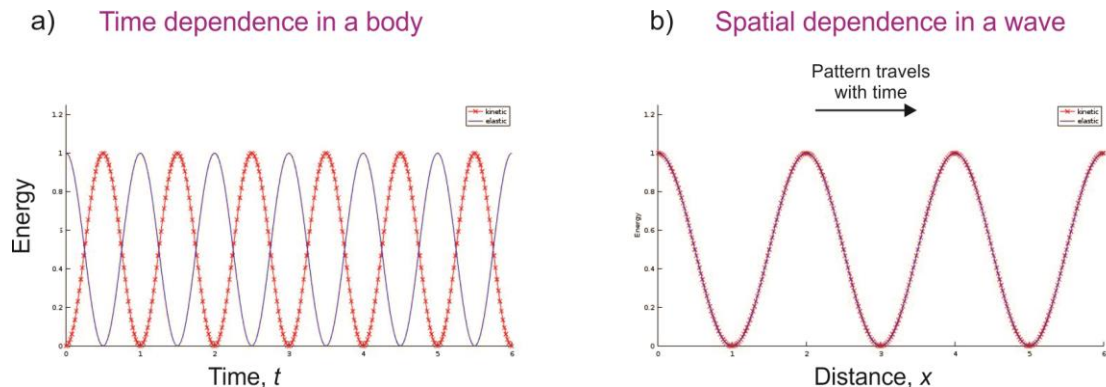


FIGURE 4.4

Equipartitioning of elastic and kinetic energies during harmonic oscillations: a) time dependencies in a body, b) distance dependencies in a wave. Blue line is the elastic energy, and red line with crosses is the kinetic energy.

$$\omega_0 \approx \omega'_0 - i\chi. \quad (4.53)$$

where ω'_0 is the ordinary angular frequency of the oscillation. This quantity χ is the temporal attenuation coefficient

$$\chi \approx \omega'_0 \frac{\text{Im} \widehat{E}_p}{2\widehat{E}_p}. \quad (4.54)$$

Quantity χ describes the logarithmic decay of oscillation amplitude with time. For an oscillation at frequency ω_0 , the amplitude decreases with time as

$$A(t) = A(0)e^{-\chi t}. \quad (4.55)$$

The attenuation coefficient χ is a fundamental quantity which applies not only to the viscoelastic case (eq. 4.54). More generally, 2χ is the ratio of the average total mechanical-energy dissipation rate $\dot{\bar{E}}_{mech}$ to the current level of this average energy \bar{E}_{mech} . This definition simply arises from the amplitude decay in eq. (4.55). Since the energy of the oscillation is proportional to A^2 , it should decay with time as $e^{-2\chi t}$. Therefore, the general definition of the attenuation coefficient is

$$\chi = -\frac{\dot{\bar{E}}_{mech}}{2\bar{E}_{mech}}. \quad (4.56)$$

The Q -factor of a resonator (oscillator, or a given free-oscillation mode) is a secondary quantity defined by taking a ratio of χ to the oscillation frequency:

$$Q^{-1} = \frac{2\chi}{\omega_0}. \quad (4.57)$$

This and other definitions of Q for forced oscillations are discussed in the next section.

In the viscoelastic case (eq. 4.54), the inverse Q -factor (4.57) equals $Q^{-1} \approx \frac{\text{Im} \widehat{E}_p}{\widehat{E}_p}$

However, looking again at eq. (4.51), note that the above “imaginary shift in the potential energy” $\text{Im } \widehat{E}_p = \frac{1}{2} \omega_0^2 D_{ij} \widehat{q}_i \widehat{q}_j$ is produced by the dashpots and is generally unrelated to the elastic or kinetic energies. For example, in the model in Figure 4.3, it is impossible to say how to attribute the effects of the two dashpots to the nine elastic moduli in order to interpret them as “viscoelastic” moduli. Therefore, attenuation should not be linked to elastic moduli or to any other specific part of the mechanical system. Attenuation is a property of the entire deformation of the body, similar to the natural frequency ω_0 .

4.10 Quality factors

For complex mechanical systems like rock, there exist several types of definitions of quality factors. These factors depend on the oscillation mode, the way this oscillation mode is excited by external loading, and also on the general goals of investigation.

4.10.1 Q of a free-oscillation mode

The Q -factor for a linear oscillation mode arises from the time dependence of solution (4.54), as a ratio of its logarithmic decrement to the natural frequency: $Q^{-1} = 2\text{Im}\omega'_0/\text{Re}\omega'_0$, which equals:

$$Q^{-1} = \frac{2\mathcal{X}}{\omega_0} \approx \xi. \quad (4.58)$$

This Q^{-1} is a constant belonging to the entire oscillator and relates to its only natural frequency. Therefore, the Q^{-1} for an oscillation mode has no frequency dependence, and it cannot be attributed to the spring constant k .

4.10.2 Q -factors in forced oscillation experiments

To look at varying frequencies, the concept of Q^{-1} needs to be extended to forced oscillations at non-resonant frequencies. This is not so easy to do. Depending on the ways this extension is performed, the same linear, damped mechanical oscillator can have

multiple “quality factors.” To see them, we need to start from the basic definition of the inverse Q^{-1} as the ratio of the mechanical energy decay in one period, $T\dot{\hat{E}}_{mech}$, to some reference energy level, E_{ref} :

$$Q^{-1} = \frac{1}{2\pi} \frac{-T\dot{\hat{E}}_{mech}}{E_{ref}} = \frac{-\dot{\hat{E}}_{mech}}{\omega E_{ref}}. \quad (4.59)$$

The key question, and also the entire uncertainty here is in the selection of E_{ref} . For forced oscillations, energy is not equipartitioned, and neither E_k , E_p , nor E_{mech} uniquely describe the state of the system. It can neither be said which of these energies truly “dissipates.” Different measures of energy can be used for E_{ref} , leading to several types of Q described in the following subsections.

Kinetic-, potential-, and total-energy based Qs

For example, the above relation of D to kinetic energy suggest that the natural choice for E_{ref} might be the peak *kinetic* energy: $E_{ref} = \hat{E}_k/2$ (denominator 2 here is because we use the peak amplitude of $E_k(t) = \hat{E}_k(1 + \cos 2\omega t)/2$ as a measure of its average level). Therefore, from eq. (4.59), the “*kinetic*” quality factor Q_k is proportional to frequency (Figure 4.5):

$$Q_k = \frac{\omega \hat{E}_k}{2\dot{\hat{E}}_{mech}} = \frac{\omega}{\omega_0} Q. \quad (4.60)$$

Alternately, if we relate the dissipation to the *peak potential* energy, $E_{ref} = \hat{E}_p/2$, as it is done in seismology (Aki and Richards, 2002), then such quality factor becomes inversely proportional to frequency (Figure 4.5):

$$Q_p = \frac{\omega \hat{E}_p}{2\dot{\hat{E}}_{mech}} = \frac{\hat{E}_p}{\hat{E}_k} Q_k = \frac{\omega_0}{\omega} Q, \quad (4.61)$$

because $\hat{E}_p = (\omega_0/\omega)^2 \hat{E}_k$ in a forced oscillation. Next, if we define the quality factor Q_t from

the relative loss of the *peak total mechanical energy*, then:

$$Q_t = \frac{\omega \hat{E}_{mech}}{\dot{\hat{E}}_{mech}} = \begin{cases} Q_p & \text{for } \omega < \omega_0, \\ Q_k & \text{for } \omega \geq \omega_0, \end{cases} \quad (4.62)$$

since \hat{E}_{mech} equals \hat{E}_p or \hat{E}_k for $\omega < \omega_0$ and $\omega \geq \omega_0$, respectively (Figure 4.5).

Further, possibly the most robust choice for E_{ref} in (4.59) could be the *total mechanical energy averaged over a period*. This also corresponds to the definition of viscoelastic Q by Buchen (1971). Peak energies, which are attained only once or twice during a period, rarely have consistent relations with the average $\dot{\hat{E}}_{mech}$. At resonance, $\bar{E}_{mech} = \hat{E}_{mech}$, and for $\omega \neq \omega_0$, the mechanical energy oscillates between \hat{E}_k and \hat{E}_p above, and its average level equals $(\hat{E}_k + \hat{E}_p)/2$. Consequently, we can define the “*average total-energy Q-factor*” as:

$$Q_a = \frac{\omega \bar{E}_{mech}}{\dot{\hat{E}}_{mech}} = \frac{Q_k + Q_p}{2}. \quad (4.63)$$

This seems to be the most logical choice for the oscillator’s Q away from the resonance. Note that it stays near constant for $\omega \approx \omega_0$ (Figure 4.5).

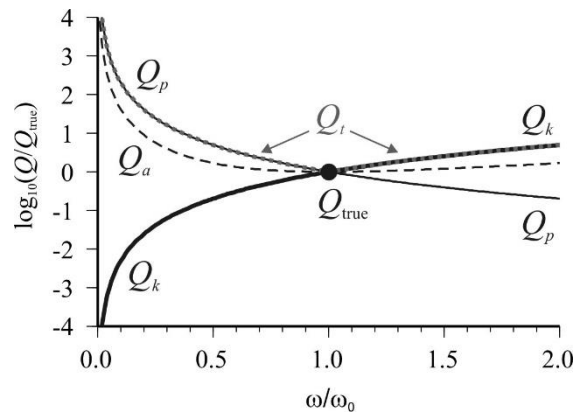


FIGURE 4.5

Frequency dependences for several types of Q definitions (4.60)–(4.63) for a linear driven oscillator. At the resonant frequency $\omega = \omega_0$, all of these values equal the true quality factor (4.58) denoted Q_{true} here.

Strain-stress phase-lag Q

Another definition of Q comes from force-displacement phase lags δ in sub-resonant lab measurements of seismic attenuation and observations of Earth's tides (Agnew, 2009). If we consider a harmonic force $f(t) = \hat{f}e^{-i\omega t}$ and a logarithmic amplitude decay rate χ , then from eq. (4.54), the stationary solution for displacement is

$$u(\omega) = \frac{\hat{f}}{\omega_0^2 - 2i\chi\omega - \omega^2}. \quad (4.64)$$

This displacement lags the force by phase angle δ :

$$\delta = \text{Arg}(\omega_0^2 - \omega^2 + 2i\chi\omega) = \begin{cases} \arctan \frac{2\chi\omega}{\omega_0^2 - \omega^2} & \text{for } \omega < \omega_0, \\ \frac{\pi}{2} & \text{for } \omega = \omega_0, \\ \pi - \arctan \frac{2\chi\omega}{\omega^2 - \omega_0^2} & \text{for } \omega > \omega_0. \end{cases} \quad (4.65)$$

At low frequencies $\omega \ll \omega_0$, the phase lag is nearly proportional to the frequency of the loading force:

$$\delta \approx \frac{2\chi}{\omega_0} \frac{\omega}{\omega_0} = \xi \frac{\omega}{\omega_0}. \quad (4.66)$$

Cotangent of the phase lag δ is usually interpreted as the quality factor in lab observations: (Lakes, 2009):

$$Q_\delta \equiv \frac{1}{\tan \delta}. \quad (4.67)$$

This quantity approximates the quality factors Q_p and Q_t above, and it is inversely proportional to the frequency (Figure 4.5):

$$Q_\delta = \frac{\omega_0^2 - \omega^2}{2\chi\omega} \approx \frac{\omega_0^2}{2\chi\omega} = Q_p. \quad (4.68)$$

4.10.3 Conclusion about Q

As we saw above, a well-defined and meaningful Q -factor only exists for an oscillator (resonator), or oscillation mode for a complex mechanical system. For forced oscillations or waves at variable frequencies, values of Q and their frequency dependencies are sensitive to the measurement procedures and definitions.

Multiple types of forced-oscillation Q -factors can be defined for a linear oscillator, based on somewhat different physical ideas and approximations. Most of these definitions contain strong and variable frequency dependencies (Figure 4.5). These extensions of the “true” resonance Q away from the natural frequency characterize not so much the oscillator itself but mostly our ideas about the energy E_{ref} which we consider to be “dissipating.” However, in reality, friction is not associated with any particular type of energy, and the choice of E_{ref} is only guided by convenience. Therefore, when applied to rocks and oscillatory processes in different environments, the “quality factors” (4.59) and (4.60)–(4.63) should be compared to each other very carefully, because they may represent quite different physical characteristics of the system.

Conventionally, the phase-lag Q (eqs. ((4.67) and (4.68)) is used in laboratory experiments. When using this quantity, note that with this definition, the attenuation Q^{-1} contains an inherent increase proportional to the frequency even for the simplest mechanical system (oscillator). Thus, the material property that can be inferred from such measured $Q^{-1}(f)$ dependence is not Q^{-1} itself but rather its ratio to the observation frequency:

$$\frac{Q^{-1}}{\omega} = \frac{2\chi}{\omega_0^2}. \text{ For a mechanical resonator with damping } \xi \text{ and natural frequency } \omega_0, \text{ this ratio equals } \frac{Q^{-1}}{\omega} = \frac{\xi}{\omega_0}.$$

However, there is also another useful transformation of the measured Q^{-1} , namely transforming it into a frequency-dependent (empirical) attenuation coefficient:

$$\chi(\omega) = \frac{\omega Q^{-1}}{2} = \pi f Q^{-1}. \quad (4.69)$$

This transformation refers to amplitude dependence as a function of travel time t in a

seismic wave: $A(t) = A(0)\exp\left(-\frac{\omega Q^{-1}}{2}t\right) = A(0)\exp[-\chi(\omega)t]$. From seismic amplitude data, it is often found that this $\chi(\omega)$ has a simple dependence on frequency with nonzero limit $\chi(0) = \gamma$:

$$\chi(\omega) \approx \gamma + \omega \frac{Q_e^{-1}}{2} + \omega^2 \frac{\tau}{2} + \dots, \quad (4.70)$$

where Q_e^{-1} is a frequency-independent “effective Q^{-1} ,” and τ is a viscous-relaxation type property (characteristic viscosity divided by characteristic modulus).

4.11 Laboratory assignments

In the following exercises, you will model a simple “digital rock” using the mechanical model in Figure 4.3 (page 101). You can also design a similar model of your own.

Lab 4.1: Model the mechanical system in Figure 4.3

Use **Matlab or Octave to solve** for the spectrum of oscillation frequencies in the system shown in Figure 4.3. Write the program assuming that all masses, spring rigidities, and damping parameters may be different from each other. For example, use adjustable parameter vectors ‘m’, ‘k’, ‘eta’, etc. to hold the respective mechanical parameters.

Then calculate the eigenfrequencies for the case of equal masses, $m = 1$, all spring constants $k = 1$, and both dashpots having $\eta = 0.01$.

Lab 4.2: Calculate the Q spectrum for the system in Figure 4.3

Using results of Lab 0, **calculate numerically** the Q values for each oscillation mode. Plot the dissipation factors Q^{-1} versus frequencies of the mode. Comment on their “frequency dependence.” However, **note** that the dependence is actually not on the frequency but on deformation type within the modes.

Lab 4.3: Model forced oscillations of the system in Figure 4.3

Also using the program of Lab 0, calculate additional averaged properties of the oscillation patterns in Figure 4.3:

- 1) Root mean square (RMS) average of displacements in X and Y directions.
- 2) Average elastic and kinetic energies. Are they equal for each mode?
- 3) Average energy dissipation rate (value of the dissipation function).
- 4) Optional: Construct some other averages, such as eigenvalues of the cross-energy matrix.

Plot these quantities as bar charts versus mode numbers or as graphs versus mode frequencies. When plotting vs. frequency, sort the values by increasing frequencies, so that the graphs look as recorded in an experiment.

5 Lagrangian Mechanics of Macroscopic Solids or Fluids

Key points:

- Macroscopic material properties
- Lagrangian descriptions of isotropic materials
- General Linear Solid (GLS) rheology
- Biot's poroelasticity as a case of GLS
 - Extensions of Biot's model
- Viscoelasticity as a case of GLS
 - GLS forms of viscoelastic linear solids
- Extended generalized standard linear solid
- Effective media and homogenization

Here and below, we consider small and reversible (seismic) deformations of a continuous or discretized elastic medium. For such deformations, displacements u_i (where $i = 1, 2, \text{ or } 3$) at each point $\mathbf{x} = (x, y, z)$ are usually selected as the generalized coordinates. These displacements represent components of displacement vectors $\mathbf{u}(\mathbf{x}, t)$ at each point. As above, the time derivatives are denoted by an overdot, and therefore \dot{u}_i are the generalized velocities. Zero displacements $\mathbf{u} = \mathbf{0}$ corresponds to the state of equilibrium without seismic waves or oscillations.

In analytical mechanics, the problem of obtaining all equations of motion for $\mathbf{u}(\mathbf{x}, t)$ consists in finding the functions $L\{\mathbf{u}, \dot{\mathbf{u}}\}$ and $D\{\mathbf{u}, \dot{\mathbf{u}}\}$. These functions are actually functionals themselves, because their arguments are functions of \mathbf{x} : $\mathbf{u}(\mathbf{x})$ and $\dot{\mathbf{u}}(\mathbf{x})$. These functionals are integrals over the entire volume of the medium: $L\{\mathbf{u}, \dot{\mathbf{u}}\} = \int L dV$ and

$D\{\mathbf{u}, \dot{\mathbf{u}}\} = \int DdV$, where L and D in the integrands are the densities of the Lagrangian and dissipation functions of the medium. For simplicity of notation, I use the same symbols L and D for the density and the total volume integrals. The total action of the elastic field is given by the integration over the whole volume and time interval: $S = \iint LdVdt$.

The definition of functions L and D requires considering the principles of physics, and not merely modifications of mathematics as this may seem from the conventional viscoelastic model. To recognize the possible forms of L and D , we need to identify the meanings of such key concepts as linearity, elastic and kinetic energies, viscous friction, and symmetries, such as the dependence or independence of mechanical properties on spatial locations, orientations, and time. In particular, the linearity and the condition that $\mathbf{u} = \mathbf{0}$ corresponds to an equilibrium (i. e., minimum of the elastic energy) means that functions L and D should be quadratic with respect to \mathbf{u} and $\dot{\mathbf{u}}$. This is a very strong constraint on the possible forms of L and D , and the following considerations show that there exist *only several possible quadratic functional forms* for L and D in an isotropic medium:

- 1) All energies are scalar quantities, which are explicitly independent of the coordinates and time and rotationally-invariant. All energy functions are composed by summations of contributions from the elementary volumes dV within the body (as shown by relations $L\{\mathbf{u}, \dot{\mathbf{u}}\} = \int LdV$ and $D\{\mathbf{u}, \dot{\mathbf{u}}\} = \int DdV$ above).
- 2) The quadratic forms of the kinetic energy T and function D depend on particle velocities \dot{u}_i only, and the quadratic form for U is formulated with respect to displacements u_i .
- 3) The elastic energy U can in principle depend on the displacement \mathbf{u} directly and also on the strain tensor $\varepsilon_{ij} \stackrel{\text{def}}{=} (\partial_i u_j + \partial_j u_i)/2$. Further, because U is a scalar quantity and the medium is isotropic, U can only depend on scalar combinations of u_i and ε_{ij} called rotational invariants of the displacement and strain, respectively. There exist only one such invariant for vector u_i , which

is its square $u_i u_i$. For the strain tensor $\boldsymbol{\varepsilon}$, there are two invariants, which are $\Delta = I_1 \stackrel{\text{def}}{=} \varepsilon_{ii}$ (first order in $\boldsymbol{\varepsilon}$) and $I_2 = \tilde{\varepsilon}_{ij} \tilde{\varepsilon}_{ij}$ (second order), where Δ is the dilatational strain, and $\tilde{\varepsilon}_{ij} \stackrel{\text{def}}{=} \varepsilon_{ij} - (\Delta/3)\delta_{ij}$ is the deviatoric (zero-trace) strain, and summation over all pairs of repeated indices is implied as usual.

- 4) The dissipation function D only depends on the time derivatives and \dot{u}_i (particle velocity) and $\dot{\varepsilon}_{ij}$ (strain rate), also in the form of rotational invariants (for strain rate) similar to Δ and I_2 .

With physical constraints 1) – 4), there are only six possible forms of the terms in functions L (Lagrangian) and D (dissipation-function densities) reduce to only six terms:

$$\begin{cases} L = \frac{\rho}{2} \dot{u}_i \dot{u}_i - \left(\frac{\zeta}{2} u_i u_i + \frac{K}{2} \Delta^2 + \mu \tilde{\varepsilon}_{ij} \tilde{\varepsilon}_{ij} \right), \\ D = \frac{d}{2} \dot{u}_i \dot{u}_i + \left(\frac{\eta_K}{2} \dot{\Delta}^2 + \eta_\mu \dot{\tilde{\varepsilon}}_{ij} \dot{\tilde{\varepsilon}}_{ij} \right). \end{cases} \quad (5.1a)$$

In these expressions, the terms enclosed in parentheses represent the elastic energy (in L) and viscous friction (in D). The coefficients in front of the various combinations of \mathbf{u} and $\boldsymbol{\varepsilon}$ represent the macroscopic material properties. Thus, for an isotropic medium with no internal structure (described only by displacements \mathbf{u} and the corresponding strain), there exist only six possible material properties. Factor ρ is the mass density, and the corresponding term is the kinetic energy density. Factors K and μ are the bulk and shear elastic moduli, respectively. Together with ρ , these terms describe the dynamics of the medium.

The term proportional to $u_i u_i$ in the first eq. (5.1a) would lead to an elastic force returning the medium to the equilibrium point $\mathbf{u} = \mathbf{0}$. For media without internal variables, this term would violate translational invariance, i.e. the invariance with respect to shifting the whole body to a different place. For this reason, the corresponding material property $\zeta = 0$ for a material without internal structure. However, for materials with internal structure (section 5.1), this ζ could be a viable material property.

In function D in eqs. (5.1a), the first term containing factor d describes the first-order linear friction, such as occurring in an acoustic or electrical resonator, or mechanical oscillator in the preceding section. However, although possible, this term (friction with respect to displacement rate without strain) does not seem to occur in media without internal structure, for which we can take $d = 0$. However, this term is most important friction in Biot's poroelastic model, although there, variables u_i also represent vectors in a 2-D model space (section 5.6). Pore-flow effects are likely the dominant internal-friction mechanism for explaining the seismic wave attenuation in sedimentary rock.

Parameters η_K and η_μ in D (eqs. (5.1)) represent the solid viscosity of the rock for dilatations and shear deformations, respectively. Viscosity is the standard mechanism of internal-friction in grainy solids, and metals, and it leads to the well-known Navier-Stokes equations for fluids. In contrast to the first term in function D containing the ground velocity \dot{u}_i , this type of internal friction is caused by the strain rate $\dot{\varepsilon}_{ij}$. Note that the solid viscosity of subsurface rocks was first measured by Ricker in 1941. In in number of papers (e.g., Deng and Morozov, 2016), we showed that the bulk and shear solid viscosities can be produced by "squirt flows" within porous rock with microcracks. This mechanism should be significant in many sedimentary rocks and granite.

Alternatively, the same functions (5.1a) can be expressed using the components of the complete strain tensor ε_{ij} instead of the deviatoric stress $\tilde{\varepsilon}_{ij}$. In this form, the bulk modulus K is replaced with Lamé modulus λ , and a similar replacement is made for the bulk viscosity parameter:

$$\begin{cases} L = \frac{\rho}{2} \dot{u}_i \dot{u}_i - \left(\frac{\zeta}{2} u_i u_i + \frac{\lambda}{2} \Delta^2 + \mu \varepsilon_{ij} \varepsilon_{ij} \right), \\ D = \frac{d}{2} \dot{u}_i \dot{u}_i + \left(\frac{\eta_\lambda}{2} \dot{\Delta}^2 + \eta_\mu \dot{\varepsilon}_{ij} \dot{\varepsilon}_{ij} \right). \end{cases} \quad (5.1b)$$

This representation may be slightly easier to implement in numerical modeling.

5.1 *Media with internal structure (“General Linear Solid”)*

Real rock almost always contains internal structure, such as grains of various shapes and mechanical properties and various pores (partially) saturated with fluids. Macroscopically, these structures can be described by additional internal variables, such as displacements of pore fluids relative to the average rock frame. It was actually our group who proposed a general Lagrangian model for such arbitrary macroscopic structure (several papers by Morozov and Deng since 2016). This model was called the General Linear Solid (GLS), to give a resemblance but also an alternative to the well-known Generalized Standard Linear Solid model (GSLs; see chapter 2). The GLS is a much more general concept, and it includes the GSLs, all other “linear solids,” Biot’s poroelasticity, and other models with linear elasticity and Newtonian viscosity. I will illustrate these models in sections 5.6 and 0 below.

There are two types of GLS models depending on the character of the additional internal variables recognized within rock. Subsection 5.1.1 describes the case when internal variables have meanings of spatial displacements, such as macroscopic movements of pore fluids, groups of mineral grains, etc. In addition, other internal variables may exist, such as variations of porosity, capillary effects, variations of temperature, electrical charges developing within rock, etc.. Such general internal variables are described in subsection 5.1.2.

5.1.1 GLS with displacement-type internal variables

The first form of the GLS is a straightforward generalization of eqs. (5.1) to media with additional internal variables with meanings of vector displacements. Such vector variables can be movements of pore fluids or displacements of groups of grains within the rock frame. Thus, we can simply consider a mechanical continuum with N vector variables \mathbf{u}_j . The first of these variables is normally the observable displacement \mathbf{u} of a macroscopic point within the material, and others can be the relative displacements of pore fills or some other properties. Equations (5.1) are then generalized to additional matrix products in the N -dimensional space of variables:

$$\begin{cases} L = \frac{1}{2} \dot{\mathbf{u}}_i^T \boldsymbol{\rho} \dot{\mathbf{u}}_i - \left(\frac{1}{2} \mathbf{u}_i^T \boldsymbol{\zeta} \mathbf{u}_i + \frac{1}{2} \Delta^T \mathbf{K} \Delta + \tilde{\boldsymbol{\varepsilon}}_{ij}^T \boldsymbol{\mu} \tilde{\boldsymbol{\varepsilon}}_{ij} \right), \\ D = \frac{1}{2} \dot{\mathbf{u}}_i^T \mathbf{d} \dot{\mathbf{u}}_i + \left(\frac{1}{2} \dot{\Delta}^T \boldsymbol{\eta}_K \dot{\Delta} + \dot{\tilde{\boldsymbol{\varepsilon}}}_{ij}^T \boldsymbol{\eta}_\mu \dot{\tilde{\boldsymbol{\varepsilon}}}_{ij} \right), \end{cases} \quad (5.2)$$

In these equations, all material properties become $N \times N$ matrices: $\boldsymbol{\rho}$ is the density matrix, \mathbf{K} and $\boldsymbol{\mu}$ are the elastic moduli matrices, $\boldsymbol{\eta}_K$ and $\boldsymbol{\eta}_\mu$ are their viscosity counterparts, and (as before) $i, j = 1, 2, 3$ denote the spatial coordinates. Matrices $\boldsymbol{\rho}$, \mathbf{K} , $\boldsymbol{\mu}$, \mathbf{d} , $\boldsymbol{\eta}_K$, and $\boldsymbol{\eta}_\mu$ should be symmetric and positive definite, to ensure that the kinetic and elastic energies are non-negative for *arbitrary* deformations. Similar to the conditions $\zeta = 0$ and $d = 0$ mentioned above, elements ζ_{11} and d_{11} of matrices $\boldsymbol{\zeta}$ and \mathbf{d} (corresponding to the observable deformation of the whole rock) must equal zero. Because one of the matrices $\boldsymbol{\rho}$, \mathbf{d} , $\boldsymbol{\zeta}$, and $\boldsymbol{\eta}$ can always be diagonalized by appropriately selecting the internal variables, model (5.2) contains $N(3N + 2)$ independent mechanical properties.

5.1.2 GLS with arbitrary scalar internal variables

In addition to N displacement-type variables \mathbf{u} in eqs. (5.2), let us consider a vector of N_θ scalar variables $\boldsymbol{\theta}$ representing some macroscopic-scale variations occurring within rock during deformation. For example, for Biot's GLS model considered later (section 5.6) variables $\boldsymbol{\theta}$ would represent local dilatation of the drained rock frame, i.e. rock with drained Biot's pores but potentially containing fluids trapped within parts of the pore volume. Microstructures contributing to such variables may include planar (or other) micropores with "squirt" flows, dilatations of certain mineral-grain assemblages or parts of the pore volume, patches of saturation containing WIFF, capillary effects, or more general effects of viscosity within the drained frame.

Considering only local effects, the contributions from the scalar field $\boldsymbol{\theta}$ to the Lagrangian and dissipation function should contain products $\Delta \boldsymbol{\theta}$, no coupling with the displacement of the rock or pore fluid ($\boldsymbol{\theta} \mathbf{u}$) and no spatial derivatives of internal deformations ($\partial_i \boldsymbol{\theta}$). Focusing on the bulk-deformation terms for brevity, the most general extension of the model in eqs. (5.2) consists in adding the following four quadratic terms

containing $\boldsymbol{\theta}$ and $\dot{\boldsymbol{\theta}}$ to it¹⁰:

$$\begin{cases} L = L_0 + \frac{1}{2} \dot{\boldsymbol{\theta}}^T \boldsymbol{\rho} \dot{\boldsymbol{\theta}} - \frac{1}{2} \boldsymbol{\theta}^T \mathbf{P} \boldsymbol{\theta} + \boldsymbol{\Delta}^T \mathbf{Q} \boldsymbol{\theta}, \\ D = D_0 + \frac{1}{2} \dot{\boldsymbol{\theta}}^T \mathbf{P}' \dot{\boldsymbol{\theta}} - \dot{\boldsymbol{\Delta}}^T \mathbf{Q}' \dot{\boldsymbol{\theta}}, \end{cases} \quad (5.3)$$

where L_0 and D_0 are the Lagrangian and dissipation functions from eqs. (5.2). Here, the $N_\theta \times N_\theta$ matrix \mathbf{P} describes the elastic response of the internal deformations $\boldsymbol{\theta}$, the $N \times N_\theta$ matrix \mathbf{Q} describes its elastic coupling to volumetric strains ($\boldsymbol{\Delta}$), and matrices \mathbf{P}' and \mathbf{Q}' have similar meanings for viscosity and viscous coupling. The signs of the terms containing matrices \mathbf{Q} and \mathbf{Q}' will be clear when we get to the equations of motion.

Equations (5.2) and (5.3) contain all possible combinations of the variables and their time derivatives satisfying the requirements of locality and linearity. The first-order approximation for realistic porous rock is the well-known Biot's model, which is given by selecting $N = 2$, $N_\theta = 0$, and setting material-property matrices $\boldsymbol{\zeta} = \mathbf{0}$, $\boldsymbol{\eta}_K = \boldsymbol{\eta}_\mu = \mathbf{0}$, matrix $\boldsymbol{\mu}$ of a simple form with only one nonzero element, and matrix $\boldsymbol{\rho}$ corresponding to unidirectional ("global") pore-fluid flow (section 5.6 below). Extensions of this selection give numerous other models:

- 1) With $\boldsymbol{\zeta} = \mathbf{0}$, $N > 2$, and $N_\theta = 0$, multiple-porosity and permeability models are obtained.
- 2) With $\boldsymbol{\zeta} = \mathbf{0}$, $N_\theta \geq 1$, *all* squirt-flow, WIFF, and other models of rock containing locally heterogeneous pore-fluid flows. In these cases, the scalar variable θ_i represent different patterns of divergent local flows (i.e. any flows different from a coherent flow defined by variable u_{2i} in Biot's model; cf. section 5.6 below). In particular, if a squirt-flow model is formulated in a macroscopic GLS form, matrix elements Q_{1j} describe the elasticity of J^{th} set of compliant pores, P'_j would be the effect of

¹⁰ Note that variables $\boldsymbol{\theta}$ can also couple with internal displacements and velocities (terms with material properties $\boldsymbol{\zeta}$ and \mathbf{d} in eqs. (5.2)) but we do not consider this coupling here.

viscosity within these pores. Together with matrices \mathbf{P} and \mathbf{Q} , matrix \mathbf{K} contains all effects of the elastic rock frame and Biot's pore fluid.

- 3) With $\zeta \neq \mathbf{0}$ and $N_\theta = 0$, the model should describe phenomena related to partial saturation, such as surface tension (deformations of capillary menisci and contact angles). The same phenomena should likely be described by using $\zeta = \mathbf{0}$ and $N_\theta \geq 1$, with variable θ representing the average shapes or capillary surfaces.
- 4) As shown in general terms in section 4.5 and with physical detail in chapter 6 below, variable θ may include temperature variations caused by thermoelastic effects within grains and pockets of pore fluids. Note that because the pore fluid is compressible (certainly more than rock frame), all WIFF effects are generally accompanied by variations of temperature. Therefore, temperature variables θ_i are closely related to those representing divergent flows, and these variables need generally to be considered together.

Equations (5.3) are invariant with respect to scaling (selection of measurement units) of the internal variables $\theta \rightarrow \mathbf{C}^{-1}\theta$ and material-property matrices $\mathbf{Q} \rightarrow \mathbf{Q}\mathbf{C}$, $\mathbf{P} \rightarrow \mathbf{C}^T\mathbf{P}\mathbf{C}$, $\mathbf{Q}' \rightarrow \mathbf{Q}'\mathbf{C}$, and $\mathbf{P}' \rightarrow \mathbf{C}^T\mathbf{P}'\mathbf{C}$, where \mathbf{C} is an arbitrary diagonal matrix. By utilizing this invariance, we can select variables θ as non-dimensional (analogous to dilatation Δ) and fix the value of the elastic matrix for parameters θ :

$$\mathbf{P} = K_\theta \mathbf{I}, \quad (5.4)$$

where \mathbf{I} is the identity matrix and K_θ is some characteristic (scaling) modulus. For example, for porous rock (Biot's model, section 5.6 below), it is convenient to take this modulus equal the elastic modulus of the drained frame. If thermal effects are included in the model, temperatures would be naturally scaled to this modulus using the specific heat and coefficient of thermal expansion (see chapter 6 for detail).

5.2 Equations of motion

Equations of motion are obtained by taking variational derivatives of separate terms

of the Hamiltonian action $S = \iint L dV dt$ and the corresponding dissipation functional $\iint D dV dt$. For an ordinary macroscopic, isotropic medium without internal variables, Euler derivatives (eq. 4.11) using the functions L and D in eqs. (5.1) (with $\zeta = 0$ and $d = 0$) give partial differential equations of motion for the medium:

$$\rho \ddot{u}_i = \partial_j \sigma_{ij}, \quad (5.5)$$

where σ_{ij} is the stress tensor equal

$$\sigma_{ij} = \left(K \Delta \delta_{ij} + 2\mu \tilde{\epsilon}_{ij} \right) + \left(\eta_K \dot{\Delta} \delta_{ij} + 2\eta_\mu \dot{\tilde{\epsilon}}_{ij} \right). \quad (5.6)$$

In this expression, the first pair of parentheses contains the elastic stress (bulk and shear), and the second pair contains the corresponding parts of the viscous stress.

For a general GLS medium, the above equations remain the same but attain matrix form. For porous rock, material property \mathbf{d} is often important, and I retain it in the equations:

$$\rho \ddot{\mathbf{u}}_i = -\zeta \mathbf{u}_i - \mathbf{d} \dot{\mathbf{u}}_i + \partial_j \sigma_{ij}, \quad (5.7)$$

where the strain-related (elastic and viscous) stress tensor equals:

$$\sigma_{ij} = \left(\mathbf{K} \Delta \delta_{ij} + 2\mu \tilde{\epsilon}_{ij} \right) + \left(\eta_K \dot{\Delta} \delta_{ij} + 2\eta_\mu \dot{\tilde{\epsilon}}_{ij} \right). \quad (5.8a)$$

Using moduli λ , μ , and the corresponding viscosities, this equation can also be written through strain ϵ_{ij} :

$$\sigma_{ij} = \left(\lambda \Delta \delta_{ij} + 2\mu \epsilon_{ij} \right) + \left(\eta_\lambda \dot{\Delta} \delta_{ij} + 2\eta_\mu \dot{\epsilon}_{ij} \right). \quad (5.8b)$$

As shown in the next subsection, matrix differential equations lead to solutions for harmonic waves, which are also of matrix form. Further, spatial discretization of the model makes *all* equations matrix (see sections 4.5 and 5.11).

If scalar deformation variables $\boldsymbol{\theta}$ are used, omnidirectional elastic and viscous stresses are added to eqs. (5.8a and b):

$$\boldsymbol{\sigma}_{ij} \rightarrow \boldsymbol{\sigma}_{ij} + \delta_{ij} (\mathbf{Q}\boldsymbol{\theta} - \mathbf{Q}'\dot{\boldsymbol{\theta}}). \quad (5.8c)$$

and the Euler-Lagrange equation for variables $\boldsymbol{\theta}$ is

$$\boldsymbol{\rho}_\theta \ddot{\boldsymbol{\theta}} = -\mathbf{P}\boldsymbol{\theta} - \mathbf{P}'\dot{\boldsymbol{\theta}} - \mathbf{Q}^T \boldsymbol{\Delta} + \mathbf{Q}'^T \dot{\boldsymbol{\Delta}}. \quad (5.8d)$$

In most applications further in this text, I do not consider¹¹ the elasticity directly related to displacement \mathbf{u}_i and set $\boldsymbol{\zeta} = 0$.

5.2.1 Wave modes

Generally, a GLS medium with N variables supports N P-wave modes and $2N$ S-wave modes with different polarizations. Equations (5.7) or (5.8) need to be written specifically for each wave type, using a time-spatial dependence harmonic in time and exponentially decaying along axis X :

$$\mathbf{u} = \text{Re} \left[\mathbf{A} \exp(-i\omega t + ikx - \alpha x) \right], \quad (5.9)$$

where A_j is the complex amplitude (including the relative phase shift) of the J^{th} variable, ω is the frequency, k is the wavenumber, and α is the spatial damping factor (attenuation coefficient). This damping factor is merely the observed logarithmic spatial decrement of the amplitude, which can be due to multiple physical reasons such as geometric spreading, scattering, or intrinsic internal friction. Denoting the complex-valued wavenumber $k^* \equiv k + i\alpha$ and $\gamma \equiv (k^*)^2 / \omega^2$, eqs. (5.7) or (5.8) always reduce to solving a generalized eigenvalue equation for eigenvector (polarization in model space) $\mathbf{v}^{(n)}$ and eigenvalue $\gamma^{(n)}$ (with $n = 1 \dots N$):

¹¹ The necessity and physical meaning of this term in the general Lagrangian is currently under investigation. This term may contain the elastic effects of surface tension of saturating fluid in porous rock. However, in observations, these effects may be difficult to separate from those of the elastic moduli \mathbf{K} and $\boldsymbol{\mu}$.

$$\boldsymbol{\rho}^* \mathbf{v}^{(n)} = \gamma^{(n)} \mathbf{M}^* \mathbf{v}^{(n)}, \quad (5.10)$$

where $\boldsymbol{\rho}^* \equiv \boldsymbol{\rho} + i\mathbf{d}/\omega$ and \mathbf{M}^* is a complex-valued, matrix modulus corresponding to the selected wave type. Several examples of these moduli are given in chapter 7.

The eigenvector problem (5.10) has normally N eigenvectors corresponding to the modes waves possible in this medium. For example, in Biot's poroelasticity (section 5.6), $N = 2$, and the eigenvectors represent the primary and Biot's secondary P waves. From the corresponding values of γ , the phase velocity of the wave is obtained for each mode:

$$V_{\text{phase}} \equiv \frac{\omega}{k} = \frac{1}{\text{Re} \sqrt{\gamma}}, \quad (5.11a)$$

and the energy-dissipation factor, defined by $Q^{-1} \equiv \alpha/(2k)$:

$$Q^{-1} = \frac{\text{Im} \sqrt{\gamma}}{2 \text{Re} \sqrt{\gamma}}. \quad (5.11b)$$

With weak dissipation, for an eigenmode n satisfying eqs. (5.11) and (5.10), the kinetic and potential energies included in the Lagrangian L in eqs. (5.5) equal each other. This equation of energy equipartitioning (Rayleigh principle; section 4.8) is useful for calculating the amount of wave dispersion and attenuation in heterogeneous media.

5.3 Constitutive relations

In physics and engineering, constitutive equations, constitutive laws, or constitutive relations are understood as relations between two physical quantities that are specific to the material or substance. A constitutive relation represents the response of the material to some external factor, so that parameters of this response represent an important ('constitutive') property of the material. For example, when heat δQ is injected into a unit volume of material, the corresponding constitutive relation states that the temperature will increase by $\delta T = \delta Q/c_V$, and c_V (specific heat at constant volume) is the material property.

In elastostatics, constitutive relations are usually understood as relations between

strain $\boldsymbol{\varepsilon}$ and stress $\boldsymbol{\sigma}$. In the viscoelastic theory, this relation is extended to time-dependent and/or frequency-dependent relations (chapter 2), and two-way time-dependent relations $\boldsymbol{\varepsilon}(t) \leftrightarrow \boldsymbol{\sigma}(t)$ are called constitutive relations or rheologic laws. However, this empirical understanding of constitutive relations is inappropriate in mechanics. In mechanics (see the end of chapter 2): i) there exists no fixed relation between the time histories of strain and stress, ii) there exist forces not included in $\boldsymbol{\sigma}$, and iii) there are forces related to displacement \mathbf{u} instead of $\boldsymbol{\varepsilon}$. The one-to-one relation $\boldsymbol{\varepsilon}(t) \leftrightarrow \boldsymbol{\sigma}(t)$ only exists in special cases in which these i)–iii) cases do not take place: quasi-static deformations without body-force friction, and in the absence of certain types of structures within the studied body.

The correct constitutive relations in mechanics represent the deformation-to-stress relations produced by the different terms in the Lagrangian description (5.2). These relations are contained in equations (5.7) and (5.8) and discussed separately in the following subsections. I use the general GLS case (5.2); however, note that with a single variable ($N = 1$), these relations also refer to the usual isotropic elastic solid or fluid with (optional) linear viscous internal friction. I also discuss only elasticity and viscosity and disregard the effects of temperature and heat flows.

5.3.1 Elasticity: Hooke's law

The equation of motion (5.8) with time-independent deformation at constant temperature $\mathbf{T} = \mathbf{T}_0$ gives the elastic stress tensor produced by a given strain tensor at any point within the medium:

$$\boldsymbol{\sigma}_{ij} = \mathbf{K}\Delta\delta_{ij} + 2\boldsymbol{\mu}\tilde{\boldsymbol{\varepsilon}}_{ij}. \quad (5.12)$$

This is the Hooke's law for a continuous solid. With $\boldsymbol{\mu} = \mathbf{0}$, this relation also applies to a fluid or gas. By listing all $6N$ components of strain and stress as vectors:

$$\boldsymbol{\varepsilon} = \begin{pmatrix} \varepsilon_{xx} \\ \varepsilon_{yy} \\ \varepsilon_{zz} \\ \varepsilon_{xy} \\ \varepsilon_{xz} \\ \varepsilon_{yz} \end{pmatrix} \quad \text{and} \quad \boldsymbol{\sigma} = \begin{pmatrix} \sigma_{xx} \\ \sigma_{yy} \\ \sigma_{zz} \\ \sigma_{xy} \\ \sigma_{xz} \\ \sigma_{yz} \end{pmatrix}, \quad (5.13)$$

this relation becomes matrix multiplication:

$$\boldsymbol{\sigma} = \mathbf{M}\boldsymbol{\varepsilon}, \quad (5.14)$$

where \mathbf{M} is a $6N \times 6N$ matrix of the elastic modulus. This relation works two-way, so that strain can be uniquely obtained from stress by $\boldsymbol{\varepsilon} = \mathbf{J}\boldsymbol{\sigma}$, where $\mathbf{J} = \mathbf{M}^{-1}$ is the elastic compliance matrix. This compliance matrix is useful for obtaining effective-media properties for porous media (section 5.4 below).

In the presence of scalar variables $\boldsymbol{\theta}$, the elastic stress is modified (by taking variational derivatives of the modified Lagrangian L in eqs.(5.3)):

$$\sigma_{ij} = \mathbf{K}\Delta\delta_{ij} + 2\boldsymbol{\mu}\tilde{\varepsilon}_{ij} - \mathbf{Q}\boldsymbol{\theta}\delta_{ij}. \quad (5.15)$$

5.3.2 Viscous surface friction: Navier-Stokes law

If we consider the terms proportional to strain rates in eq. (5.8) (those produced by the viscosity-related parts of the dissipation function), the viscous stress tensor is obtained:

$$\sigma_{ij} = \boldsymbol{\eta}_K \dot{\Delta}\delta_{ij} + 2\boldsymbol{\eta}_\mu \dot{\tilde{\varepsilon}}_{ij}. \quad (5.16)$$

This strain-rate to viscous-stress relation is well-known as the Navier-Stokes law in fluid

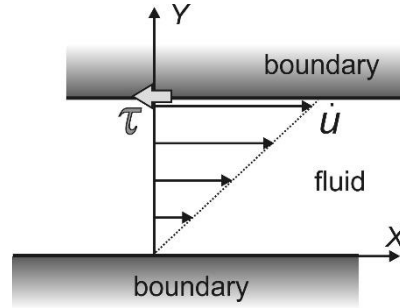


FIGURE 5.1.

Velocity distribution and traction force applied to the moving boundary (τ) in viscous fluid flow between two boundaries.

mechanics, but it also applies to solids.

$$\boldsymbol{\sigma} = \boldsymbol{\eta} \dot{\boldsymbol{\varepsilon}}, \quad (5.17)$$

where $\boldsymbol{\eta}$ is a $6N \times 6N$ matrix of viscosities.

Although eq. (5.16) is also a constitutive relation, its use is strongly limited to cases in which the elastic stress is zero or known. Such cases include steady-state flow processes (Figure 5.1). The inverse relation expressing $\boldsymbol{\varepsilon}(\boldsymbol{\sigma})$ from eq. (5.16) is nonunique and hardly useful on its own, because: 1) in addition to the viscous stress here, there usually exists an inhomogeneous elastic stress which causes the flow, 2) the inverse is also affected by static level of $\boldsymbol{\varepsilon}$, 3) matrix $\boldsymbol{\eta}$ often contains many zero elements and is not invertible, and 4) there may also be a body-force friction adding to the resistance top the flow (Figure 5.1; next subsection).

In the presence of scalar variables $\boldsymbol{\theta}$, the viscous stress (proportional to time derivatives of the variables) becomes

$$\boldsymbol{\sigma}_{ij} = \boldsymbol{\eta}_K \dot{\Delta} \delta_{ij} + 2\boldsymbol{\eta}_\mu \dot{\boldsymbol{\varepsilon}}_{ij} - \mathbf{Q}' \dot{\boldsymbol{\theta}} \delta_{ij}. \quad (5.18)$$

5.3.3 Body-force drag friction: Darcy's law

To describe Darcy's law, we need to consider a porous material with saturating fluid, i.e. the case of $N = 2$ (discussed in detail in section 5.6 below). Considering a slow flow

(so that the inertial force can be disregarded), the equations of motion (5.7) give a steady-state force balance relation:

$$-\mathbf{d}\dot{\mathbf{u}}_i + \partial_j \boldsymbol{\sigma}_{ij} = \mathbf{0}. \quad (5.19)$$

This equation is the differential form of Darcy's law. This law will predict the velocities of the fluid components of the rock from a known spatially-variable stress $\boldsymbol{\sigma}$. Note that the stress here includes both elastic and solid-viscosity parts in eqs. (5.8).

5.4 *Effects of micropores on material properties*

The observable macroscopic material properties (elastic moduli, viscosities, electrical and thermal conductivities, etc.) are modified if pores or microcracks present within the rock frame. In this section, we consider the effects of microcracks. Microcracks can be described by the second-order crack-density tensor α_{ij} (Sayers and Kachanov, 1991):

$$\alpha_{ij} = \frac{1}{V} \sum_c \gamma_c n_i^{(c)} n_j^{(c)}, \quad (5.5)$$

where c is the crack number, V is the averaging volume, $\mathbf{n}^{(c)}$ is the unit normal vector to the c th crack, and γ_c is the weight with this crack contributes to the desired physical material property.

For calculating elastic properties and density of the effective medium, we can take γ_c equal volumes of the penny-shaped cracks of radii a_c and aspect ratios σ_c : $\gamma_c = \pi \sigma_c a_c^3$. Then, the trace of this tensor equals the porosity of the microcracks, which I denote ϕ_s (for 'secondary' pores):

$$\text{tr } \boldsymbol{\alpha} = \alpha_{ii} = \frac{1}{V} \sum_c \gamma_c = \phi_s. \quad (5.61)$$

Thus, the crack density tensor (5.5) is a generalization of the concept of porosity. Along

with the microcrack porosity value (as its trace), this tensor contains information about the preferred or correlated orientations of cracks.

Let us now consider a GLS model in eqs. (5.2) describing some internal rock structure, such as, for example, a rock with Biot's pores (with $N = 2$). Let us now assume that this rock also contains secondary microcracks with distribution given by eq. (5.5). The question we want to solve is how the material-property matrices $\boldsymbol{\rho}$, \mathbf{K} , $\boldsymbol{\mu}$, $\boldsymbol{\eta}_\kappa$, $\boldsymbol{\eta}_\mu$, and \mathbf{d} in eq. (5.2) would be modified by this secondary porosity. We will introduce no additional GLS variable in vector \mathbf{u} to describe the microcracks (which we could!). Instead, we will assume that the macrocracks behave quasi-statically and look for their effect in terms of changing the effective material properties in the primary model.

In the presence of microcracks, the kinetic and elastic-energy and dissipation-function terms in eqs. (5.2) would change by linear and/or quadratic terms with respect to the values of tensor α_{ij} . The quadratic forms will be of the same forms as in eqs. (5.2), with modified material-property matrices. Because the energy terms are scalars, there are only few ways in which these matrices can vary with variable α_{ij} . The density matrix should only be sensitive to the secondary porosity (trace of α_{ij}):

$$\boldsymbol{\rho}^{\text{mod}} = \boldsymbol{\rho}(1 - \phi_s) + \phi_s \boldsymbol{\rho}'. \quad (5.62)$$

Here, the first term is the reduction of density due to the secondary porosity ϕ_c , and the additional term is just another possible modification of matrix $\boldsymbol{\rho}$ associated with introduction of ϕ_c . For example, the microcracks are typically assumed to be located within the solid rock matrix (first term in eq. (5.62)), but they also might actually occur on the edges of the primary pores and thus modify the pore space and tortuosity. These effects would be contained in matrix $\boldsymbol{\rho}'$. Because secondary porosity is usually very small, $\boldsymbol{\rho}' = \mathbf{0}$ or even $\boldsymbol{\rho}^{\text{mod}} = \boldsymbol{\rho}$ should likely be a good approximation.

Matrix \mathbf{d} has a role similar to $\boldsymbol{\rho}$ in Lagrange energy forms (eqs. 5.2), and therefore its variation due to secondary porosity should be similar: $\mathbf{d}^{\text{mod}} = \mathbf{d} + \phi_s \mathbf{d}'$ (there is no need to isolate factor $(1 - \phi_s)$ in this case).

To obtain modifications of the strain-related matrices \mathbf{K} , $\boldsymbol{\mu}$, $\boldsymbol{\eta}_K$, and $\boldsymbol{\eta}_\mu$ it is easier to start from the elastic-energy or viscous-dissipation terms in eqs. (5.2). Because we will be varying porosity at constant stress (not strain), we need to use the stress tensor σ_{ij} as the independent variable. In terms of the applied stress, the elastic energy density in eqs. (5.2) equals $U = \frac{1}{2} \boldsymbol{\sigma}_{ii}^T \mathbf{J}_K \boldsymbol{\sigma}_{jj} + \tilde{\boldsymbol{\sigma}}_{ij}^T \mathbf{J}_\mu \tilde{\boldsymbol{\sigma}}_{ij}$, where $\mathbf{J}_K = \mathbf{K}^{-1}$ is the bulk compliance and $\mathbf{J}_\mu = \boldsymbol{\mu}^{-1}$ is the shear compliance. Due to the effect of microcracks, this energy is modified by adding a term which is also quadratic with respect to the stress tensor σ_{ij} and linear with respect to porosity α_{ij} . The most general form of such modified potential-energy expression is

$$U^{\text{mod}} = U + \alpha_{jk} \boldsymbol{\sigma}_{kj}^T \mathbf{b}_1 \boldsymbol{\sigma}_{ii} + \alpha_{ik} \boldsymbol{\sigma}_{kj}^T \mathbf{b}_2 \boldsymbol{\sigma}_{ji}. \quad (5.63)$$

where \mathbf{b}_1 and \mathbf{b}_2 are symmetric matrices in the $N \times N$ GLS model space. These matrices contain new model parameters describing the sensitivity of elastic properties of the material to the density of microcracks. Viscosity terms in the dissipation function ($D_{\text{visc}} = \frac{1}{2} \dot{\boldsymbol{\Delta}}^T \boldsymbol{\eta}_K \dot{\boldsymbol{\Delta}} + \dot{\tilde{\boldsymbol{\epsilon}}}_{ij}^T \boldsymbol{\eta}_\mu \dot{\tilde{\boldsymbol{\epsilon}}}_{ij}$ in eqs. 5.2) should modify analogously, with their own pair of parameter matrices \mathbf{b}_1 and \mathbf{b}_2 .

Parameters \mathbf{b}_1 and \mathbf{b}_2 in eq. (5.63) need to be determined by solving the problem for static equilibrium of a medium with specific shapes and distribution of cracks. Since tensor α_{ij} is a sum of contributions from individual cracks (eq. 5.5), matrices \mathbf{b}_1 and \mathbf{b}_2 can also be found for individual cracks, and the results added together.

Once matrices \mathbf{b}_1 and \mathbf{b}_2 are found, they can be transformed into modifications of the bulk and shear matrices, so that the modified elastic energy (5.63) is as in eq. (5.2):

$$U^{\text{mod}} = \frac{1}{2} \boldsymbol{\sigma}_{ii}^T \mathbf{J}_K^{\text{mod}} \boldsymbol{\sigma}_{jj} + \tilde{\boldsymbol{\sigma}}_{ij}^T \mathbf{J}_\mu^{\text{mod}} \tilde{\boldsymbol{\sigma}}_{ij}, \quad (5.64)$$

and therefore, the modification of elastic energy by the secondary porosity is:

$$U^{\text{mod}} - U = \frac{1}{2} \boldsymbol{\sigma}_{ii}^T \delta \mathbf{J}_K \boldsymbol{\sigma}_{jj} + \tilde{\boldsymbol{\sigma}}_{ij}^T \delta \mathbf{J}_\mu \tilde{\boldsymbol{\sigma}}_{ij} = \alpha_{jk} \boldsymbol{\sigma}_{kj}^T \mathbf{b}_1 \boldsymbol{\sigma}_{ii} + \alpha_{ik} \boldsymbol{\sigma}_{kj}^T \mathbf{b}_2 \boldsymbol{\sigma}_{ji}. \quad (5.65a)$$

This change of the elastic energy density of the medium can also be represented by compliance of the distribution of microcracks, which is a fourth-order tensor \mathbf{J}_{ijkl} :

$$U^{\text{mod}} - U = \frac{1}{2} \boldsymbol{\sigma}_{ij}^T \mathbf{J}_{ijkl} \boldsymbol{\sigma}_{kl}, \quad (5.65b)$$

and therefore \mathbf{J}_{ijkl} is a combination of a_{ij} , \mathbf{b}_1 and \mathbf{b}_2 . To find these combinations, it is convenient to use spatial coordinate axes (indices i, j, k, l , etc.) in the directions of the eigenvectors of the crack density matrix $\boldsymbol{\alpha}$. In these coordinates, the crack density has the

form $\boldsymbol{\alpha} = \begin{bmatrix} \alpha_{11} & 0 & 0 \\ 0 & \alpha_{22} & 0 \\ 0 & 0 & \alpha_{33} \end{bmatrix}$, and eqs. (5.65) give the nonzero components of crack

compliance (no summations over the subscripts ‘ p ’ and ‘ q ’ here):

$$\begin{aligned} \mathbf{J}_{pqpq} &= (2\mathbf{b}_1 + \mathbf{b}_2) \alpha_{pq} \delta_{pq} + \frac{\mathbf{b}_2}{2} (\alpha_{pp} + \alpha_{qq}), \\ \mathbf{J}_{ppqq} &= \mathbf{b}_1 (\alpha_{pp} + \alpha_{qq}) + 2\mathbf{b}_2 \alpha_{pq} \delta_{pq}. \end{aligned} \quad (5.66)$$

This compliance tensor will need to be further decomposed into \mathbf{J}_K and \mathbf{J}_μ . However, \mathbf{J}_K and \mathbf{J}_μ can also be very simply obtained from arbitrary \mathbf{b}_1 and \mathbf{b}_2 by a numerical matrix calculation (see Lab 5.4).

Finally, note that for an ordinary isotropic solid without internal variables ($N = 1$) with randomly oriented ‘penny-shaped’ microcracks (for which the crack tensor is diagonal and equal $\alpha_{ij} = \frac{1}{3} \phi_s \delta_{ij}$), the above solution of equation (5.65) shows that the modification of the shear compliance is always equal 4/15 of the modification of the bulk compliance:

$$\delta \left(\frac{1}{\mu} \right) = \frac{4}{15} \delta \left(\frac{1}{K} \right). \quad (5.67)$$

This simple proportionality occurs because in eq. (5.65), quantities $\mathbf{b}_1 = b_1$ and $\mathbf{b}_2 = b_2$ are scalars in this case, and the ratio of compliance corrections $\delta J_\mu / \delta J_K$ is only determined by the ratio b_1/b_2 , which is fixed by the selected pore geometry.

5.5 *Wave-Induced Fluid Flows (WIFF)*

In hundreds of papers in rock-physics research literature and also above in this course, “wave-induced pore-fluid flows” (WIFF) are broadly described as the principal cause of seismic wave velocity dispersion and attenuation in porous rock. Numerous pore structures supporting WIFF at multiple spatial scales are illustrated by analytical estimates and numerical modeling. However, there still exists no rigorous definition of what the WIFF mechanisms mean physically, in terms of macroscopic Lagrangian model like shown by eqs. (5.1) or (5.2). In this section, I give such physical definitions.

As described in chapter 4, the first task in formulating a Lagrangian model for a mechanical system always consists in defining the appropriate set of generalized variables. Because of the extreme complexity of rock microstructure and its redundancy for describing a macroscopic behavior, it is impossible to use variables related to some specific dimensions or geometrical shapes of pores or grains¹². Instead of specific dimensions, local-scale averages of the microstructure must be used as dynamic variables of the medium. However, to define these average quantities, two questions need to be considered: 1) what type of variable to use, and 2) what mathematical form to select for this spatial averaging.

To answer the above questions, consider the difference between WIFF phenomena which are usually called “global” and “local” (chapter 1). This difference is usually explained by references to the spatial scales of the pore-fluid flows produced during deformation (Müller et al., 2010). Global flows are associated with larger and interconnected primary pores, and local flows are mutually disconnected and occur within compliant micropores (squirt) or patches of saturation of various shapes. However, we need to differentiate between these mechanisms based not on certain shapes or dimensions of the resultant flows but vice versa, based on the characters of physical interactions causing these flows. Figure 5.2 schematically shows how this can be by recognizing *two different types of pore-fluid flows*.

¹² Note that for this reason alone, most current models using “pore shapes”, “pore connectivity”, “aspect ratios of penny-shaped pores”, or “squirt-flow lengths” as parameters of the microstructure are inadequate. These parameters are impossible to define and measure independently, and they are only used as tuning parameters to empirically fit laboratory data.

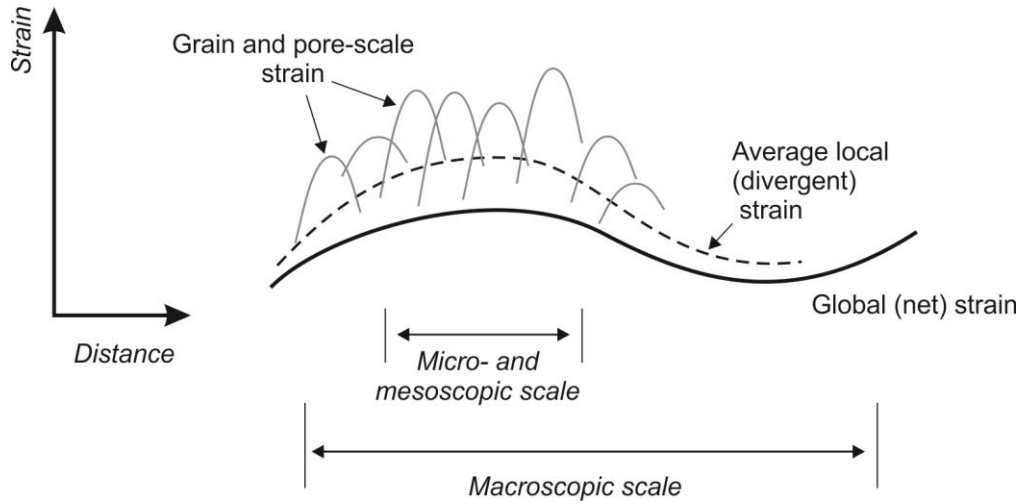


FIGURE 5.2.

Schematic illustration of spatial variation of strain within porous rock. The “global” or “net” strain (thick black line) is the observable deformation of the rock and pore fluid. At grain and pore scales, the strain is a random field with short correlation length (gray lines), which can be characterized by macroscopically variant average level (“divergent” strain, dashed line).

Consider the displacement field u and the strain field ε within porous rock on which a macroscopic deformation is imposed, such as caused by a seismic wave (Figure 5.2). The macroscopic (locally-averaged) displacement and strain within rock are combinations of a macroscopic average flow and a zero-mean divergent (or convergent) local flow:

$$\bar{u} \approx u_{\text{net}}, \quad \text{and} \quad \bar{\varepsilon} \approx \varepsilon_{\text{net}} + \bar{\varepsilon}_{\text{div}}. \quad (5.68)$$

The net-flow component is the observable deformation of macroscopic rock and/or pore fluid, in which the strain is related to the displacement by usual differential relations (e.g., $(\varepsilon_{\text{net}})_{ij} = [\partial_i (u_{\text{net}})_j + \partial_j (u_{\text{net}})_i] / 2$). For the divergent component, the average displacement is zero (as it is included in u_{net}), but the local strain is a rapidly variable stochastic field (gray lines in Figure 5.2). This random strain has a generally nonzero mean value, which we denote $\bar{\varepsilon}_{\text{div}}$ (eq. (5.68), dashed line in Figure 5.2). Thus, the principal difference between these two types of deformations consists not in their spatial scales but in different characters of the respective generalized variable:

- 1) For the “net-displacement” deformation, the generalized variable is the measurable

displacement vector $\underline{u}_{\text{net}}$, from which strain ε_{net} and other macroscopic quantities (velocities, strain rates, stresses, etc.) can be determined.

- 2) For “divergent-displacement” deformation, the *displacement vector equals zero*, and its generalized variable is the strain $\bar{\varepsilon}_{\text{div}}$ averaged on the local scale (Figure 5.2). This variable is generally a tensor quantity, which reduces to scalar dilatation in simple and isotropic cases.

Note that although the above differentiation of variables is applied to WIFF here, it is unrelated to fluids and also applies to grains, shapes of primary pores, and other heterogeneities within the rock microstructure. Also note that the existence of vector and scalar variables is independent of observation scales. The conventional “global-scale” WIFF is associated with the “net-displacement” movement of pore fluid, and the “microscopic-“ and “mesoscopic-scale” WIFF are indistinguishable and related to “divergent-displacement” deformations.

5.6 Biot’s Poroelastic Model

For the best description of Biot’s poroelastic model, I refer the reader to the book by Bourbié, et al. (1987). These authors (as well as Biot himself) also use Lagrangian formulation which is readily rendered in our matrix GLS form. The complete Biot’s model is obtained from eqs. (5.2) by considering two variables ($N = 2$), zero matrix ζ , matrix μ consisting of only one element (shear stiffness of rock frame), and zero viscosity matrices ($\eta = \mathbf{0}$):

$$\begin{cases} L^B = \frac{1}{2} \dot{\mathbf{u}}_i^T \rho \dot{\mathbf{u}}_i - \left(\frac{1}{2} \Delta^T \mathbf{K} \Delta + \tilde{\boldsymbol{\varepsilon}}_{ij}^T \mu \tilde{\boldsymbol{\varepsilon}}_{ij} \right), \\ D^B = \frac{1}{2} \dot{\mathbf{u}}_i^T \mathbf{d} \dot{\mathbf{u}}_i, \end{cases} \quad (5.20)$$

The displacement variable \mathbf{u}_1 is the observable deformation of the whole fluid-saturated rock, and the internal variable \mathbf{u}_2 is be the filtration displacement (relative displacement between the fluid and its unperturbed position in host matrix) multiplied by minus porosity ϕ : $\mathbf{u}_2 \equiv -\mathbf{w} \equiv -\phi(\mathbf{u}_{\text{fluid}} - \mathbf{u}_1)$.

Accordingly to the two forms of deformations (of the rock as a whole and its pore fluid), there are two types of stresses: the solid stress tensor σ_{ij} and the pore pressure p . As in the Lagrangian model above and in the more general thermodynamics, these stresses are given by derivatives of the potential energy U :

$$\sigma_{ij} = \frac{\partial U}{\partial \varepsilon_{ij}}, \quad \text{and} \quad p = \frac{\partial U}{\partial \xi}, \quad (5.21)$$

where the scalar quantity $\xi \equiv -\text{div } \mathbf{w}$ is called the fluid content.

The potential energy U is a quadratic function of two variables ε_{ij} and ξ . Therefore, for bulk deformation, U should be given by three terms proportional to squares of ε_{ij} and ξ , and their product. The shear-deformation part of U is not affected by pore fluid. Consequently, from such very general considerations, U is given by the following quadratic expressions (basically, again all possible combinations of scalar invariants $I_1 = \Delta$, $I_2 = \tilde{\varepsilon}_{ij}\tilde{\varepsilon}_{ij}$, and ξ):

$$U = \frac{1}{2} K_U \Delta^2 - \alpha M \Delta \xi + \frac{1}{2} M \xi^2, \quad \text{and} \quad U_{\text{shear}} = \mu \tilde{\varepsilon}_{ij} \tilde{\varepsilon}_{ij}. \quad (5.22)$$

In the notation of eqs. (5.2), the dilatational and deviatoric strains associated with the two displacement fields are $\Delta_1 \equiv \Delta$, $\Delta_2 \equiv \xi$, $\tilde{\varepsilon}_{1ij} \equiv \tilde{\varepsilon}_{ij}$, and $\tilde{\varepsilon}_{2ij} = 0$. Therefore, eq. (5.22) is the elastic part of the Lagrangian (eqs. 5.2):

with 2×2 matrix moduli (I enclose in boxes the most important formulas in Biot's model):

$$\mathbf{K} = \begin{bmatrix} K_U & -\alpha M \\ -\alpha M & M \end{bmatrix} \text{ (bulk modulus)} \quad \text{and} \quad \boldsymbol{\mu} = \begin{bmatrix} \mu & 0 \\ 0 & 0 \end{bmatrix} \text{ (shear)}. \quad (5.23)$$

In these equations, parameter K_U is the “undrained” bulk modulus explained in the next subsection. Parameter M is the pressure that needs to be exerted on the fluid in order to increase the fluid content ξ by a unit value at constant volume (when $\Delta = 0$). Parameter $\alpha \in [0, 1]$ is called the Biot-Willis coefficient (also called Skempton A), which measures the proportion of the dilatational strain caused by variations in fluid content at constant

pressure. These parameters are related to the bulk modulus of a drained rock frame, K_D , as $\alpha^2 M = K_U - K_D$ (next subsection).

The kinetic energy density in the poroelastic model equals (Bourbié et al., 1987):

$$E_{kin} = \frac{\rho}{2} \dot{u}_i \dot{u}_i + \rho_f \dot{u}_i \dot{w}_i + \frac{a\rho_f}{2\phi} \dot{w}_i \dot{w}_i, \quad (5.24)$$

where ρ_f is the density of the pore fluid and $a \geq 1$ is the tortuosity of the pore space. This expression is again contained in the Lagrangian in eqs. (5.2), with 2×2 density matrix:

$$\mathbf{\rho} = \begin{bmatrix} \rho & -\rho_f \\ -\rho_f & \frac{a}{\phi} \rho_f \end{bmatrix}. \quad (5.25)$$

In a porous medium, internal friction occurs by the friction of pore fluid being squeezed through pores (Darcy law). The force of this friction is opposite in direction and proportional to the rate of pore flow \dot{w}_i . In Biot's model, this friction described by the dissipation function $D = \eta \dot{w}_i \dot{w}_i / (2\kappa)$, where η is the pore-fluid viscosity and κ is the permeability. This D corresponds to the D in eqs. (5.2) with matrix \mathbf{d} equal

$$\mathbf{d} = \begin{bmatrix} 0 & 0 \\ 0 & \eta/\kappa \end{bmatrix}. \quad (5.26)$$

In matrix \mathbf{d} in eq. (5.26), the first row and column are always zero (chapter 5), and the remaining block corresponding to the internal variables can be interpreted as an inverse mobility matrix. In Biot's model, this matrix consists of a single quantity $\eta/\kappa = 1/m$, where quantity $m = \kappa/\eta$ is called the fluid mobility in Darcy flow.

5.6.1 Relations between displacements, strains, and elastic parameters

The three parameters of the bulk elastic-moduli matrix \mathbf{K} are related to the empirical moduli measured in experiments:

- 1) The undrained modulus K_U measured in an experiment with zero pore flow ($\Delta_2 = 0$). This regime is obtained by jacketing the sample (for example, hydraulically insulating the sample by covering it with epoxy).
- 2) The drained modulus K_D measured in an experiment in which the pore-fluid pressure is unchanged. This regime can be (at least hypothetically) achieved by providing a hydraulic connection of the pore fluid to the outside of the sample. This regime is also approximated by measurements with dry rock.
- 3) The modulus of the solid skeleton (or solid grains) K_s . This modulus is obtained by measuring the pressure/strain ratio while ensuring that the pressure of the pore fluid equals the pressure on the solid grains. This means that the sample must beunjacketed, and the measurement must be quasi-static to allow equilibration of all pressures.
- 4) The elastic modulus of the pore fluid K_f . This modulus is usually measured separately, by using only the pore fluid.

All of these moduli can be calculated from matrix \mathbf{K} by considering several types of experiments with a rock volume. Let us use here the notation $\begin{pmatrix} \Delta \\ \xi \end{pmatrix} \stackrel{\text{def}}{=} \begin{pmatrix} \Delta_1 \\ \Delta_2 \end{pmatrix}$ popular in discussions of poroelasticity. The stresses applied to the whole rock and its pore fluid are given by the matrix product

$$\begin{pmatrix} \sigma \\ -p \end{pmatrix} = \mathbf{K} \begin{pmatrix} \Delta \\ \xi \end{pmatrix}. \quad (5.27)$$

The inverse of this equation is

$$\begin{pmatrix} \Delta \\ \xi \end{pmatrix} = \mathbf{J} \begin{pmatrix} \sigma \\ -p \end{pmatrix}, \quad (5.28)$$

where \mathbf{J} is the compliance matrix:

$$\mathbf{J} = \mathbf{K}^{-1} = \frac{1}{K_D} \begin{bmatrix} 1 & \alpha \\ \alpha & K_U/M \end{bmatrix}, \quad (5.29)$$

In which, from the rule of calculating the matrix inverse

$$K_D = \frac{\det \mathbf{K}}{M} = K_U - \alpha^2 M . \quad (5.30)$$

As shown in the next paragraph, this quantity is the drained modulus, and you can notice that $K_D \leq K_U$. The compliance matrix \mathbf{J} gives the deformations of the whole rock ($\Delta = \Delta_1$) and of the change in fluid content ($\xi = \Delta_2$) caused by given confining and pore pressures.

By taking different combinations of Δ , ξ , σ , and p , the different experiments listed above are obtained:

- 1) Taking fluid flow $\xi = 0$, and $\sigma = K_U \Delta$. Thus, the upper-left element of matrix \mathbf{K} is the undrained modulus. It can be measured by taking an experimental ratio

$$K_U = \frac{\sigma}{\Delta} .$$

- 2) Taking $p = 0$, the drained case is obtained, and from the compliance equation

$$\text{above, } \Delta = \frac{\sigma}{K_D} . \text{ Thus, the } \underline{\text{drained modulus}} \text{ equals } K_D = \frac{\sigma}{\Delta} = \frac{1}{J_{11}} .$$

Also from the compliance equation (5.28), if we ensure $p = 0$ (drained experiment) and apply stress σ to the whole rock sample, then its deformations will be $\begin{pmatrix} \Delta \\ \xi \end{pmatrix} = \frac{\sigma}{K_D} \begin{pmatrix} 1 \\ \alpha \end{pmatrix}$,

i. e. $\xi = \alpha \Delta$. This relation shows that

$$\alpha = \left. \frac{\xi}{\Delta} \right|_{p=0} , \quad (5.31)$$

i.e. the Biot-Willis coefficient α is the amount of relative compression of the pore volume when applying pressure to a drained rock. Thus, it is a property of the drained rock frame and independent of the pore fluid. This quantity must obey constraints $\phi \leq \alpha \leq 1$.

To see how the moduli K_s and K_f are included in matrix \mathbf{K} , we need to first express the dilatations of the material of the frame and pore fill from the macroscopic variables Δ

and ξ :

$$\begin{pmatrix} \Delta_s \\ \Delta_f \end{pmatrix} = \mathbf{U} \begin{pmatrix} \Delta \\ \xi \end{pmatrix}, \quad (5.32)$$

where matrix \mathbf{U} is

$$\mathbf{U} = \begin{bmatrix} 1 & -1 \\ 1 & -1/\phi \end{bmatrix}. \quad (5.33)$$

In the drained experiment (eq. (5.28) with $p = 0$), from relation (5.32), the dilatations of the solid and fluid phases equal

$$\begin{pmatrix} \Delta_s \\ \Delta_f \end{pmatrix} = \mathbf{U} \begin{pmatrix} \Delta \\ \xi \end{pmatrix} = \frac{\sigma}{K_D} \begin{pmatrix} 1-\alpha \\ 1-\alpha/\phi \end{pmatrix}. \quad (5.34)$$

From this equation, $\Delta_s = \frac{\sigma}{K_D}(1-\alpha)$. At the same time, when pores are empty ($p = 0$), the entire deformation and strain energy in the rock belongs to the solid, and consequently $\Delta_s = \frac{\sigma}{K_s}$. Therefore, parameter α is also related to the ratio of the dry and solid-grain moduli:

$$\alpha = 1 - \frac{K_D}{K_s}. \quad (5.35)$$

To find the meaning of modulus K_f , consider another experiment in which both the confining and pore pressures are held equal p (and therefore stress $\sigma = -p$). From eq. (5.28), the deformation of the solid and fluid phases are

$$\begin{pmatrix} \Delta_s \\ \Delta_f \end{pmatrix} = \mathbf{U} \mathbf{J} \begin{pmatrix} -p \\ p \end{pmatrix} = \frac{p}{K_D} \begin{pmatrix} 2\alpha - K_U/M - 1 \\ \alpha - K_U/(\phi M) - 1 + \alpha/\phi \end{pmatrix}. \quad (5.36)$$

The volumetric strain within the fluid should satisfy $\Delta_f = \frac{-p}{K_f}$, which gives (after some simplification) the relation for the bulk modulus of pore fluid K_f :

$$\frac{\phi}{K_f} = \frac{1}{M} - \frac{\alpha - \phi}{K_s}. \quad (5.37)$$

This relation also shows how the elastic coupling M in matrix \mathbf{K} can be determined from the measured K_s and K_f :

$$\frac{1}{M} = \frac{\phi}{K_f} + \frac{\alpha - \phi}{K_s}. \quad (5.38)$$

This relation shows that M can be viewed a Reuss (harmonic) average of moduli K_s and K_f , with α acting as the total volume occupied by the compound within a unit volume of rock.

5.6.2 Gassmann's equation

Because there are four empirically measured moduli (K_U , K_D , K_s , and K_f) but only three independent elastic moduli in matrix \mathbf{K} , the empirical moduli must be mutually related for any material. This automatic relation is called the Gassmann's equation.

Gassmann's equation is usually presented as answering the following question: If the drained bulk modulus K_D , modulus of solid grains K_s , and pore fluid modulus K_f are measured for a porous rock with porosity ϕ , what is the bulk modulus of this rock K_U in a saturated state? The answer to this question is given very compactly by eq. (5.30):

$$K_U = K_D + \alpha^2 M, \quad (5.39)$$

where α and M can be determined from eqs. (5.35) and (5.38). There are many forms of final relations for the undrained modulus, for example:

$$K_U^{-1} = \frac{K_s^{-1} + \phi' K_D^{-1}}{1 + \phi'}, \quad (5.40)$$

where $\phi' \equiv \phi \frac{K_f^{-1} - K_s^{-1}}{K_D^{-1} - K_s^{-1}} = \frac{\phi}{\alpha} K_D (K_f^{-1} - K_s^{-1})$.

5.6.3 Wave modes

Again using the generalized eigenvalue equation

$$\mathbf{p}^* \mathbf{v}^{(n)} = \gamma^{(n)} \mathbf{M}^* \mathbf{v}^{(n)}, \quad (5.10 \text{ repeated})$$

with longitudinal and transverse spatial polarizations of vector $u_1 \mathbf{i}$, Biot's model predicts two P-wave and one S-wave modes. Phase velocities V and attenuation (spatial attenuation coefficients $\alpha = \chi/V$) of these modes are shown in Figures 5.3–5.5. These dependencies are controlled by the characteristic frequency (Biot's frequency)

$$f_c = \frac{\phi \eta}{2\pi \rho_f \kappa}. \quad (5.41)$$

This relation shows that the velocity dispersion and attenuation effects are caused by inertial forces acting on the pore fluid (hence ρ_f in the denominator and no elastic moduli in this expression). Biot's frequency f_c is *proportional to fluid viscosity* η , which is opposite to the characteristic frequency due to viscous-friction terms with matrices $\boldsymbol{\eta}_K$ and $\boldsymbol{\eta}_m$ in the Lagrangian (these terms would describe the mesoscopic-scale fluid-flow friction).

At low frequencies, velocities of the primary modes tend to the corresponding elastic limits:

$$V_P = \sqrt{\frac{\lambda + 2\mu}{\rho}} \quad \text{and} \quad V_S = \sqrt{\frac{\mu}{\rho}}, \quad (5.42)$$

and the velocity of the secondary (dissipative) P wave tends to zero (Figures 5.3a–5.5a). The attenuation coefficients in Figures 5.3ba–5.5b are scaled by levels

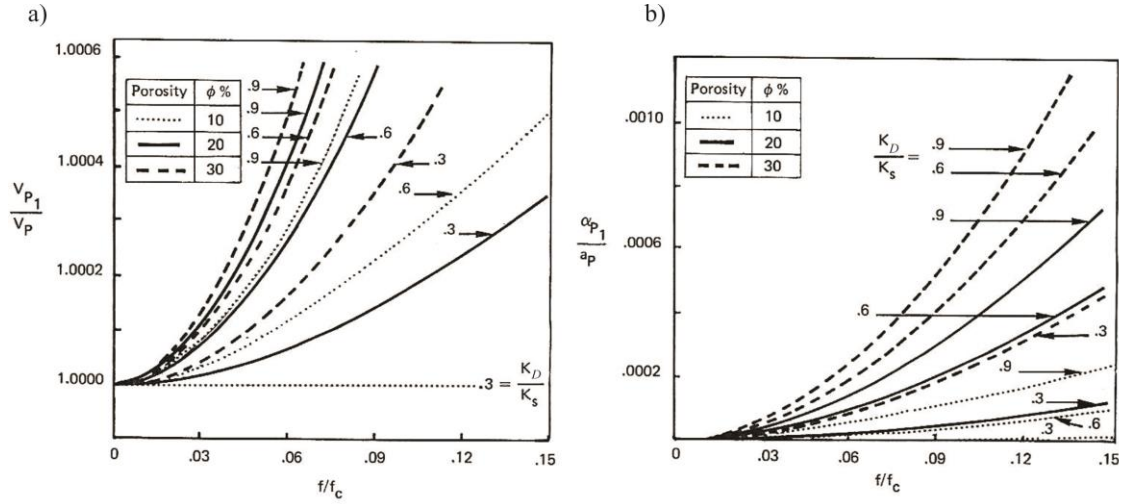


FIGURE 5.3.

Primary (“fast”) P waves in Biot’s model for several porosity values and ratios K_D/K_S (from Bourbié et al., 1987): a) velocity, b) attenuation coefficient α . Frequencies are relative to Biot’s frequency f_c , velocities are relative to the zero-frequency limit.

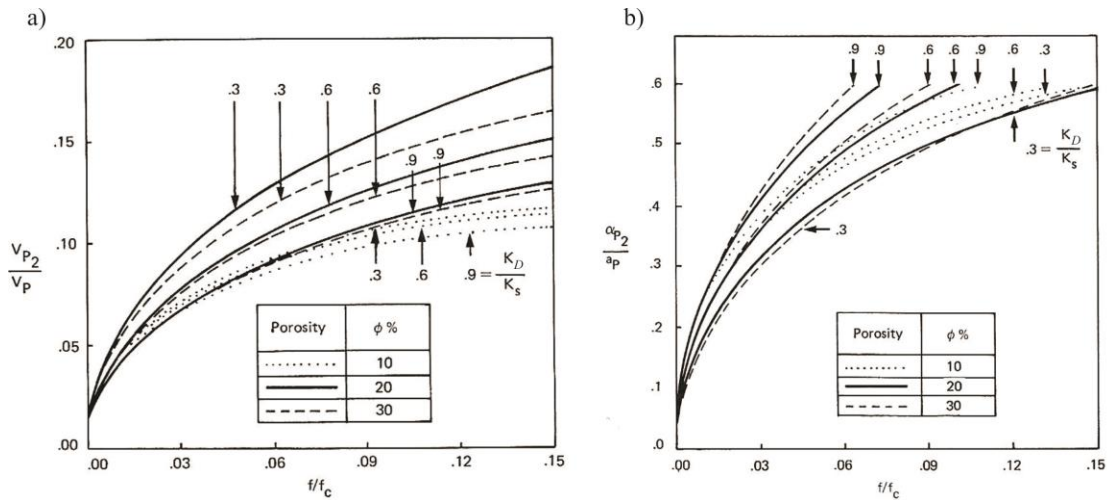


FIGURE 5.4.

Secondary (“slow”, “diffusive”) P waves in Biot’s model for several porosity values and ratios K_D/K_S (from Bourbié et al., 1987): a) velocity, b) attenuation coefficient α . Frequencies are relative to Biot’s frequency f_c , velocities are relative to the zero-frequency limit.

$$\alpha_P = \frac{2\pi f_c}{V_P} \quad \text{and} \quad \alpha_S = \frac{2\pi f_c}{V_S}, \quad (5.43)$$

which correspond to temporal attenuation coefficients (section 4.9) $\chi_P = \chi_S = 2\pi f_c = \omega_c$.

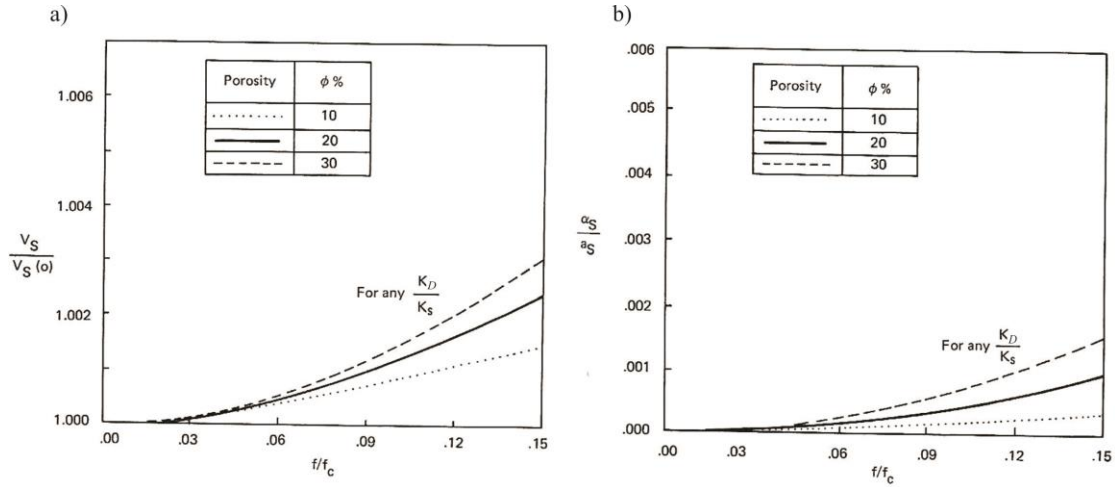


FIGURE 5.5.

S waves in Biot's model for several porosity values and ratios K_D/K_S (from Bourbié et al., 1987): a) velocity, b) attenuation coefficient α . Frequencies are relative to Biot's frequency f_c , velocities are relative to the zero-frequency limit.

The Biot's characteristic frequency f_c is extremely variable but typically large (from 30 kHz to 1 GHz for water), and consequently the dispersion and attenuation effects are weak at seismic frequencies ($f/f_c \sim 10^{-2}$ or less) (Figures 5.3–5.5).

The $Q^{-1}(f)$ shows an asymmetric peak at $f=f_c$ (not shown in these figures). At a fixed frequency $f < f_c$, the attenuation coefficients and Q^{-1} decreases with increasing η . The same trend of attenuation decreasing with increasing pore-fluid η is observed for the viscoelastic attenuation mechanism at frequencies above the relaxation peak, $f > f_c$.

5.7 Biot's model with variable secondary porosity

Starting from Biot's poroelastic model, as the next approximation to a realistic grain and pore structure, we need additional macroscopic parameters describing the secondary porosity. Such additional detail including pore or grain-contact orientations and anisotropy can be represented by the porosity tensor α_{ij} or by higher-rank averages of the microstructure using products of three or more vectors $n_j^{(p)}$ in eq. (5.5). It appears that for practical applications and for rendering most current WIFF models, planar contacts are

most important, and the second-rank tensor α_{ij} (eq. (5.5)) is sufficient as the generalized variable. Sayers and Kachanov (1991) used this tensor in a variational principle for finding elastic properties of effective media with many types of inclusions. Maximov (2010) used a similar, albeit abstractly defined tensorial variable for adding shear elasticity and relaxation of pore fluid to Biot's model.

Treating the spatial vectors \mathbf{u}_i and tensor α_{ij} as generalized variables of the system, the most general model for linear interactions can be obtained by adding to Biot's functions L^B and D^B (section 5.6) scalar quadratic forms of $\boldsymbol{\varepsilon}_{ij}$, and α_{ij} . It is convenient to separate the dilatational and pure shear parts in these tensors:

$$\boldsymbol{\varepsilon}_{ij} = \Delta \delta_{ij} + \tilde{\boldsymbol{\varepsilon}}_{ij}, \quad \alpha_{ij} = \Delta_\alpha \delta_{ij} + \tilde{\alpha}_{ij}, \quad (5.44)$$

where $\Delta_\alpha = \delta\alpha_{ii}$, and traces of $\tilde{\boldsymbol{\varepsilon}}_{ij}$ and $\delta\tilde{\alpha}_{ij}$ equal zero. There exist only four quadratic invariants of these tensors containing $\delta\alpha_{ij}$: $(\Delta_\alpha)^2$, $\Delta\Delta_\alpha$, $\tilde{\boldsymbol{\varepsilon}}_{ij}\delta\tilde{\alpha}_{ij}$, and $\delta\tilde{\alpha}_{ij}\delta\tilde{\alpha}_{ij}$. Therefore, the general modification of eqs. (5.20) by a deformation of porosity α_{ij} is

$$\begin{cases} L = L^B + \frac{1}{2} \rho_1 \dot{\Delta}_\alpha^2 + \tilde{\rho}_1 \dot{\tilde{\alpha}}_{ij} \dot{\tilde{\alpha}}_{ij} - \left[\frac{1}{2} e_1 \Delta_\alpha^2 - \boldsymbol{\Delta}^T \mathbf{e}_2 \Delta_\alpha \right] - \left[\tilde{e}_1 \tilde{\boldsymbol{\varepsilon}}_{ij} \tilde{\boldsymbol{\varepsilon}}_{ij} - 2 \tilde{\boldsymbol{\varepsilon}}_{ij}^T \tilde{\mathbf{e}}_2 \tilde{\boldsymbol{\varepsilon}}_{ij} \right], \\ D = D^B + \left[\frac{1}{2} \eta_1 \dot{\Delta}_\alpha^2 - \dot{\boldsymbol{\Delta}}^T \boldsymbol{\eta}_2 \dot{\Delta}_\alpha \right] + \left[\eta_1 \dot{\tilde{\alpha}}_{ij} \dot{\tilde{\alpha}}_{ij} - 2 \tilde{\boldsymbol{\varepsilon}}_{ij}^T \tilde{\boldsymbol{\eta}}_2 \dot{\tilde{\alpha}}_{ij} \right], \end{cases} \quad (5.45)$$

where the terms enclosed in square brackets contain modifications of the bulk and shear parts of the elastic energy and dissipation function. In these expressions, material properties e_1 , \tilde{e}_1 , ρ_1 , and $\tilde{\rho}_1$ represent analogs of bulk and shear elasticity and density with respect to deforming porosity and/or grain contacts. The inertial coupling between $\dot{\Delta}$ and $\dot{\Delta}_\alpha$ equals zero because the divergent flow is random and uncorrelated with $\dot{\Delta}$.

If the perturbation of the porosity distribution is always isotropic, then

$$\alpha_{ij} = \frac{\delta_{ij}}{3} \delta\phi, \quad \text{and} \quad \Delta_\alpha = \delta\phi, \quad (5.46)$$

and the perturbation of porosity $\delta\phi$ becomes an example of the scalar GLS variable θ in section 5.1. This is the case of isotropic “spherical” pores often used to illustrate Biot’s model (although the shapes and sizes of pores are actually insignificant).

Exercise
Show that if the perturbation of porosity satisfies eqs. (5.46), the L and D functions in eqs. (5.45) become those in eqs. (5.3).

In an isotropic medium (including isotropic distribution of heterogeneities and pores), the principal directions of porosity tensor coincide with those of the strain ϵ_{ij} , and therefore tensor α_{ij} can be represented by variations of porosity in these principal directions. These variations of the eigenvalues of α_{ij} can be combined in a three-component model vector θ , used in subsection 5.1.2. In chapter 7, I illustrate these variables and the corresponding material properties for a classical model of isotropically distributed “penny-shaped” microcracks.

5.8 *Rigorous continuum-mechanics (GLS) form of the viscoelastic model*

In this section, I use the GLS continuum-mechanics framework to re-describe the axiomatic viscoelastic model (chapter 2). As shown in the following subsections, for all mechanically implementable viscoelastic models (those which can be represented by spring-dashpot diagrams), rigorous physical meanings can be obtained. Such viscoelastic systems can be solved with great accuracy and detail by using Lagrangian mechanics.

The conventional viscoelastic models are obtained from GLS models by:

- 1) Using mechanical diagrams to approximate the desired behavior of the viscoelastic model.
- 2) From the mechanical diagram, selecting the appropriate number of

variables N . As shown in the examples below, this number equals one (for the observable deformation) plus the number of joints between the mechanical elements which are not directly connected to the measured strain.

- 3) Using only elasticity terms (with factors \mathbf{K}) and viscosity terms (with factors $\boldsymbol{\eta}$) in the Lagrangian. Terms containing matrices \mathbf{d} and $\boldsymbol{\zeta}$ are absent in the viscoelastic model.

The principal conclusion from this GLS model is that the true physical properties of the medium (elastic matrices \mathbf{M} and $\boldsymbol{\eta}$, and density ρ) are frequency-independent and not directly measured in any experiment. The measured viscoelastic moduli $M(t)$, compliances $J(t)$, and the corresponding frequency-domain spectra $M(f)$, $J(f)$, or $Q^{-1}(f)$ only belong to observations with certain specific systems, such as waves of different kinds or deformations of rock samples of certain shapes and under certain boundary conditions. Such observation-method specific quantities are called ‘apparent.’ These functions are determined not only by material properties but also by the size and shape of the body being tested, its heterogeneity (such as subsurface layering), and other factors. For example, the same sample of fluid-saturated sandstone shows strongly different $M(f)$ when measured in an unjacketed or jacketed states.

Thus, the goal of interpretation of any experiment with anelastic rock consists in revealing the true (frequency-independent) mechanical properties through the observed frequency-dependent apparent properties.

5.8.1 Linear solids

In the following subsections, I show material properties for five types of the classic linear solids described in chapter 2.

Maxwell’s solid

The Maxwell’s solid requires one observable and one additional internal variable shown by white circle in Figure 5.6. Therefore, the GLS dimensionality $N = 2$ in this case, and the 2×2 material-property matrices are

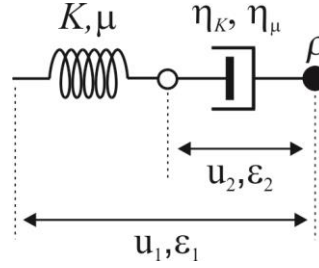


FIGURE 5.6.

Maxwell's linear solid. This diagram describes the bulk-deformation (labeled K) and shear-deformation (labeled μ) parts of the Lagrangian and dissipation function. Black dot labeled ρ indicates the density in the Lagrangian, the open dot shows the internal variable, and labels u_1 , u_2 and ϵ_1 , ϵ_2 indicate the displacement variables and strains, respectively.

$$\boldsymbol{\rho} = \begin{bmatrix} \rho & 0 \\ 0 & 0 \end{bmatrix}, \quad \mathbf{M} = \begin{bmatrix} M & -M \\ -M & M \end{bmatrix}, \quad \text{and} \quad \boldsymbol{\eta} = \begin{bmatrix} 0 & 0 \\ 0 & \eta \end{bmatrix}, \quad (5.43)$$

where the modulus M denotes any type of elastic moduli, and η denotes the corresponding solid viscosity. The characteristic form of the elastic matrix \mathbf{M} in eqs. (5.43) corresponds to the expression for the strain (for example, shear) energy of the 'spring' depending on the on the difference of the strains of variable 1 (observed) and 2(internal) (Figure 5.6):

$$U_{\text{shear}} = \mu (\tilde{\epsilon}_{1ij} - \tilde{\epsilon}_{2ij}) (\tilde{\epsilon}_{1ij} - \tilde{\epsilon}_{2ij}) = \mu \tilde{\epsilon}_{1ij} \tilde{\epsilon}_{1ij} - 2\mu \tilde{\epsilon}_{1ij} \tilde{\epsilon}_{2ij} + \mu \tilde{\epsilon}_{2ij} \tilde{\epsilon}_{2ij}. \quad (5.44)$$

The mechanical-energy dissipation is only caused by the strain rate of the internal variable in this model:

$$D_{\text{shear}} = \frac{1}{2} \eta_\mu \dot{\tilde{\epsilon}}_{2ij} \dot{\tilde{\epsilon}}_{2ij}. \quad (5.45)$$

Note that the diagram in Figure 5.6 contains more information than is usually shown in the diagrams of linear solids. Because this diagram summarizes not only the strain-stress response but also the complete structure of the Lagrangian and dissipation function, it shows the observable displacement variable (black dot), the internal variable (open white dot), the definition of the internal displacement and strain (u_2 and ϵ_2 , measuring the deformation of the 'dashpot'), and density matrix $\boldsymbol{\rho}$. In the conventional linear solid

models, the internal variable u_2 (open dot in Figure 5.10) is massless, which is another physical drawback of these models.

To obtain the characteristic frequency-dependent spectra $M(f)$ for a Maxwell' solid, we need to consider some specific experiment. For example, assume that a cylindrical rock sample in a laboratory experiment is being deformed by an oscillating force applied to the end of the cylinder, and the displacement is measured at the same point. Taking this measured displacement as the generalized variable \mathbf{q} (a two-element vector in the GLS model space), we can express the average strain $\boldsymbol{\varepsilon}$ through this \mathbf{q} . Using this strain, we can further express the Lagrangian (L) and dissipation density (D) for the sample through \mathbf{q} and its time derivative $\dot{\mathbf{q}}$. The L and D functions will have the same forms as in the mass-stiffness-damping matrix system in eq. (4.12) (simply because there are no other forms possible):

$$\begin{cases} L = \frac{1}{2} \dot{\mathbf{q}}^T \mathbf{M} \dot{\mathbf{q}} - \frac{1}{2} \mathbf{q}^T \mathbf{S} \mathbf{q}, \\ D = \frac{1}{2} \dot{\mathbf{q}}^T \mathbf{D} \dot{\mathbf{q}}, \end{cases} \quad (5.46)$$

Since the oscillating loading force is applied to the end of the cylinder only (and not to the internal variable), then it can be taken equal $\mathbf{f} = \begin{pmatrix} 1 \\ 0 \end{pmatrix}$. Using these equations, the response of the deformation to the applied load will be (see eqs. (4.15) and (4.16))

$$\mathbf{r} = \left(-\omega^2 \mathbf{M} - i\omega \mathbf{D} + \mathbf{S} \right)^{-1} \begin{pmatrix} 1 \\ 0 \end{pmatrix}. \quad (5.47)$$

In this vector \mathbf{r} , the first element corresponds to the displacement of the top of the cylinder, which means that it is the desired complex-valued modulus $M(\omega) = r_1$. The second element r_2 shows the displacement of the internal variable.

The force-deformation response vector (5.47) contains the relaxation spectrum $M(\omega)$ of the ordinary viscoelastic Maxwell's solid, but it also contains additional information:

- 1) The free oscillation of the sample and the Q associated with this oscillation;

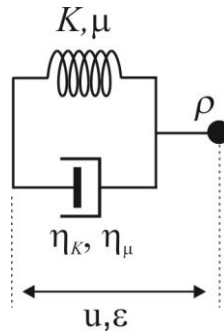


Figure 5.7. Kelvin-Voigt's linear solid. Labels and notation are as in Figure 5.6.

2) The deformation of the internal variable.

You can study these features in the laboratory assignments at the end of this chapter.

Kelvin-Voigt solid

For a Kelvin-Voigt solid (Figure 5.7), there are no internal variables, and the corresponding 1×1 constitutive matrices are

$$\boldsymbol{\rho} = [\rho], \quad \mathbf{M} = [M], \quad \text{and} \quad \boldsymbol{\eta} = [\eta]. \quad (5.48)$$

With nonzero η , waves in this medium are always dissipative, similar to waves in a Newtonian fluid.

Using these material-property matrices, this system can be studied completely similarly to the Maxwell's case (eqs. (5.46) and (5.47)).

Standard linear (Zener's) solid

The Zener's linear solid can be obtained in two ways: by using a Maxwell's solid with an additional elastic element attached in parallel with it (Figure 5.8a) or using a Kelvin-Voigt body with an additional spring connected in series (Figure 5.8b). In either case, the model requires one internal variable ($N = 2$), and the 2×2 material-property matrices represent the Maxwell's model with additional elasticity added to either the observable strain ε_{1ij} or internal strain ε_{2ij} . The difference between the two models is in the selection of the secondary modulus M_2 (or K_2, μ_2), so that both the zero-frequency and the

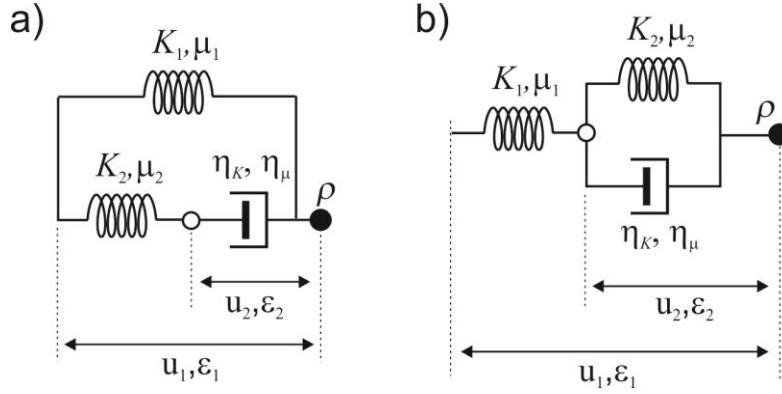


FIGURE 5.8.

Two forms of Zener's linear solid (also called the Standard linear solid, SLS): a) using a Maxwell's body with a spring attached in parallel, b) using a Kelvin-Voigt body with a spring in series. Labels and notation are as in Figure 5.6.

high-frequency limits of the response and frequency f_c are the same. For the first type (Figure 5.8a), the matrices represent the Maxwell's model with additional elasticity due to the observable strain ε_{1ij} :

$$\boldsymbol{\rho} = \begin{bmatrix} \rho & 0 \\ 0 & 0 \end{bmatrix}, \quad \mathbf{M} = \begin{bmatrix} M_1 + M_2 & -M_2 \\ -M_2 & M_2 \end{bmatrix}, \quad \text{and} \quad \boldsymbol{\eta} = \begin{bmatrix} 0 & 0 \\ 0 & \eta \end{bmatrix}. \quad (5.49)$$

For the model in Figure 5.8b, the form of matrix \mathbf{M} in the expression for the elastic energy is different:

$$\mathbf{M}' = \begin{bmatrix} M'_1 & -M'_1 \\ -M'_1 & M'_1 + M'_2 \end{bmatrix}, \quad \text{and} \quad \boldsymbol{\eta}' = \begin{bmatrix} 0 & 0 \\ 0 & \eta' \end{bmatrix}. \quad (5.50)$$

and the rigidity of the 'springs' and viscosity η' are also different from the case in Figure 5.8a. These quantities must be selected so that:

- 1) The 'unrelaxed' modulus (upper-left element M_{11} of matrix \mathbf{M}) equals M_{11} in eq. (5.49);
- 2) The 'relaxed' compliance (upper-left element of matrix $\mathbf{J} = \mathbf{M}^{-1}$) also equal that for matrix \mathbf{M} in eq. (5.49).

Exercise

From the above, it is obvious that $M'_1 = M_1 + M_2$. Try also obtaining M'_2 and η' .

To obtain η' , consider a pure internal deformation with fixed $\varepsilon_1 = 0$. For this deformation, the characteristic frequency is $f_c = M_{22}/2\pi\eta$, and this frequency must be the same for the two implementations of Zener's body.

Again using a specific experimental parameters and eqs. (5.46) and (5.47), the behavior of the Zener's body can be modeled completely and in detail (see Lab 5.2 below). This modeling yields the Zener's equation and all the characteristic relation for relaxation times and frequency-dependent attenuation and dispersion spectra (see section 2.4).

Burgers' solid

The Burger's solid adds to Zener's one an additional degree of freedom (variable number three in Figure 5.9) for which free static deformation is allowed. Therefore, this viscoelastic system is described by the GLS case $N = 3$, with 3×3 material-property matrices

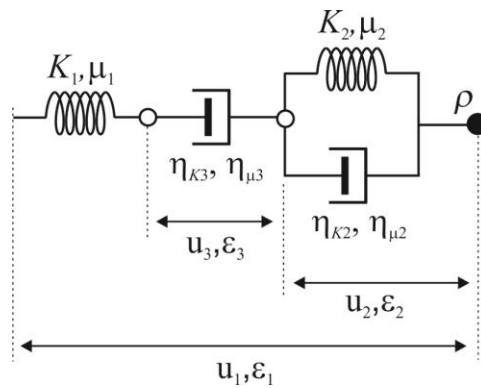


Figure 5.9.

Burgers' linear solid. Labels and notation are as in Figure 5.6.

$$\boldsymbol{\rho} = \begin{bmatrix} \rho & 0 & 0 \\ 0 & 0 & 0 \\ 0 & 0 & 0 \end{bmatrix}, \quad \mathbf{M} = \begin{bmatrix} M_1 & -M_1 & -M_1 \\ -M_1 & M_1 + M_2 & -M_1 \\ -M_1 & -M_1 & M_1 \end{bmatrix}, \quad \text{and} \quad \boldsymbol{\eta} = \begin{bmatrix} 0 & 0 & 0 \\ 0 & \eta_2 & 0 \\ 0 & 0 & \eta_3 \end{bmatrix}. \quad (5.51)$$

Generalized standard linear solid

The GSLS model of material rheology (Figure 5.10) is a combination of multiple SLS (Zener's) bodies with an additional spring. This arrangement of mechanical elements (terms in equations) is commonly used to implement band-limited attenuation in finite-difference codes for modeling seismic wavefield.

In finite-difference modeling software, the GSLS structure is implemented by including in the time-stepping several Maxwell's solids shown by red in Figure 5.10. The effects of Maxwell's solids are implemented by adding terms r_{ij} called 'memory variables' to the elastic stresses σ_{ij} within the medium. From Figure 5.10, these memory variables can be roughly visualized as deformations of the dashpots (which are initially zero and vary with time).

The GSLS (Figure 5.10; which is also the Standard linear solid for $N=2$) is constructed by using $L \equiv N-1$ internal (or memory) variables (usually, $L=5$ or 6 in finite-difference modeling; Zhu et al., 2013). Its GLS matrices are (Figure 5.10):

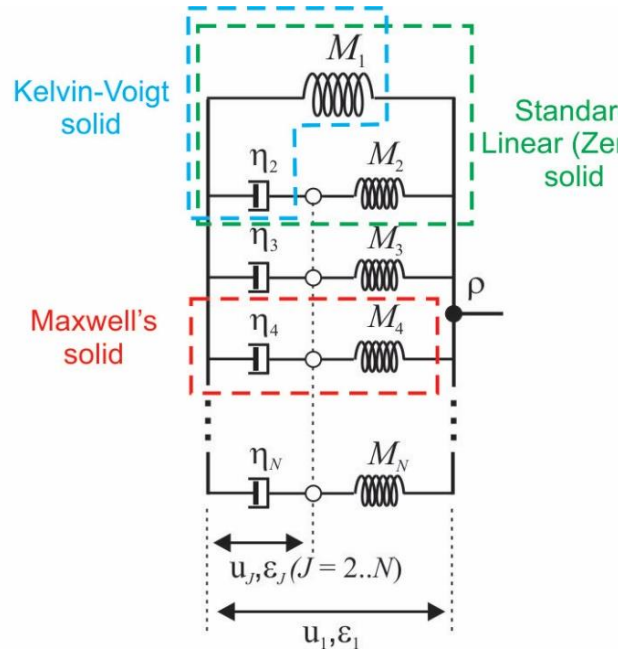


FIGURE 5.10.

Generalized standard linear solid. Color boxes indicate the Kelvin-Voigt, Maxwell's, and Standard Linear (Zener) solids. Moduli M_1, M_2, \dots and the corresponding viscosity parameters of the dashpots may refer to any type of elastic modulus (bulk, shear, Young's, or P-wave). Variable u_1 and its gradients ϵ_1 represent the observable variable, and variables \mathbf{u}_J ($J=2 \dots N$) are the internal variables added to implement band-limited seismic attenuation.

$$\boldsymbol{\rho} = \begin{bmatrix} \rho & 0 & 0 & \cdots & 0 \\ 0 & 0 & 0 & \cdots & 0 \\ 0 & 0 & 0 & \ddots & 0 \\ \vdots & \vdots & \ddots & \ddots & \vdots \\ 0 & 0 & 0 & \cdots & 0 \end{bmatrix}, \quad \mathbf{M} = \begin{bmatrix} \sum_{J=1}^N M_J & -M_2 & -M_3 & \cdots & -M_N \\ -M_2 & M_2 & 0 & \cdots & 0 \\ -M_3 & 0 & M_3 & \ddots & 0 \\ \vdots & \vdots & \ddots & \ddots & \vdots \\ -M_N & 0 & 0 & \cdots & M_N \end{bmatrix}, \quad (5.52a)$$

$$\text{and } \boldsymbol{\eta} = \begin{bmatrix} 0 & 0 & 0 & \cdots & 0 \\ 0 & \eta_2 & 0 & \cdots & 0 \\ 0 & 0 & \eta_3 & \cdots & 0 \\ \vdots & \vdots & \vdots & \ddots & \vdots \\ 0 & 0 & 0 & \cdots & \eta_N \end{bmatrix}. \quad (5.52b)$$

The values of M_J and η_J are usually selected to achieve a near-constant Q -factor within the frequency band of interest. Figure 5.11 shows such attenuation and wave velocity dispersion spectra calculated using the eigenmode eq. (5.10) for a GSLS rheology with five Maxwell's bodies listed in Table 5.1. Only one mode is valid (all other modes involving massless internal variables have infinite velocities) and shows a broad-band near constant spectrum of $Q^{-1}(f)$ (Figure 5.11a) and a near-linear interval of velocity increase across this band (Figure 5.11b).

If we try nonzero densities of the internal variables, N wave modes appear (Figure 5.12). There exists a small “critical” level of these densities, so that for densities

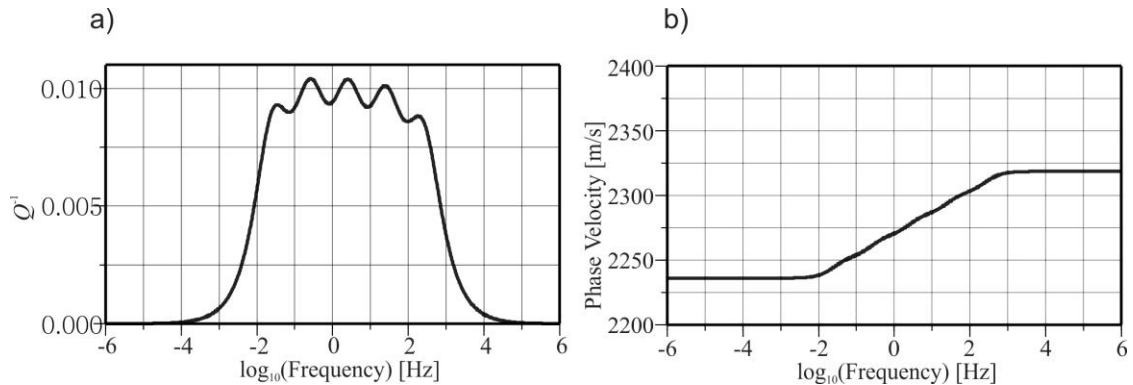


FIGURE 5.11

Characteristics of a plane P wave in a GSLS medium (Table 5.1): a) attenuation, b) phase velocity.

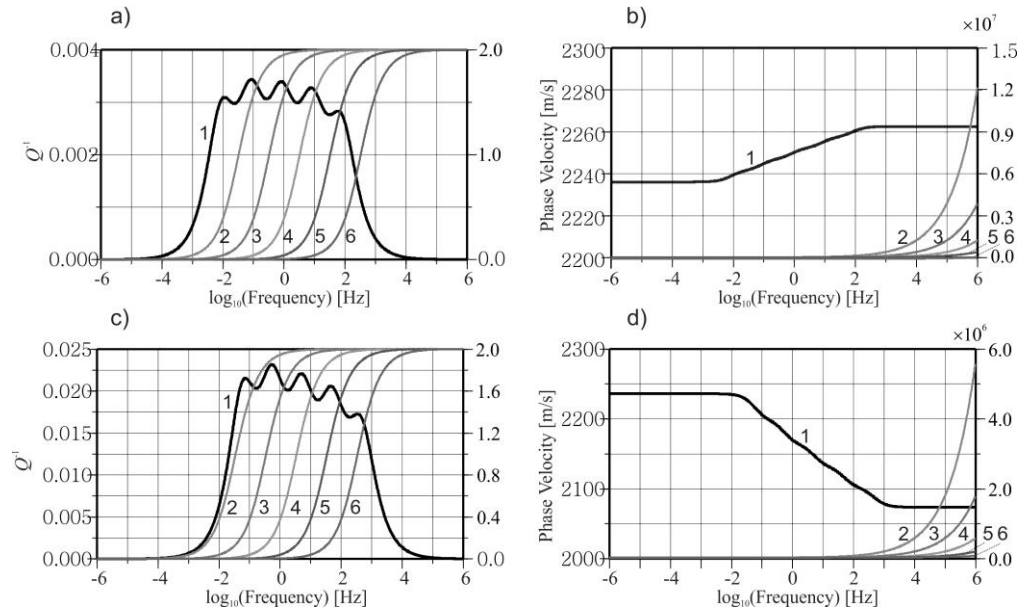


FIGURE 5.12

Propagation of a plane P wave in a GSLS medium with densities assigned to the internal variables: a) attenuation for internal density levels of 1% of the main density (Table 5.1), b) phase velocity for internal-density factor $a = 0.01$, c) and d) – the same for $a = 0.05$ (Table 5.1). The numbers of wave modes are labeled. Black lines indicate the primary mode, and gray lines are the additional modes due to internal densities..

above this level, the primary-mode velocity dispersion is positive (solid line in Figure 5.12b; this type of dispersion is actually called “inverse” in optics and seismology). The level of this critical density is about q/Q , which is about 1% of the density of the rock. For internal densities below this critical level, the velocity trend with frequency is negative (Figure 5.12d; “normal” dispersion). The attenuation (Q^{-1}) can still be kept exactly the same (Figure 5.12a and c). Thus, as this example shows, internal densities cause significant

Table 5.1. Mechanical Parameters of the Generalized Standard Linear Solid (GSLS) medium in Figures 5.11 and 5.12

J	M_J , (GPa)	η_J (Pa·s)	GSLS model	GSLS with 1% (5%)
			(Figure 5.12a, b)	internal densities (Figure 5.12c, d)
			ρ_J (kg/m ³)	ρ_J (kg/m ³)
1	10	0	2000	2000
2	0.15	$9.3 \cdot 10^8$	0	20 (100)
3	0.15	$9.3 \cdot 10^7$	0	20 (100)
4	0.15	$9.3 \cdot 10^6$	0	20 (100)
5	0.15	$9.3 \cdot 10^5$	0	20 (100)
6	0.15	$9.3 \cdot 10^4$	0	20 (100)

effects on the wave mode content and velocity dispersion even with the same attenuation spectrum $Q^{-1}(f)$.

5.8.2 Kinetic (massless) internal variables

To understand the behavior of generalized linear solids, it is instructive to consider an elementary system consisting of a Maxwell body connected in parallel with some other mechanical system (Figure 5.13). This system represents partitioning of the Generalized Standard Linear Solid in Figure 2.10a, and the serial arrangement in Figure 2.10b can be treated similarly. The two parts of this system share the “observable” strain ε and strain rate $\dot{\varepsilon}$, whereas the strain ε' is contained entirely within the Maxwell body. This strain is considered not measured and viewed as an internal variable. Our goal here is to show that if the Maxwell body is massless, this internal variable obeys a kinetic equation.

As usual, to solve this problem, we need to write the Lagrangian and dissipation function for the entire system. For simplicity of notation, we choose the deformation of the “internal spring” as the internal variable (Figure 5.13), so that $\varepsilon' = 0$ in both the initial (at $t = 0$) and “relaxed” ($t \rightarrow \infty$ and $\dot{\varepsilon} = 0$) states. Therefore,

$$L = L_0 - \frac{k}{2} \varepsilon'^2, \text{ and } D = D_0 + \frac{\eta}{2} (\dot{\varepsilon} - \dot{\varepsilon}')^2. \quad (5.53)$$

For a massless variable ε' , the Lagrangian is independent of the generalized velocity, $\dot{\varepsilon}'$, and therefore the corresponding Euler-Lagrange equation is:

$$-\frac{\partial L}{\partial \varepsilon'} + \frac{\partial D}{\partial \dot{\varepsilon}'} = k\varepsilon' + \eta\dot{\varepsilon}' - \eta\dot{\varepsilon} = 0. \quad (5.54)$$

Therefore, the rate $\dot{\varepsilon}'$ is uniquely determined by the external deformation rate and the current value of ε' :

$$\dot{\varepsilon}' = \dot{\varepsilon} - \frac{1}{\tau} \varepsilon', \quad (5.55)$$

where $\tau = k/\eta$ can be called the “relaxation time.” This is the kinetic equation commonly

used for describing chemical reaction rates and often used to describe viscoelastic solids (e.g., Nowick and Berry, 1972). If after some moment t_0 , the external strain becomes stationary ($\dot{\varepsilon} = 0$), then the internal strain exponentially relaxes to zero as $\varepsilon'(t-t_0) = \varepsilon'(t_0) \exp[-(t-t_0)/\tau]$ for $t \geq t_0$. The external strain rate, $\dot{\varepsilon}(t)$, serves as a source continuously displacing $\varepsilon'(t)$ from the stationary solution.

Equation (5.55) shows that $\varepsilon'(\omega)$, which is the Fourier amplitude and phase of the internal deformation at frequency ω , is uniquely determined by $\varepsilon(\omega)$:

$$\varepsilon'(\omega) = \frac{-i\omega\tau}{1-i\omega\tau} \varepsilon(\omega), \quad (5.56)$$

The internal degree of freedom follows the observed deformation with phase lag $\text{Arg}[i\omega\tau/(1-i\omega\tau)]$, which is determined by τ alone. This is the reason for the “stress-strain” phase lags used in viscoelasticity, and also for “relaxation times” τ controlling most popular strain-stress relations. Once again, such properties are only possible because of the assumed pure massless internal variables.

As shown in Problem 5.3, a solution to eq. (5.55) can be written in the form of a Volterra integral over the preceding time history of $\dot{\varepsilon}(t)$. However, the significance of this

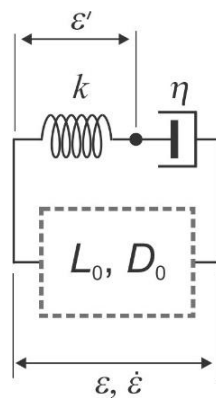


FIGURE 5.13

Maxwell's body connected in parallel with an arbitrary mechanical system (L_0, D_0). The two elements share the “observable” variables (strain ε and strain rate $\dot{\varepsilon}$). The “internal” strain ε' belongs to the Maxwell's body and accounts for its retarded response.

solution as “memory” inherent in the system should not be overstated, as it simply follows from the differential eq. (5.55). Physically, the ability to produce a kinetic equation (5.55) and a solution completely determined by $\dot{\epsilon}(t)$ arises from the absence of mass in the Maxwell body (Figure 5.13). This is characteristic of the kinetic (or quasi-static) approximation inherent in the viscoelastic model (see section 2.8).

5.9 Extended Generalized Standard Linear Solid

In this section, we consider a GLS model called the extended Generalized Standard Linear Solid (extended GSLS). This model differs from the conventional viscoelastic models and has no pictorial representation by a collection of springs (like in Figure 5.10). The purpose of this model is to describe the rock matrix with multiple porosities. Because of a close similarity to Biot’s model, this structure is likely more appropriate for describing rocks than the usual GSLS.

The extended GSLS is obtained by noting that the bulk-modulus matrix \mathbf{K} for Biot’s model (eq. 5.23) becomes that of the SLS (Zener’s; eq. (5.50)) model when Biot-Willis parameter α is set equal one. Using this connection, we can generalize the elastic matrix of the GSLS (eq. 5.52a) by including parameters α_J for each internal variable $J = 2, \dots, N$:

$$\mathbf{M} = \begin{bmatrix} M_1 + \sum_{J=2}^N \alpha_J^2 M_J & -\alpha_2 M_2 & -\alpha_3 M_3 & \cdots & -\alpha_N M_N \\ -\alpha_2 M_2 & M_2 & 0 & \cdots & 0 \\ -\alpha_3 M_3 & 0 & M_3 & \ddots & 0 \\ \vdots & \vdots & \ddots & \ddots & \vdots \\ -\alpha_N M_N & 0 & 0 & \cdots & M_N \end{bmatrix}. \quad (5.57)$$

For the Biot’s poroelastic case ($N = 2$), this extended SLS is exactly the bulk-modulus matrix. The analogy also suggests that α_J is limited by relation $\phi_J \leq \alpha_J \leq 1$ in which the lower limit $\phi_J \geq 0$ is a geometrical property serving as “porosity” for component J of the composite material. The lower limit $\alpha_J = \phi_J$ means zero analog of the pore-fluid modulus K_f (eq. 5.37). The upper limit $\alpha_J = 1$ means that the drained frame (modulus M_1 in eq. 5.57) contains no stiffness due to this variable (compare to eq. (5.35)). In this limit, the elastic

frame contains a deformation mode (the “drained,” or quasi-static state) in which variable J has no impact on the wave propagation.

Having defined the possible elastic structure, we need to consider solid viscosity. Generally, a GLS medium with N variables supports N P-wave modes and $2N$ S-wave modes with different polarizations. As shown in section 5.2, these waves can be found as solutions $\mathbf{v}^{(n)}$ (with $n = 1 \dots N$) of the generalized eigenvalue equation

$$\boldsymbol{\rho}^* \mathbf{v}^{(n)} = \gamma^{(n)} \mathbf{M}^* \mathbf{v}^{(n)}, \quad (5.10 \text{ repeated})$$

where $\boldsymbol{\rho}^* \equiv \boldsymbol{\rho} + i\mathbf{d}/\omega$ and $\mathbf{M}^* = \mathbf{M} - i\omega\boldsymbol{\eta}_M$ are the complex-valued, matrix density and P-wave modulus, respectively, and $\gamma^{(n)}$ is the eigenvalue containing the phase velocity and attenuation of the wave. Without viscosity or Darcy friction ($\mathbf{d} = \mathbf{0}$, $\boldsymbol{\eta} = \mathbf{0}$), all these eigenvalues will be real-valued, and all N wave modes will propagate to arbitrary distances. However, in practice, only one primary mode with weak attenuation is usually observed for each wave type. All other modes such as Biot’s secondary waves are suppressed by solid viscosity. Thus, matrices $\boldsymbol{\eta}$ and \mathbf{d} should generally be constructed so that they exert relatively weak friction on the primary mode (involving the strongest deformation of the observable displacement variable u_{Ji} , with $J = 1$) but strong friction on other modes with $J \geq 2$.

5.9.1 Selection of internal-friction material properties

In Biot’s model (section 5.6) and in the usual GSLS (eqs. 5.52), the diagonal matrices of internal friction \mathbf{d} and $\boldsymbol{\eta}_K$ are defined in exactly the way described in the preceding paragraph. All elements of the first rows and columns of these matrices equal zero, and therefore, viscous forces are only applied to the internal variables number $J \geq 2$. However, in the extended GSLS model (eq. 5.57) with $\alpha_j \neq 1$, such purely diagonal friction is insufficient. If using a diagonal matrix $\boldsymbol{\eta}$, the primary wave mode also turns out to be dissipative, as in the Kelvin-Voigt body (see subsection above). However, as shown below, the appropriate matrices $\boldsymbol{\eta}$ and/or \mathbf{d} can be found for any selection of parameters α_j , and even for any arbitrary elastic matrices \mathbf{K} and $\boldsymbol{\mu}$.

If the observed dispersion spectrum for some modulus (for example, P-wave) $M(\omega)$ possesses a high-frequency plateau $M(\omega) \approx M_U$, this plateau means that the deformation at high frequencies occurs in a mode which is insensitive to viscosity (because viscosity causes effective moduli $M(\omega)$ linearly increasing with frequency). Therefore, this wave mode must be a solution of eq. (5.10 repeated) with zero viscosity Matrices $\boldsymbol{\eta}$ and \mathbf{d} determine whether all wave modes will experience attenuation at high frequencies, i.e. of the elastic wave equation (with real-valued matrices $\boldsymbol{\rho}$ and \mathbf{M})

$$\boldsymbol{\rho}\mathbf{v}^{(n \text{ elastic})} = \gamma^{(n \text{ elastic})}\mathbf{M}\mathbf{v}^{(n \text{ elastic})}. \quad (5.58)$$

This equation can be solved giving N possible elastic-wave solutions. The non-dissipative mode should be the primary one, with the largest phase velocity and (usually) the strongest contribution from the observable displacement variable u_{1i} . Let us denote this mode by index $n = 1$, i.e. $\mathbf{v}^{(1 \text{ elastic})}$. Then, because the wave must be non-dissipative, all internal-friction matrices should satisfy

$$\boldsymbol{\eta}_K \mathbf{v}^{(1 \text{ elastic})} = \boldsymbol{\eta}_\mu \mathbf{v}^{(1 \text{ elastic})} = \mathbf{d}\mathbf{v}^{(1 \text{ elastic})} = \mathbf{0}. \quad (5.59)$$

If multiple elastic wave modes are expected (for example, are observed) to be non-dissipative, additional equations with $n > 1$ can be added to equations (5.59).

With all eigenvectors $\mathbf{v}^{(n \text{ elastic})}$ obtained from eq. (5.58), equations (5.59) represent a linear system of equations for frictional material properties (elements of matrices \mathbf{h}_K , $\boldsymbol{\eta}_m$, and \mathbf{d}). In these equations, some of these material properties, such as elements on the main diagonals, can be selected relatively arbitrarily (similar to the diagonal of matrix $\boldsymbol{\eta}$ in eq. (5.52b)), and others need to be inverted from eqs. (5.59) to produce the non-dissipative mode(s). Similar to eq. (5.52b), the arbitrary elements can be selected so that the resulting wave will have the expected attenuation spectrum of $Q^{-1}(f)$.

5.10 *Effective media (homogenization)*

The preceding subsection gave an example of homogenization (construction of

effective-media parameters) for a porous medium with noninteracting microcracks. Here, I describe how homogenization is done for a GLS.

...

5.11 *Model discretization for numerical modeling*

Discretization of continuous models into the form of finite mass-stiffness-damping models (section 4.5) can be done by numerous methods. Below, I describe two groups of such methods: 1) using “finite elements” (decomposition into spatial elements of various shapes; subsection 5.11.1), and 2) using “finite differences” on regular spatial grids subsection (5.11.2).

5.11.1 Finite-element discretization using basis functions (Galerkin’s method)

Finite-element discretization of differential equations such as the Euler-Lagrange equations of motion (eqs. 4.13) is based on the so-called weak formulation of these equations. Consider an arbitrary system of differential or integral equations for some variable field $\mathbf{q}(t, \mathbf{x})$, such as the GLS equations in section 5.1 or their extension to thermal effects in chapter 6 below. For linear interactions considered in the GLS model, these equations are linear with respect to function $\mathbf{q}(t, \mathbf{x})$. Isolating the partial derivatives with respect to time, these differential equations can be written in the following general form:

$$\sum_k D_t^{(k)} \frac{\partial^k}{\partial t^k} \mathbf{q}(t, \mathbf{x}) + \sum_m D_x^{(m)} \mathbf{q}(t, \mathbf{x}) = \mathbf{s}(t, \mathbf{x}), \quad (5.68)$$

where $D_t^{(k)}$ and $D_x^{(m)}$ are some differential operators in space and $\mathbf{s}(t, \mathbf{x})$ is some source function. Operators $D_t^{(k)}$ and $D_x^{(m)}$ contain material properties and may therefore depend on \mathbf{x} . Multiple equations of the form (5.68) may be combined to form the system of linear differential equations.

In addition to eqs. (5.68), function $\mathbf{q}(t, \mathbf{x})$ is expected to satisfy boundary conditions, such as zero stress on the side boundary of a cylinder in axial compression test, zero pore-fluid flows on sealed boundaries, or a certain temperature regime at the contact with

thermostat. These boundary conditions can be simply added to eqs. (5.68) or included in the construction of basis functions as discussed in subsection “Implementation of boundary conditions” below.

In a “weak formulation” of eqs. (5.68), an approximate solution is sought in the form of a linear combination of a set of basis functions $f_n(\mathbf{x})$:

$$q_J(t, \mathbf{x}) = \sum_n q_n(t) f_n(\mathbf{x}). \quad (5.69)$$

where the uppercase subscript J denotes GLS (and other) model-space variables, index n enumerates the basis functions in some way. For models with internal variables ($N > 1$ or possibly internal variables $\boldsymbol{\theta}$ and/or temperature) this enumeration should include J , spatial components of displacement as well as spatial mode numbers such as orders of Fourier-Bessell functions, etc. The coefficients q_n become scalar and discrete generalized variables, and the problem reduces to modeling their variations with time $q_n(t)$. Taken together, all variables q_n form a (possibly large) model vector denoted $\bar{\mathbf{q}}$ below.

To implement the decomposition (5.69) and other equations, one needs to define a measure of mutual scalar product of two arbitrary functions $\varphi_1(\mathbf{x})$ and $\varphi_2(\mathbf{x})$, in the functional space. In linear algebra, this scalar product is also called the inner product, or dot product for conventional vectors. This measure is often denoted $\langle \varphi_1 | \varphi_2 \rangle$, and for functions, defined as

$$\langle \varphi_1 | \varphi_2 \rangle = \int \varphi_1^*(\mathbf{x}) \varphi_2(\mathbf{x}) d\mathbf{x}, \quad (5.70)$$

where the integration is performed over the entire space or volume of interest, and complex conjugation “*” is used working with complex-valued fields $\mathbf{q}(t, \mathbf{x})$ and basis functions. The product of a vector (function) $\varphi(\mathbf{x})$ with itself gives its L_2 norm as $\|\varphi\| = \sqrt{\langle \varphi | \varphi \rangle}$.

To simplify subsequent calculations, it is useful to use orthogonal and normalized basis functions satisfying relations

$$\langle f_n | f_k \rangle = \delta_{nk}, \quad (5.71)$$

for arbitrary n and k , where δ_{nk} is the Kronecker delta. With such functional basis, the coefficient vector q_n equals (inverse of relation (5.69)):

$$q_n(t) = \langle f_n | \mathbf{q}(t, \mathbf{x}) \rangle. \quad (5.72)$$

This expression represents a projection of field $\mathbf{q}(t, \mathbf{x})$ onto the spatial basis function $f_n(\mathbf{x})$.

The Galerkin's method for solving eq. (5.68) consists in projecting both sides of this equation onto each of the basis functions and solving the resulting matrix equations. Considering the usual values $k = 1$ and 2 , one m , and one component of output model vector for simplicity of notation, for the l^{th} basis function and, eq. (5.68) becomes

$$\sum_n \langle f_l | D_t^{(2)} f_n \rangle \ddot{q}_n + \sum_n \langle f_l | D_t^{(1)} f_n \rangle \dot{q}_n + \sum_n \langle f_l | D_x f_n \rangle q_n = \langle f_l | s \rangle. \quad (5.73)$$

In matrix form for the complete model vector $\bar{\mathbf{q}}$, this equation is

$$\mathbf{A}^{(2)} \ddot{\bar{\mathbf{q}}} + \mathbf{A}^{(1)} \dot{\bar{\mathbf{q}}} + \mathbf{C} \bar{\mathbf{q}} = \mathbf{s}, \quad (5.74)$$

where the matrix and vector elements are

$$A_n^{(k)} = \langle f_l | D_t^{(k)} f_n \rangle, \quad C_n = \langle f_l | D_x f_n \rangle, \quad \text{and} \quad s_l = \langle f_l | s \rangle. \quad (5.75)$$

In addition to equations of mechanics, vector $\bar{\mathbf{q}}$ should satisfy a set of boundary conditions. Boundary-condition equations can be added directly to the system of linear system of eq. (5.74); however, it is useful to utilize them separately, prior to considering the actual motion of the system. This solution provides a characterization of possible deformation types and reduces the dimensionality of the inverse problem. As shown in the subsection "Implementation of boundary conditions," boundary conditions lead to vector $\bar{\mathbf{q}}$ of the form

$$\bar{\mathbf{q}} = \mathbf{F}\mathbf{q}, \quad (5.76)$$

where \mathbf{q} is a vector of *mutually independent* variables and \mathbf{F} is a matrix implementing the boundary conditions. If vector $\bar{\mathbf{q}}$ contains N_q elements and the number of independent boundary conditions is N_b , then vector \mathbf{q} contains $(N_q - N_b)$ variables, and the dimensions of matrix \mathbf{F} are $(N_q - N_b)$ rows and N_q columns. Equations (5.74) finally become

$$\mathbf{A}^{(2)}\mathbf{F}\ddot{\mathbf{q}} + \mathbf{A}^{(1)}\mathbf{F}\dot{\mathbf{q}} + \mathbf{C}\mathbf{F}\mathbf{q} = \mathbf{s}. \quad (5.77)$$

In frequency domain, this equation can be inverted as

$$\mathbf{q}_\omega = \left(-\omega^2 \mathbf{A}^{(2)}\mathbf{F} - i\omega \mathbf{A}^{(1)}\mathbf{F} + \mathbf{C}\mathbf{F} \right)^{-1} \mathbf{s}_\omega. \quad (5.78)$$

Note that the matrix eqs. (5.77) and (5.78) represent the motion of a mass-stiffness damping (MSD) system (section 4.5 on page 86) with mass matrix $\mathbf{M} = \mathbf{A}^{(2)}\mathbf{F}$, damping matrix $\mathbf{D} = \mathbf{A}^{(1)}\mathbf{F}$, and stiffness matrix $\mathbf{S} = \mathbf{C}\mathbf{F}$. Thus, even if thermoelastic effects are involved, the macroscopic body (rock sample, seismic wave) behaves as a mechanical system, and therefore it can be described by Lagrangian mechanics with energy dissipation.

Recipe for solving GLS equations using Galerkin's method

In summary, to solve a system of GLS (or other) equations using Galerkin's method, one needs to:

- 1) Define a convenient enumeration $n = 1, 2, \dots, N_b$ of variables $q_n(t)$ in eq. (5.69) including all observable and internal variables, one or multiple temperatures if desired, and all spatial locations or harmonics.
- 2) Construct an initial set of basis functions corresponding to geometry of the problem and the desired sampling style (for example, spatial gridding or

- Fourier harmonics), and providing sufficient spatial detail of the solution.
- 3) Transform the initial set of basis functions 2) to satisfy boundary conditions. This step is described in subsection “Implementation of boundary conditions.”
 - 4) Optional step: If this is not included in step 3), further transform the basis functions to satisfy the orthonormality relations in eqs. (5.71). This procedure is standard in linear algebra and described in the Appendix (section 9.3).
 - 5) Evaluate (analytically or numerically) the spatial averages of products of basis functions with the appropriate differential operators and material properties. This gives matrix equation (5.75).
 - 6) Perform modeling by integration of the differential equation eq. (5.77) in time or by Laplace-transform or frequency-domain methods.

Implementation of boundary conditions

Boundary conditions are usually of the form of homogeneous differential equations similar to eq. (5.68):

$$D_x^{(b)} \mathbf{q}(t, \mathbf{x}) = 0, \quad (5.79)$$

where $D_x^{(b)}$ is some spatial differentiation operator. For example, eq. (5.79) can require zero displacements, strains, or stresses at some boundaries, constant temperatures or zero heat flows at boundaries, or linear combinations of such constraints. Multiple equations of the type (5.79) correspond to evaluating the boundary conditions at different point or area, such as on a side of the cylinder or at its end. Using eq. (5.69)) and projecting these differential equations onto the l^{th} basis function gives a matrix equation

$$\mathbf{B}\bar{\mathbf{q}} = \mathbf{0}, \quad (5.80)$$

where the matrix elements are similar to eq. (5.75)

$$\mathbf{B}_{ln} = \langle f_l | D_x^{(b)} f_n \rangle. \quad (5.81)$$

The subspace of vectors $\bar{\mathbf{q}}$ satisfying eqs. (5.80) can be found from the singular value decomposition (SVD) of \mathbf{B} :

$$\mathbf{B} = \sum_{k=1}^{N_b} \sigma_k \mathbf{u}_k \mathbf{v}_k^+. \quad (5.82)$$

where \mathbf{u}_k and \mathbf{v}_k are the k^{th} left and right singular vectors, respectively, and σ_k are the corresponding singular values. In this expression, superscript ‘+’ denotes the Hermitian conjugation (complex conjugate and transposed \mathbf{v}), and N_b is the rank of matrix \mathbf{B} which is expected to be smaller than the number of elements in vector $\bar{\mathbf{q}}$ denoted N_q . Vectors \mathbf{u}_k and \mathbf{v}_k are also mutually orthogonal and normalized to unit magnitude. Note that N_b is also found from the SVD as the number of nonzero singular values. If the boundary condition equations are linearly dependent, N_b may be smaller than the number of rows in matrix \mathbf{B} .

Equations (5.80) and (5.82) show that for a deformation allowed by the boundary conditions, vector $\bar{\mathbf{q}}$ must be orthogonal to each of the vectors \mathbf{v}_k . This subspace of vectors orthogonal to \mathbf{v}_k is called the orthogonal linear complement of the subspace given by vectors $\{\mathbf{v}_1, \mathbf{v}_2, \dots, \mathbf{v}_{N_b}\}$. Vectors of this orthogonal complement can be represented by matrix product

$$\bar{\mathbf{q}} = \mathbf{F} \underline{\mathbf{q}}, \quad (5.83)$$

where \mathbf{F} is a matrix of $N_f = N_q - N_b$ basis vectors in the orthogonal complement and $\underline{\mathbf{q}}$ is an arbitrary vector of dimension N_f . Columns of matrix \mathbf{F} can be found in various ways. For example, starting from known vectors $\{\mathbf{v}_1, \mathbf{v}_2, \dots, \mathbf{v}_{N_b}\}$, one can set random values to N_f additional vectors and apply to them the ortho-normalization procedure described in the Appendix (section 9.3).

Finally, after inclusion of boundary conditions, vector $\underline{\mathbf{q}}$ can be viewed as a vector of *all independent generalized variables of the problem*. Similar to eq. (5.69), the modeled

field is represented by a combination of basis functions (finite elements):

$$q_J(t, \mathbf{x}) = \sum_k q_k(t) \underline{f}_k(\mathbf{x}). \quad (5.84)$$

where the shape of deformation in k^{th} finite element is (from eq. (5.83))

$$\underline{f}_n(\mathbf{x}) = \sum_n F_{nk} f_n(\mathbf{x}). \quad (5.85)$$

As in eq. (5.69), the summation in eq. (5.84) is performed over all values relevant to index J and location \mathbf{x} .

Construction of basis functions

Construction of the set of appropriate basis functions f_n depends on the size, symmetry, and shape of modeled body. In the following subsections, I describe three of the most common cases for finite bodies: bodies consisting of rectangular shapes and bodies with cylindrical or spherical symmetries.

Rectangular shapes (gridded functions)

For bodies represented by combinations of rectangular objects, the easiest shape of the finite-element functions is a product of some localized spline functions of the individual coordinates. For example, for three dimensions:

$$f_n(x, y, z) = f_i^{(x)}(x) f_j^{(y)}(y) f_k^{(z)}(z), \quad (5.86)$$

where n is a unique index spanning all basis functions and (i, j, k) are the indices in each of the spatial dimensions. Because equations (5.88), () represent only the initial set of basis functions which need to be further orthogonalized and scaled to satisfy the orthogonality relations, eqs. (5.86) do not require scaling factor.

The 1-D functions in eq. (5.86) (for example, $f_i^{(x)}(x)$) are usually constructed so that the value at the i^{th} node equals one and it falls off to zero at the adjacent nodes $(i-1)$ and $(i+1)$. Two types of shapes are commonly used:

1) Piecewise-linear “saw tooth” function

$$\begin{aligned} f_i^{(x)}(x) &= 1 - (x - x_i) / (x_{i-1} - x_i) \quad \text{for } x \in [x_{i-1}, x_i], \\ f_i^{(x)}(x) &= 1 - (x - x_i) / (x_{i+1} - x_i) \quad \text{for } x \in [x_i, x_{i+1}], \\ f_i^{(x)}(x) &= 0 \quad \text{elsewhere.} \end{aligned} \quad (5.87)$$

This function is simple but has a discontinuous derivative (constant between grid points), which may be undesirable and inaccurate when using not very dense gridding.

2) If continuous derivatives are desired, “Wiggins basis functions” can be used. These are actually *two* sets of functions, each of which combines two cubic polynomial within intervals $[x_{i-1}, x_i]$ and $[x_i, x_{i+1}]$ (Figure 5.14). The coefficients of these polynomial are defined by four requirements: zero value $f_i^{(x)} = 0$ and zero derivative $df_i^{(x)}/dx = 0$ at the adjacent points $x = x_{i\pm 1}$, and at point $x = x_i$:

a) For the first set, $f_i^{(x)}(x_i) = 1$ and $\frac{d}{dx} f_i^{(x)}(x_i) = 0$;

b) For the second set, $f_i^{(x)}(x_i) = 0$ and $\frac{d}{dx} f_i^{(x)}(x_i) = 1$.

The derivatives for these functions are easily calculated. Within any grid interval, the functions have the form $f_i^{(x)}(x) = ax^3 + bx^2 + cx + d$, and therefore the derivative is

$$\frac{d}{dx} f_i^{(x)}(x) = 3ax^2 + 2bx + c.$$

Discs and cylinders (Bessel functions)

Mechanical rock-physics experiments are typically conducted with cylindrical cores (e.g., Figure 1.7), and it is therefore natural to use cylindrical coordinates to model them. Consider a cylinder of radius R and length L . In cylindrical coordinates (r, φ, z) ¹³, the basis functions for the interior of the cylinder are taken as

¹³ To avoid confusion with density, I denote the radial distance r instead of the conventional notation ρ .

$$f_n(r, \varphi, z) = f_j^{(z)}(z) f_k^{(r)}(r) f_m^{(\varphi)}(\varphi), \quad (5.88)$$

where $m = 0, 1, 2, \dots$ is the number of the azimuthal harmonic, $k = 0, 1, 2, \dots$ is the radial order, $f_j^{(z)}(z)$ is the basis function for the dependence on the axial coordinate, $f_k^{(r)}(r)$ is the radial basis function, and $f_m^{(\varphi)}(\varphi)$ is the azimuthal dependence. Index n enumerates all basis functions sequentially, and spatial indices l, m , and j are functions of n .

For azimuthal dependencies, due to the periodicity of this domain, complex exponential functions are commonly used:

$$f_m^{(\varphi)}(\varphi) = e^{2\pi i m \varphi}. \quad (5.89)$$

However, gridding of the interval $\varphi \in [0, 2\pi]$ can also be used. For typical axisymmetric cases in rock physics, a single function $f_m^{(\varphi)}(\varphi) = 1$ (with $m = 0$) is sufficient.

For the axial dependence $f_j^{(z)}(z)$, any kind of gridded functions from the preceding subsection can be used. Alternatively, a sine and cosine or complex exponential function

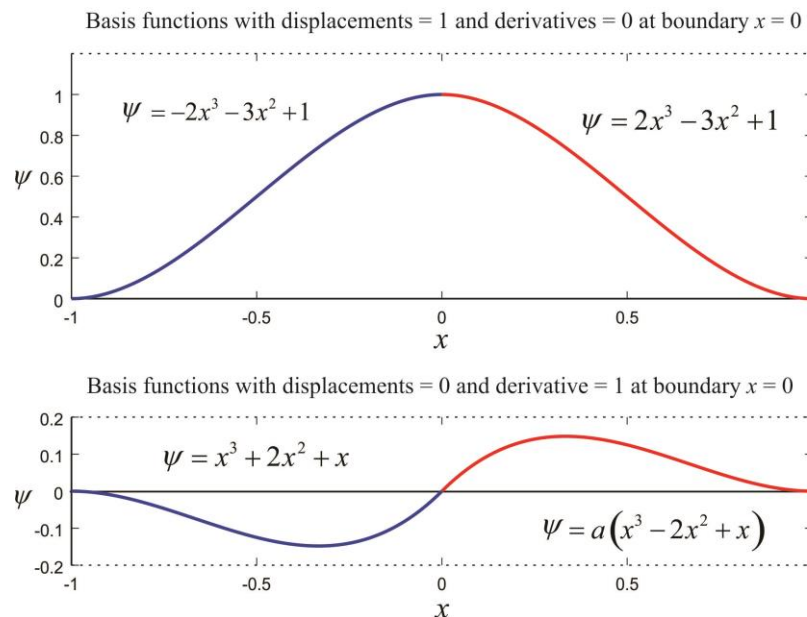


FIGURE 5.14.

Two types of Wiggins basis functions associated with node at $x_i = 0$ and adjacent nodes at ± 1 .

obtained by a Fourier transform in z can be used. These functions can be useful when specific kinds of boundary conditions are required at the ends of the cylinder, such as

$$f_j^{(z)}(z)\Big|_{z=0,L} = 0 \text{ or } f_j^{(z)'}(z)\Big|_{z=0,L} = 0. \text{ In such cases, sine or cosine functions of } \pi zj/L \text{ can}$$

be selected as axial basis functions.

For the dependence on r , again gridded or harmonic functions defined within interval $[0,R]$ should work. Because of the azimuthal symmetry, a decomposition into Bessel functions is often useful. Because of the singularity at point $r = 0$, two different forms of basis functions $f_k^{(r)}(r)$ are needed. For scalar quantities or the axial component of displacements, the basis function should satisfy constraint $f_k^{(r)'} = 0$ at $r = 0$. Hence we can use a constant function $f_0^{(r)}(r) = 1$ for $k = 0$ and two or three Bessel functions for $k \geq 1$:

$$\begin{aligned} f_k^{(r)}(r) &= 1 && \text{for } k = 0, \\ f_k^{(r)}(r) &= J_0\left(\frac{r}{\kappa_k R}\right) && \text{for } k \geq 1. \end{aligned} \quad (5.90a)$$

Here, the zero-order Bessel function J_0 is used because of the absence of singularity at $r = 0$ for descriptions of an interior of a cylinder. This function is analogous to $\cos(\dots)$ function for the radial direction in polar coordinates. Parameters κ_k are nonzero roots of functions $J_0(\kappa)$ or $J_1(\kappa)$ (which is analogous to $\sin(\dots)$). For radial displacement, let us denote these function $f_k^{(r1)}(r)$ in cases of possible ambiguity. This basis functions should satisfy $f_k^{(r1)} = 0$ at $r = 0$, and we can use

$$f_k^{(r1)}(r) = J_1\left(\frac{r}{\kappa_k R}\right) \text{ for } k \geq 1. \quad (5.90b)$$

When evaluating norms in the space of basis functions and their orthogonality (eq. 5.70), the integration over volume takes the form

$$\int f d\mathbf{x} = \int_0^R r dr \int_0^{2\pi} d\varphi \int_0^L f dz. \quad (5.91)$$

Components of gradients are also modified to

$$\nabla_r f = \frac{\partial f}{\partial r}, \quad \nabla_\varphi f = \frac{1}{r} \frac{\partial f}{\partial \varphi}, \quad \text{and} \quad \nabla_z f = \frac{\partial f}{\partial z}. \quad (5.92)$$

Ellipsoidal bodies (Spherical functions)

...

5.11.2 Finite-difference discretization by spatial gridding

To produce equations for modeling of seismic waves, the model needs to be discretized on some type of grid or mesh. To produce such gridded equations, one can use finite-element methods of the preceding subsection, with n^{th} basis functions of some form described in subsection 5.11.1. Alternatively (and equivalently), for regularly spaced grids, matrix equations can be obtained by discretizing the partial differential equations of motion directly. This approach is called finite-difference and reviewed in this subsection. Effects of temperature are not considered here although they can be added in a straightforward way.

For simplicity, consider the case of ordinary with $N = 1$ and $d_{ij} = 0$ (eqs. 5.1) and wavefield sampled on a uniform 1-D grid (layering), 2-D, or 3-D grid (or even) with

constant spacing in each direction. Let us denote $\mathbf{u} = \begin{pmatrix} \mathbf{u}_x \\ \mathbf{u}_y \\ \mathbf{u}_z \end{pmatrix}$ the vector combining all values

of the three components of displacement at all grid points. This will usually be a very large vector, but nevertheless, all equations involving this vector will be simple. By using this vector, we can first define matrix operators extracting the x , y , and z components of the vector wavefield:

$$\mathbf{U}_x = [\mathbf{I} \ \mathbf{0} \ \mathbf{0}], \quad \mathbf{U}_y = [\mathbf{0} \ \mathbf{I} \ \mathbf{0}], \quad \text{and} \quad \mathbf{U}_z = [\mathbf{0} \ \mathbf{0} \ \mathbf{I}], \quad (5.93)$$

where the matrix blocks are of the same dimension as \mathbf{u} . Further, three spatial differentiation operators can be defined for each block of spatial directions $i = x, y, z$ (or 1,

2, 3) (see the GEOL884 notes): the forward derivative

$$\mathbf{D}_i^+ = \frac{1}{\Delta x_i} \begin{bmatrix} \dots & 1 & 0 & \dots & \dots & \dots \\ 0 & -1 & 1 & 0 & 0 & \dots \\ \dots & 0 & -1 & 1 & 0 & \dots \\ \dots & 0 & 0 & -1 & 1 & \dots \\ \dots & 0 & 0 & 0 & -1 & 1 \\ \dots & \dots & \dots & \dots & 0 & \dots \end{bmatrix}, \quad (5.94a)$$

and the backward one:

$$\mathbf{D}_i^- = -\mathbf{D}_i^{+T} = \frac{1}{\Delta x_i} \begin{bmatrix} \dots & 0 & 0 & \dots & \dots & \dots \\ -1 & 1 & 0 & 0 & 0 & \dots \\ \dots & -1 & 1 & 0 & 0 & \dots \\ \dots & 0 & -1 & 1 & 0 & \dots \\ \dots & 0 & 0 & -1 & 1 & 0 \\ \dots & \dots & \dots & \dots & -1 & \dots \end{bmatrix}. \quad (5.94b)$$

Combining these operators applied to each of the (x,y,z) blocks of vector \mathbf{u} , it is straightforward to obtain an expression for gridded strain corresponding to the definition

$$\varepsilon_{ij}^{\text{def}} = (\partial_i u_j + \partial_j u_i) / 2 \quad (\text{i.e., } \mathbf{E}_{ij}^+ = (\mathbf{D}_i^+ \mathbf{U}_j + \mathbf{D}_j^+ \mathbf{U}_i) / 2):$$

$$\boldsymbol{\varepsilon}_{ij} = \mathbf{E}_{ij}^+ \mathbf{u}. \quad (5.95)$$

The dilatational strain at every point within the grid is obtained as the spatial trace of this matrix, which gives another matrix operator $\boldsymbol{\Omega}^+$ (and its counterpart $\boldsymbol{\Omega}^-$):

$$\Delta^+ = \boldsymbol{\Omega}^+ \mathbf{u}, \quad \text{where} \quad \boldsymbol{\Omega}^+ = \mathbf{E}_{11}^+ + \mathbf{E}_{22}^+ + \mathbf{E}_{33}^+. \quad (5.96)$$

By using this $\boldsymbol{\varepsilon}$ and the λ - μ - ρ description of material properties (eqs. 5.1b), Generalized viscoelastic model for the body where all terms containing \mathbf{u} and $\dot{\mathbf{u}}$ are combined in three new matrix operators:

- 1) the mass matrix \mathbf{M} consisting of all density values on the diagonal;

- 2) the stiffness matrix $\mathbf{S} = \mathbf{\Omega}^{+T} \boldsymbol{\lambda} \mathbf{\Omega}^+ + 2\mathbf{E}^{+T} \boldsymbol{\mu} \mathbf{E}^+$, where λ and μ are similar diagonal matrices of the elastic moduli at each grid point. This matrix is often denoted \mathbf{K} , but I reserve this symbol for bulk modulus and for the poroelastic model.
- 3) the damping matrix $\mathbf{D} = \mathbf{\Omega}^{+T} \boldsymbol{\eta}_\lambda \mathbf{\Omega}^+ + 2\mathbf{E}^{+T} \boldsymbol{\eta}_\mu \mathbf{E}^+$ containing similar values of viscosity parameters on the diagonal. This matrix is often denoted \mathbf{C} , but we will use ‘ \mathbf{D} ’ for association with “damping”.

In time-domain modeling with attenuation using the empirical “viscoelastic” model, the governing equations deviate from the rigorous Lagrangian and thermodynamical equations above. The difference consists in replacing the internal variables with hypothetical “memory” variables which carry information about the previous time history deformation at every point. Boundary conditions for Unfortunately, this difference is practically never appreciated, but nevertheless, the viscoelastic model is the dominant approach to describing attenuation.

5.12 Problems and laboratory assignments

Lab 5.1: Model a Maxwell’s body

- 1) Using relations (5.43), derive matrices \mathbf{M} , \mathbf{S} , and \mathbf{D} for unidirectional extension of a cylindrical Maxwell’s body of length l . Disregard the Poisson’s effect of transverse contraction, i.e. assume that the body only deforms in the axial direction.
- 2) Using these matrices, model the frequency-dependent strain-stress response \mathbf{r} in this experiment.

Lab 5.2: Model a Zener’s body

- 1) Modify the code of Lab 5.1 to model a rock cylinder

Lab 5.3: Zener’s body with finite internal mass

Modify the code of Lab 5.2 to include a nonzero mass density for the internal variable (white dot in Figure 5.8). Compare the $M(f)$ spectra and deformations of the internal

variable for different values of the internal mass.

Lab 5.4: Modification of bulk and shear elastic moduli by secondary porosity

For a medium with $N = 1$, **write a Matlab function which takes arbitrary parameters b_1 and b_2** and an arbitrary crack tensor (symmetric matrix) α_{ij} in eq. (5.65) and returns the corresponding modifications of bulk and shear compliances $\delta(1/K)$ and $\delta(1/\mu)$.

To implement the function, consider two mutually independent trial values for stress

tensor, for example $\boldsymbol{\sigma}_1 = \begin{bmatrix} 1 & 0 & 0 \\ 0 & 0 & 0 \\ 0 & 0 & 0 \end{bmatrix}$ (unidirectional extension) and $\boldsymbol{\sigma}_2 = \begin{bmatrix} 0 & 1 & 0 \\ 1 & 0 & 0 \\ 0 & 0 & 0 \end{bmatrix}$ (shear).

Ideally, you need to select these trial stresses in the directions of eigenvectors of matrix $\boldsymbol{\alpha}$; otherwise, there is a chance that the resulting system of equations will be singular. Using these trial stress tensors, evaluate the right-hand-side of eq. (5.65) and the coefficients with δJ_K and δJ_μ in its left-hand side. Using these coefficients, solve for δJ_K and δJ_μ .

Using this function and values $b_1 = \dots$ and $b_2 = \dots$ for planar cracks, **verify eq. (5.67)** for an isotropic distribution of cracks (matrix α_{ij} proportional to an identity matrix).

Problem 5.1: Creep in the standard linear solid

Model creep of a Standard Linear Solid analytically. Use the configuration shown on the left in Figure 5.8. Write the Euler-Lagrange equations, and solve them numerically for constant stress σ , starting from zero initial conditions. As a result, you will obtain $\varepsilon(t)$ and $\varepsilon(\tau)$.

Problem 5.2: Equivalence of two forms of the SLS

Show that the two configurations of the Standard Linear Solid shown in Figure 5.8 are equivalent when $m = 0$. To achieve this, repeat derivation from eq. (5.53) to (5.56) for each of these bodies and determine τ . For the case on the right, determine the values of k_1 and k_2 so that the values of τ and the potential energies in the static limit ($\omega = 0$) are the

same as for the other case.

Problem 5.3: Memory equation for strain

Show that the solution to equation (5.55) can be written in "memory" form, i.e. as a convolutional integral of the preceding history of the external strain rate:

$$\varepsilon'(t) = \int_{-\infty}^t \dot{\varepsilon}(t_0) \exp\left(-\frac{t-t_0}{\tau}\right) dt_0, \quad (5.P1)$$

Problem 5.4: Memory equation for stress

Assuming that the mechanical system (L_0, D_0) in Figure 5.13 is a single spring of rigidity k_0 , derive the stress $\sigma(t)$ in an integral form similar to eq. (5.P1).

Problem 5.5: Strain-stress relations for SLS

Using the results of problems 5.3 and 5.4, derive the stress-strain rate relation for the Generalized Standard Linear Solid in Figure 2.10a.

6 Effects of Temperature

Key points:

- Adiabatic and isothermal deformations
 - Heat flows within the General Linear Solid
 - Kinetic equations
-

Temperature has two effects on mechanical properties of rocks. First, for example, in an oil or hydrothermal reservoir, the ambient temperatures may change by hundreds of degrees, and these variations cause variations of mechanical properties. In particular, properties related to pore fluids or bitumen are affected by temperature. Among these properties, the most sensitive mechanical properties are viscosity and effective porosity. Pore-fluid viscosity, and consequently also the solid viscosity of the whole rock quickly reduces with increasing ambient temperature. The dependencies of material properties on temperature are documented experimentally and explained by empirical and kinetic models similar to explanations of chemical reactions. Here, I will not consider these dependencies and focus on the second physical effect of temperature variations called the thermoelastic effect.

Thermoelasticity studies local variations of temperature caused by deformation itself. When a seismic wave passes through a medium, the compressed areas become hotter and the expanded ones become cooler. In addition, in a grainy and porous medium (like any rock), grains with contrasting elastic properties or thermal properties, and pores filled with fluids attain substantial temperature contrasts. These temperature contrasts cause additional stresses within the medium, and also heat flows between the hotter and colder parts of the medium. The exchange of heat causes a gradual loss of the average mechanical energy in the wave, which is ultimately observed as attenuation and velocity dispersion in the seismic wave. Our goal here is to describe these complex microscopic processes by certain averaged properties of the medium and macroscopic equations, similar to the Lagrangian

energy functions in section 5.

Consider a rock body and denote T_0 its temperature in an undeformed state and without sources of heat. If the temperature of the body changes to a spatially variable T , because of the phenomenon of thermal expansion, different parts of the body will tend to expand unevenly, and consequently the body will become deformed. Thus, the vector of temperature gradient **grad** T acts as a body force causing additional deformation. This deformation is somewhat analogous to the action of the gravity vector **g**, only **grad** T is usually not constant and often dependent on the deformation itself.

In addition to body forces produced by temperature gradients, temperature variations have two other types of effects on the elastic moduli and viscosities of the material:

- 1) Material properties themselves are sensitive to the ambient temperature. In particular, viscosity of pore fluids strongly reduces with increasing temperature. For a composite material such as porous rock, the whole rock and its pore space possess generally different coefficients of thermal expansion, and consequently the porosity and the drained and undrained moduli will also change with temperature.
- 2) The elastic moduli and the corresponding viscosities also depend on whether heat is added to or withdrawn from the material during the deformation. If there is no heat exchange (good insulation or quick deformation, usually a good approximation for seismic waves), the adiabatic elastic moduli are observed. Alternatively, if the temperature is maintained constant (by means of adding or removing heat), isothermal elastic moduli are observed. The adiabatic moduli are always larger than the isothermal ones. These moduli will be discussed more in section 6.1. Presumably the same relation should exist between the adiabatic and isothermal viscosities, although these concepts are not studied so much.

To describe these above phenomena mathematically, note that the elastic energy in the Lagrangian (5.2) is actually the thermodynamic (or Helmholtz) free energy. In thermodynamics, the term “free” means “able to produce mechanical work.” The formula for the free energy is $F = E - TS$, where E is the internal energy, T is the temperature,

and S is the entropy. As always in analytical mechanics, to obtain the free energy for arbitrary T from the second term in L in eq. (5.2) ($\frac{1}{2}\Delta^T \mathbf{K}\Delta + \tilde{\boldsymbol{\varepsilon}}_{ij}^T \boldsymbol{\mu} \tilde{\boldsymbol{\varepsilon}}_{ij}$), we need to consider what most general form add to it a term which would be: a) a scalar in both the coordinate and model spaces, b) proportional to temperature deviation from equilibrium $T - T_0$, c) linear with respect to strain $\boldsymbol{\varepsilon}$, and d) sensitive to the volume change only, i.e. trace of the strain tensor $\Delta = \boldsymbol{\varepsilon}_{ii}$. The most general expression satisfying these requirements is

$$F(T) = F_0(T) + \frac{1}{2} \mathbf{u}_i^T \boldsymbol{\zeta} \mathbf{u}_i + \frac{1}{2} \Delta^T \mathbf{K}\Delta + \tilde{\boldsymbol{\varepsilon}}_{ij}^T \boldsymbol{\mu} \tilde{\boldsymbol{\varepsilon}}_{ij} - \Delta^T \mathbf{K}\boldsymbol{\alpha}(\mathbf{T} - \mathbf{T}_0), \quad (6.1)$$

where \mathbf{T}_0 denotes an N -element vector with all elements equal T_0 , and $F_0(T)$ is the free energy of the rock due to its temperature alone (i.e., due to the vibrations and interactions of its molecules). Do not confuse the transposition symbol T with temperature \mathbf{T} .

Note that the generality of expression (6.1) suggests that \mathbf{T} must be a vector in the N -dimensional GLS model space. Elements of this vector represent temperatures of each component of the rock (such as the average rock and pore fluid within it). The different components of the medium should generally have different temperatures because they have different bulk moduli, coefficients of thermal expansion, and specific heat capacities, and consequently they are heated differently by thermoelastic processes. The matrix product $\mathbf{K}\boldsymbol{\alpha}$ coupling \mathbf{T} to Δ can of course be represented by a single material-property matrix, but it is factorized in this form so that $\boldsymbol{\alpha}$ has the dimensionality of 1/degree and simple meaning of the thermal expansion coefficient at constant pressure (explained below). The negative sign of the last term in eq. (6.1) is selected for the same reason.

For the case $N = 1$ (ordinary isotropic material without internal variables), there is only a single temperature T and all material properties are scalar, and the above expression for the free energy is

$$F(T) = F_0(T) + \frac{1}{2} K \Delta^2 + \tilde{\boldsymbol{\varepsilon}}_{ij} \boldsymbol{\mu} \tilde{\boldsymbol{\varepsilon}}_{ij} - \alpha K (T - T_0) \Delta. \quad (6.2)$$

Differentiating the scalar function F in eq. (6.1) at constant temperature with respect

to $\boldsymbol{\varepsilon}_{ij}$, the elastic stress tensor is obtained:

$$\boldsymbol{\sigma}_{ij}^{\text{elastic}} = \left(\frac{\partial F}{\partial \boldsymbol{\varepsilon}_{ij}^T} \right)_T = \mathbf{K}\boldsymbol{\Delta}\delta_{ij} + 2\boldsymbol{\mu}\tilde{\boldsymbol{\varepsilon}}_{ij} - \mathbf{K}\boldsymbol{\alpha}(\mathbf{T} - \mathbf{T}_0)\delta_{ij}, \quad (6.3)$$

where the second term is the thermoelastic stress caused by the temperature variation, and the subscript ‘ T ’ means that the partial derivative is taken along a path with constant T (i.e., when deforming the body isothermally).

To understand the meaning of the material-property matrix $\boldsymbol{\alpha}$, consider a body with no external stresses applied and increase its temperature. The stress in eq. (6.3) must remain equal zero, and therefore the volume of the body will increase so that $\mathbf{K}\boldsymbol{\Delta} = \mathbf{K}\boldsymbol{\alpha}(\mathbf{T} - \mathbf{T}_0)$, and consequently $\boldsymbol{\Delta} = \boldsymbol{\alpha}(\mathbf{T} - \mathbf{T}_0)$. This relation shows that matrix $\boldsymbol{\alpha}$ (scalar for ordinary medium without pores or internal structure) has a meaning of dilatational deformation $\boldsymbol{\Delta}$ caused by a change of the temperature of each component by one degree at constant pressure. This matrix $\boldsymbol{\alpha}$ is the coefficient of thermal expansion of the composite material.

From the same considerations of generality, we can expect that the dissipation function can also be modified by thermal effects. Although I can offer no rigorous thermodynamic argument, this analogy suggests that the viscous stress should also be generally modified by temperature as

$$\boldsymbol{\sigma}_{ij}^{\text{viscous}} = \boldsymbol{\eta}_K \dot{\boldsymbol{\Delta}}\delta_{ij} + 2\boldsymbol{\eta}_\mu \dot{\tilde{\boldsymbol{\varepsilon}}}_{ij} - \boldsymbol{\eta}_K \boldsymbol{\beta} \dot{\mathbf{T}}\delta_{ij}, \quad (6.4)$$

where $\boldsymbol{\beta}$ is another material-property matrix analogous to $\boldsymbol{\alpha}$. However, such detail of description appears redundant for viscosity because: 1) viscosity matrices $\boldsymbol{\eta}_K$ and $\boldsymbol{\eta}_\mu$ themselves are poorly known, 2) viscosities themselves should also vary (usually reduce) with temperature, and 3) in granular media like metals and rocks, the thermoelastic effect leads to additional, temperature-independent but scale-length dependent contributions to viscosity (see §34 and §35 in Landau and Lifshitz, 1986).

6.1 *Adiabatic and isothermal elastic moduli*

The various thermodynamic types of deformation are bounded by two end-member types defined by preservation of either temperature or entropy. Adiabatic deformation occurs when there is no heat flow in or out of the volume. The change of heat is given by relation $\delta Q = TdS$, where dS is the change of entropy, and therefore absence of heat generation (or absorption) means $dS = 0$, or constant entropy in an adiabatic process. By contrast, in an isothermal process, the change of temperature is kept equal zero: $dT = 0$, which usually requires a change of heat content.

Both isothermal and adiabatic deformations (and also those under other heat-flow regimes) can be elastic. Production of heat at some place and part of the wave cycle does not mean “attenuation” of the wave. For example, assume we are maintaining a perfectly constant temperature T_0 in a rock-physics experiment by keeping the sample in perfect contact with an infinitely large thermostat. The deformation of the sample will then be reversible and elastic, with equal amounts of heat flowing in and out of the body during a loading-unloading cycle. Similarly, if we provide a complete thermal insulation of the body, there will be no heat exchange, and the deformation will again be elastic.

Because of the flow of heat in and out of the body, in isothermal deformation, the material is “softer” than in the adiabatic one. The isothermal bulk and shear elastic moduli are given by the coefficients with Δ and $\tilde{\epsilon}_{ij}$ in eq. (6.3) at constant temperature $\mathbf{T} = \mathbf{T}_0$. These coefficients are \mathbf{K} and $\boldsymbol{\mu}$, which means that the moduli in the Lagrangian functions (5.2) are the isothermal moduli.

To obtain the adiabatic moduli, we need to consider the derivatives not of the free energy F but the internal energy $E = F + TS$ at constant entropy S (which means zero heat flow). The entropy S is the derivative of the free energy with respect to temperature: $S = -\partial F / \partial T$, and therefore), the entropy is also a vector in the space of the different components of the material, which we denote \mathbf{S} . From eq. (6.1), in the presence of deformation Δ , the entropy vector is:

$$\mathbf{S}(\mathbf{T}) = \mathbf{S}_0(\mathbf{T}) + (\Delta^T \mathbf{K} \boldsymbol{\alpha})^T = \mathbf{S}_0(\mathbf{T}) + \boldsymbol{\alpha}^T \mathbf{K}^T \Delta. \quad (6.5)$$

where \mathbf{S}_0 is the deformation-independent part of entropy due to the microstructure of the material. With constant $\mathbf{S} = \text{const}$ (adiabatic deformation) and fixed deformation Δ , if we increase the temperature of the material from \mathbf{T}_0 to \mathbf{T} , $\mathbf{S}_0(\mathbf{T})$ should change by amounts $d\mathbf{S}_0 = \mathbf{S}_0(\mathbf{T}) - \mathbf{S}_0(\mathbf{T}_0) = -\boldsymbol{\alpha}^T \mathbf{K}^T \Delta$. The amounts of heat (per unit volume) within each component are related to the increments of the internal entropy $d\mathbf{S}_0$ $d\mathbf{Q}_0 = \text{diag}(\mathbf{T}_0) d\mathbf{S}_0 = -\text{diag}(\mathbf{T}_0) \boldsymbol{\alpha}^T \mathbf{K}^T \Delta$, where $\text{diag}(\mathbf{T}_0)$ is a diagonal $N \times N$ matrix of background temperatures. These increments of stored heat $d\mathbf{Q}_0(\mathbf{T})$ are related to the specific heat capacity at constant volume \mathbf{c}_v , which is also a diagonal $N \times N$ matrix:

$$d\mathbf{Q}_0 = \mathbf{c}_v (\mathbf{T} - \mathbf{T}_0). \quad (6.6)$$

From these two expressions for $d\mathbf{Q}_0$, the change of temperature during the adiabatic deformation is proportional to the dilatational strain Δ :

$$d\mathbf{T} = -\mathbf{c}_v^{-1} \text{diag}(\mathbf{T}_0) \boldsymbol{\alpha}^T \mathbf{K}^T \Delta. \quad (6.7)$$

Note that the negative sign here means that when a medium is expanded without adding heat, the temperatures of all of its components should reduce (this is how the refrigerator

Substitution of the temperature variation from eq. (6.7) into eq. (6.3) gives the elastic stress-strain response under adiabatic conditions:

$$\boldsymbol{\sigma}_{ij} = \left[\mathbf{K} + \mathbf{K} \mathbf{a} \mathbf{c}_v^{-1} \text{diag}(\mathbf{T}_0) \boldsymbol{\alpha}^T \mathbf{K}^T \right] \Delta \delta_{ij} + 2\boldsymbol{\mu} \tilde{\boldsymbol{\epsilon}}_{ij}. \quad (6.8)$$

Exercise

Using eq. (6.7), show that as mentioned above, the adiabatic stress equals the derivative of the internal energy $E = F + TS$ with respect to the strain at constant entropy:

$$\boldsymbol{\sigma}_{ij} = \left(\frac{\partial E}{\partial \boldsymbol{\epsilon}_{ij}^T} \right)_S .$$

Similar to eq. (6.7), equation (6.8) represents the Hooke's law, but with a different bulk modulus:

$$\mathbf{K}_{\text{adiabatic}} = \mathbf{K} + \mathbf{K} \boldsymbol{\alpha} \boldsymbol{\alpha}^{-1} \text{diag}(\mathbf{T}_0) \boldsymbol{\alpha}^T \mathbf{K}^T . \quad (6.9)$$

This is the adiabatic bulk modulus of a GLS medium.

For an ordinary isotropic medium ($N = 1$), all factors in this expression become scalar quantities. For such a medium, heat flows within the wave can only occur at the wavelength scale, temperature gradients are small, and consequently the thermoelastic dissipation is weak and the deformation regime is close to adiabatic. However, with $N > 1$ such as in a porous rock, heat flows exist on the scales of grain sizes, temperature gradients can be large, and therefore heat exchanges may likely occur on the characteristic time scales of seismic wave oscillations. In such cases, the bulk moduli would be close to isothermal ones at low frequencies and to adiabatic ones at high frequencies. This transition from near-isothermal to near-adiabatic effective moduli with increasing frequencies is an example of what is called the (effective, or empirical) modulus dispersion. In section 1, I'll give more examples of similar dispersion phenomena.

6.2 Heat flows

Due to the thermoelastic effects described in the preceding section, whenever the deformation of a body is spatially inhomogeneous, the associated temperature variations are also heterogeneous, and gradients of temperatures cause flows of heat. The heat flows

go in the direction from hotter (compressed) areas toward the colder (decompressed) ones, which causes mechanical-energy dissipation (i.e., wave attenuation) and reduction of the average elastic moduli (i.e., wave dispersion). Because heat flows require time, these effects are frequency-dependent: stronger at low frequencies and weaker at high frequencies. This means that as a result of thermoelastic heat dissipation, high-frequency waves are faster than low-frequency waves (this relation between velocities is called inverse dispersion, in contrast to the normal dispersion usually observed for surface waves). The transition between the low-velocity and higher-velocity regimes occurs at characteristic frequency corresponding to the maximum average heat within the medium.

According to the spatial scales of the causal heterogeneous deformation, there exist two types of heat flows:

- 1) In the first type, heat flows occur on the wavelength scale, by heat flowing between adjacent areas with contrasting average deformation and temperature. This mechanism does not involve the internal structure and is available for any material. This mechanism can be called the “global” heat flow, by analogy with Biot’s pore-fluid flows occurring on the wavelength scale and also often called global. However, similarly to Biot’s effect, for seismic waves in rocks, this thermoelastic mechanism causes weak attenuation which is noticeable only at very high frequencies.
- 2) In addition to the above mechanism, in a medium with $N \geq 2$, there always exist strong local temperature contrasts between the different components (such as rock frame and pore fluid) located at the same macroscopic point. These contrasts are described by the different elements of our temperature vector \mathbf{T} . These temperature contrasts cause “local” heat flows, which similarly produce mechanical-energy loss and relaxation (reduction) of the observed moduli.

In the following subsections, these two types of thermoelastic attenuation effects are discussed separately.

6.2.1 Macroscopic heat flow

The macroscopic heat flow involves the average medium, and therefore I will only describe it for the case $N = 1$ (i.e., averaging out all of the internal structure). Without change of deformation, the rate of heat increase per unit volume is given by $\dot{Q} = -\text{div} \mathbf{q}$, where \mathbf{q} is the heat flux density (as above, overdots denote time derivatives, e.g. $\dot{q} \equiv \partial q / \partial t$). The heat flux is usually caused by the gradient of temperature: $\mathbf{q} = -\kappa \mathbf{grad} T$ (this relation is often called the Fourier's law), and heat density Q is related to the temperature as $Q = cT$, where c is some type of specific heat capacity. Depending on boundary conditions and geometry of the heat flow, in some cases (see §32 in Landau and Lifshitz, 1986), c can be taken at constant volume, c_v , and in some cases – at constant pressure, c_p , or their combinations. However, the difference between c_v , and c_p is small for solids. The equation of heat flow (“equation of continuity of heat”) then becomes a diffusion equation for temperature. Allowing a spatially variable thermometric conductivity $\chi = \kappa/c$ (conductivity evaluated for temperature variations, also called thermal diffusivity), the diffusion equation is

$$\dot{T} = \nabla(\chi \nabla T), \quad (6.10)$$

where ∇ is the vector differential operator for gradient. In subscript form, this equation reads $\dot{T} = \partial_i(\chi \partial_i T)$. With constant χ , this relation is often written as $\dot{T} = \chi \Delta T$ by using the Laplacian operator $\Delta \equiv \partial_i \partial_i$, but I refrain from this notation because of using symbol Δ for volumetric strain.

To couple this equation with temperature variations caused by deformation, the adiabatic deformation relation (6.7) (for the case $N = 1$) is usually used: $dT = -c_v^{-1} T_0 \alpha K \Delta$. Time derivative of this equation gives the temperature increase rate due to dilatation rate: $\dot{T} = -c_v^{-1} T_0 \alpha K \dot{\Delta}$. Adding this rate to eq. (6.10), the final equation for temperature variation within a deforming body is:

$$\dot{T} = -c_v^{-1} T_0 \alpha K \dot{\Delta} + \partial_i(\chi \partial_i T). \quad (6.11)$$

This equation for temperature variations should be added to the equations of motion for deformation.

6.2.2 Local (internal) heat flow

For a medium with $N \geq 2$ components, equation (6.11) is naturally generalized for multiple temperatures \mathbf{T} by returning to eq. (6.7) and adding two kinetic coefficient matrices κ_1 and κ_2 for heat exchanges between the components:

$$\dot{\mathbf{T}} = -\mathbf{c}_v^{-1} \text{diag}(\mathbf{T}_0) \boldsymbol{\alpha}^T \mathbf{K}^T \dot{\Delta} - \chi_1 (\mathbf{T} - \mathbf{T}_0) + \partial_i (\chi_2 \partial_i \mathbf{T}), \quad (6.12)$$

where we also define the thermometric conductivities $\chi_1 = \mathbf{c}_v^{-1} \kappa_1$ and $\chi_2 = \mathbf{c}_v^{-1} \kappa_2$. The meaning of thermal conductivity κ_2 (and χ_2) is in describing the “global” heat flux into each component of the composite material from the adjacent areas in the medium, analogously to κ and χ in eq. (6.11).

Note that the measurement units of χ_1 and χ_2 are different. Parameter χ_2 is the usual thermal conductivity measured in Watts per meter·Kelvin. Parameter χ_1 has units of *1/time*, i.e. it can be simply estimated from the characteristic frequency of thermoelastic transition observed in a modulus-dispersion or attenuation experiment. Accordingly, the units of κ_1 are the specific heat capacity per second.

Similar to the usual thermoelastic internal friction, the effect of the global thermal conductivity χ_2 should be relatively weak at seismic frequencies. However, the effect of the local mechanism given by parameters κ_1 or χ_1 should be dominant in observations. These material properties describe the heat exchange between the components of rock (such as the entire average rock and its pore fluid) at the same macroscopic point, i.e. across the closely spaced grain and fluid boundaries. Temperature gradients are much greater at these distances, and the heat flows are much stronger.

6.3 General Linear Solid with multiple temperatures (GLST)

In this section, I summarize the complete GLS model with arbitrary scalar (“local”) variables and temperature (eqs. (5.2), (5.3), and (6.29)). The mechanical part of the model has the form of eqs. (5.2) and (5.3) combined with (6.1) and extended (similar to eq. (6.1)) with free energy corresponding to a coupling between $\boldsymbol{\theta}$ and \mathbf{T} :

$$\left\{ \begin{array}{l} L = \frac{1}{2} \dot{\mathbf{u}}_i^T \boldsymbol{\rho} \dot{\mathbf{u}}_i - \left(\frac{1}{2} \mathbf{u}_i^T \boldsymbol{\zeta} \mathbf{u}_i + \frac{1}{2} \boldsymbol{\Delta}^T \mathbf{K} \boldsymbol{\Delta} + \tilde{\boldsymbol{\epsilon}}_{ij}^T \boldsymbol{\mu} \tilde{\boldsymbol{\epsilon}}_{ij} \right) - \boldsymbol{\Delta}^T \mathbf{K} \boldsymbol{\alpha} (\mathbf{T} - \mathbf{T}_0) - \\ \quad - \frac{1}{2} \boldsymbol{\theta}^T \mathbf{P} \boldsymbol{\theta} + \boldsymbol{\Delta}^T \mathbf{Q} \boldsymbol{\theta} - \boldsymbol{\theta}^T \mathbf{P} \boldsymbol{\alpha}_\theta (\mathbf{T} - \mathbf{T}_0), \\ D = \frac{1}{2} \dot{\mathbf{u}}_i^T \mathbf{d} \dot{\mathbf{u}}_i + \left(\frac{1}{2} \dot{\boldsymbol{\Delta}}^T \boldsymbol{\eta}_K \dot{\boldsymbol{\Delta}} + \dot{\tilde{\boldsymbol{\epsilon}}}_{ij}^T \boldsymbol{\eta}_\mu \dot{\tilde{\boldsymbol{\epsilon}}}_{ij} \right) + \frac{1}{2} \dot{\boldsymbol{\theta}}^T \mathbf{P}' \dot{\boldsymbol{\theta}} - \dot{\boldsymbol{\Delta}}^T \mathbf{Q}' \dot{\boldsymbol{\theta}}, \end{array} \right. \quad (6.13)$$

where the combined model-space and spatial vector \mathbf{u}_i represents the “global” spatial movement of the rock frame and multiple assemblages of rock grains, parts of pore space, and pore fluids, and model vector $\boldsymbol{\theta}$ represents various kinds of “local” (spatial scalars) deformations, such as expansions of microcracks or patches of pore fluid. Similar to the (matrix) thermal expansion coefficient $\boldsymbol{\alpha}$, matrix $\boldsymbol{\alpha}_\theta$ represents thermal expansion coefficients for such internal structures.

Taking Euler derivatives of eqs. (6.13) with respect to \mathbf{u}_i gives mechanical equations of motion similar to eqs. (5.8):

$$\boldsymbol{\rho} \ddot{\mathbf{u}}_i = -\boldsymbol{\zeta} \mathbf{u}_i - \mathbf{d} \dot{\mathbf{u}}_i + \partial_j \boldsymbol{\sigma}_{ij}, \quad (6.14)$$

where the stress tensor is modified by the thermoelastic effect:

$$\boldsymbol{\sigma}_{ij} = \left(\mathbf{K} \boldsymbol{\Delta} \delta_{ij} + 2 \boldsymbol{\mu} \tilde{\boldsymbol{\epsilon}}_{ij} \right) + \left(\boldsymbol{\eta}_K \dot{\boldsymbol{\Delta}} \delta_{ij} + 2 \boldsymbol{\eta}_\mu \dot{\tilde{\boldsymbol{\epsilon}}}_{ij} \right) + \delta_{ij} \left[\left(\mathbf{Q} \boldsymbol{\theta} - \mathbf{Q}' \dot{\boldsymbol{\theta}} \right) - \left(\mathbf{K} \boldsymbol{\alpha} + \mathbf{P} \boldsymbol{\alpha}_\theta \right) (\mathbf{T} - \mathbf{T}_0) \right]. \quad (6.15)$$

Similarly, Euler derivative with respect to variable $\boldsymbol{\theta}$ give eq. (5.8d) with an additional term due to thermoelasticity:

$$\rho_{\theta} \ddot{\boldsymbol{\theta}} = -\mathbf{P}\boldsymbol{\theta} - \mathbf{P}'\dot{\boldsymbol{\theta}} - \mathbf{Q}^T \Delta + \mathbf{Q}'^T \dot{\Delta} - \mathbf{P}\boldsymbol{\alpha}_{\theta} (\mathbf{T} - \mathbf{T}_0). \quad (6.16)$$

If variable $\boldsymbol{\theta}$ is massless ($\rho_{\theta} = \mathbf{0}$) but matrix \mathbf{P}' is invertible (as it should be), the equation for $\boldsymbol{\theta}$ becomes of kinetic type:

$$\dot{\boldsymbol{\theta}} = \mathbf{P}'^{-1} \left[-\mathbf{P}\boldsymbol{\theta} - \mathbf{Q}^T \Delta + \mathbf{Q}'^T \dot{\Delta} - \mathbf{P}\boldsymbol{\alpha}_{\theta} (\mathbf{T} - \mathbf{T}_0) \right]. \quad (6.17)$$

As shown in the preceding and also next sections, the temperature vector \mathbf{T} can also be included in $\boldsymbol{\theta}$ and treated as a kinetic variable of a Lagrangian mass-stiffness-damping mechanical system. However, to formulate the complete GLST model let us keep the equation for \mathbf{T} separate. Adding to eq. (6.12) work performed by the thermoelastic forces acting on variables $\boldsymbol{\theta}$, the temperature variation rate becomes

$$\dot{\mathbf{T}} = -\mathbf{c}_v^{-1} \text{diag}(\mathbf{T}_0) (\boldsymbol{\alpha}^T \mathbf{K}^T \dot{\Delta} + \boldsymbol{\alpha}_{\theta}^T \mathbf{P}' \dot{\boldsymbol{\theta}}) - \chi_1 (\mathbf{T} - \mathbf{T}_0) + \partial_i (\chi_2 \partial_i \mathbf{T}). \quad (6.18)$$

Note that apart from the (insignificant) last term related to the “global” Fourier heat flow, temperature \mathbf{T} behaves as a kinetic variable $\boldsymbol{\theta}$. For the case of $N = 2$, this similarity was illustrated in detail in subsection 6.2.2. Thus, internal temperature variations are closely related to purely mechanical effects such as viscosity, and generally, they should hardly be separable.

In chapter 7, we will transform equations (6.14) through (6.18) into matrix form using two approaches:

- 1) Transform the Lagrangian and dissipation functions, and equation (6.18) into the Mass-Stiffness-Damping model (next section);
- 2) Transform the differential equations directly using Galerkin’s finite-element method (section 5.11 on page 158).

These approaches are closely related and equivalent.

6.4 Biot’s Model with Internal Temperatures

The above observation of the dominant effect of the term containing χ_1 leads to two

useful simplifications of the above equations. Let us illustrate them on Biot's model of porous rock (GLS with $N = 2$; section 5.6). We can assume that in a composite material, the constituent components exchange heat locally without exchanging with other areas of the body, and therefore its average temperature is constant: $T = T_0$. Since the average amount of heat is preserved, there are $(N - 1)$ independent temperature contrasts occur between different the components of the material. Therefore, for Biot's model, there is only one independent internal-temperature parameter which I denote θ here¹⁴. If the temperature of component 1 (average rock) increases in a seismic wave by θ degrees, the temperature of component 2 (pore fluid) reduces, and the total temperature vector is

$$\mathbf{T} - \mathbf{T}_0 = \theta \mathbf{T}_{rel}, \quad (6.19)$$

where the dimensionless vector of relative temperature variation $\mathbf{T}_{rel} = \begin{pmatrix} 1 \\ -p \end{pmatrix}$,

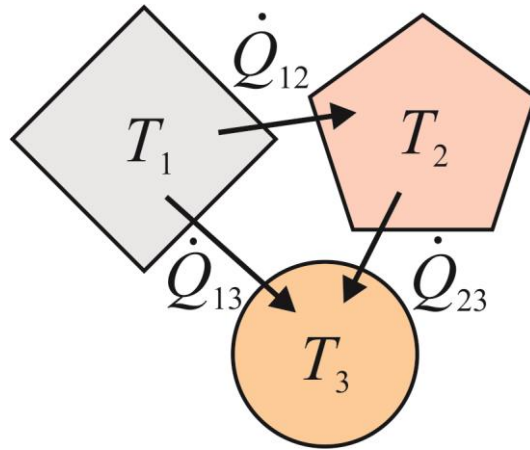


FIGURE 6.1.

Schematic illustration of heat exchange in a grainy material with grains or pore fluids at different temperatures $T_1 > T_2 > T_3$ (labels 'T'). Heat flows within pairs of grains at rates proportional to temperature differences (labels 'Q' and arrows).

¹⁴ In chapter 5, symbol θ was used to denote arbitrary scalar variables describing some aspects of the internal structure of the rock. Here, the same symbol is used to denote specifically the deformation-related temperature variation of the average rock. This identical notation is used on purpose, to show that temperature perturbations represent just one example of the broader internal variable θ .

$p = \frac{\phi_1 \rho_1 c_{V1}}{\phi_2 \rho_2 c_{V2}}$, ϕ_1 and ϕ_2 are the volume fractions of the two components, ρ_1 and ρ_2 are their respective densities, and c_{V1} and c_{V2} are the specific heat capacities at constant volume. Inversely, θ can be obtained from the temperature vector as

$$\theta = \boldsymbol{\theta}_{rel}^T (\mathbf{T} - \mathbf{T}_0), \quad \text{where} \quad \boldsymbol{\theta}_{rel} = \frac{1}{2} \begin{pmatrix} 1 \\ -1/p \end{pmatrix}. \quad (6.20)$$

With the above simplification of the temperature vector, the total stress within Biot's medium with thermoelasticity becomes (eq. (6.15)):

$$\boldsymbol{\sigma}_{ij} = (\mathbf{K}\Delta\delta_{ij} + 2\mu\tilde{\boldsymbol{\epsilon}}_{ij}) - \delta_{ij}\theta\mathbf{K}\boldsymbol{\alpha}\mathbf{T}_{rel}. \quad (6.21)$$

Thus, additional pressure develops in areas of increased temperature difference between the rock and its pore fluid.

Another useful simplification of the model in eq. (6.12) relates to the structure of matrix $\boldsymbol{\chi}_1$. For a material with inclusions like porous rock, it is reasonable to assume that heat flows only occur between pairs of components, so that the heat flow between i^{th} and j^{th} components is proportional to the temperature difference between them (Figure 6.1):

$$\dot{Q}_{ij} = -\chi_{ij}(T_i - T_j). \quad (6.22)$$

where a positive value of \dot{Q}_{ij} means heat flowing into component I , and η_{ij} is the thermal conductivity associated with this pair of components (arrow in the Figure). This relation means that matrix $\boldsymbol{\chi}_1$ is of the characteristic form similar to the elastic modulus \mathbf{M} for the generalized standard linear solid (see eq. (5.52) on page 151)). For the above case $N = 2$, this matrix contains only one parameter:

$$\boldsymbol{\chi}_1 = \begin{bmatrix} \chi & -\chi \\ -\chi & \chi \end{bmatrix}. \quad (6.23)$$

Using the above approximations, dropping the term with conductivity $\boldsymbol{\chi}_2$, and

multiplying by $\boldsymbol{\theta}_{rel}^T$ on the left, and evaluating matrix products, eq. (6.12) becomes an equation for the internal temperature perturbation θ :

$$\dot{\theta} = -\frac{\boldsymbol{\theta}_{rel}^T \mathbf{c}_v^{-1} \boldsymbol{\alpha}^T \mathbf{K}^T}{T_0} \dot{\Delta} - \chi_\theta \theta, \quad (6.24)$$

where the effective relaxation rate for θ equals

$$\chi_\theta = \boldsymbol{\theta}_{rel}^T \boldsymbol{\chi}_1 \mathbf{T}_{rel} = \chi \left(1 + p + \frac{1}{p} \right). \quad (6.25)$$

Equation (6.24) is easy to interpret. The first term describes the increase of temperature contrasts between grains and/or pores caused by compression (the thermoelastic effect). In the absence of compression, the second term describes relaxation of this temperature contrast due to heat exchange between grains. In laboratory measurements, this internal thermal relaxation should produce an attenuation peak at frequency $f \sim \chi_\theta$.

6.5 *Mass-Stiffness-Damping model with temperature (MSDT)*

In this section, I consider temperature effects in a very general form, in the spirit of the MSD model. This gives an ‘‘MSD model with temperature,’’ or MSDT.

Similar to the vector of generalized coordinates \mathbf{q} , temperature variations ($\mathbf{T} - \mathbf{T}_0$) within the body can be viewed as an additional model vector \mathbf{q}_T . For example, this vector can combine temperatures at different parts of the body and/or different temperatures for rock matrix and pore fluid in a porous rock. Temperature variations are described by diffusion equation of the form $c\dot{T} = \text{div}(\boldsymbol{\kappa} \mathbf{grad} T) + J_{ext}$, where c is the specific heat, and $\boldsymbol{\kappa}$ is the thermal conductivity, and J_{ext} is an external source of heat density (injected power per unit volume). In terms of the generalized parameter vector \mathbf{q}_T , this equation is

$$\mathbf{C}\dot{\mathbf{q}}_T - \boldsymbol{\Psi}\mathbf{q}_T = \mathbf{J}_{ext}, \quad (6.26)$$

where matrix \mathbf{C} is the distribution of specific heat at constant volume, and matrix $\boldsymbol{\Psi}$ represents the differential operator $\text{div}(\kappa \mathbf{grad}(\dots))$. These material properties can be understood as follows: if vector \mathbf{q}_T represents temperature variations for parts of the body, then products $\mathbf{C}\mathbf{q}_T$ give the heat density stored in them, and $\mathbf{J} = \boldsymbol{\Psi}\mathbf{q}_T$ is the amount of heat entering these parts of the body.

Equation (6.26) can be viewed as an Euler-Lagrange equation for dynamic variable \mathbf{q}_T with elastic Lagrangian $L_T = -\frac{1}{2}\mathbf{q}_T^T \boldsymbol{\Psi}\mathbf{q}_T$ and dissipation function

$$D_T = \frac{1}{2}\dot{\mathbf{q}}_T^T \mathbf{C}\dot{\mathbf{q}}_T. \quad (6.27)$$

Note that since $\boldsymbol{\Psi}$ consists of sums of second spatial derivatives, L_T is a positive-definite quadratic form.

Equation (6.26) for pure heat exchange is valid in the absence of deformation, i.e. when $\mathbf{q} = \text{const}$. If both \mathbf{q} and \mathbf{q}_T are variable, a deformation-temperature coupling term is subtracted from the free energy $\delta F = -\alpha K \delta T \Delta$, where Δ is the dilatation, δT is the perturbation of temperature, α is the coefficient of thermal expansion, and K is the bulk modulus of the material (for more detail, see section 6). In our generalized notation, this shift in the elastic energy corresponds to another deformation-temperature coupling in the Lagrangian:

$$L_T = -\frac{1}{2}\mathbf{q}_T^T \boldsymbol{\Psi}\mathbf{q}_T + \mathbf{q}_T^T \mathbf{A}\mathbf{q}, \quad (6.28)$$

where the non-square matrix \mathbf{A} contains differential operations producing dilatation of \mathbf{q} and its multiplication by the (generally spatially variable) material properties α and K . Because L_T is a scalar quantity, it can also be written in transposed form: $\mathbf{q}_T^T \mathbf{A}\mathbf{q} = \mathbf{q}^T \mathbf{A}^T \mathbf{q}_T$. These expressions allow easy evaluation of the partial derivatives of L_T with respect to \mathbf{q}

and \mathbf{q}^T .

Combining vectors \mathbf{q} and \mathbf{q}_T in model vector $\bar{\mathbf{q}} = \begin{pmatrix} \mathbf{q} \\ \mathbf{q}_T \end{pmatrix}$ and including functions L_T and D_T in the MSD model, the MSDT model for deformations with temperature variations is:

$$\begin{cases} L_{MSDT} = \frac{1}{2} \dot{\bar{\mathbf{q}}}^T \bar{\mathbf{M}} \dot{\bar{\mathbf{q}}} - \frac{1}{2} \bar{\mathbf{q}}^T \bar{\mathbf{S}} \bar{\mathbf{q}}, \\ D_{MSDT} = \frac{1}{2} \dot{\bar{\mathbf{q}}}^T \bar{\mathbf{D}} \dot{\bar{\mathbf{q}}}. \end{cases} \quad (6.29)$$

where $\bar{\mathbf{M}} = \begin{bmatrix} \mathbf{M} & \mathbf{0} \\ \mathbf{0} & \mathbf{0} \end{bmatrix}$, and $\bar{\mathbf{S}} = \begin{bmatrix} \mathbf{S} & -\mathbf{A} \\ -\mathbf{A}^T & \Psi \end{bmatrix}$, and $\bar{\mathbf{D}} = \begin{bmatrix} \mathbf{D} & \mathbf{0} \\ \mathbf{0} & \mathbf{C} \end{bmatrix}$.

Thus, deformations with thermoelastic temperature variations can be described by the same equations as (4.13) through (4.30) with expanded mass, stiffness, and damping matrices (eqs. (6.29)). The external force vector \mathbf{f} (mechanical source) is similarly combined with the source of heat as $\bar{\mathbf{f}} = \begin{pmatrix} \mathbf{f} \\ \mathbf{J}_{ext} \end{pmatrix}$. Because of the structure of matrix $\bar{\mathbf{M}}$, variables \mathbf{q}_T behave quasi-statically, and they can be separated during time-domain forward modeling as described in section 4.5.

Note that from the variational principle given by eqs. (6.29), the thermoelastic effect modifies the equation for heat diffusion (eq. 6.26) to

$$\mathbf{C} \dot{\mathbf{q}}_T = \mathbf{J}_{ext} - \Psi \mathbf{q}_T - \mathbf{A} \mathbf{q}. \quad (6.30)$$

Also note that if $\mathbf{D} = \mathbf{0}$ (no viscous friction in the material) the Lagrangian and dissipation function in eq. (6.29) look like those of Biot's model of porous rock (section 5).

6.6 Temperature Waves

If thermal effects are considered, the average temperature $T(t, \mathbf{x})$ or temperature vector field $\mathbf{T}(t, \mathbf{x})$ need to be added to the model variables $\boldsymbol{\theta}$ (eq. (6.13)), with the

corresponding changes in the system of linear differential equations (5.7) and (5.8). An interesting question arises from including fields $\mathbf{T}(t, \mathbf{x})$ in the system of dynamic equations: will additional wave modes analogous to Biot's secondary P waves appear because of the added temperature field(s)? These secondary waves are called temperature waves, or T-waves.

Modeling of temperature waves leads to a significant paradox which needs to be considered. The temperature variables are kinetic in nature, and the corresponding equations for T are of kinetic (diffusion) and not wave type. The quasi-static mode dominated by eq. (6.11) appears to be nonphysical, as it represents a certain exponential shape of distribution of the strain and temperature in space, with magnitude exponentially changing in time simultaneously. If viewing this mode as a "T-wave", the wave turns out to be of infinite velocity, which appears unsatisfactory. However, this behavior of the solution is expected from Fourier's law of heat conduction, in which the heat spreads from the source

To guarantee that the T-wave propagates at finite velocity, many researchers (e.g., Lord and Schulman ??) arbitrarily introduce "thermal relaxation" terms proportional to $\ddot{\Delta}$ in eq. (6.11). Such terms are also equivalent to assuming inertial properties of temperature perturbations. However, this approach does not seem to be physically justified. Temperature or heat are not something that would possess inertia or (always related to it) gravitational attraction. Temperature also does not change with time by a "memory-type" process but varies due to spatial heat flows.

To resolve the above paradox in a more meaningful way, note that the near-exponential thermal relaxation is due to two different causes:

- 1) temperature contrasts between adjacent grains ("local" heat flows), and
- 2) average temperature gradient within the medium ("global" heat flows).

The paradox only occurs when interpreting the resulting temperature distribution as resulting from cause 2) above, i.e. from a heat spreading from the source according to the Fourier heat conduction law. However, within rock, this mechanism should be much less significant than mechanism 1) (local heat flows). For local heat flows, temperature gradients are several orders of magnitude stronger, and contrasts in material properties

between adjacent grains and pockets of gas and fluid are also much stronger than for the global Fourier heat flow. For mechanism 2), temperature variations occur simultaneously at all points within the volume, and the spatial pattern of temperature is not a wave. The heat source is delivered at each point through deformation, i.e. through (fast or slow) P or S waves traveling at finite speeds.

Another side of the above paradox is that it arises only when considering a T-waves in a boundless medium. However, in most practical applications, finite bodies or layers are considered, and the nonphysical traveling T-waves are superseded by near-constant spatially and time-variant temperatures of the bodies. In such environments, the effect of heat spreading “too fast” by the Fourier-law term is also insignificant, and it should be removed by evaluating boundary conditions.

Note that a similar problem with nonphysical solutions exponentially increasing downward is encountered for surface waves. There, the problem is also removed in the same way, by not allowing the wave amplitudes to exponentially grow at the infinity.

In finite-difference modeling, the above difficulty of a nonphysical temperature-related mode is manifested by propagation of numerical errors when evaluating wave propagation. This problem can similarly be resolved by carefully constructing the algorithm and suppressing the nonphysical solutions.

6.7 *Problems and Laboratory Assignments*

... still needs some work ...

7 Applications

Key points:

- Specific model parameterizations and boundary conditions must be utilized for modeling each type of experiment
-

In this chapter, we consider specific applications of the models developed in this course. To solve equations from the preceding section, specific experimental environments need always to be followed as much as possible. These environments determine the boundary and initial conditions that need to be added to the equations of motion. In this section, I consider several key cases useful for modeling practical experiments with rock samples and waves in the field. These key cases are: 1) static equilibrium, 2) plane harmonic waves, and 3) quasi-static forced oscillations of a small body, such as a subresonant attenuation experiment with a rock specimen. Each of these cases samples somewhat different parts of the general mechanical problem (section 5), and therefore the explanations of similar observations may be different. Thus, in the static case 1), viscous properties of the medium (\mathbf{d} , $\boldsymbol{\eta}_\kappa$, and $\boldsymbol{\eta}_\mu$) are not tested. For plane waves (case 2)), all properties are involved, but spatial heterogeneity of the medium is not considered. However, most problems of interest relate to finite bodies or heterogeneous structures. For forced oscillations, the inertial properties (matrix $\boldsymbol{\rho}$) are typically insignificant, but the effects of the shape and size of the body may become very strong and complex.

In experiments involving harmonic oscillations (cases 2) and 3) above), the key observations which are expected to be explained by the model are schematically shown in Figure 7.1. With increasing the testing frequency, some type of empirical modulus M shows an increase by amount δM . This increase occurs across a well-pronounced frequency band centered at frequency f_0 , and the attenuation factor Q^{-1} shows a peak at the same frequency (Figure 7.1). The goal of the theory consists in explaining both of the plateaus in $M(f)$, the magnitude of the peak $Q^{-1}(f)$, the transition frequency f_0 , and possibly the whole

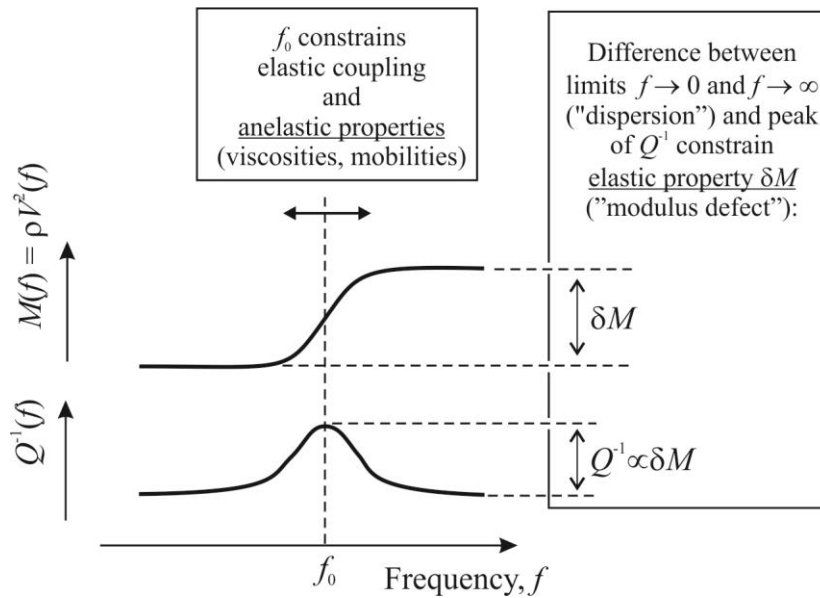


FIGURE 7.1.

Cartoons of typical observations of modulus or wave-velocity dispersion (gradual step in the curve by δM) and the corresponding peak in the attenuation factor Q^{-1} .

shapes of these spectra.

Some fundamental observations about the mechanical structure can be made directly from the modulus dispersion curve in Figure 7.1. Insets in this Figure point out that the dispersion always occurs because of a transition between some quasi-elastic modes of deformation within the rock. For example, in a sample of porous rock, the “drained-undrained” transition occurs from the drained regime at low frequencies to undrained regime at high frequencies. At low frequencies, there is enough time to equilibrate the variation of pore pressure to zero level (and hence the regime is called drained), and at high frequency, pore flows tend to zero. Similarly, for thermoelastic dispersion, the transition occurs between the isothermal and adiabatic heat-flow regimes. These pairs of complementary regimes are characterized by the difference of the moduli, δM in Figure 7.1, which is called the “modulus defect”.

Interestingly, for band-limited dispersion as in Figure 7.1, the $Q^{-1}(f)$ is not an independent observation. Regardless of the mechanism (but provided that it is causal, which is expected from mechanical testing of a rock body), the attenuation function is close

to a derivative of the logarithm of the modulus with respect to the logarithm of frequency:

$$Q_M^{-1} \approx \frac{1}{2} \frac{d[\ln(\operatorname{Re} M)]}{d[\ln f]} \approx \frac{1}{2} \frac{\delta M}{\bar{M}} \frac{f_0}{\Delta f}, \quad (7.1a)$$

where Δf is the frequency band width of the attenuation peak, and \bar{M} is some average level of the measured modulus, for which the relaxed modulus $M_R = M(f \rightarrow 0)$ can be taken.

This equation is one of the so-called nearly local Kramers-Krönig causality relations. Equation (7.1) shows that the peak in $Q^{-1}(f)$ occurs at the same frequency f_0 as the dispersion of $\operatorname{Re} M$, and the magnitude of this peak is proportional to δM (Figure 7.1). For the standard linear solid (Zener) model (which is commonly used to model relaxation spectra in Figure 7.1; subsection 0), the peak Q^{-1} equals

$$Q_M^{-1} \approx \frac{\delta M}{2M_R}. \quad (7.1b)$$

For the SLS, the notion of bandwidth Δf for its peak Q^{-1} is rather arbitrary, but it can be obtained by taking $\Delta f = f_0$, which reconciles the two equations (7.1).

The constancy of the relaxed and unrelaxed limits (horizontal plateaus in Figure 7.1) and vanishing attenuation ($Q^{-1} \rightarrow 0$) in them shows that the deformations in these limits are predominantly elastic. In seismic applications, the only exception from this transition between two elastic modes is the case of P-wave dispersion in Biot's poroelastic model. In this case, the increase of wave velocity at high frequencies occurs because of an effective reduction of inertial properties via the material property matrix \mathbf{d} .

Thus, despite the notation as a “quality factor”, the peak value of $Q^{-1}(f)$ is actually an elastic property. By contrast, frequency f_0 of the transition is an indicator of internal friction within the rock. Variations of f_0 can be caused by the solid and pore-fluid viscosity, permeability, or heat dissipation. For example, with increasing viscosity η , the transition frequency f_0 reduces so that product $f_0\eta$ remains comparatively invariant. In addition, f_0 is sensitive to the elastic coupling between the different deformation modes, which is described by off-diagonal elements of matrices \mathbf{K} and $\boldsymbol{\mu}$.

7.1 *Static equilibrium*

Static equilibrium is the first case one considers when studying a mechanical system. In this case, the deformation \mathbf{u} is independent of time, and equation (5.7) becomes

$$\partial_j \boldsymbol{\sigma}_{ij} = \mathbf{0}, \quad \text{with} \quad \boldsymbol{\sigma}_{ij} = \lambda \Delta \delta_{ij} + 2\mu \boldsymbol{\varepsilon}_{ij}. \quad (7.2)$$

For simplicity, let us assume that material properties λ and μ are constant within the zone of interest. Then, plugging into these equations the definition of strain $\boldsymbol{\varepsilon}_{ij} = (\partial_i \mathbf{u}_j + \partial_j \mathbf{u}_i)/2$, we obtain the differential equation satisfied by the displacement \mathbf{u} , (verify this!):

$$(\lambda + \mu) \partial_i \partial_j \mathbf{u}_j + \mu \partial_j \partial_j \mathbf{u}_i = \mathbf{0}. \quad (7.3)$$

Note that this is a vector equation in both the usual 3-D coordinate space (given by the free subscript i) and in the N -dimensional GLS space of model variables (represented by bold characters).

If the force of gravity is significant but spatially uniform on the scale of the experiment (for example, when considering the lithostatic or hydrostatic pressure within a reservoir), then the first equation (7.2) is modified as $\partial_j \boldsymbol{\sigma}_{ij} = -\rho \mathbf{g}_i$, and consequently eq. (7.3) becomes

$$(\lambda + \mu) \partial_i \partial_j \mathbf{u}_j + \mu \partial_j \partial_j \mathbf{u}_i = -\rho \mathbf{g}_i. \quad (7.4)$$

In addition, if the body is non-uniformly heated, then the stress tensor in eq. (7.2) must contain an additional term $-\mathbf{K}\boldsymbol{\alpha}(\mathbf{T} - \mathbf{T}_0)\delta_{ij}$ (where \mathbf{K} is the bulk modulus, $\boldsymbol{\alpha}$ is the coefficient (matrix in the general GLS case) of thermal expansion, \mathbf{T} is a vector of temperatures, and \mathbf{T}_0 is the temperature at the state of equilibrium; see section 0), and therefore equation (7.3) is

$$(\lambda + \mu) \partial_i \partial_j \mathbf{u}_j + \mu \partial_j \partial_j \mathbf{u}_i = -\rho \mathbf{g}_i + \mathbf{K}\boldsymbol{\alpha} \partial_i \mathbf{T}. \quad (7.5)$$

In a perfectly static case, $\partial_i \mathbf{T} = 0$, and therefore there is no thermoelastic effect. However, thermoelastic stresses may become significant if slow, quasi-static deformations are considered, such as a subresonant mechanical testing of a rock sample in the laboratory or a seismic wave in the field (next subsections).

7.2 Plane Waves

For understanding and modeling seismic waves, the simplest and most important shape of deformation is given by plane harmonic (sinusoidal) waves in a spatially uniform medium. Such solutions are used in frequency-domain modeling, such as by using the Thomson-Haskell propagator for layered media described later. Such wave solutions take the form of harmonic plane waves with amplitudes exponentially decaying with distance due to internal friction.

Let us derive the frequency-dependent phase velocity and attenuation for a most general uniform GLS medium with N variables. In the following subsections, I will consider a plane P wave in some detail, and then briefly describe the modifications needed for modeling S waves and extensional-mode waves. The extensional-mode (longitudinal) waves are particularly important for modeling “Young’s modulus” laboratory experiments with uniaxial deformation of cylindrical rock samples.

7.2.1 P waves

Consider a plane P wave in which all spatial displacements are oriented in the direction of axis X : $u_{jk} = u_j \delta_{k1}$, where the upper-case subscript ‘ j ’ enumerates model variables, and the lower-case ‘ k ’ refers to spatial coordinates. The strain for J^{th} phase equals $\varepsilon_{jik} = u'_j \delta_{i1} \delta_{k1}$, where the prime denotes the spatial derivative in X . Consequently, the dilatation $\Delta_j = \varepsilon_{jii} = u'_j$, and the equation of motion (5.5) then simplifies to:

$$\rho \ddot{\mathbf{u}} = -\mathbf{d}\dot{\mathbf{u}} + \mathbf{M}\mathbf{u}'' + \boldsymbol{\eta}_M \dot{\mathbf{u}}'' , \quad (7.6)$$

where $\mathbf{M} \equiv \mathbf{K} + 4\boldsymbol{\mu}/3$ is the (matrix) P-wave modulus and $\boldsymbol{\eta}_M \equiv \boldsymbol{\eta}_K + 4\boldsymbol{\eta}_\mu/3$ is the P-wave

viscosity.

eq. (7.6) shows that the complex-valued wave modes $\mathbf{v}^{(n)}$ and the corresponding eigenvalues $\gamma^{(n)}$ can be obtained from the following generalized eigenvector problem:

$$\boldsymbol{\rho}^* \mathbf{v}^{(n)} = \gamma^{(n)} \mathbf{M}^* \mathbf{v}^{(n)}. \quad (5.10 \text{ repeated})$$

In this equation, $\boldsymbol{\rho}^* \equiv \boldsymbol{\rho} + i\mathbf{d}/\omega$ is the complex-valued effective density matrix and $\mathbf{M}^* \equiv \mathbf{M} - i\omega\boldsymbol{\eta}_M$ is the viscoelastic-type, matrix P-wave modulus. If thermoelastic effects are considered as described in section 7.3, they can also be included in this modulus \mathbf{M}^* .

7.2.2 S waves

For an S wave propagating in the direction of axis X and polarized along axis Y , the displacement is $u_{jk} = u_j \delta_{k2}$, the nonzero strain components equal $\varepsilon_{j12} = \varepsilon_{j21} = u'_j/2$, and $\Delta_j = 0$. Therefore, only shear material-property contribute to the equation of motion (5.5), which is simply:

$$\boldsymbol{\rho}\ddot{\mathbf{u}} = \boldsymbol{\mu}\mathbf{u}'' + \boldsymbol{\eta}_\mu \dot{\mathbf{u}}''. \quad (7.10)$$

By solving this equation for eigenmodes as in the preceding subsection, all plane S-wave properties are obtained. For Biot's model, the right-hand side of this equation contains all zeros, which means that the pore fluid is not involved in wave motion, and there is only one S-wave mode. However, if $\boldsymbol{\eta}_\mu \neq \mathbf{0}$, this mode will show velocity dispersion and attenuation.

7.2.3 Extensional waves in an infinite rod

Consider an axisymmetric wave (also called extensional, longitudinal) propagating along a rod oriented in the direction of axis X . For simplicity (and practical applications), let us consider the case of Biot's porous rock ($N = 2$) with the cylindrical surface of the rod sealed for pore fluid. This means that the transverse fluid motion is zero: $u_{jk} = 0$ with $J = 2$ and $k = 2$ or 3 , and therefore the fluid displacement is described by a single variable

$u_{2x} = u_f$ (here, I temporarily switch to the more intuitive notation for coordinates $x_2 \equiv y$ and $x_3 \equiv z$). The nonzero components of these fields can be described by two fields (generalized variables, functions of x and t): a GLS vector of rock and fluid displacement along the rod \mathbf{u}_x , and the radial strain of the rod ε_r (here, I temporarily switch to the more intuitive notation for coordinates $x_2 \equiv y$ and $x_3 \equiv z$). Let us combine variables \mathbf{u}_x , ε_r , and their derivatives with respect to x $f' = \partial f / \partial x$ in one vector

$$\boldsymbol{\psi} = \begin{pmatrix} \mathbf{u}_x \\ \mathbf{u}'_x \\ \varepsilon_r \\ \varepsilon'_r \end{pmatrix}. \quad (7.11)$$

Next, we need to express the strains and the Lagrangian and dissipation functions through this vector $\boldsymbol{\psi}$. The spatial components of the GLS displacement vector (vectors in the 2-D space of poroelastic displacements) are given by matrix products $\mathbf{u}_i = \mathbf{U}_i \boldsymbol{\psi}$, where

$$\mathbf{U}_x = \begin{bmatrix} \mathbf{I} & \mathbf{0} & 0 & 0 \\ \mathbf{0} & \mathbf{0} & 0 & 0 \end{bmatrix}, \quad \mathbf{U}_y = \begin{bmatrix} \mathbf{0} & \mathbf{0} & y & 0 \\ \mathbf{0} & \mathbf{0} & 0 & 0 \end{bmatrix}, \quad \text{and} \quad \mathbf{U}_z = \begin{bmatrix} \mathbf{0} & \mathbf{0} & z & 0 \\ \mathbf{0} & \mathbf{0} & 0 & 0 \end{bmatrix}, \quad (7.12)$$

where the boldface symbols denote 2×2 matrices, and \mathbf{I} is the identity matrix. The components of strain equal $\boldsymbol{\varepsilon}_{ij} = \mathbf{E}_{ij} \boldsymbol{\psi}$, with the following nonzero matrices \mathbf{E}_{ij} :

$$\begin{aligned} \mathbf{E}_{xx} &= \begin{bmatrix} \mathbf{0} & \mathbf{I} & 0 & 0 \\ \mathbf{0} & \mathbf{0} & 0 & 0 \end{bmatrix}, & \mathbf{E}_{yy} = \mathbf{E}_{zz} &= \begin{bmatrix} \mathbf{0} & \mathbf{0} & 1 & 0 \\ \mathbf{0} & \mathbf{0} & 0 & 0 \end{bmatrix}, \\ \mathbf{E}_{xy} = \mathbf{E}_{yx} &= \begin{bmatrix} \mathbf{0} & \mathbf{0} & 0 & y/2 \\ \mathbf{0} & \mathbf{0} & 0 & 0 \end{bmatrix}, & \mathbf{E}_{xz} = \mathbf{E}_{zx} &= \begin{bmatrix} \mathbf{0} & \mathbf{0} & 0 & z/2 \\ \mathbf{0} & \mathbf{0} & 0 & 0 \end{bmatrix}. \end{aligned} \quad (7.13)$$

The dilatation has the same form of matrix product $\boldsymbol{\Delta} = \boldsymbol{\Omega} \boldsymbol{\psi}$, where

$$\boldsymbol{\Omega} = \mathbf{E}_{ii} = \begin{bmatrix} \mathbf{0} & \mathbf{I} & 2 & 0 \\ \mathbf{0} & \mathbf{0} & 0 & 0 \end{bmatrix}. \quad (7.14)$$

The deviatoric strain similarly is $\tilde{\boldsymbol{\varepsilon}}_{ij} = \tilde{\mathbf{E}}_{ij} \boldsymbol{\psi}$, where $\tilde{\mathbf{E}}_{ij} = \mathbf{E}_{ij} - \boldsymbol{\Omega} \delta_{ij} / 3$ equal

$$\begin{aligned}\tilde{\mathbf{E}}_{xx} &= \begin{bmatrix} \mathbf{0} & 2\mathbf{I}/3 & -2/3 & 0 \\ & & 0 & 0 \end{bmatrix}, & \tilde{\mathbf{E}}_{yy} = \tilde{\mathbf{E}}_{zz} &= \begin{bmatrix} \mathbf{0} & \mathbf{0} & 1/3 & 0 \\ & & 0 & 0 \end{bmatrix}, \\ \tilde{\mathbf{E}}_{xy} = \tilde{\mathbf{E}}_{yx} &= \mathbf{E}_{xy}, & \tilde{\mathbf{E}}_{xz} = \tilde{\mathbf{E}}_{zx} &= \mathbf{E}_{xz}.\end{aligned}\quad (7.15)$$

From eq. (5.6), the components of stress also have a similar matrix form $\sigma_{ij}^{\text{elastic}} = \mathbf{S}_{ij}\boldsymbol{\psi}$ and $\sigma_{ij}^{\text{viscous}} = \mathbf{H}_{ij}\boldsymbol{\psi}$, with nonzero matrices \mathbf{S}_{ij} and \mathbf{H}_{ij} equal:

$$\begin{aligned}\mathbf{S}_{xy} = \mathbf{S}_{yx} = \mathbf{S}_{xz} = \mathbf{S}_{zx} &= 2\mu\tilde{\mathbf{E}}_{xy}, \\ \mathbf{S}_{ij} &= \mathbf{K}\boldsymbol{\Omega} + 2\mu\tilde{\mathbf{E}}_{ij} \quad \text{for } i = j, \\ \mathbf{H}_{xy} = \mathbf{H}_{yx} = \mathbf{H}_{xz} = \mathbf{H}_{zx} &= 2\eta_{\mu}\tilde{\mathbf{E}}_{xx}, \\ \mathbf{H}_{ij} &= \eta_K\boldsymbol{\Omega} + 2\eta_{\mu}\tilde{\mathbf{E}}_{ij} \quad \text{for } i = j.\end{aligned}\quad (7.16)$$

Using the representations for strain (eqs. 7.14 and 7.15), the Lagrangian and dissipation density (eq. 5.2) can be expressed in terms of variable $\boldsymbol{\psi}(x,t)$ and then averaged over the cross-section of the rod. This gives the L and D functions identical to those in eqs. (4.12):

$$\begin{cases} L = \frac{1}{2}\dot{\boldsymbol{\psi}}^T \mathbf{M}\dot{\boldsymbol{\psi}} - \frac{1}{2}\boldsymbol{\psi}^T \mathbf{S}\boldsymbol{\psi}, \\ D = \frac{1}{2}\dot{\boldsymbol{\psi}}^T \mathbf{D}\dot{\boldsymbol{\psi}}, \end{cases}\quad (7.17)$$

where matrices $\mathbf{M} = \langle \mathbf{U}_i^T \boldsymbol{\rho} \mathbf{U}_i \rangle$, $\mathbf{S} = \bar{\mathbf{K}} + 2\bar{\mu}$, and $\mathbf{D} = \langle \mathbf{U}_i^T \mathbf{d} \mathbf{U}_i \rangle + \bar{\eta}_K + 2\bar{\eta}_{\mu}$ are the mass, stiffness, and damping matrix, respectively. In these matrices, the averaged elastic moduli and viscosities are

$$\begin{aligned}\bar{\mathbf{K}} &= \boldsymbol{\Omega}^T \mathbf{K} \boldsymbol{\Omega}, \quad \bar{\mu} = \langle \tilde{\mathbf{E}}_{ij}^T \mu \tilde{\mathbf{E}}_{ij} \rangle, \\ \bar{\eta}_K &= \boldsymbol{\Omega}^T \eta_K \boldsymbol{\Omega}, \quad \bar{\eta}_{\mu} = \langle \tilde{\mathbf{E}}_{ij}^T \eta_{\mu} \tilde{\mathbf{E}}_{ij} \rangle.\end{aligned}\quad (7.18)$$

From the ‘‘oscillator’’ functions L and D , the equation of motion for $\boldsymbol{\psi}$ is

$$\mathbf{M}\ddot{\boldsymbol{\psi}} + \mathbf{D}\dot{\boldsymbol{\psi}} + \mathbf{S}\boldsymbol{\psi} = \mathbf{0}.\quad (7.19a)$$

The ranks of matrices \mathbf{M} , \mathbf{D} , and \mathbf{S} equal two (the number of variables in our original GLS model), and therefore we need four additional equations for the 6-element vector $\boldsymbol{\psi}$. Three of these equations come from the initial selection of the third, fourths, and sixth variable in $\boldsymbol{\psi}$ being spatial derivative of a preceding one (eq. 7.11):

$$\begin{aligned}\frac{\partial \psi_1}{\partial x} - \psi_3 &= 0, \\ \frac{\partial \psi_2}{\partial x} - \psi_4 &= 0, \\ \frac{\partial \psi_5}{\partial x} - \psi_6 &= 0.\end{aligned}\tag{7.19b}$$

The last equation comes from the free-surface boundary condition, which requires that the transverse stress $\sigma_{yy} = \sigma_{zz}$ equals zero (eqs. 7.16):

$$\left(\mathbf{S}_{yy}\right)_1 \boldsymbol{\psi} = 0,\tag{7.19c}$$

Equations (7.19) can be used for time-domain simulations of deformation of the rod, including its longitudinal extension, transverse strain, and longitudinal pore-fluid flow. When considering a harmonic wave at frequency ω and complex-valued wavenumber k^* (as in eq. (5.9)), the derivatives in these equations can be replaced by multiplications: $\frac{\partial}{\partial x} \rightarrow ik^*$, $\frac{\partial}{\partial t} \rightarrow -i\omega$. After this replacement, eqs. (7.19) become an eigenvalue problem, with eigenvalue of the matrix in the left-hand side equal zero. Therefore, denoting this matrix $\boldsymbol{\Theta}$, this matrix must satisfy equation

$$\det(\boldsymbol{\Theta}) = 0.\tag{7.20}$$

For any given ω , this equation gives a nonlinear (in fact, quadratic) function of k^* , and therefore two roots can be found numerically. These roots $k_1^*(\omega)$ and $k_2^*(\omega)$ give the velocity dispersion and attenuation relations for the primary and secondary (slow and dissipative) extensional waves within the porous rod (as in eqs. 5.11).

$$V_{\text{phase}} \equiv \frac{\omega}{\text{Re } k^*}, \quad (7.21a)$$

and the energy-dissipation factor, defined by $Q^{-1} \equiv \alpha/(2k)$:

$$Q^{-1} = \frac{\text{Im } k^*}{2 \text{Re } k^*}. \quad (7.21b)$$

7.3 *Low-frequency forced oscillations of cylindrical rock samples*

In low-frequency forced-oscillation laboratory measurements (see Figures 1.7 and 1.8), a range of values for the loading frequency f is tested. At each angular frequency $\omega = 2\pi f$, the stress-strain ratio Y is measured, and the magnitude $|Y(\omega)|$ and the ratio $Q = -\text{Re } Y/2\text{Im } Y$ is reported. In particular, in a “Young’s modulus” experiment (also called extensional-mode, longitudinal), this ratio is the ratio of axial strains measured by strain gages attached to the sample and an aluminum cylinder attached to it (Figure 1.8):

$$Y = E_{\text{aluminum}} \frac{\varepsilon_{\text{standard}}}{\varepsilon_{\text{sample}}} = \frac{\sigma}{\varepsilon_{\text{sample}}}. \quad (7.22)$$

This ratio is scaled by the known elastic modulus of the standard (aluminum), so that Y has the meaning of Young’s modulus (E) of the sample. The use of the standard is needed because it is difficult to measure the stress σ applied to the top of the rock sample, and so this stress is estimated as the product $\sigma = E_{\text{aluminum}} \varepsilon_{\text{standard}}$ (eq. 7.22).

Another ratio measured in such experiments is the empirical Poisson’s ratio (Figure 1.8):

$$Y = -\frac{\varepsilon_{\text{transverse}}}{\varepsilon_{\text{axial}}}. \quad (7.23)$$

This ratio is used as a direct measure of the Poisson’s ratio (ν) of the rock.

The ratios (7.22), (7.23), and in fact any other measurement in this experiment is represented by a sinusoidal function at the given loading frequency, with a certain phase lag φ relative to the strain in the standard (Figure 1.8). This sine function can be represented by a complex-valued quantity

$$Y = |Y| e^{-i\varphi}, \quad (7.24)$$

which is a function of frequency ω . Using this function, analogs of the pair of quantities (7.21) is obtained:

$$\text{The “empirical modulus” (or Poisson’s ratio) } |Y|, \text{ and} \quad (7.25a)$$

$$\text{The corresponding “attenuation” for } Y: \quad Q_Y^{-1} = \arctan \varphi. \quad (7.25b)$$

The above shows that an empirical “modulus” and a “ Q ” can be defined for practically any pair of readings in an experiment like those discussed in chapter 1. Not all of these ratios are equally useful. For example, there exists an empirical Q (phase lag) for the Poisson’s ratio, although it has no physical meaning as any type of wave attenuation.

7.3.1 Approximation of uniform deformation

In practical laboratory work, a much simpler model than described in the preceding subsection is typically used. The observations above are replaced with rather drastic approximations:

- 1) The axial and transverse strains are assumed to be constant across the whole volume.
- 2) Pore fluid flow is also uniform. In most experiments, jacketed samples under undrained conditions are assumed. These conditions mean that the macroscopic fluid content remains constant.
- 3) No temperature variations and no effects occurring outside of the sample are considered.

In addition to these simplifying assumptions, conventional models focus only on explaining the specific sinusoidal-pressure loading test (Figure 1.8), i.e. only on predicting

the amplitudes and phases of the measured stress-strain ratios like (7.25). Such prediction is easy to do by assuming frequency-dependent effective viscoelastic moduli of the material. However, the effective moduli measured in a small sample may differ from those in a seismic wave *in situ* (subsection 1.6). Therefore, instead of the conventional frequency-dependent effective moduli, I will only consider rigorous physical effects described in section 5 and 6 in this text.

The viscosity of fluid included in Biot's drag (Darcy, our matrix \mathbf{d}) and solid viscosity of the rock (our matrices $\boldsymbol{\eta}_K$ and $\boldsymbol{\eta}_\mu$) are the principal mechanisms that should explain the observations, such as shown in Figures 7.1 and 1.8. As shown in subsection 0, at seismic frequencies, thermoelastic effects can likely be always viewed as part of solid viscosity.

Another cautionary remark about using approximations for interpreting laboratory data is related to assuming elastic formulas for relations between moduli. For example, it is usually assumed that at finite frequencies, the Poisson's ratio ν is related to the bulk modulus K and shear modulus μ by relation

$$\nu = \frac{3K - 2\mu}{2(3K + \mu)}, \quad (7.31a)$$

or that modulus K or P-wave modulus M can be calculated from a measured Young's modulus E by using relations

$$K = \frac{E}{3(1-2\nu)} \quad \text{and} \quad M = \frac{E(1-\nu)}{(1+\nu)(1-2\nu)}. \quad (7.31b)$$

The Poisson's ratio ν is often assumed to be frequency-independent. However, none of the above formulas are accurate for porous rock at nonzero frequencies. There exist no equations like eqs. (7.31) uniquely relating the measured quantities K , μ , E , ν , etc. because these quantities additionally depend on the patterns of pore-fluid flows within the rock. These flow patterns are controlled by boundary conditions of the experiment. Thus, to properly examine the properties of porous rock, both drained and undrained conditions must be tested, and rigorous theories used instead of *ad hoc* formulas like (7.31).

Therefore, further in this section, I consider both undrained and drained cases but still assuming simple patterns of pore-fluid flows constant along the length of the cylindrical sample.

If the sample is uniformly deformed (as in Figure 1.7, left), it is convenient to describe its deformation by two GLS vectors: $\boldsymbol{\varepsilon}_x$ (axial strain) and $\boldsymbol{\varepsilon}_r$ (radial strain). We can combine these vectors in one model vector of generalized coordinates:

$$\mathbf{q} = \begin{pmatrix} \boldsymbol{\varepsilon}_x \\ \boldsymbol{\varepsilon}_r \end{pmatrix}. \quad (7.32)$$

Consider a point within the sample at coordinate x along the symmetry axis and distance r from the axis. Assuming that the base of the cylindrical sample is fixed and impermeable for pore-fluid flow, the axial displacement of a point within the sample equals $\mathbf{u}_x = \boldsymbol{\varepsilon}_{xx}x$, the radial displacement is $\mathbf{u}_r = \boldsymbol{\varepsilon}_r r$, dilatation $\boldsymbol{\Delta} = \boldsymbol{\varepsilon}_x + 2\boldsymbol{\varepsilon}_r$, and components of deviatoric strain $\tilde{\boldsymbol{\varepsilon}}_x = \frac{2}{3}\boldsymbol{\varepsilon}_x - \frac{2}{3}\boldsymbol{\varepsilon}_r$ and $\tilde{\boldsymbol{\varepsilon}}_r = -\frac{1}{2}\tilde{\boldsymbol{\varepsilon}}_x$. The Lagrangian and dissipation functions (eq. 5.2) are then of the general discretized form in eq. (4.12):

$$\begin{cases} L = \frac{1}{2} \dot{\mathbf{q}}^T \begin{bmatrix} \boldsymbol{\rho}_{xx} & \mathbf{0} \\ \mathbf{0} & \boldsymbol{\rho}_{rr} \end{bmatrix} \dot{\mathbf{q}} - \frac{1}{2} \mathbf{q}^T \begin{bmatrix} \mathbf{S}_{xx} & \mathbf{S}_{xr} \\ \mathbf{S}_{xr} & \mathbf{S}_{rr} \end{bmatrix} \mathbf{q}, \\ D = \frac{1}{2} \dot{\mathbf{q}}^T \begin{bmatrix} \mathbf{D}_{xx} & \mathbf{D}_{xr} \\ \mathbf{D}_{xr} & \mathbf{D}_{rr} \end{bmatrix} \dot{\mathbf{q}}, \end{cases} \quad (7.33)$$

where the nonzero blocks of the mass and stiffness matrices are

$$\boldsymbol{\rho}_{xx} = \langle x^2 \rangle \boldsymbol{\rho} = \frac{r_0^2}{3} \boldsymbol{\rho}, \quad \boldsymbol{\rho}_{rr} = \langle y^2 + z^2 \rangle \boldsymbol{\rho} = \frac{r_0^2}{4} \boldsymbol{\rho}, \quad (7.34a)$$

$$\mathbf{S}_{xx} = \mathbf{K} + \frac{2}{3} \boldsymbol{\mu}, \quad \mathbf{S}_{rr} = 4\mathbf{K} + \frac{2}{3} \boldsymbol{\mu}, \quad \mathbf{S}_{xr} = -\frac{2}{3} \boldsymbol{\mu}, \quad (7.34b)$$

where $\langle \dots \rangle$ means averaging over the volume of the cylinder, and r_0 is its radius. The damping matrix consists of similar terms but applied to strain rates:

$$\mathbf{D}_{xx} = \frac{r_0^2}{3} \mathbf{d} + \boldsymbol{\eta}_K + \frac{2}{3} \boldsymbol{\eta}_\mu, \quad \mathbf{D}_{rr} = \frac{r_0^2}{4} \mathbf{d} + \frac{2}{3} \boldsymbol{\eta}_\mu, \quad \mathbf{D}_{xr} = -\frac{2}{3} \boldsymbol{\eta}_\mu. \quad (7.34c)$$

For forced oscillations of the cylinder at frequency ω much lower than the frequencies of its normal oscillations (called subresonant), the deformation of the cylinder will be given by eq. (4.29):

$$\mathbf{q} = \mathbf{J} \mathbf{f}, \quad (7.35)$$

where the compliance matrix \mathbf{J} equals

$$\mathbf{J} = \left\{ \begin{bmatrix} \mathbf{S}_{xx} & \mathbf{S}_{xr} \\ \mathbf{S}_{xr} & \mathbf{S}_{rr} \end{bmatrix} - i\omega \begin{bmatrix} \mathbf{D}_{xx} & \mathbf{D}_{xr} \\ \mathbf{D}_{xr} & \mathbf{D}_{rr} \end{bmatrix} \right\}^{-1}. \quad (7.36)$$

This solution is valid for any type of stress applied to the cylinder and any boundary conditions. Similar to vector \mathbf{q} , the stress and pore pressure are constant across the cylinder. Let us consider a GLS rheology with N variables, so that the case $N = 2$ will give the Biot's poroelastic model. If we consider a Young's-modulus (extensional) type experiment with free side surface of the cylinder, then the $2N$ -element stress vector equals

$$\mathbf{f} = \begin{pmatrix} \sigma \\ \mathbf{p} \\ 0 \\ \mathbf{p} \end{pmatrix}, \quad (7.37)$$

where σ is the arbitrary axial stress applied by the actuator and \mathbf{p} is a vector of $(N-1)$ induced variations of pore pressures (the only pore pressure in Biot's model). This vector also shows that the radial stress must be zero because of the free boundary conditions on the sides of the cylinder, and the pore pressure must be equal in both directions. Now let us consider two different cases for pore flow.

Open (drained) boundary conditions for all pore fluids. In this case, $\mathbf{p} = \mathbf{0}$ in eq. (7.37), and eq. (7.35) gives the ratios of both components of strain to the applied stress:

$$\begin{pmatrix} \boldsymbol{\varepsilon}_x/\sigma \\ \boldsymbol{\varepsilon}_r/\sigma \end{pmatrix} = \mathbf{J} \begin{pmatrix} 1 \\ \mathbf{0} \\ 0 \\ \mathbf{0} \end{pmatrix} = \mathbf{J}_{:,1}. \quad (7.38)$$

Here and below, I use Matlab notation for selecting rows and columns of matrix \mathbf{J} (the first column is used in this equation). Specifically, this solution contains $2N$ quantities ($2N = 4$ for ordinary rock with single porosity) which are (in principle) measurable in this experiment:

Table 9.1	
Properties measurable in an extensional-mode experiment with <u>drained</u> rock sample	
1) Empirical Young's modulus of the sample:	$E = \frac{\sigma}{\varepsilon_{1x}} = \frac{1}{J_{11}};$
2) Empirical Poisson's ratio:	$\nu = -\frac{\varepsilon_{1r}}{\varepsilon_{1x}} = -\frac{J_{(N+1),1}}{J_{11}};$
3) Analog of Young's modulus for I^{th} pore fluid:	$E_{fl} = \frac{\sigma}{\varepsilon_{Ix}} = \frac{1}{J_{I1}};$
4) Analog of Poisson's ratio for I^{th} pore fluid:	$\nu_{fl} = -\frac{\varepsilon_{Ir}}{\varepsilon_{Ix}} = -\frac{J_{(N+I),1}}{J_{I1}}.$

where Matlab notation $J_{(N+1),1}$ is used again. Note that the pore fluid index I above starts counting from $I = 2$, as in all GLS model vectors.

Closed (undrained) boundary conditions for all pore fluids. In this case, vector \mathbf{p} is unknown, and the solution (7.35) is

$$\begin{pmatrix} \boldsymbol{\varepsilon}_x/\sigma \\ \boldsymbol{\varepsilon}_r/\sigma \end{pmatrix} = \mathbf{J}_{:,1} + \mathbf{J}_{:,2:N} \frac{\mathbf{p}}{\sigma}. \quad (7.39)$$

where ' f ' denotes all columns related to pore fluids matrix \mathbf{J} . The induced pressure variation p must be such that it ensures zero dilatation for I th fluid: $\Delta_I = \varepsilon_{Ix} + 2\varepsilon_{Ir} = 0$. Solving this equation for \mathbf{p}/σ gives:

$$\frac{\mathbf{p}}{\sigma} = -\left(\mathbf{J}_{2:N,2:N} + 2\mathbf{J}_{(N+2):2N,2:N}\right)^{-1} \left(\mathbf{J}_{2:N,1} + 2\mathbf{J}_{(N+2):2N,1}\right). \quad (7.40a)$$

Let us denote this ratio by a GLS vector β . With $N = 2$ (poroelastic case), this ratio is a single number:

$$\beta = -\frac{J_{21} + 2J_{41}}{J_{22} + J_{42} + 2(J_{24} + J_{44})}. \quad (7.40b)$$

Thus, in the experiment with undrained rock cylinder, there also are $2N$ measurable quantities:

Table 9.2		
Properties measurable in an extensional-mode experiment with an <u>undrained</u> rock sample		
1) Empirical Young's modulus:	$E = \frac{\sigma}{\varepsilon_{1x}}$	from eq. (7.40);
2) Empirical Poisson's ratio:	$\nu = -\frac{\varepsilon_{1r}}{\varepsilon_{1x}}$	from eq. (7.40);
3) Analog of Young's modulus for I^{th} pore fluid:	$E_f = \frac{\sigma}{\varepsilon_{Ix}}$	from eq. (7.39);
4) Induced pore pressure ratio:	$\beta_I = \frac{p_I}{\sigma}$	from eq. (7.40).

From the above results, note that the Young's modulus and Poisson's ratio for the cylindrical rock sample depend on the boundary conditions for pore fluid. Also, even under undrained conditions, the pore flow does not equal zero (only the dilatation is zero), and therefore the Young's modulus and Poisson's ratio depend on material properties included in matrix \mathbf{d} , that is on the permeability of the sample and viscosity of the fluid within primary pores. This dependence seems to be unnoticed in most Young's modulus experiments.

7.3.2 Detailed modeling of Biot's rock with thermoelastic effects

In this subsection, we use Galerkin's method (section 5.11 on page 158) to model subresonant forced-oscillation axial loading of a cylindrical rock sample (Figure 7.2). We will use the general GLS rheology with thermoelastic effects and take into account the variation of the shape of the specimen, and the effect of the "dead volume" (an inlet and tube with oil) attached to one end of the rock cylinder. For a specific application, we will use Biot's poroelastic model (GLS with $N = 2$; section 5.6). Material properties are constant within each of the elements of the structure. To describe the thermoelastic effects, we will use the simplified local-heat transfer model in subsection 6.2.2 (page 182).

Construction of finite elements and basis functions

The approach to finite-element model discretization is described in section 5.11

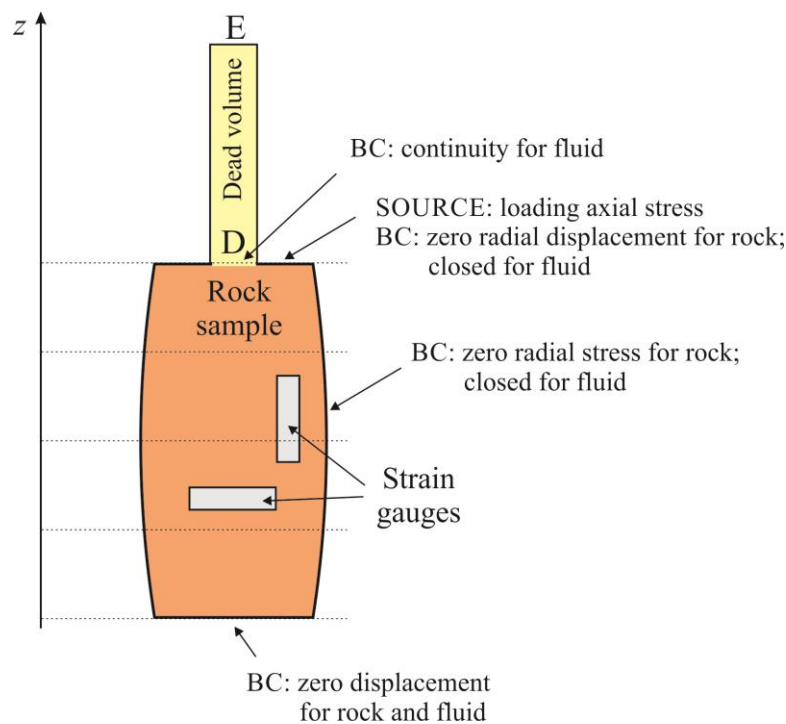


FIGURE 7.2.

Modeling a subresonant rock-physics experiment with axial loading. Curved side surfaces of the sample and the positions of strain gages are indicated schematically. Dotted lines indicate the nodes of the finite-element grid in direction Z . The volume of oil outside of the sample ("dead volume") is modeled as a cylinder hydraulically connected to the pore fluid volume, with fluid moving in the axial direction. Source and boundary conditions are indicated by labels 'SOURCE' and 'BC', respectively.

(page 158). First, a set of basis functions (finite elements, FE below) $f_{jk}(r, \varphi, z)$ is defined for the interior of the cylinder as:

$$f_{jk}(z, r) = f_j^{(z)}(z) f_k^{(r)}(r). \quad (7.41)$$

These functions are indexed by a pair of spatial indices j and k indicating grid locations in the axial and radial directions, respectively. In the axial direction Z , we can use Wiggins functions centered on the levels shown by the dotted lines in Figure 7.2. Wiggins functions are smooth and will be sufficient with a relatively coarse gridding. In the radial direction, we need to use two different forms of basis functions $f_k^{(r)}(r)$ for radial displacements and all other cases (eqs. (5.90) on page 167). In the azimuthal direction, we consider no variations of material properties or field variables.

Using the selected basis function (eq. (7.41)), it is convenient to define basis functions for their spatial derivatives. Let us denote them using commas in subscripts:

$$f_{jk,z}(z, r) = \frac{\partial f_{jk}}{\partial z} = f_j^{(z)'}(z) f_k^{(r)}(r) \quad \text{and} \quad f_{jk,r}(z, r) = \frac{\partial f_{jk}}{\partial r} = f_j^{(z)}(z) f_k^{(r)'}(r), \quad (7.42a)$$

and the azimuthal derivative is zero: $f_{jk,\varphi}(z, r) = \frac{\partial f_{jk}}{\partial \varphi} = 0$. Similarly, second derivatives of the basis functions are

$$\begin{aligned} f_{jk,zz}(z, r) &= f_j^{(z)''}(z) f_k^{(r)}(r), & f_{jk,rr}(z, r) &= f_j^{(z)}(z) f_k^{(r)''}(r), \\ \text{and } f_{jk,zr}(z, r) &= f_{jk,rz}(z, r) = f_j^{(z)'}(z) f_k^{(r)'}(r). \end{aligned} \quad (7.42a)$$

Using the above functions, if q_n denotes some scalar quantity $q(z, r)$ stored in the n^{th} element of our model vector $\bar{\mathbf{q}}$, and (j, k) are the spatial indices of the FE to which this q_n is related, then the spatial variation of this quantity within this FE equals

$$q(z, r) = q_n f_{jk}(z, r), \quad (7.43)$$

and the two nonzero components of its gradient can also be obtained from q_n :

$$\begin{pmatrix} \frac{\partial q}{\partial z} \\ \frac{\partial q}{\partial r} \end{pmatrix} = q_n \begin{pmatrix} f_{jk,z}(z, r) \\ f_{jk,r}(z, r) \end{pmatrix}, \quad (7.44)$$

and similarly the second derivatives. If indices n_z and n_r correspond to the axial and radial components of some displacement vector at the same FE (j, k) (i.e., the displacement vector

$$\begin{pmatrix} u_z^{(jk)} \\ u_r^{(jk)} \end{pmatrix} = \begin{pmatrix} q_{n_z} \\ q_{n_r} \end{pmatrix}), \text{ then, from eq. (7.44), the nonzero components of the strain tensor are}$$

given by matrix product

$$\begin{pmatrix} \mathcal{E}_{zz}^{(jk)} \\ \mathcal{E}_{rr}^{(jk)} \\ \mathcal{E}_{\varphi\varphi}^{(jk)} \\ \mathcal{E}_{zr}^{(jk)} \end{pmatrix} = \mathbf{E}_{jk}(z, r) \begin{pmatrix} q_{n_z} \\ q_{n_r} \end{pmatrix}, \quad (7.45a)$$

where the matrix-valued basis function is

$$\mathbf{E}_{jk}(z, r) = \begin{bmatrix} f_{jk,z}(z, r) & 0 \\ 0 & f_{jk,r}^{(r1)}(z, r) \\ 0 & \frac{1}{r} f_{jk}^{(r1)}(z, r) \\ \frac{1}{2} f_{jk,r}(z, r) & \frac{1}{2} f_{jk,z}^{(r1)}(z, r) \end{bmatrix}, \quad (7.45b)$$

Note that radial basis functions $f_{jk}^{(r1)}(z, r)$ are used here (see eqs. (5.90b)). From this expression, the spatial function for dilatational strain within the FE number (j, k) is similarly

$$\Delta^{(jk)} = \Omega_{jk}(z, r) \begin{pmatrix} q_{n_z} \\ q_{n_r} \end{pmatrix}, \quad (7.46a)$$

where the matrix-row basis function is

$$\Omega_{jk}(z, r) = \left(f_{jk,z}(z, r) \quad f_{jk,r}(z, r) \right). \quad (7.46b)$$

The deviatoric strain contains a diagonal component in the azimuthal direction:

$$\begin{pmatrix} \tilde{\varepsilon}_{zz}^{(jk)} \\ \tilde{\varepsilon}_{rr}^{(jk)} \\ \tilde{\varepsilon}_{\varphi\varphi}^{(jk)} \\ \tilde{\varepsilon}_{zr}^{(jk)} \end{pmatrix} = \begin{pmatrix} \varepsilon_{zz}^{(jk)} \\ \varepsilon_{rr}^{(jk)} \\ 0 \\ \varepsilon_{zr}^{(jk)} \end{pmatrix} - \frac{\Delta^{(jk)}}{3} \begin{pmatrix} 1 \\ 1 \\ 1 \\ 0 \end{pmatrix} = \tilde{\mathbf{E}}_{jk}(z, r) \begin{pmatrix} q_{n_z} \\ q_{n_r} \end{pmatrix}. \quad (7.47a)$$

where

$$\tilde{\mathbf{E}}_{jk}(z, r) = \begin{bmatrix} \frac{2}{3} f_{jk,z}(z, r) & -\frac{1}{3} f_{jk,r}^{(r1)}(z, r) \\ -\frac{1}{3} f_{jk,z}(z, r) & \frac{2}{3} f_{jk,r}^{(r1)}(z, r) \\ -\frac{1}{3} f_{jk,z}(z, r) & -\frac{1}{3} f_{jk,r}^{(r1)}(z, r) \\ \frac{1}{2} f_{jk,r}(z, r) & \frac{1}{2} f_{jk,z}^{(r1)}(z, r) \end{bmatrix}. \quad (7.47b)$$

The expressions for observables and FE equations below will also use spatial derivatives of strain. These derivatives can also be represented by matrix products:

$$\partial_i \Delta^{(jk)} = \Omega_{jk,i}(z, r) \begin{pmatrix} q_{n_z} \\ q_{n_r} \end{pmatrix}, \quad (7.48a)$$

where subscripts ‘ i ’ can be ‘ z ’ or ‘ r ’, and the matrix-row valued functions are

$$\Omega_{jk,i}(z, r) = \left(f_{jk,zi}(z, r) \quad f_{jk,ri}(z, r) \right). \quad (7.48b)$$

Similarly, gradients of the deviatoric strain components are

$$\partial_i \begin{pmatrix} \tilde{\epsilon}_{zz}^{(jk)} \\ \tilde{\epsilon}_{rr}^{(jk)} \\ \tilde{\epsilon}_{\varphi\varphi}^{(jk)} \\ \tilde{\epsilon}_{zr}^{(jk)} \end{pmatrix} = \tilde{\mathbf{E}}_{jk,i}(z, r) \begin{pmatrix} q_{n_z} \\ q_{n_r} \end{pmatrix}. \quad (7.49a)$$

where

$$\tilde{\mathbf{E}}_{jk,i}(z, r) = \begin{bmatrix} \frac{2}{3} f_{jk,zi}(z, r) & -\frac{1}{3} f_{jk,ri}(z, r) \\ -\frac{1}{3} f_{jk,zi}(z, r) & \frac{2}{3} f_{jk,ri}(z, r) \\ -\frac{1}{3} f_{jk,zi}(z, r) & -\frac{1}{3} f_{jk,ri}(z, r) \\ \frac{1}{2} f_{jk,ri}(z, r) & \frac{1}{2} f_{jk,zi}(z, r) \end{bmatrix}, \quad (7.49b)$$

with subscripts ‘ i ’ again being ‘ z ’ or ‘ r ’.

Construction of model vector

The model is represented by vector $\bar{\mathbf{q}}$ with the number of elements denoted N_q and elements defined as shown in Table 7.1. For the last element describing the dead volume, we define a special basis function linearly decreasing from value $f_{N_q}(z)=1$ at level D to $f_{N_q}(z)=0$ at level E (Figure 7.2). This function describes a uniform compression or expansion of pore fluid within the dead-volume tube.

Table 7.1 Mapping of finite-element model variables in Figure 7.2

<i>Indices in vector $\bar{\mathbf{q}}$</i>	<i>Model variables</i>
$n = 1, \dots, (N_q - 1)$	Groups of <u>five variables</u> corresponding to each spatial finite element (j, k) within the interior of the rock cylinder (combination of indices j and k in eqs. (7.41)): 1) Axial and radial displacements of rock;

	2) Axial and radial displacements of pore fluid; 3) Thermoelastic temperature disbalance θ for Biot's rock (page 184).
$n = N_q$	<u>Axial displacement</u> of the fluid within the dead volume near its contact with rock (at point D)

Observables

To express observables such as displacements and stresses at arbitrary points within the model, we need to use the decomposition of these observables as products of elements of vector $\bar{\mathbf{q}}$ with the corresponding FE basis function (eq. (5.69) on page 159). In matrix form, a vector \mathbf{a} combining any observables of the system can be expressed as

$$\mathbf{a}(z, r) = \mathbf{U}_a(z, r)\bar{\mathbf{q}} + \mathbf{V}_a(z, r)\dot{\bar{\mathbf{q}}}, \quad (7.50)$$

where rows of matrices $\mathbf{U}_a(z, r)$ and $\mathbf{V}_a(z, r)$ contain basis functions for variables \mathbf{a} at point (z, r) . These matrices are sparse, with nonzero columns corresponding to the elements of vector $\bar{\mathbf{q}}$ related to the FE covering location (z, r) and the desired GLS variable J . For example, for rock or pore-fluid displacement, eq. (7.50) is

$$u_{ji}(z, r) = \sum_{n(J,i,z,r)} q_n f_{jk}(z, r), \quad (7.51)$$

where the summation over n is performed over all elements of vector $\bar{\mathbf{q}}$ corresponding to the model variable J , spatial component of displacement i , and finite elements (indices (j, k)) containing point (z, r) . A similar equation gives the temperature disbalance $\theta(z, r)$. Using these displacement values, the strain measured by an axial strain gauge attached to points z_1 and z_2 (Figure 7.2) can be obtained from model $\bar{\mathbf{q}}$ as

$$\varepsilon_{zz}^{\text{gauge}}\left(\frac{z_1 + z_2}{2}, R\right) = \frac{u_{1z}(z_2, R) - u_{1z}(z_1, R)}{z_2 - z_1}. \quad (7.52)$$

For a strain gauge oriented azimuthally at level z , the radial strain is measured:

$$\varepsilon_{rr}^{\text{gauge}}(z, R) = \frac{u_{1r}(z, R)}{R}. \quad (7.53)$$

The measured strains can be obtained from the complete distribution of strain, which is obtained by extracting the rows corresponding to the desired components of strain ε_{jij} from eqs. (7.45) and summing them over all pairs (j,k) whose FEs contain the target point (z,r) . The rows extracted from matrices $\mathbf{E}_{jk}(z, r)$ in eq. (7.45b) will comprise matrix $\mathbf{U}_\varepsilon(z, r)$ (with a being strain) in eq. (7.50). Matrix $\mathbf{V}_\varepsilon(z, r) = \mathbf{0}$ for strain.

By forming¹⁵ a vector \mathbf{a} in eq. (7.50) containing all GLS and spatial components of strain combined with the temperature disbalance θ at a given point (z,r) , the corresponding components of Cauchy stress at any point (z,r) can be obtained by implementing the GLS model-space matrix products in eq. (6.21):

$$\boldsymbol{\sigma}_{ij} = \delta_{ij} \mathbf{K} \Delta + 2\mu \tilde{\boldsymbol{\varepsilon}}_{ij} - \delta_{ij} \theta \mathbf{K} \boldsymbol{\alpha} \mathbf{T}_{rel}, \quad (7.54a)$$

for porous rock, where parameters θ and \mathbf{T}_{rel} (and also $\boldsymbol{\theta}_{rel}$ and T_0 in the next subsection) are explained in section 6.4. For fluid within the dead volume, the equation is scalar in model space and tensorial in coordinate space (eq. (5.16) on page 124 and Figure 7.2):

$$\sigma_{ij} = \delta_{ij} K \Delta + 2\mu \tilde{\varepsilon}_{ij} + \eta_K \dot{\Delta} \delta_{ij} + 2\eta_\mu \dot{\tilde{\varepsilon}}_{ij}. \quad (7.54b)$$

Note that in this equation, we keep the bulk viscosity of oil η_K along with the ordinary (shear) viscosity η_μ . Viscosity η_K is usually ignored, but in this case, it should be likely more significant than η_μ . We also disregard the variation of flow rate across the dead-volume tube¹⁶. Also note that eqs. (7.54b) are of the same form and can be implemented

¹⁵ In a computer program, this operation would likely mean writing a function to return all components of the strain tensor for given coordinates (z,r) .

¹⁶ This variation can easily be included by approximating the tubular flow by a Poiseuille-type flow, but this should hardly affect the results significantly. This approximation should also be much less significant than the uncertainty of the value of the bulk viscosity of oil or water. The bulk viscosity (also called volume viscosity, or second viscosity) is not well known but it is likely about three times the shear viscosity.

by the same code as eqs. (7.54a). The differences between these equations are in using viscosity matrices in addition to elasticity, using matrices \mathbf{V}_σ in eqs. (7.50), and absence of the thermoelastic pressure terms.

Governing equations

For spatially-constant material properties within the two parts of the system (Figure 7.2), the governing equations for the interior of the cylinder are (from eqs. (5.7), (5.8), (6.21), and (7.54a)):

$$\rho \ddot{\mathbf{u}}_i + \mathbf{d} \dot{\mathbf{u}}_i - \mathbf{K} \partial_i \Delta - 2\mu \partial_j \dot{\tilde{\epsilon}}_{ij} + \mathbf{K} \alpha \mathbf{T}_{rel} \partial_i \theta = 0. \quad (7.55a)$$

where and subscript ‘ i ’ can be ‘ z ’ or ‘ r ’. For the dead volume, the equation is scalar, contains no elastic shear effects or Darcy drag but includes viscous friction (eq. (7.54b)):

$$\rho \ddot{u}_i - K \partial_i \Delta - \eta_K \partial_i \dot{\Delta} - 2\eta_\mu \partial_i \dot{\tilde{\epsilon}}_{ij} = 0. \quad (7.55b)$$

For the internal temperature disbalance within the porous-rock cylinder, we have another scalar equation from eq. (6.24):

$$\dot{\theta} + \frac{1}{T_0} \boldsymbol{\theta}_{rel}^T \mathbf{c}_v^{-1} \boldsymbol{\alpha}^T \mathbf{K}^T \dot{\Delta} + \chi_\theta \theta = 0. \quad (7.55b)$$

By using the FE decomposition of the variable fields and their derivatives (subsection “Observables”), each term in eqs. (7.55) can be presented in the form of eq. (7.50) with some matrix-valued functions $\mathbf{U}_a(z, r)$ or $\mathbf{V}_a(z, r)$. For example, the third term in eq. (7.55a) becomes

$$\mathbf{a}(z, r) = \mathbf{U}_{-K\partial\Delta}(z, r) \bar{\mathbf{q}}, \quad (7.56)$$

where vector $\mathbf{a}(z, r)$ contains all GLS model-space and spatial components of the elastic force density applied at point (z, r) . To produce the weak-formulation (Galerkin’s) matrix equations, these equations need to be projected onto the basis functions corresponding to the elements of vector $\bar{\mathbf{q}}$. Let us write this projection for the n^{th} element of vector \mathbf{a} and l^{th}

basis function using an explicit integration and the implicit index summation notation for matrix products:

$$\begin{aligned}
 \langle f_l | a_n \rangle &= 2\pi \int f_l^*(z, r) a_n(z, r) r dr dz = \\
 &= 2\pi \int f_l^*(z, r) [U_{-\mathbf{k}\partial\Delta}(z, r)]_{nm} q_m r dr dz = \\
 &= [A_{-\mathbf{k}\partial\Delta}^l]_{nm} q_m,
 \end{aligned} \tag{7.57}$$

which in matrix form reads $\langle f_l | \mathbf{a} \rangle = \mathbf{A}_{-\mathbf{k}\partial\Delta}^l \bar{\mathbf{q}}$, where matrix $\mathbf{A}_{-\mathbf{k}\partial\Delta}^l$ is obtained from matrix function $\mathbf{U}_{-\mathbf{k}\partial\Delta}(z, r)$ by multiplying each of its elements by $f_l^*(z, r)$ and spatial integration. These integrations can be performed analytically or numerically, and matrices $\mathbf{A}_{-\mathbf{k}\partial\Delta}^l$ and similar matrices for other terms in eqs. (7.55) can be calculated and stored during initialization of the FE model. Finally, a matrix form of all combined eqs. (7.55) will be obtained (eq. (5.74)):

$$\mathbf{A}^{(2)} \ddot{\bar{\mathbf{q}}} + \mathbf{A}^{(1)} \dot{\bar{\mathbf{q}}} + \mathbf{C} \bar{\mathbf{q}} = \mathbf{0}. \tag{7.58}$$

The source term \mathbf{s} is set equal zero in this expression. Due to the linearity of the problem, we can model starting with a simple step-function initial displacement or harmonic deformation applied to some point (e.g., point D in Figure 7.2), and then rescale the final model to match the measured applied pressure.

Boundary conditions

Boundary conditions for this problem are represented by a homogeneous system of linear equations $\mathbf{B} \bar{\mathbf{q}} = \mathbf{0}$ (eq. (5.80) on page 162). Rows of matrix \mathbf{B} are obtained by transforming into matrix form equations for observables listed in Table 7.2. The procedure for transforming these equations is shown in eq. (7.57).

Table 7.2 Boundary conditions for the model in Figure 7.2

<i>Boundary condition</i>	<i>Equation</i>

Zero transverse stress on side surfaces	$\sigma_{Jrr}(z,R)$ in eqs. (7.54a), with $J = 1$ and z taken at each of the levels in grid Z
Zero pore-fluid flow on side surfaces, bottom flange, and top flange outside of the tube	$\sigma_{Jrr}(z,R)$ in eqs. (7.54a), with $J = 2$ and z taken at each of the levels in grid Z
Pore-flow continuity at point D	$u_{2z}(z,r) _{\text{Rock}} - u_z(z,r) _{\text{Dead volume}} = 0$ at the axis at point D
Pore-fluid pressure continuity at point D	$\sigma_{2zz}(z,r) _{\text{Rock}} - \sigma_{zz}(z,r) _{\text{Dead volume}} = 0$ at the axis at point D

Solution

Using matrix \mathbf{B} above, construct matrix \mathbf{F} as explained on page on page 162. Using this matrix, the final solution can be expressed as $\bar{\mathbf{q}} = \mathbf{F}\mathbf{q}$, where \mathbf{q} is a vector of independent variables (eq. (5.83)). With respect to this vector, the governing equation will be (eq. (5.77))

$$\mathbf{A}^{(2)}\mathbf{F}\ddot{\mathbf{q}} + \mathbf{A}^{(1)}\mathbf{F}\dot{\mathbf{q}} + \mathbf{C}\mathbf{F}\mathbf{q} = \mathbf{0}. \quad (7.59)$$

7.3.3 Detailed modeling of Biot's rock with local extended SLS

In this subsection, we use the finite-element approximation in the preceding subsection (Figure 7.2) to model local WIFF effects (such as squirt or partial-saturation) instead of the thermoelastic effects. To represent the secondary porosity, we consider a double-porosity model (i.e., GLS with $N = 3$) with the following simplifications:

- 1) Disregard the inertial effects completely or consider inertial effects

proportional to the divergence of the flow rate. This corresponds to considering only random divergent secondary pore flow. We can also test kinetic-energy parts of L proportional to the dissipation function D , according to the principle of Rayleigh damping.

- 2) For the elastic response of the secondary porosity, use the extended GSLS (section 5.9) with a single variable (i.e., the extended SLS).

...

The results should be similar to those of the preceding subsection, with variable θ becoming the divergence of the secondary pore flow: $\theta = \Delta_2$.

....

7.3.4 Detailed modeling of Biot's rock with local WIFF

In this subsection, we use the finite-element approximation in subsection 7.3.2 (Figure 7.2) to model local WIFF effects (such as squirt or partial-saturation) instead of the thermoelastic effects. To represent the secondary porosity, we use the variable porosity tensor α_{ij} in section 5.7. We consider two types of deformation of tensor α_{ij} :

- 1) Isotropic expansion or contraction of all pores. In this case, the scalar parameter θ in subsection 7.3.2 becomes variation of the average pore radii. This model should correspond to models of "patchy saturation."
- 2) Anisotropic oscillation of planar microcracks. This model corresponds to many model of "squirt flows."

....

Again, observationally, the results should be very similar to those of the preceding subsections. The above thermoelastic and WIFF models are just impossible to differentiate based on a single macroscopic subresonant-oscillation or time-domain creep experiment.

...

7.4 *Laboratory assignments*

Several labs below use material properties of Berea sandstone given in Tables 7.1 and 7.2. Table 7.1 shows an example of a typical poroelastic model with single porosity, and Table 7.2 gives a double-porosity model with relaxation within the drained frame. This relaxation can be caused by “wave-induced fluid flows” or thermoelastic effects discussed in this text.

Table 7.1. Properties of Berea sandstone (from ...)

Table 7.2. Properties of Berea sandstone with double porosity (from ...)

Lab 7.1: Velocity dispersion and attenuation of plane P and S waves

In this lab, you will use Matlab to model the propagation of plane waves in an unbounded porous fluid-saturated medium with or without solid viscosity.

- 1) Using equations of section 7.2, write a Matlab program to model velocity dispersion and attenuation of plane P and S waves in Berea sandstone.

Properties of the sandstone are listed in Table 7.2. Use frequency range from 10^{-2} to 10^9 Hz, sampled logarithmically.

- 2) First, consider no solid viscosity ($\boldsymbol{\eta}_K = \boldsymbol{\eta}_\mu = \mathbf{0}$). Plot the attenuation (Q^{-1}) and velocity dispersion curves on logarithmic scale of frequencies. Identify Biot's dissipation peak and velocity dispersion for the primary and secondary P waves.
- 3) Is there any dispersion and attenuation for S waves? Why? Is there a secondary S wave in this case?
- 4) Repeat the modeling and plotting with nonzero $\boldsymbol{\eta}_K$ and $\boldsymbol{\eta}_\mu$ (Table 7.2). Do additional transition in velocity and attenuation peak appear?
- 5) Do secondary wave, velocity dispersion and attenuation peaks appear for S waves?
- 6) Compare the frequencies of the peaks with the characteristic frequencies $f_c = \|\mathbf{M}\|/2\pi\|\boldsymbol{\eta}_M\|$ for P waves and $f_c = \|\boldsymbol{\mu}\|/2\pi\|\boldsymbol{\eta}_\mu\|$ for S waves, where \mathbf{M} is the matrix of P-wave modulus, $\boldsymbol{\eta}_M$ is the corresponding viscosity, and $\|\dots\|$ denotes some norm of the matrices. For the high-frequency peak, compare its frequency with Biot's frequency $f_c = \phi\eta_f/2\pi\kappa\rho$.
- 7) Save the modeled P- and S-wave dispersion-attenuation spectra for use in subsequent labs.

Lab 7.2: Extensional waves in a rod

In this lab, you will model extensional (longitudinal) waves in a solid rod of porous rock and compare the results with those from Lab 1. Take the diameter of the rod equal 3 cm.

- 1) Using equations in the last part of section 7.2, write Matlab function `Theta(f, k)` which will take frequency f and complex-valued wavenumber k^* as parameters and return matrix Θ given by eqs. (7.19). Use parameters of sandstone in Table 7.2.
- 2) Verify that $\det(\Theta)$ is a quadratic polynomial function of k^* . To do this, note that matrix Θ contains only three elements containing variable k^* , in the rows

corresponding to eqs. (7.19). For harmonic wave, these equations are:

$$\begin{cases} ik^* \psi_1 - \psi_3 = 0, \\ ik^* \psi_2 - \psi_4 = 0, \\ ik^* \psi_5 - \psi_6 = 0, \end{cases}$$

which mean that elements (3,1), (4,2), and (5,5) of matrix Θ equal ik^* . Is this so? Then if exclude rows 3, 4, and 5 and columns 1, 2, and 5 (containing these elements). The resulting matrix should have zero determinant. Is this so in your matrix? This determinant equals plus or minus the coefficient of $(ik^*)^3$ in the polynomial expression for $\Theta(k^*)$ (at any selected frequency f or ω).

- 3) Write another function `eigenmodesTheta(f)`, which would use function `Theta` to solve eq. (7.20) for k^* , and return: 1) two solutions for k^* , and 2) the two corresponding solutions ψ_1 and ψ_2 of equation $\Theta\psi = \mathbf{0}$ (eqs. 7.19). Since $\det(\Theta)$ is a quadratic polynomial of k^* , its roots (values of k^* at which $\det(\Theta) = 0$) can be obtained by the following procedure:

- Use your program to evaluate $y = \det(\text{Theta}(f, k))$ at three trial points k_1, k_2 , and k_3 ;
- Derive coefficients a, b , and c of a polynomial function $f(k) = ak^2 + bk + c$ equal to the determined values of y at each of these points;
- Then determine the two roots of $f(k)$ by the usual formula

$$k_{1,2} = \frac{-b \pm \sqrt{b^2 - 4ac}}{2a}.$$

- 4) **Optional task for bonus points:** A better way for obtaining coefficients a, b , and c is to consider all matrix minors (determinants of matrices obtained by removing one row and one column) for the elements containing ik^* . For example, you can do this by:

- Defining a recursive function `polydet(A)` which would take a square matrix \mathbf{A} and output the polynomial coefficients of its determinant with respect to argument $z = ik^*$.

- b. To implement this recursive function, use the formula for determinant of a matrix expressed through a sum of its minors M_{ij} for any row i :

$$\det \mathbf{A} = \sum_j (-1)^{i+j} A_{ij} M_{ij},$$

where A_{ij} is an array of polynomial coefficients for element (i,j) and M_{ij} is returned by the same function `polydet()` for a matrix obtained from \mathbf{A} by dropping the row i and column j . The product $A_{ij}M_{ij}$ should be evaluated using polynomial calculations; this can be done by function `conv()` in Matlab.

- 5) Using the same frequency sampling as in Lab 1, use function `eigenmodesTheta(f)` to calculate the phase velocity and attenuation of the primary and secondary longitudinal (extensional) wave within the rod (eqs. 7.21). Plot graphs of velocity and Q^{-1} .

- 6) Also calculate the extensional-mode velocity and Q differently, by taking the complex-valued V_P and V_S results from Lab 1 (the primary modes only) and combining them using the standard formula for elastic Young's modulus:

$$E = \frac{\mu(3M - 4\mu)}{M - \mu}, \text{ where } M = \rho V_P^2 \text{ and } \mu = \rho V_S^2 \text{ are the empirical (complex}$$

valued and frequency-dependent) P- and S-wave moduli, and $E = \rho V_E^2$ is accordingly the expected viscoelastic extensional-mode modulus. Therefore,

the predicted extensional-wave velocity will be $V_E = \frac{1}{\text{Re} \sqrt{\rho/E}}$, and the

expected attenuation $Q_E^{-1} = -\frac{\text{Im} E}{\text{Re} E}$.

- 7) Plot the above viscoelastic estimates of $V_E(f)$ and $Q_E^{-1}(f)$ and compare them to the results of rigorous modeling using matrix Θ .

Lab 7.3: Modeling Young's modulus experiment with rock cylinder

In this lab, you will model laboratory rock-physics experiments with a porous rock

sample under different boundary conditions.

In laboratory experiments, the measured Young's moduli are defined as complex-valued stress-strain ratios given in eqs. (7.22) and (7.23). Using Matlab, model these ratios for a cylindrical sample of double-porosity sandstone described in Table 7.2, with length 8 cm and diameter 3 cm.

- 1) Implement function `compliance(f)` (or use another name of your choice) taking an arbitrary frequency and returning the compliance matrix \mathbf{J} for the cylinder (eq. (7.36) on page 205).
- 2) Using this function, for a range of seismic frequencies, calculate the four properties measurable for drained and undrained sample (Tables 9.1 and 9.2 on page 206).
- 3) Plot the calculated quantities on separate plots. For each quantity Y , plot its absolute value $|Y|$ and the corresponding $Q^{-1} = -\frac{\text{Im} Y}{\text{Re} Y}$.
- 4) Discuss the similarities and differences between the drained and undrained cases.

Lab 7.4: Poisson's ratios for poroelasticity

In this lab, you will examine the Poisson's and related ratios for poroelastic model and other similar ratios of observable strains modeled in the preceding labs. Our goal is to determine whether the Poisson's ratio can be considered as elastic and/or independent of the boundary conditions for pore flow.

- 1) Modify your program from Lab 3 to use the poroelastic model of Berea sandstone (set $N = 2$ and use material properties from Table 7.1). Note that in this case, there is only one pore fluid, and matrix inverses become simple divisions (eq. 7.40b).
- 2) Model the cases of drained and undrained rock at frequencies from 1 to 1000 Hz. Plot absolute values and the corresponding Q^{-1} of the resulting Poisson's ratios ν and additional ratios shown in Tables 9.1 and 9.2 (page 206).

- 3) In the plots of $|\nu|$, also plot the elastic Poisson's ratios (constant with frequency) calculated by using the usual formula $\nu = \frac{3K - 2\mu}{2(3K + \mu)}$ (eq. 7.31a) for drained and undrained moduli K .
- 4) Discuss the frequency dependencies of the modeled $|\nu|$ and the corresponding Q^{-1} . Are they close to the drained or undrained elastic ν ? Is the accuracy of $\nu(f) \approx \nu_{\text{elastic}}$ good enough for measuring an inverse Q^{-1} of about 0.03 (corresponding to $Q \approx 30$)?

8 Bibliography

The bibliography is still incomplete...

Aki, K. and P. G. Richards, 2002, Quantitative seismology, Second ed.: University Science Books, Sausalito, California.

Blanch, J.O., J.O.A. Robertsson, and W.W. Symes, 1995, Modeling of a constant Q : methodology and algorithm for an efficient and optimally inexpensive viscoelastic technique: *Geophysics*, **60**, 176–184.

Bohlen T. 2002. Parallel 3-D viscoelastic finite difference seismic modelling. *Computers & Geosciences* **28**, 887–899.

Bourbié, T., Coussy, O., and Zinsiger, B. 1987, Acoustics of porous media: Editions TECHNIP, France, ISBN 2-7108-0516-2.

Fuchs, K. and G. Müller, 1971, Computation of synthetic seismograms with the reflectivity method and comparison with observations: *Geophysical Journal International*, **23**, 417–433, doi: 10.1111/j.1365-246X.1971.tb01834.x.

Griggs, D. T. (1940). Experimental flow of rocks under conditions favoring recrystallization, *Bull. Geol. Soc. Am.* **51**, 1001–22.

Kennett, B. L. N., 1983, Seismic wave propagation in stratified media: Cambridge University Press.

Krebes, E.S. and Daley, P.F., 2007. Difficulties with computing anelastic plane-wave reflection and transmission coefficients, *Geophysical Journal International*, 170, 205–216.

Landau, L., and E. Lifshitz. 1986, Course of theoretical physics, volume 7 (3rd English edition): Theory of elasticity, Butterworth-Heinemann, ISBN 978-0-7506-2633-0.

Pratt, R. G., 1999, Seismic waveform inversion in the frequency domain, Part I: Theory and verification in a physical scale model: *Geophysics*, 64, 888–901.

Ruud, B.O., 2006. Ambiguous reflection coefficients for anelastic media, *Stud. Geophys. Geod.* 50, 479–498.

Sayers, C. M., and M. Kachanov, 1991. A simple technique for finding effective of cracked solids for arbitrary crack orientation statistics, *Int. J. of Solids and Structures*, 27, 671–680.

Vavryčuk, V., 2010. Behavior of rays and interfaces in anisotropic viscoelastic media, *Geophysical*

Journal International, 181, 1665–1677.

9 Appendices

9.1 *Variational principles for heat transfer*

It is interesting to see whether equations of heat transfer can be presented as mechanical equations, in the form of some variational principle (section 1.1). The answer to this question consists of two statements:

- 1) For stationary heat flow (steady-state, without changes of temperature with time at any point), a variational principle can be found. Consequently, the temperature at any point can be obtained by minimizing the corresponding Euler functional.
- 2) For nonstationary heat flow (with temperatures variable in time), there exists no variational principle in terms of minimizing some ordinary functional. However, a variational principle can be obtained after a Laplace or Fourier transform in time, i.e. when considering exponentially decaying or oscillating temperature fields.

These two cases are briefly discussed in the following subsections.

Stationary heat conduction

For stationary heat conduction, the equation of heat transfer (e.g., eq. (6.11) with variable κ and heat source $f(\mathbf{x})$, but time derivatives equal zero) is

$$\partial_j (\kappa \partial_j T) = f(\mathbf{x}) \quad (9.1a)$$

within the volume of the body V . In addition, there may be boundary conditions of several kinds:

$$\text{fixed temperature at the boundary of } V, \text{ denoted } S_1: \quad T = T_1(\mathbf{x}), \quad (9.1b)$$

$$\text{fixed heat flow on some boundary } S_2: \quad -\kappa n_j (\partial_j T) = q_2(\mathbf{x}), \quad (9.1c)$$

$$\text{heat flow due to temperature contrast on boundary } S_3: -\kappa n_j (\partial_j T) = h(T - T_3(\mathbf{x})), \quad (9.1d)$$

where unit vector \mathbf{n} (with components n_j) is the normal to the respective boundary, directed outward from the volume V .

For the equation operator with double differentiation (eq. 9.1a), the Fréchet derivative is symmetric (eq. 3.16), and therefore the variational principle exists. The corresponding Euler functional can be obtained similar to the Lagrangian for elastic field (section 0) – by considering the most general scalar, quadratic form dependent on $\mathbf{grad}T$ and source term $Tf(\mathbf{x})$:

$$\begin{aligned} \Phi\{T(\mathbf{x})\} = & \int_V \left[\frac{\kappa}{2} (\partial_j T)(\partial_j T) + Tf(\mathbf{x}) \right] dV + \\ & + \int_{S_2} q_2 T dS + \int_{S_3} \frac{h}{2} (T - T_3)^2 dS, \end{aligned} \quad (9.2)$$

where the first integral yields eq. (9.1a), and the last two terms generate the boundary conditions (9.1c) and (9.1d). The first-kind boundary condition $T = T_1(\mathbf{x})$ on S_1 is satisfied automatically by considering only functions $T(\mathbf{x})$ satisfying this condition. For any function $T(\mathbf{x})$ (even not satisfying equations (9.1) and boundary conditions), this Φ is a real number, which means that it is indeed a functional.

Let us now illustrate how the differential equation (eq. 9.1a) with all boundary conditions (eq. 9.1b-d) are obtained from this Euler functional $\Phi\{T\}$. Basically, we need to perturb the temperature: $T(\mathbf{x}) \rightarrow T(\mathbf{x}) + \delta T(\mathbf{x})$ and express the resulting perturbation $\delta\Phi = \Phi\{T + \delta T\} - \Phi\{T\}$ as an integral expression linear in δT , of the form $\delta\Phi = \int_V F_1(T) \delta T dV + \int_S F_1(T) \delta T dS$. This can be done by Fréchet differentiation (eq. 3.14):

$$\begin{aligned} \delta\Phi = & \frac{\partial}{\partial \varepsilon} \left[\Phi(T + \varepsilon \delta T) \right] \Big|_{\varepsilon=0} = \int_V \left[\kappa (\partial_j T)(\partial_j \delta T) + \delta T f(\mathbf{x}) \right] dV + \\ & + \int_{S_2} q_2 \delta T dS + \int_{S_3} h (\delta T - T_3) dS, \end{aligned} \quad (9.3)$$

Using relation $\kappa(\partial_j T)(\partial_j \delta T) = \partial_j [\kappa(\partial_j T) \delta T] - \kappa \partial_j \partial_j T \delta T$, denoting vector $E_j = \kappa(\partial_j T) \delta T$, and using for it the divergence theorem $\int_V \partial_j E_j dV = \int_{S_1} E_j n_j dS$ (where S_1 is the boundary of volume V and \mathbf{n} is the outside normal), this expression becomes of the above form with δT entering the integrands without derivatives:

$$\begin{aligned}
 \delta\Phi = & \int_V \delta T [-\kappa \partial_j \partial_j T + f(\mathbf{x})] dV + \\
 & + \int_{S_1} \delta T [\kappa n_j \partial_j T] dS + \\
 & + \int_{S_2} \delta T [q_2 + \kappa n_j \partial_j T] dS + \\
 & + \int_{S_3} \delta T [h(\delta T - T_3) + \kappa n_j \partial_j T] dS.
 \end{aligned}
 \tag{9.4}$$

According to the variational principle, this $\delta\Phi$ must equal zero for arbitrary function $\delta T(\mathbf{x})$. Therefore, each of the expressions in square brackets must equal zero, giving the Poisson's equation and boundary conditions in eq. (9.1). Note that the integral over surface S_1 is satisfied automatically because the trial function $\delta T(\mathbf{x})$ is always taken equal zero at the boundaries of the volume.

Stationary heat convection

For stationary heat convection and conduction, the source of heat comes from a flow of material with known velocity v_i :

$$\chi \partial_j \partial_j T = v_i \partial_i T, \tag{9.5}$$

where χ is the thermal diffusivity (eq. 6.10). The difference from the thermal conduction is the presence of the single temperature gradient $\partial_i T$ in the right-hand side, but because of this term, the Fréchet derivative is non-symmetric, and there exists no variational principle for this equation.

Exercise

For $F(u) = v_i \partial_i u$, evaluate \hat{F}'_u by $\hat{F}'_u \phi = \left. \frac{\partial}{\partial \varepsilon} [F(u + \varepsilon \phi)] \right|_{\varepsilon=0}$ (eq. 3.14), and show that it gives $\int \psi \hat{F}'_u \phi dV \neq \int \phi \hat{F}'_u \psi dV$ for arbitrary different function ϕ and ψ .

Nonstationary heat conduction

Consider the thermal diffusion equation with variable temperature:

$$\frac{\partial T}{\partial t} = \alpha \partial_i \partial_i T \quad , \quad (9.6a)$$

with initial and boundary conditions

$$T = T_0 \quad \text{at time } t = 0 \quad \text{and} \quad T = T_1 \quad \text{on boundary } S_1. \quad (9.6b)$$

Because of the lone derivative $\partial T / \partial t$, the Fréchet derivative is also non-symmetric for this equation, and therefore there exists no variational principle for it. However, if we take the Laplace transform of this equation, a variational principle will exist.

The Laplace transform is a transformation of a function $f(t)$ defined for $t \geq 0$ into another function $\bar{f}(s)$ defined on $s \geq 0$:

$$\bar{f}(s) = \int_0^s f(t) e^{-st} dt \quad . \quad (9.7)$$

After applying this transformation to both sides of eq. (9.6a), this equation becomes

$$s\bar{T} - T_0 = \alpha \partial_i \partial_i \bar{T} \quad . \quad (9.8)$$

This equation contains no time derivative (it was replaced by the multiplication by s), and

as shown in the first example, it has a variational principle. After dividing this equation by s , the Euler function for this principle is:

$$\Phi\{\bar{T}(\mathbf{x})\} = \int_V \left[\frac{\alpha}{2s} (\partial_j \bar{T})(\partial_j \bar{T}) + \frac{1}{2} \bar{T}^2 T - \frac{1}{s} \bar{T} T_0 \right] dV . \quad (9.9)$$

Exercise
Evaluate variation $\delta\Phi = 0$ of this function as in the preceding examples and show that condition $\delta\Phi = 0$ leads to eq. (9.6a).

In addition to using the Laplace transform, other variational principles for this equation have been constructed using convolutional integrals in time or space. I do not consider them here because they imply non-local or non-instantaneous interactions. However, the transformation from time to Laplace variable s is in fact also an example of non-instantaneous transformation, and so our general conclusion is that heat diffusion or convection equations like (9.5) and (9.6) do not integrate well with the variational principles of mechanics, and therefore they should be considered separately.

9.2 *Symmetry of the kinetic-coefficient matrix*

Like all other material-property matrices, the kinetic coefficient matrices $\kappa_{1,2}$ and $\chi_{1,2}$ defined in chapter 6 must be non-negative definite and symmetric. The symmetry of kinetic coefficients can be explained as follows. The general meaning of kinetic equations consists in describing the behavior of a statistical system in the vicinity of its equilibrium. If variable \mathbf{x} measures the deviation from the equilibrium at $\mathbf{x} = \mathbf{0}$, then the kinetic equation states that \mathbf{x} will be moving toward the equilibrium with the rates of change $\dot{\mathbf{x}}$ proportional to the gradient of some function $\Phi(\mathbf{x})$:

$$\dot{\mathbf{x}} = -\gamma \mathbf{grad}\Phi , \quad (9.10a)$$

or in subscript notation with implicit summation over repeated indices:

$$\dot{x}_a = -\gamma_{ab} \frac{\partial \Phi}{\partial x_b}. \quad (9.10b)$$

In these relations, γ_{ab} are the kinetic coefficients. If such a function $\Phi(\mathbf{x})$ exists and has a minimum at $\mathbf{x} = \mathbf{0}$, then in the vicinity of this point, $\Phi(\mathbf{x})$ can be approximated by a quadratic form (combination of all possible pairs of coordinates): $\Phi(\mathbf{x}) = \frac{1}{2} x_a \Phi_{ab} x_b$.

Matrix Φ_{ab} can always be considered as symmetric because of the symmetry of the product $x_a x_b = x_b x_a$.

The symmetry $\gamma_{ab} = \gamma_{ba}$ of the kinetic coefficients is a very general property of eq. (9.10) called the *Onsager principle* in statistical physics. This principle states that for a fluctuating statistical system, time averages over its trajectory equal averages over an ensemble of states. From this principle, the correlation function between two variables x_a and x_b taken at different times: $\phi_{ab}(t' - t) = \langle x_a(t') x_b(t) \rangle$ has a symmetry property with respect to time reversal: $\phi_{ab}(\tau) = \phi_{ab}(-\tau)$. This symmetry is related to the time-reversal symmetry of the equations of mechanics for particles within the body. If the directions of velocities are reversed for all particles in the system, its movement will remain valid and satisfying all equations of motion (however, in the absence of a magnetic field!). Because of this symmetry, the correlation function $\langle x_a(t') x_b(t) \rangle$ is the same regardless of which of the quantities x_a or x_b are taken earlier or later in time. In addition, from its definition above, the correlation has a pure mathematical symmetry. From these two relations, it follows that the correlation functions are symmetric in two ways: $\phi_{ab}(\tau) = \phi_{ba}(\tau) = \phi_{ab}(-\tau)$.

Finally, it can be easily shown that if random functions $x_a(t)$ satisfy kinetic eq. (9.10), then their correlations also satisfy the same equations:

$$\frac{d}{d\tau} \phi_{ab}(\tau) = -\gamma_{ac} \phi_{cb}(\tau). \quad (9.11)$$

Therefore, since both ϕ_{ab} and ϕ_{cb} are symmetric matrices in this equation, we can conclude (not very rigorously, but this can be proved better) that γ_{ab} must also be symmetric.

For the specific case of internal thermal diffusion within a GLS solid, the equilibrium state can be described by the heat density vector \mathbf{Q}_0 , and the deviation from the equilibrium can be measured by variable $\mathbf{x} = \mathbf{Q} - \mathbf{Q}_0$ used here. At the state of equilibrium, entropy S attains a maximum, and therefore this state minimizes function $\Phi(\mathbf{x}) = -T_0^2(S - S_0)$, where S_0 is the entropy at this state, and T_0 is its temperature. Gradients of entropy with respect to \mathbf{x} equal temperature variations: $\frac{\partial(S - S_0)}{\partial Q} = \frac{1}{T} - \frac{1}{T_0} \approx -\frac{T - T_0}{T_0^2}$. Therefore, for heat variation rate with time $\dot{\mathbf{x}}$, we have the kinetic equations (9.10).

9.3 Orthogonalization and normalization of finite-element basis functions

After an initial set of basis functions is constructed for a finite-element decomposition (section 5.11), it can be transformed into another basis of mutually orthogonal and normalized functions satisfying the condition $\langle f_n | f_k \rangle = \delta_{nk}$ (eq. (5.71)). This orthogonalization is performed using the so-called Gram-Schmidt process. Treating functions as vectors in a linear space, a projection operator projecting an arbitrary vector \mathbf{v} onto vector \mathbf{u} is defined:

$$\hat{P}_{\mathbf{u}} \mathbf{v} = \frac{\langle \mathbf{v} | \mathbf{u} \rangle}{\langle \mathbf{u} | \mathbf{u} \rangle} \mathbf{u}. \tag{9.10}$$

For a zero vector \mathbf{v} , the projection is also zero: $\hat{P}_{\mathbf{u}} \mathbf{v} = \mathbf{0}$. The meaning of this operator is that the resulting vector $\mathbf{v}' = \hat{P}_{\mathbf{u}} \mathbf{v}$ is proportional to \mathbf{u} and its inner product with \mathbf{u} is the same as for \mathbf{v} : $\langle \mathbf{u} | \hat{P}_{\mathbf{u}} \mathbf{v} \rangle = \langle \mathbf{u} | \mathbf{v} \rangle$. Then, if $\{\mathbf{v}_1, \mathbf{v}_1, \dots, \mathbf{v}_N\}$ is a set of linearly independent vectors (functions), then a set of mutually orthogonal vectors $\{\mathbf{u}_1, \mathbf{u}_1, \dots, \mathbf{u}_N\}$ can be obtained as follows (Gram-Schmidt process):

$$\begin{aligned}
 \mathbf{u}_1 &= \mathbf{v}_1, \\
 \mathbf{u}_2 &= \mathbf{v}_2 - \hat{\mathbf{P}}_{\mathbf{u}_1} \mathbf{v}_2, \\
 \mathbf{u}_3 &= \mathbf{v}_3 - \hat{\mathbf{P}}_{\mathbf{u}_1} \mathbf{v}_3 - \hat{\mathbf{P}}_{\mathbf{u}_2} \mathbf{v}_3, \\
 &\dots, \\
 \text{and generally, } \mathbf{u}_k &= \mathbf{v}_k - \sum_{i=1}^{k-1} \hat{\mathbf{P}}_{\mathbf{u}_i} \mathbf{v}_k.
 \end{aligned} \tag{9.11}$$

It can be easily verified that $\langle \mathbf{u}_i | \mathbf{u}_j \rangle$ for any $i \neq j$. From the orthogonal set of vectors \mathbf{u}_i , normalized vectors $\{\mathbf{e}_1, \mathbf{e}_1, \dots, \mathbf{e}_N\}$ are finally obtained as

$$\mathbf{e}_i = \frac{\mathbf{u}_i}{\|\mathbf{u}_i\|} \equiv \frac{\mathbf{u}_i}{\sqrt{\langle \mathbf{u}_i | \mathbf{u}_i \rangle}}. \tag{9.12}$$

9.4 Frequency-dependent effective moduli with thermal effects

To interpret results of lab experiments in terms of true physical properties of the samples, we need to use rigorous and sufficiently detailed continuum-mechanics models described above. In low-frequency forced oscillations like shown in Figures 1.7 and 1.8, the inertial, gravity, and global thermoelastic forces are insignificant compared to elastic forces, but viscous and *local* thermoelastic stresses are significant. The resulting quasi-static equations can then be obtained by combining the equilibrium equations (7.2) with the terms for viscous and thermoelastic stress σ_{ij} from eq. (5.8b), Darcy friction (drag), and temperature variation from eq. (6.12):

$$\begin{cases}
 (\lambda^* + \mu^*) \partial_i \partial_j \mathbf{u}_j + \mu^* \partial_j \partial_j \mathbf{u}_i - \mathbf{d} \dot{\mathbf{u}}_i - \mathbf{K} \alpha \partial_i \theta = 0, \\
 \dot{\theta} = -\mathbf{c}_v^{-1} \mathbf{T}_0 \alpha^T \mathbf{K}^T \partial_j \dot{\mathbf{u}}_j - \mathbf{c}_v^{-1} \kappa_1 \theta + \mathbf{c}_v^{-1} \kappa_2 \partial_j \partial_j \theta,
 \end{cases} \tag{7.26}$$

where $\theta = \mathbf{T} - \mathbf{T}_0$ is the deviation from the equilibrium temperature, and $\lambda^* = \lambda + \eta_\lambda \frac{\partial}{\partial t}$ and

$\mu^* = \mu + \eta_\mu \frac{\partial}{\partial t}$ denote differential operators combining the effects of elasticity and

viscosity.

For harmonic oscillations, time dependencies of the fields can be taken in the form $\mathbf{u}_j(\mathbf{x}, t) = \text{Re}\left[e^{-i\omega t} \mathbf{u}_j(\mathbf{x})\right]$ and $\boldsymbol{\theta}(\mathbf{x}, t) = \text{Re}\left[e^{-i\omega t} \boldsymbol{\theta}(\mathbf{x})\right]$, where $\mathbf{u}_j(\mathbf{x})$ and $\boldsymbol{\theta}_j(\mathbf{x})$ are complex-valued fields satisfying boundary conditions for the given shape of the body. Time derivatives become multiplications by $-i\omega$, and operators $\boldsymbol{\lambda}^*$ and $\boldsymbol{\mu}^*$ become multiplications by complex-valued matrices $\boldsymbol{\lambda}^* = \boldsymbol{\lambda} - i\omega\boldsymbol{\eta}_\lambda$ and $\boldsymbol{\mu}^* = \boldsymbol{\mu} - i\omega\boldsymbol{\eta}_\mu$.

The last term in the second eq. (7.26) (“global” thermal flow) is likely insignificant at seismic frequencies. Dropping this term, the harmonic oscillation of temperature can be calculated from the variations of displacement:

$$\boldsymbol{\theta} = -\left(\mathbf{I} + \frac{i}{\omega} \mathbf{c}_v^{-1} \boldsymbol{\kappa}_1\right)^{-1} \mathbf{c}_v^{-1} \mathbf{T}_0^T \boldsymbol{\alpha}^T \mathbf{K}^T \partial_j \mathbf{u}_j, \quad (7.27)$$

where \mathbf{I} is the identity matrix. This equation shows that at high frequencies $\omega \rightarrow \infty$, adiabatic temperature variations occur (see eq. (6.7)). At low frequencies $\omega \rightarrow 0$, the system approaches the isothermal regime ($\boldsymbol{\theta} \rightarrow 0$) as $\boldsymbol{\theta} = i\omega \mathbf{c}_v^{-1} \mathbf{T}_0^T \boldsymbol{\alpha}^T \mathbf{K}^T \partial_j \mathbf{u}_j$. Factor ‘ i ’ here shows that the low-frequency temperature variations are lagging the deformation by 90° in phase. These effects are the same as the deformation of the internal variable (internal spring) in the mechanical model for the standard linear solid.

Substituting eq. (7.27) into the first eq. (7.26), we obtain an equation for spatial variation of displacement \mathbf{u}_i :

$$\left(\tilde{\boldsymbol{\lambda}}^* + \boldsymbol{\mu}^*\right) \partial_i \partial_j \mathbf{u}_j + \boldsymbol{\mu}^* \partial_j \partial_j \mathbf{u}_i + i\omega \mathbf{d} \mathbf{u}_i = 0, \quad (7.28)$$

where the effect of thermoelastic stresses (term containing $\partial_i \partial_j \mathbf{u}_j$) leads to a frequency-dependent modification of modulus $\boldsymbol{\lambda}$:

$$\tilde{\boldsymbol{\lambda}}^* = \boldsymbol{\lambda} - i\omega\boldsymbol{\eta}_\lambda + \mathbf{K}\boldsymbol{\alpha} \left(\mathbf{I} + \frac{i}{\omega} \mathbf{c}_v^{-1} \boldsymbol{\kappa}_1\right)^{-1} \mathbf{c}_v^{-1} \mathbf{T}_0^T \boldsymbol{\alpha}^T \mathbf{K}^T, \quad (7.29)$$

and to a similar modification of the bulk modulus.

Equations (7.28) and (7.29) can be used to explain low-frequency laboratory experiments such as discussed in chapter 1. Note the three key conclusions from these equations:

- 1) In permeable porous rock (with $\mathbf{d} \neq 0$), when fluid flow is allowed by boundary conditions, the distribution of \mathbf{u} and the dynamic stress-strain ratio (at $\omega \neq 0$) is not described by only a pair of viscoelastic moduli. Body-force term $i\omega \mathbf{d} \mathbf{u}_i$ (eq. 7.28) has a comparable effect, which may be dominant if the pore fluid is allowed to flow.
- 2) Thermoelastic effects can be viewed as a frequency-dependent modification of the bulk modulus (eq. 7.29).
- 3) At low frequencies, the thermoelastic effect simply adds bulk solid viscosity to the medium: $\tilde{\lambda}^* \approx \lambda - i\omega \boldsymbol{\eta}_\lambda - i\omega \boldsymbol{\eta}_T$, where

$$\boldsymbol{\eta}_T = \mathbf{K} \boldsymbol{\alpha} \boldsymbol{\alpha}_1^{-1} \mathbf{T}_0^T \boldsymbol{\alpha}^T \mathbf{K}^T \quad (7.30)$$

is the additional viscosity produced by thermoelastic friction. This relation illustrates one likely mechanism of solid viscosity in multicomponent media.

In an experiment like shown in Figure 1.7 (page 27), the deformation of the porous rock sample is relatively complex:

- 1) Under axial compression, the side surface of the cylinder attains a barrel-like shape, with stronger oscillations or radius at the middle of the cylinder and weaker deformations at its ends (need to give a Figure ...);
- 2) There is an oscillatory pore fluid flow is concentrated toward the center of the upper end of the cylinder, where the tube controlling the pore pressure is connected.
- 3) The fastest fluid flow occurs within the connecting tube and the “dead volume” to which it is connected. This pore fluid flow is difficult to avoid, and it violates the usual assumption of “undrained” conditions (zero pore fluid flow) of the sample. In studies with variable dead volumes, it was found

that with small dead volumes, the recorded stress-strain response (eq. 7.22) approaches the expected undrained case, and with larger volume and lower frequencies, the measured modulus in eq. (7.22) is close to the drained one (with zero pore pressure variations).

- 4) There exist temperature contrasts between the pore fluid and rock frame, which produce solid viscosity (eq. 7.30).